

# Digital Construction

Parametric structural & environmental design of a 3D printed concrete bridge





# Digital Construction

## Parametric structural & environmental design of a 3D printed concrete bridge

By

Karel A.A. van Dongen

in partial fulfilment of the requirements for the degree of

**Master of Science**  
in Civil Engineering

at the Delft University of Technology,  
to be defended publicly on Friday the 16<sup>th</sup> of November 2018 at 14:00

Supervisor:	Prof. dr. ir. H.E.J.G. Schlangen,	TU Delft
Thesis committee:	Ir. J.A. Bolhuis,	BAM Infraconsult
	Dr.ir. J.L. Coenders,	White Lioness technologies
	Dr. H.M. Jonkers,	TU Delft
	Dr.ir. H.R. Schipper,	TU Delft

*This thesis is confidential and cannot be made public until December 31, 2020.*

An electronic version of this thesis is available at <http://repository.tudelft.nl/>.





## Preface

Before you lies the report of research study “Digital Construction, parametric structural and environmental design of a 3D printed concrete bridge”. This report is in partial fulfilment of the degree of Master of Science in Civil Engineering. I was engaged in research and writing the report from January to November 2018.

To me, this project is very special because it allowed me to use a multi-disciplinary approach to achieve the research objective. My background in Architecture drives me to be creative and search for possibilities to combine multiple design aspects. The three design aspects combined in this project, parametric-/structural-/environmental-design, are well known topics in the construction industry. However, a combination of these design aspects is less common. Another factor that makes this research project interesting is the combination of a digital design model with 3D printing of concrete. I believe that a combination of digital design and digital fabrication, such as 3D printing, can contribute to a transaction in the construction industry towards digital construction.

This research project was initiated and performed in cooperation with Johan Bolhuis from BAM Infraconsult. I want to thank Johan for his time, help and involvement in the project. During the project, Johan taught me a great deal about project and (non) related topics. He helped me find people to learn from and introduced me to Jeroen Coenders, Herman Oogink, Erik Schlangen and many others. Thank you Johan, you have been a great mentor to me!

Early in the project, Jeroen Coenders and his company White Lioness technologies became involved. Jeroen and his team helped me develop the parametric structural design model. I want to thank Jeroen for his involvement in the project and for challenging me to do better. Especially his help in writing the report was very useful to me. I would also like to thank the White Lioness team, in particular Babette Hohrath and Maarten Mathot, for their time/help and the enlightening discussions during lunch.

At a later stage in the project, Herman Oogink and Gino Vanstraelen from SCIA became involved. Together they helped develop a connection between Grasshopper and SCIA Engineer. They also helped to write a publication about the project in a Dutch construction magazine (Cementonline). I therefore want to thank Herman and Gino for their help and involvement in the project.

Many thanks to the TU Delft committee for their involvement. Their feedback helped me identify critical elements of the project and improve the report. Thank you Erik, Henk and Roel for your time and involvement in the project. Even though all of you had a very busy schedule, you always had time to answer my questions during the project.

Last but not least, I would like to thank my friends and family for listening to me going on and on about the project. The topic probably did not interest them as much as me, however it did not stop them from listening and they always supported me. A special thanks to my father P. van Dongen, my sister J. van Dongen and “De Vagga Boyz” for reviewing draft versions and for providing me with distractions.

*K.A.A. van Dongen  
Delft, November 2018*



# Contents

<b>Abstract.....</b>	<b>11</b>
<b>1. Introduction .....</b>	<b>13</b>
1.1. Problem definition .....	17
1.2. Research question .....	18
<b>2. Model Intent .....</b>	<b>19</b>
2.1. Defining simulation intent .....	20
2.2. Model simulation intent .....	22
2.3. Software comparison .....	24
<b>3. Parametric geometry .....</b>	<b>27</b>
3.1. Parametric design .....	28
3.2. Component methodology .....	29
3.3. Parametric geometry component .....	32
<b>4. Structural analysis .....</b>	<b>41</b>
4.1. Structural design .....	42
4.2. Structural analysis context .....	45
4.3. Component methodology .....	51
4.4. Structural analysis component .....	63
<b>5. Environmental analysis .....</b>	<b>73</b>
5.1. Towards sustainable construction .....	74
5.2. Component methodology .....	77
5.3. Environmental analysis component .....	81
<b>6. Model analysis.....</b>	<b>85</b>
6.1. Result validation .....	86
6.2. Structural efficiency comparison.....	90
6.3. Environmental impact comparison .....	94
<b>7. Discussion .....</b>	<b>99</b>
7.1. Reflection on research project .....	100
7.2. Project limitations.....	102
<b>8. Conclusions.....</b>	<b>105</b>
<b>9. Recommendations .....</b>	<b>106</b>
<b>Bibliography .....</b>	<b>107</b>
<b>Annex A – Grasshopper components.....</b>	<b>111</b>
A1. Geometry component .....	112
A2. Pre-processing component .....	115
A3. XML export and execute analysis component .....	117
A4. Result interpretation component .....	119
A5. Environmental analysis component .....	122
<b>Annex B – Design drawings.....</b>	<b>125</b>

B1. Print path design .....	126
B3. Varying tendon location in print path .....	127
B3. Inner/outer tendon location .....	128
<b>Annex C – Eurocode documentation .....</b>	<b>129</b>
C1. Eurocode load combinations .....	130
C2. Eurocode standards .....	132
C3. Method statement .....	138
<b>Annex D – XML documentation .....</b>	<b>150</b>
D1. XML identification document .....	151
<b>Annex E – Calculation control document .....</b>	<b>162</b>
E1. Geometric properties .....	163
E2. Load generation .....	164
E3. Bending induced stresses .....	167
E4. Shear force .....	168
E5. Post-tensioning force losses .....	169
<b>Annex F – Environmental analysis input .....</b>	<b>170</b>
F1. Volvo truck emissions .....	171
F2. Road transport truck dimensions .....	174
F3. Bending induced stresses .....	177

## Index

### Equations:

Equation 1.1-1.3 .....	35
Equation 2.1-2.2 .....	37
Equation 3.1-3.4 .....	37-38
Equation 4.1-4.2 .....	53
Equation 5.1-5.4 .....	58
Equation 6.1-6.2 .....	59
Equation 7.1-7.5 .....	59
Equation 8.1-8.2 .....	59
Equation 9.1-9.2 .....	60
Equation 10.1-10.4 .....	60
Equation 11.1-11.2 .....	60
Equation 12.1-12.2 .....	61
Equation 13.1-13.2 .....	61
Equation 14.1-14.4 .....	71
Equation 15 .....	77
Equation 16 .....	77
Equation 17 .....	78
Equation 18.1-18.4 .....	92

### Figures:

Figure 1; Graphical representation of the BIM principle - [3] .....	13
Figure 2; Visual representation of a linear construction project organisation - [8] ....	14

Figure 3; Schematic representation of a digital construction organisation method - [5]	15
Figure 4; Photograph of the 3DPC bridge in Gemert, The Netherlands. ....	19
Figure 5; Visualisation of the Gemert design in the article of T.A.M. Salet et al - [22]	22
Figure 6; Visualisation of the model workflow used in this research project. ....	24
Figure 7; Comparison of parametric software .....	25
Figure 8; comparison of structural analysis software .....	25
Figure 9; Comparison of process automating software.....	26
Figure 10; Example of parametric bridge design by Andreas Schnubel (2008) - [36]	27
Figure 11; Flowchart visualising the method of creating the main geometry. ....	29
Figure 12; Flowchart visualisation of the method of creating the modified geometry	29
Figure 13; Flowchart visualisation of the 3DPC cross-section geometry .....	30
Figure 14; Flowchart visualisation of the calculation of area moments .....	30
Figure 15; Flowchart visualisation of the placement of tendons in 3DPC cross-sections	31
Figure 16; Left; without distortion factors – Right; with distortion factors .....	32
Figure 17; Top left; smooth interpolated line – Top right; linear interpolated line – Bottom left; sinusoidal line – Bottom right; skewed line .....	33
Figure 18; Top left; generated cross-section – Top right; grid based on half the filament width & AutoCAD approximation – Bottom left; identified key grid points – Bottom right; straight line approximation of the print path .....	34
Figure 19; Calculated conversion factors and the average value used in the model	35
Figure 20; Top left; area for tendon placement – Top right; tendon location per cross- section – Bottom left; resulting location for straight placement per print loop – Bottom right; straight tendon configuration .....	36
Figure 21; Top left; possible horizontal tendon movement – Top right; possible vertical tendon movement – Bottom left; effect of horizontal movement on tendon placement – Bottom right; effect of vertical movement on tendon placement .....	37
Figure 22; Schematic visualisation of the stress directions in 3DPC .....	43
Figure 23; Eurocode NEN-EN 1990 equation 6.8 .....	46
Figure 24; Eurocode NEN-EN 1990 critical load combinations.....	46
Figure 25; Eurocode NEN-EN 1990 load factors .....	46
Figure 26; Eurocode NEN-EN 1990 load combination factors.....	47
Figure 27; Bending induced stresses in post-tensioned structures.....	48
Figure 28; Eurocode NEN-EN 1992-1-1 equation 6.2a and 6.2b.....	48
Figure 29; Effect of creep on the strain in post-tensioning tendons .....	49
Figure 30; Eurocode NEN-EN 1990 equation 3.6 .....	49
Figure 31; Eurocode NEN-EN 1992-1-1 Figure 3.4 .....	49
Figure 32; NEN-EN 1992-1-1 table 2.1 .....	50
Figure 33; Eurocode NEN-EN 1992-1-1 equation 3.15 and 3.16.....	50
Figure 34; Material properties of post-tensioning tendons of class Y1860S7 .....	50
Figure 35; Flowchart visualisation of the structural analysis component .....	51
Figure 36; Height over span length and height over width ratios .....	53
Figure 37; Top left; centroidal axis of the section interfaces – Top right; coordinates of the representative solid model – Bottom left; representative sections – Bottom right; representative solid model .....	55
Figure 38; Example of specifying a node of a structure for import into SCIA.....	56
Figure 39; Exported from SCIA – Mesh generated by SCIA for the Gemert design case	58
Figure 40; Percentage based difference between results obtained by the compared model representations.....	65
Figure 41; 2D plate model existing of multiple elements exported from SCIA Engineer	66

Figure 42; Relation between force and displacement in a SCIA Engineer 2D plate model .....	67
Figure 43; Stiffness matrix equations used in a SCIA Engineer 2D plate model .....	67
Figure 44; Above; correct numbering of the nodes and its result – Below; incorrect numbering of the nodes and its result .....	69
Figure 45; Python component, Python script and execute button used in Grasshopper .....	70
Figure 46; Command file created for calculating the structural behaviour in SCIA Engineer without an interface.....	71
Figure 47; Graphic representation of the current construction economy - [63] .....	73
Figure 48; Graphic representation of a circular built environment - [75] .....	76
Figure 49; Flow chart for determining the environmental impact .....	77
Figure 50; Flow chart for determining the shadow cost related to transport of final product .....	78
Figure 51; Fuel index based on a publication of the Volvo company - [77].....	81
Figure 52; Left; identified edges of the primary structure in green – Right; generated start points in green.....	82
Figure 53; Left side, top to bottom; inner layer, secondary shape and volume in the linear interpolated configuration – Right side, top to bottom; inner layer, secondary shape and volume in the sinusoidal configuration .....	83
Figure 54; Calculated accuracy of the conversion rate method .....	86
Figure 55; Internal moment distribution calculated in SCIA Engineer .....	88
Figure 56; Internal shear force distribution calculated in SCIA Engineer .....	88
Figure 57; Top left; Limit case 1 – Top right; Limit case 2 – Bottom left; Limit case 3 – Bottom right; Limit case 4.....	91
Figure 58; Utilisation ratio comparison between the limit cases .....	92
Figure 59; Comparison of environmental impact expressed in shadow costs .....	94
Figure 60; Weighted factor of the calculated impacts .....	95
Figure 61; Calculated CO2 reduction related to reusing demountable standardized elements - [78] .....	96
Figure 62; Comparison between shadow cost reduction of applying modular construction to the project .....	96
Figure 63; Load in relation to span curve to determine the required type of slab - [79] .....	97
Figure 64; Indication of shadow cost related to new and reused hollow-core slabs - [80] .....	97

#### Tables:

Table 1; Material properties determined for the 3DPC bridge in Gemert by T.A.M. Salet et al - [22] .....	<b>Fout! Bladwijzer niet gedefinieerd.</b>
Table 2; Results calculated using the design model and verification of structural safety .....	71
Table 3; Comparison of the obtained results .....	87
Table 4; Support reactions calculated in SCIA Engineer .....	87
Table 5; Result comparison of the limit case study .....	91
Table 6; Shadow cost conversion rates used in the model, based on the NDEI of 2009 .....	94

# Abstract

The objective of this research project is to verify whether 3D printing of concrete (3DPC) reduces the environmental impact by increasing the structural efficiency. During the literature study, numerous articles were identified that claimed an increase of structural efficiency by using 3DPC to reduce material use. Some of these articles suggest that an increase in structural efficiency results in a reduction of environmental impact. However, these articles do not support this potential with a research study.

This research project therefore studies the relation between structural efficiency and the environmental impact of a 3DPC bridge. This relation is studied by developing a design model that calculates structural efficiency and determines the environmental impact. The design model is developed in a visual script environment for parametrically controlling visual design software. The parametric script specifies and combines information in an XML file used for structural analysis in finite element software. This analysis is executed on command in the parametric environment and the results are used for verifying the structural safety. The structural safety is expressed in a material utilisation ratio. This ratio indicates the used proportion of strength of the material and can be used as an indicator for structural efficiency. After calculating the structural efficiency, the design model is used to determine the environmental impact of the structure expressed in shadow costs. Shadow costs quantify the environmental impact of materials and processes related to geometric quantities defined in the design model.

Multiple combinations of parameters have been compared to determine the relation between structural efficiency and environmental impact. The results of the comparison show that an increase in structural efficiency results in decreased material use. A decrease in material use reduces the environmental impact because  $\pm 59\%$  of the impact is related to 3DPC material. The environmental impact of the 3DPC bridge is then compared to a hollow-core-slab element with a similar functionality to verify the claimed potential. This comparison shows that the environmental impact of 3DPC is almost two times higher than the compared conventional method.

Therefore, using a novel design model and based on the results, following two conclusions can be drawn:

1. Increasing structural efficiency can decrease the environmental impact of a 3DPC bridge, and
2. Considering the state of 3D printing concrete technology at present, applications of this technology for bridges can result in a higher environmental impact than the compared conventional method.





# 1. Introduction

The modern-day construction industry is influenced by digitisation, especially in the design phase. Computer-aided design (CAD) software is used to visualise a design and create accurate construction drawings. Computer-aided engineering (CAE) software is used to calculate the structural behaviour of the design and generate reports. A benefit of digitisation is an increased work-rate when compared to traditional manual processes [1]. Implementing CAD and CAE software can therefore result in increased productivity of construction projects. A related influence of digitisation is experienced in the organisation of projects. CAD and CAE software create digital output that can be shared with a multitude of actors. This fuelled the development of new data sharing systems such as building information modelling (BIM). BIM systems can be used to create databases of integrated and interoperable information. As a result, information stored in BIM databases can be used seamlessly and sequentially by everyone in the database [2]. Integrating knowledge of multiple aspects of the life cycle of a project can result in early identification of consequences of design decisions. BIM can therefore be used to create added value to the process and product by integrating knowledge. Figure 1 presents a graphical explanation of the BIM principle.



**Figure 1; Graphical representation of the BIM principle - [3]**

As mentioned, BIM systems can be used to integrate multiple aspects of a project in multiple phases of the project. Integrating multiple aspects of the project can result in early identification of critical project aspects and/or phases. Therefore, the application of BIM systems to a construction project can result in a reduction of time [4]. Another benefit of BIM systems is related to collaboration in the construction industry. Implementing BIM as a project organisation system can help manage the complexity of construction projects. Construction projects can contain multiple interdependent activities between multiple corporations. In these projects a multitude of actors perform several activities with many overlap areas. Another complicating factor is the high amount of activity turnover, poor collaboration and poor information interoperability [5]. In traditional organisation systems a linear model is used, that visualises a project as a rigid sequence of phases, to manage complex projects (see Figure 2). A benefit of

managing projects in phases is that this setup allows local adaptations to local influences. Therefore, in traditional projects, construction managers considered construction projects to be managed most effectively in a decentralised manner [6]. However, a possible downside related to the decentralised organisation is transfer of information. Communication in decentralised organisations connects actors in adjacent activities. These actors share the required output for the next phase with the actor in charge of the next phase. Therefore, the communication topology in the construction industry can currently be labelled as linear. Because of the linear communication and transfer of information, information can be left out that could be valuable for other phases [7].

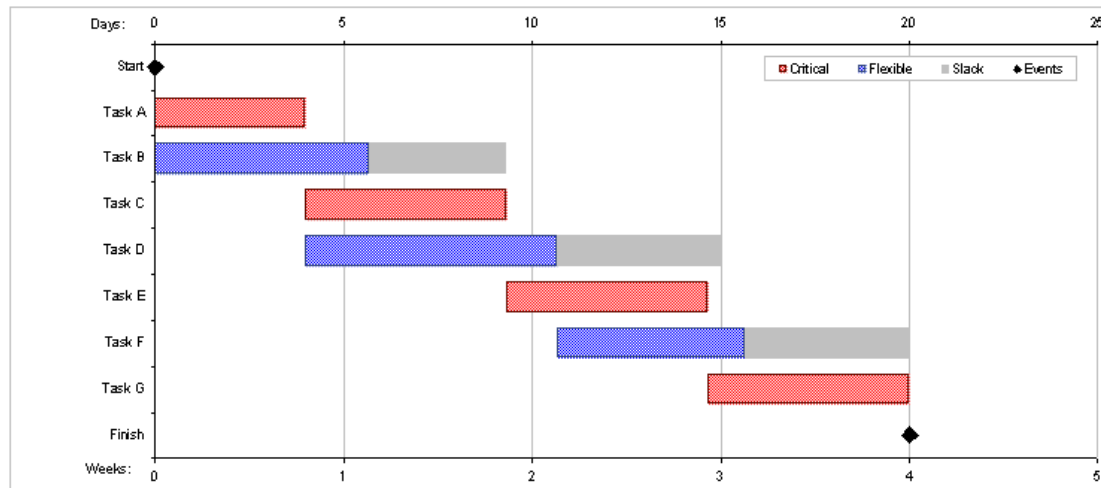


**Figure 2; Visual representation of a linear construction project organisation - [8]**

Digital construction (DC) is an organisational initiative for increasing productivity by sharing digital information using BIM systems. The goal of the initiative is to integrate processes and information throughout multiple phases of a construction project. Therefore, BIM and DC have a similar approach in storing/sharing information. The difference between BIM and DC is in the intention of the method. BIM is a technical method for integrating knowledge in a project. DC is an organisational method for communication and sharing of information in a project [9]. A benefit of applying DC organisational systems is that information is efficiently shared and communicated in the project. Therefore, increasing data interoperability and communication efficiency, previously indicated as a complicating factor in construction projects [10]. As a result, applying DC methods to construction projects can contribute to increased productivity. An example is presented in the article of C. Merschbrock and B.E. Munkvold [11]. The article describes a hospital construction project in Norway that used a DC method to organise the project. In the project, an open BIM system was used that connected actors involved in the project (client, engineer, architect supplier and contractor). The project was rewarded with the award for 'outstanding open BIM practice' by BuildingSMART in 2015. According to the conclusions of the project/article the application of the DC organisation using open BIM system resulted in;

- Improved model based decision making. Connecting previously unconnected designers resulted in increased efficiency of overcoming technical challenges.
- Cloud based infrastructure. Allowing all parties involved to either work co-located, distributed or both.
- Successfully sharing digital information. Determining the software used in the project for all parties involved increased the efficiency of sharing digital information.

- Integrated design. The holistic approach used in the project resulted in an overall 'organising vision' which result in a high level of integrated value of the design.

The project succeeded in creating a digital information system that automatically updated all information. In the application to the construction projects, this method can be seen as a step forwards towards DC [11]. The application of DC using BIM systems in the hospital project is linked connected to component-based design (CBD). CBD can be used to breakdown a project into a set of functions that can be performed by various components. In CBD, a component represents a self-sustained subsystem that can interact with other components [12]. Together the components represent the total project organisation of performed functions. Figure 3 visualises the transition towards DC in three steps by implementing BIM and CBD.

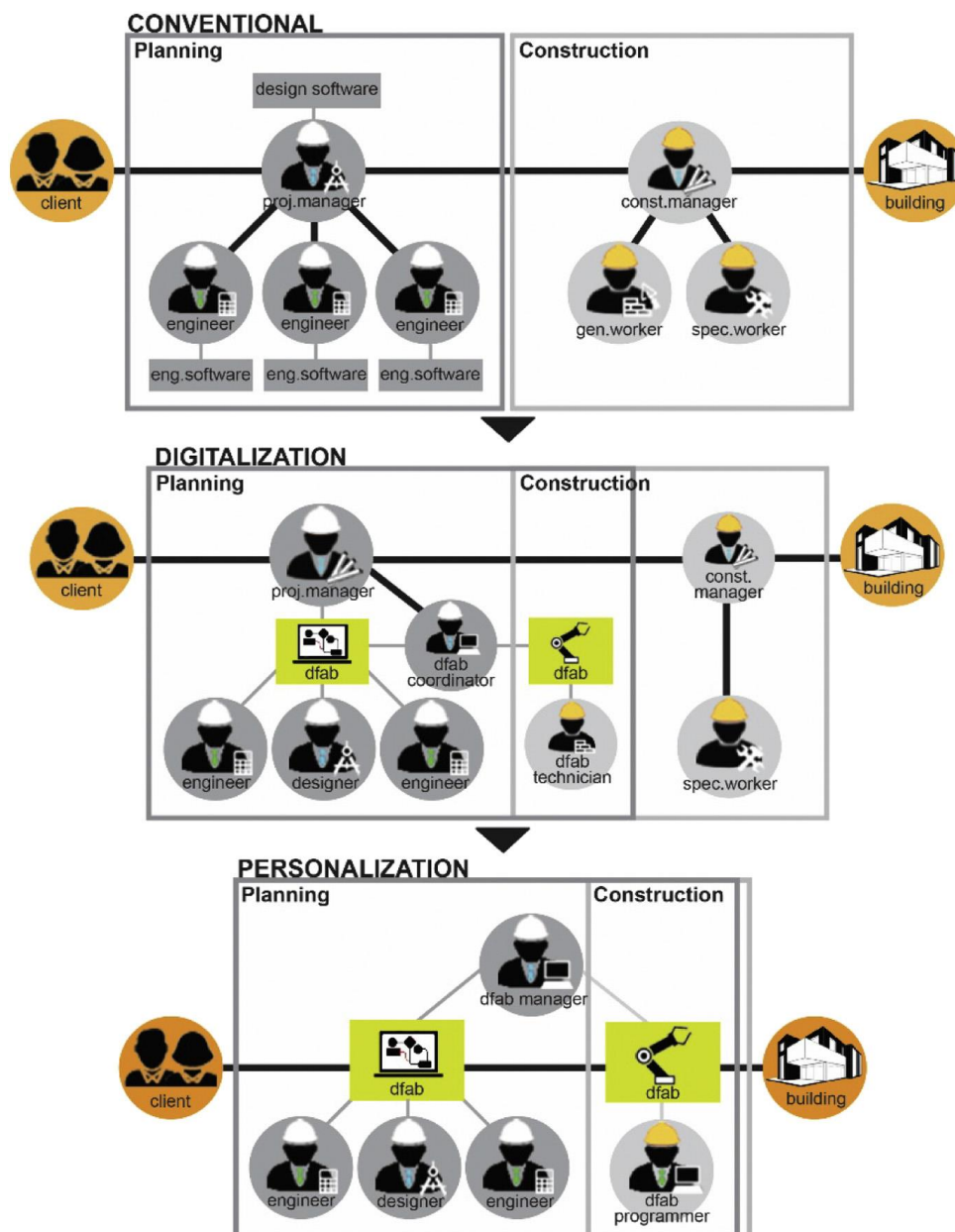


**Figure 3; Schematic representation of a digital construction organisation method - [5]**

The first step, in Figure 3, is the conventional project organisation in which CAD & CAE are used in the design/planning phase. In the second step BIM systems are implemented in the design/planning phase and partly in the construction phase. In the

design phase engineering, design and digital fabrication components are developed by their representative actor. The components are combined in a BIM system, however the on-site construction phase is not integrated. In the third step the transition to DC is completed. BIM systems are used to integrate all components of the construction project. Therefore, in the transition towards DC, all phases of a construction project should be digitised/industrialised.

In conventional projects, pre-fabricated elements are used for increasing the on-site construction speed. This method can be considered as partly industrialised. However, DC required a higher level of industrialisation. An industrialised alternative to pre-fabrication is additive manufacturing (AM). AM is an automated production process that has developed into a digitally controlled production method. One of the digitally controlled AM techniques is 3D printing. 3D printing is a production method that creates volumes by depositing material layer-by-layer [13]. A benefit of this production method is the possibility of producing complex shaped section on a large scale. This is beneficial to meet the requirements of the changing nature of the construction industry. Currently the demand of the industry is changing from mass production to mass customisation. In other words, the industry demands rapid modifications and fast but accurate production [14]. Fast and accurate production of non-standardised products is possible by using 3D printing. Rapid modification is possible by integrating all required components using DC and BIM systems. Because of the current demand of the construction industry, the combination of BIM, DC, CBD and 3D printing is of interest to the construction industry.

The application of the described combination of methods is not common in construction projects. Especially in civil construction projects where risks are much higher than in residential projects. However, civil construction projects tend to have a higher repetition factor in the design. Especially in the structural design of concrete bridges. The application of the described methods can therefore be useful to increase the productivity in civil construction projects, particularly to the construction of concrete bridges [15]. However, the application of 3D printed concrete (3DPC) to the civil and infrastructure industry is relatively new. As a result, the benefits of using the material and production process are not fully determined. The estimated benefits of 3DPC are mostly based on the difference between 3DPC and traditional production methods. Schutter et al mention, in the article *“Vision of 3D printing with concrete – Technical, economic and environmental potentials”*, three potentially beneficial aspects of digital additive fabrication [5].

1. Technical potential; placing material only where it is structurally or functionally needed increases the efficiency of the application of the material.
2. Economical potential; additive digital fabrication and reduction of material can result in increased cost-effectiveness of construction projects.
3. Environmental potential; reduction of environmental impact related to increased structural efficiency through accurate material placement.

In each of the presented potential improvements, the benefit of 3DPC is a result of the reduction in material. However, the article states that these potentials are expected and not verified. Therefore, this research project aims to verify the claimed potential of 3DPC in civil and infrastructural projects. The claimed potential will be verified by developing a DC based design model for 3DPC bridges. The developed model will be used to determine the impact of material reduction on the structural efficiency and environmental impact.

## 1.1. Problem statement

According to data gathered in 2010, 45% of world energy and 50% of water are used by buildings. When looked environmental effects; 23% of air pollution, 50% of greenhouse gas production and 40% of water pollution are caused by buildings [16]. Out of these impacts 70-90% is related to the use-phase of a structure, which is not a strange result because it exceeds all other phases in the duration of the phases [17]. Civil construction projects such as roads or bridges requires less use-phase related activities compared to residential projects. As a result, the initial environmental impact of civil construction projects is higher, especially if concrete is used as structural material. Concrete has a high environmental impact because of the required cement used in the production process of concrete [18]. A reduction in the environmental impact of civil projects containing concrete structures can therefore reduce the total environmental impact of the construction industry.

Sustainable construction is a frequently used term in the construction industry. This is the result of two developments. The first is an increase in knowledge regarding the environmental impact of construction activities. The second is the implementation of design regulations by governmental organisations. The European Commission currently request that the total level of the emission of green house gases (GHG) should be cut by 40% in 2030, 60% in 2040 and 80% in 2050 [19]. The total contribution of the construction industry to the emission of GHG is estimated as 40-50% of all global GHG emission. The production process of cement is solely responsible for 5% of all global GHG emission [20]. Construction related activities such as maintenance and demolition further increase the already high environmental impact of the industry. To conclude, the negative environmental impact of concrete structures should be reduced to meet the conditions of the European Commission. Methods to reduce the emission of GHG related to concrete, in the construction industry, can be divided in three main categories. These categories are based on the reduce, reuse and recycle principles derived from architecture [21].

1. The first category is reduction of materials in the final product that are responsible for most of the GHG emission.
2. The second category is focussed on reusing as much of the final product as possible. This can either be partial or complete reuse.
3. The third category is focussed on re-cycling as much of the final product as possible. If the final product is not reusable at the end-of-life phase then some of its content can still be useful in other applications.

All three principles have design related aspects. However, the first two principles have the most design related aspects. Therefore, In this research project the emphasis is on the first and second principle. Reduction of materials can be achieved by adjusting the geometry of a design without endangering the structural safety. Therefore, the first two function components of the proposed DC model are; generate a geometry and determine the structural safety of the geometry. A third function component is required to determine the environmental impact of the geometry. Reuse of structural elements imposes design requirements but does not require additional function components. BIM software can be used to combine the three required functions in a single interface. As presented in Figure 3, this setup can be seen as a first step in the transition towards DC. The second transition can be made by combining the BIM model with a digital construction method such as 3DPC.

This research project proposes a different organisation setup of construction projects for two reasons. The first is to increase the productivity of the civil and infrastructure industry by implementing DC. The second is to determine the relation between increasing the structural efficiency and lowering the environmental impact.

## 1.2. Research question

Based on currently available literature, a potential benefit of 3DPC in bridges is an increase in structural efficiency and a decrease of environmental impact. This research project aims to determine the relation between structural efficiency and environmental impact of 3DPC bridges. By using the described methods to determine and verify the suggested relation, this research project also functions as a proof of concept for the combination of Building Information Modelling, Component Based Design & 3DPC in a Digital Construction based project organisation. The following research question is used in this research project to verify the suggested relation and its potential;

**“Does increasing the structural efficiency in a 3D printed concrete bridge result in a decreased environmental impact that is lower compared to a conventional method?”**

As mentioned, the research question will be answered using a design model that is developed using the described methods. The model will be validated to a manual design calculation to determine the accuracy of the model. The validation model is a reconstructed calculation of the 3DPC bridge in Gemert based on Eurocode and literature [22]. The research question can be dissected into a set of sub-questions that address the three topics combined in the research question.

1. *What is the effect of changing the geometry on the structural efficiency?*
  - a. Which geometrical parameters influence the structural efficiency?
  - b. What limits the change in geometry and the resulting structural safety?
  - c. What is the accuracy of the structural analysis of the design model?
  - d. What are the restrictions related to using the design model?
2. *What is the effect of changing the geometry on the environmental impact?*
  - a. What is the influence of reducing material on the environmental impact?
  - b. What limits does reuse of structures impose on the changes in geometry?
3. *Does applying 3DPC to bridge design result in a lower environmental impact when compared to a conventional method?*
  - a. Which conventional method can 3DPC be compared to?
  - b. What is the influence of material reduction on the comparison to the conventional method?
  - c. What is the influence of reuse of the structure on the comparison to the conventional method?

The combination of methods and the components used in the design model developed in this research project should not be limited to the application to 3DPC bridges. As a result, the model methodology can be applied to other projects.



## 2. Model intention

This chapter uses the objective of the design model described in Section 1.1 and 1.2 to define the function of the three identified components. This process is known as defining the model simulation intent. The model simulation intent can be used to determine required input and output for each of the three components. The required input and output can be derived from the research question and sub-questions.

The first step in determining the model simulation intent is to further specify the function of each of the identified functional components. The second step is to determine the relation between the components. The third step links the first two steps and determines the setup of the model and visualises the process using a flow-chart diagram. This diagram links the required input/output to each of the functional components in the determined process flow.



**Figure 4; Photograph of the 3DPC bridge in Gemert, The Netherlands.**

## 2.1. Defining simulation intent

A benefit of using CAD and CAE software in a design process is the possibility of using software packages to perform difficult tasks. For example, finite element analysis (FEA) software can simplify modelling the mechanical behaviour. A downside of using FEA software can be to determine the required information for the model. Accurate input such as material properties benefit the accuracy of the result, especially when modelling concrete structures [23]. However, simulations that require a high amount of information also require more time to use. This can be a downside compared to less accurate simulations based on less detailed information [24]. Therefore, it is important to match the simulation specifications to the simulation intent. As a result, simulation intent can help reduce the amount of time spent on modelling unnecessary information in non-suitable software applications [25]. The MSI and software suited for the intent can be derived from the information that the model should generate.

As discussed in Section 1.2, the design model should determine the structural efficiency and the environmental impact. Examples of comparable design models are described in literature. For example the studies of Garcia-Segura [26] and Yepes [20] describe an optimisation of cost and CO<sub>2</sub> emission. The studies of Rumpf [27] and Bletzinger [28] describe an optimisation of form and thereby material use efficiency. All four studies have a similarities in the model used to determine the optimum. In these studies the described models all contained three functional components.

1. Geometry component; used to generate and control the form/shape of an object
2. Analysis component;
  - a. Environmental impact analysis in the CO<sub>2</sub> reduction studies
  - b. Structural analysis in the material use efficiency studies
3. Optimisation component; used to categorise a multitude of combinations based on performance to the optimum criterion

Because this research project aims to determine the relation between structural efficiency and environmental impact, both analysis components but no optimisation component are used. In the model used in the mentioned studies, the geometry was determined using parametric principles. Parametric setup of the geometry model allows rapid modifications of the design thereby decreasing the model use time [14]. The definition of parametric design and the principles of parametric modelling will be addressed in Section 3.1.

Ideally, the combination between parametric and structural design would involve a bi-directional feedback system. In bi-directional systems, each feature can be derived from its parents through its relationships and the behaviour is predicted [29]. From a geometrical construction perspective this would be the purest way to model geometry. However, bi-directional communication is a complicated process to implement in CAD software. The downside of the lack of bi-directional relationships is explained by an example; "Suppose that a designer defines line A and then defines line B as being parallel to line A. Moving line A causes line B to update to maintain itself parallel to line A. However, if line B is moved it has no effect on line A". A solution strategy for bi-directional relations, without changing software packages for the use of built-in feedback loops, is a constraint solver. In this process both line A and B are defined separately and then declares that line A and B should be constrained to be parallel (independent of the draw order) [30].

Bi-directional software communication is not common in current parametric and structural design software. For a long time software developers in CAD and CAE mainly focussed on 3D visualisation. This resulted in software focussed on generating complex geometries. After the use of CAD was established, the coupling with computer animated/automated analysis became more interesting in engineering practices. The



independent development of the two software types resulted in a mismatch between requirements for the software types [25]. An increasing demand for the combination between parametric geometric modelling and FEA calculations drives developers to shift focus to communication requirements between types of software. Theoretically, a benefit of using programs created by the same developer is in the communication between the program interfaces [31]. Because Autodesk, for example, created Revit, Dynamo and RSA the communication between the software interfaces runs smoothly. This can be beneficial for sending information backwards and forwards through the combined interfaces. A benefit of using software from the same developer is the availability of a built-in application programming interfaces (API). Therefore, multiple applications can communicate directly because of the API.

Other software packages do not offer an API for communication between software. SCIA and ABAQUS, for example, make use of import and export options to share analysis results with other software. A downside of this type of information sharing is in time requirement of importing/exporting results due to transformation of data coding [32]. A possible method of using this type of programs in combination with incompatible data structures is by using eXtensible Markup Language (xml). An XML format provides flexible and adaptable information identification since it is a meta-language, a language for describing other languages. The format, thereby, allows one to design their own customized markup language for interoperability with different data structured software. If the data structure cannot be transformed to the required format, custom formatting options must be used for cooperation of software. However, this can require advanced knowledge of data structures and coding of communication between multiple software. Examples of software that offer options for custom communication development are MATLAB and Python [33].

Negative effects of implementing design software in construction practices are mainly related to case specific applicability of models and limitations of software. Further developing CAD/CAE programs can improve design tools that are used in engineering practices, thereby increase simulation possibilities. Development of these types of software can increase the design capacity in design practices. Implementing design software in construction practices can offer non-expert designers insights in relation between parameters, structural behaviour and performance of a design [34]. In combination with design performance simulation software, designers can generate sufficient design details in topics that normally only experts would be able to generate [35]. One of such developments is parametric structural design, which is a combination between architecture and structural engineering.

## 2.2. Model simulation intent

In this research project, a design model will be developed that determines the structural efficiency and the environmental impact of a 3DPC bridge. To verify the workflow of the design model, the generated results will be compared to a test case. Because there is only one 3DPC bridge, the test case used in this project is the 3DPC cyclists and pedestrians bridge in Gemert (see Figure 4&5). The Gemert design and design input is described in the article of T.A.M. Salet et al [22]. The design model developed in this research project should therefore be able to generate a design similar to the 3DPC in Gemert, based on similar design input. However, the design model should not be limited to reproducing the Gemert design. This intent has been set for two reasons;

1. The first reason is based on the model validation. Based on the design described by T.A.M. Salet et al [22], a calculation verification document is created that can be used to validate the results of the design model. If the design model results in an accurate design approximation, the model is likely to generate meaningful results for other geometric input as well.
2. The second reason is based on the intent of the project. This project aims to verify the potential of the material production method to reduce the environmental impact of the structure. Since the Gemert bridge is the first application of 3DPC to the civil and infrastructure industry it is the only available test case to verify the reduction potential compared to conventional methods.



**Figure 5; Visualisation of the Gemert design in the article of T.A.M. Salet et al - [22]**

The article of T.A.M. Salet et al [22] describes the main geometric, material and structural design input. The following design input is used from the article;

1. Geometrical design input;
  - a. Span-length *6,50 m*
  - b. Width *3,50 m*
  - c. Section height *0,80 m*
  - d. Filament width *0,06 m (print path thickness)*
2. Material properties
  - a. Concrete strength *(presented in Section 4.2)*
  - b. Concrete time dependent behaviour *(presented in Section 4.2)*
3. Structural design input
  - a. Pre-stressing type *Post-tensioned*
  - b. Number of tendons *10 + 6 (bottom + top)*
  - c. Post-tension force *150 kN (per tendon)*
  - d. Support conditions *Hinge and slider connection*
  - e. Loading conditions *Pedestrian/cyclist load case (presented in section 4.2)*
  - f. Critical design checks *Bending induced stresses  
Post-tension losses  
Shear force*

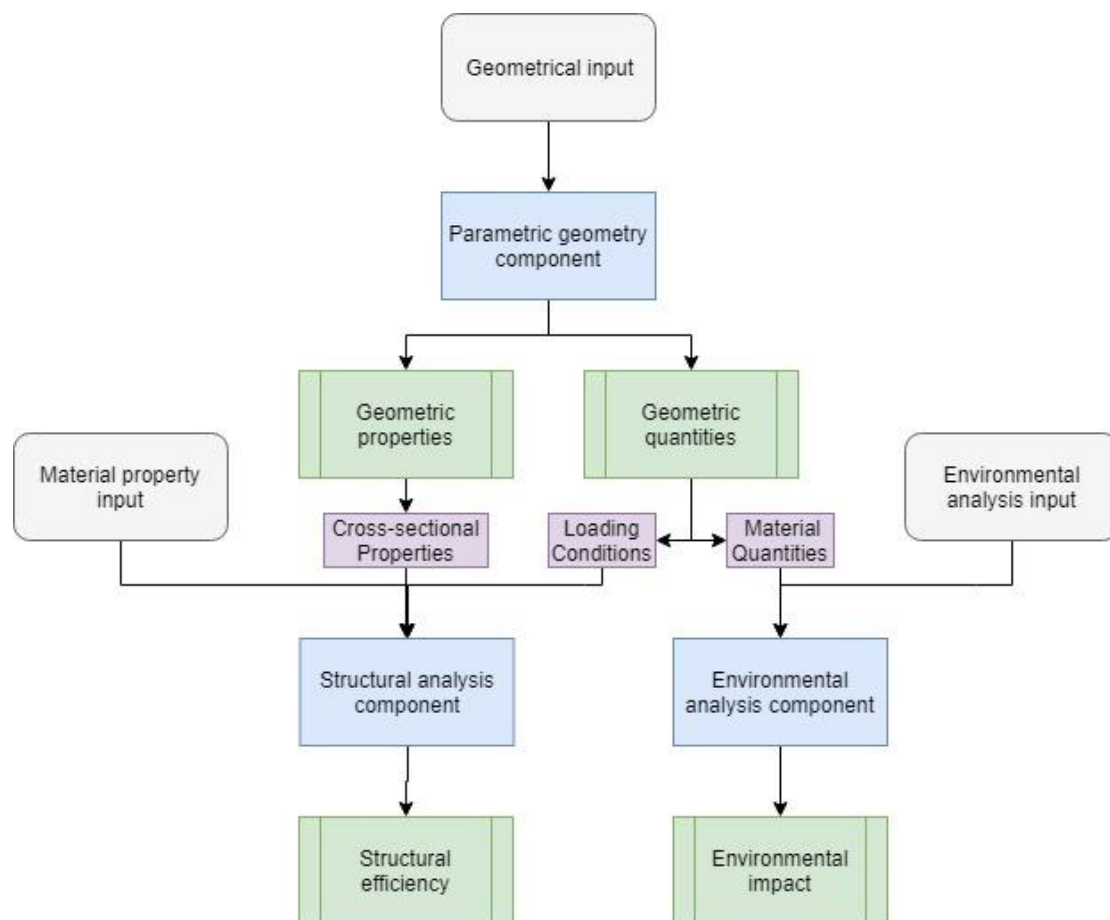
The following characteristics of the model are based on the described MSI. It is important to consider that these characteristics are used for validating the accuracy of the structural behaviour of the design model. As mentioned before, the model is not restricted to only reproducing the same design as the Gemert pedestrian/cyclist bridge.

1. Geometrical design characteristics of the design model
  - a. The same geomtric design input will be used as in the Gemert design in order to verify the work-flow of the design model. However, the use of other geometric design input should be possible.
  - b. The tendon configuration should remain straight throughout the span to avoid using tendon deviators. Tendon deviators should be avoided because tendon deviators cannot be printed into the cross-section.
  - c. The tendons cannot interfere with the shape of the cross-section (see Figure 4). Therefore, tendons are restricted to the positioning inside one of the printed loops. This requires a constant amount of loops along the span.
2. Material property characteristics of the design model
  - a. The same material properties will be used as in the Gemert design for the verification of the workflow of the model. However, the use of other material properties should be possible.
3. Structural design characteristics of the model
  - a. The same type of pre-stressing, number of tendons and post-tensioned force should be used as in the Gemert design. This ensures that only the effect of changes in the geometry influence the structural behaviour.
  - b. The same support and loading conditions will be used in the design model. Because of the focus and the limited time-span of the research project, it was decided to limit the structural design scheme to the Gemert design.
  - c. The design model should validate the critical design checks identified in the Gemert design process described in the article of T.A.M. Salet et al.

These model characteristics function as the main content of the MSI throughout this research project.

## 2.3. Model workflow and software



The described characteristics of the model are used to determine the workflow and suitable software for the design model. Based on Section 2.1 the model uses three different functional components. The first component is the parametric geometry component. This component uses the design input to create a geometric model. The model is used to determine two items; the geometric properties and geometric quantities. The generated output of the geometry component is used as input for the structural analysis (SA) component and environmental analysis component. Together with material properties, the geometric properties and quantities are used to determine the structural efficiency. The environmental analysis input is combined with geometrical quantities to determine the environmental impact. The model workflow used in this research project is visualised in Figure 6.



**Figure 6; Visualisation of the model workflow used in this research project.**

As described in Section 2.1, the process of determining the structural efficiency requires the combination of three software types. The geometry and the environmental analysis can be performed in parametric software. Calculating structural behaviour can be performed using SA software. If the two software packages are not directly compatible for data-communication, computer programming software can be used for data-communication. The software and the functions it supports or does not support influences the results generated by the model. Therefore it is important that the software used in the project matches the MSI. Based on the MSI, literature and the preferences of BAM Infraconsult the below listed software are compared on compliance to the MSI. The comparison is based on five possible rates; (--) = least desirable, (-) = not




desirable, (+-) = neutral, (+) = desirable and (++) = very desirable). The results of the comparison are visually presented separately for each comparison. Based on the results of the comparison the most suitable software will be used per function.

	Curved line support	Online forum support	Plug-in availability	User friendly
 Dynamo	+-	+	+	+-
 grasshopper	+	++	++	++

**Figure 7; Comparison of parametric software**

#### 1. Parametric generative software

- a. Dynamo is an Autodesk product that can be combined with Revit Autodesk for 3D visualisation. Dynamo is an open source graphical programming environment for design. Because Dynamo is an Autodesk product, it offers limited connections to other software applications other than import or export of unicode files.
- b. Grasshopper is visual programming environment that allows developers to model any type of connection to other software and publish the tool. The software links a visual programming interface to Rhinoceros which is a 3D visualisation software. There are multiple online platforms available for help and for downloading tools to connect to other software. For these reasons the combination between Grasshopper 0.9.0076 and Rhinoceros 5.0 is used in this research project.

	Combination with GH	Import/Export options	Used by BAM	User friendly
 MATRIX SOFTWARE	++	+	-	++
 SOFiSTiK	+	Direct plug-in available	+-	+-
 SCIA A NEMETSCHEK COMPANY	-	+	++	+



**Figure 8; comparison of structural analysis software**

#### 2. Structural analysis software

- a. Matrixframe is a very simplistic analysis software package. The input requirements are limited but sufficient for simple structures. A benefit of the program is the user friendly interface, logos are chosen to visually represent the function of the component. A downside to this programs is that the software is not currently used by BAM Infraconsult. However, it can be

introduced quite easily because the software requires limited knowledge to operate. For these reasons the analysis software is suitable.

- b. SOFiSTiK offers a direct plugin for the combination with Rhino and offers a lot of freedom in modelling the behaviour of the material, the structure and custom sectional properties. However, the software is much too complicated and advanced for obtaining simplistic linear elastic results. Although the software is used by BAM Infraconsult this software package is not desirable.
- c. SCIA Engineer is the most used structural analysis software package by BAM Infraconsult. The options for importing and exporting geometries is relatively user friendly and accurate. It is well suited for linear analysis of simplified structures and offers a lot of possibilities for extracting analysis output. For these reasons this software package is considered to be the most suitable to be applied in this research project. Therefore, in this research project SCIA Engineer 17.01 is used.

	Integration with GH	Online forum support	Library availability	User friendly
 MATLAB	-	+	+	+
 python™	++	++	++	+-

**Figure 9; Comparison of process automating software**

### 3. Process automating method

- a. Matlab is a software interface capable of running multiple programs based on command input. The software is primarily intended for numerical computations of complex systems. However, Matlab has a limited amount of described projects that combine 3D visualisation software with structural engineering processes, specifically the combination with Grasshopper.
- b. Python is an open source software with large online communities that describe most problems and combinations with other software. Grasshopper developers created a Python component, based on version 2.7, that has all the functionalities of a Python script. This component is very useful for automating the process in Grasshopper and therefore will be used in this research project.

The described software is used to develop a parametric structural design methodology based on the described MSI. The developed methodology is not limit in the application to the described design and technologies because of the structural design workflow. Most processes in structural design are generic and therefore application to a specific problem only requires updating the set of parameters and relations between parameters. This process will be further elaborated in the automated construction chapter of this thesis document. With the described characteristics in mind, the model can be developed and tested for compliance to the MSI. Therefore, the next step in the project is to develop the parametric geometry component.

## 3. Parametric geometry

This chapter describes the development of a parametric component that generates geometric output. Geometric output such as area moments are required for structural analysis. Geometric output such as material quantities are used for both structural analysis and environmental analysis. Material quantities are used in combination with structural analysis input to determine loading conditions for the analysis. However, In combination with environmental impact input the material quantities are used for environmental analysis. Therefore, the first required component in the design model is the parametric geometry component. Before developing the component, this chapter determines the definition and principles of parametric design. This is used as literature background for the function of the parametric geometry component. After defining parametric design, this chapter describes the methodology developed to generate a parametric geometry component. Based on the methodology, actions performed to develop the component are presented to elaborate the development of the component.

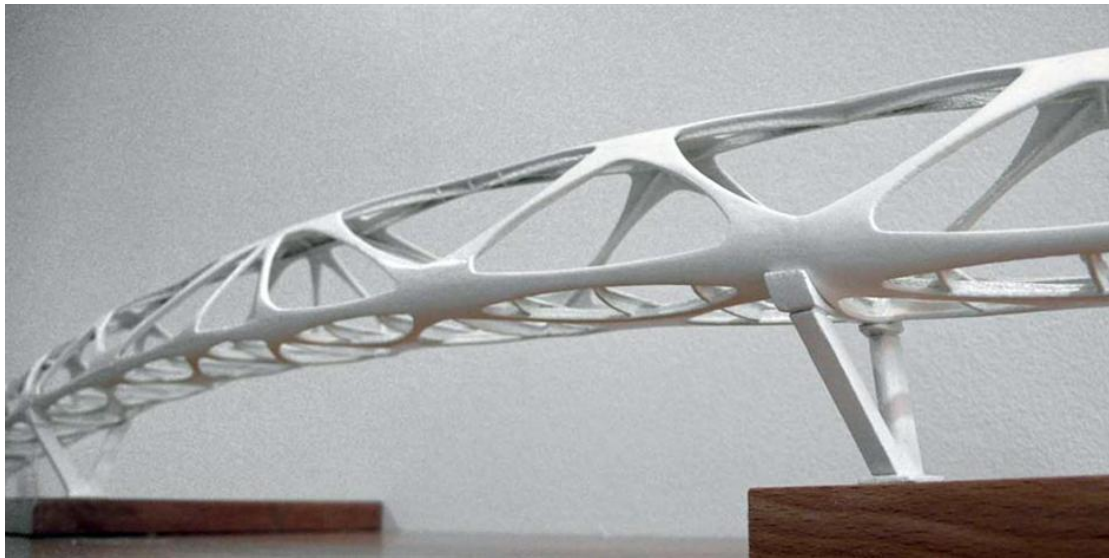


Figure 10; Example of parametric bridge design by Andreas Schnubel (2008) - [36]



### 3.1. Parametric design

Parametric design is a design method that has been used in the construction industry for quite some time and therefore is applicable to a multitude of perceptions. One definition of parametric design portrays the process as *“a method to enable the maintaining of dynamic links between parameters and their use in geometry definition for real-time, continuous modification”* [35]. Another definition of parametric design involves *“modelling the use of geometric constraints as well as dimensional relations and data to drive shape definitions. Values within parametric expressions can be modified by designers and are then propagated through a design”* [37]. A third definition uses parametric design as *“an associative systems, which in general generate an output, often geometry, from user-definable parameters and user-definable relations (associations) between those parameters. The generation process can be replayed every time one of the parameters or associations changes. This approach provides consistent design logic captured in rules in the form of parameters and associations”* [38].

Although the presented definitions have different perspectives on parametric design they share similarities. The three presented definitions describe parametric design as a method that develops design relations and identifies parameters that influence design relations. Combined with scripting of generative design instructions that describe a form, these principles are the basis of parametric design software such as Grasshopper [35]. Examples of parameters used in the construction industry are material properties, geometric properties, structural behaviour, etc. After identifying parameters, a range of variation can be set for each individual parameter. Variation of parameter input results in different alternatives that are created the same design script [39]. This process is called generative parametric modelling and is mostly used in combination with 3D visualisation software.

A downside to rule based modelling, such as parametric design, is related to the mathematical nature of the approach. Most software suitable for parametric design use mathematical relations between input and output. When encountering unpredicted inferences, the software is not equipped for the same level of efficiency in problem solving as human designers are. The human brain is able to interpret and manage relations with both internal (mathematical software) and external (material behaviour) factors [4]. However, parametric design software does not always consider the correct relation between internal and external factors. As a result, the validity of a rule based model depends on the accuracy of the mathematical representation of reality. In other words, non-mathematical relations can be difficult for rule based models to take into account [28].

An upside to parametric design are possible combinations with engineering software. However, parametrically simulating mechanical behaviour of a structure requires combining generative parametric software and calculation software. FEA software can be used to determine structural/mechanical behaviour [40]. Such a combination of parametric- and FEA-software is generally referred to as structural optimisation software because this type of software can be used to find the optimal combination of parameter values for a given set of criteria [41]. When combined with an established base-design and predetermined optimization criteria the program can determine a normalized score of compliance to the criteria for alternative solution [42]. This process uses iterative design steps and calculation checks to determine the range of models in compliance to the design rules and then determines their score.



## 3.2. Component methodology

In the description of the methodology of the parametric geometry component, five functions can be separated. The first function is generating the main geometry. The second function is adjusting the main geometry which results in a modified shape of the structure. The third function is generating the shape of the cross-section which creates the print path. The fourth function is calculating the geometric properties and quantities of the design. The fifth and final step is placement of tendons in the print path. Each of these functions will be elaborated and visualised in a flowchart.

### 1. Main geometry

The main geometry uses three components; a point-, a line- and a division-component. The points are determined based on a combination of X, Y and Z input. These points create the start-, mid- and end-section of the structure. Four points are required per section to define the top/bottom and left/right coordinate of a section. In total there are 12 points defined to create the main geometry. The line component connects points with a similar location in the section (top/bottom and left/right). This creates a set of four lines that connect the start-, mid- and end-point of the structure. These lines are connected to a divide component that creates a number of points along the four lines. These points will be used in the next function.

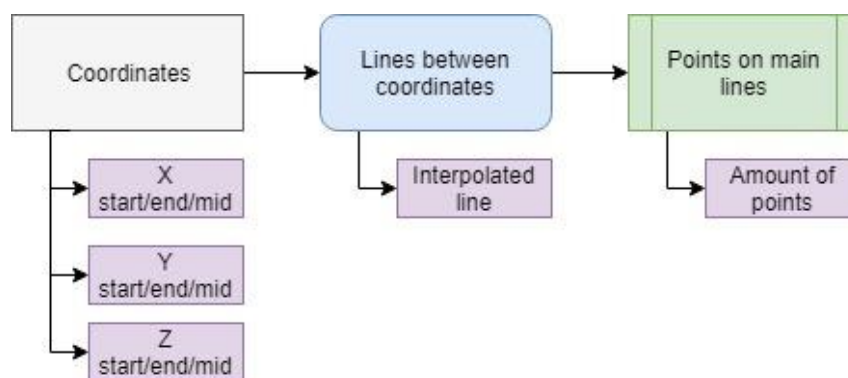


Figure 11; Flowchart visualising the method of creating the main geometry.

### 2. Modified geometry

The created set of points is connected to a modification component. The modification component moves each of the points, along a line, individually in a specified direction and pattern. After moving the points the set of points is connected to two components. The first component uses the displaced points to create the modified set of lines. The second component uses the displaced points in each of the lines (top/bottom & left/right) to create a set of cross-sections along the length of the model.

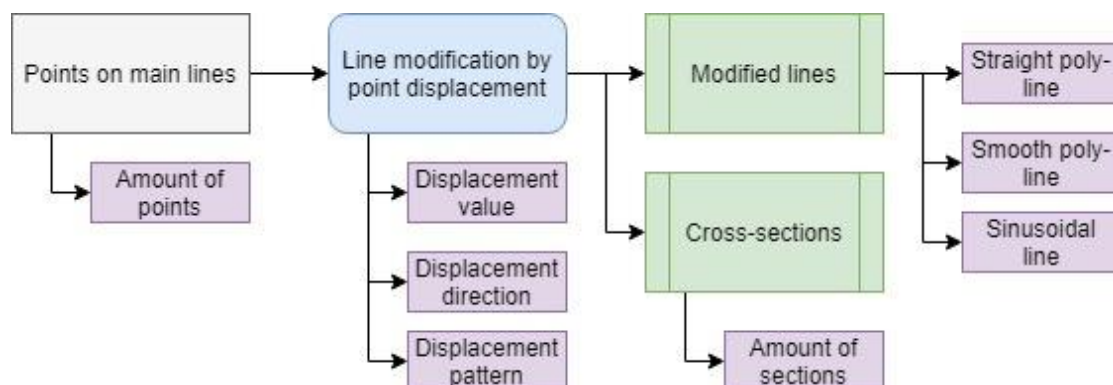


Figure 12; Flowchart visualisation of the method of creating the modified geometry

### 3. 3D printed concrete cross-section geometry

The created set of cross-sections is linked to a divide surface components. The divide surface component generates a set of grid points on each of the generated cross-sections based on a specified distance between the grid points. Some of these grid points have the same location as curves in the print path. These points are the key grid points. These key grid points can be used to generate the shape of the print path. The key grid points are connected to a line component that creates the shape of the print path on the set of cross-sections. This creates a set of 3DPC cross-sections.

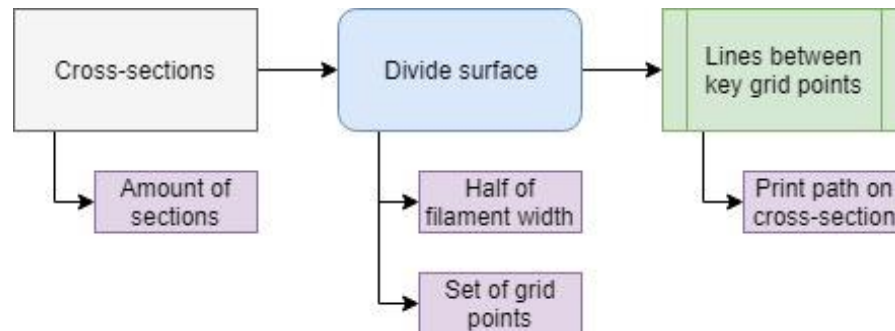


Figure 13; Flowchart visualisation of the 3DPC cross-section geometry

### 4. Geometrical properties

The created set of lines between the key grid points is connected to a trim surface component. The trim surface component determines the difference between the cross-section created in step 2 and the set of lines. This creates a set of areas in the shape of the 3DPC print path. The set of print path areas is connected to two components. The first component is the area moments component. This component calculates the centroidal axis, area and moment of inertia of each of the print path areas. The second component is a loft component. This component creates a volume that represents the 3D printed structure.

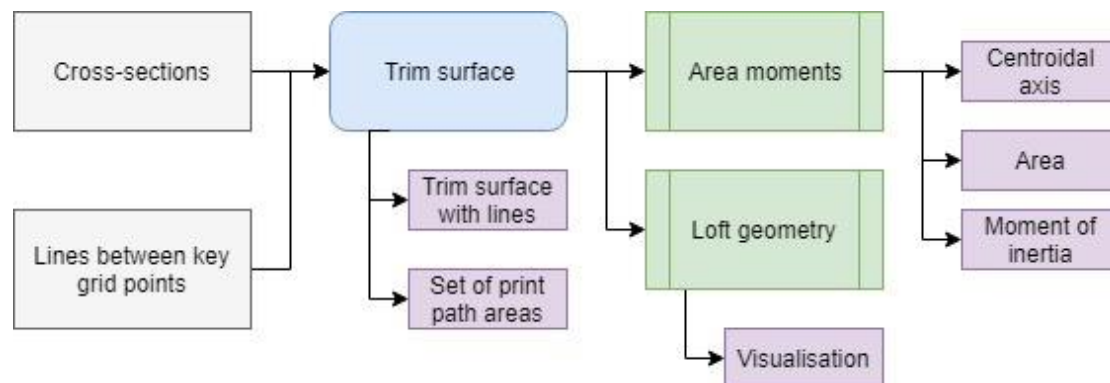
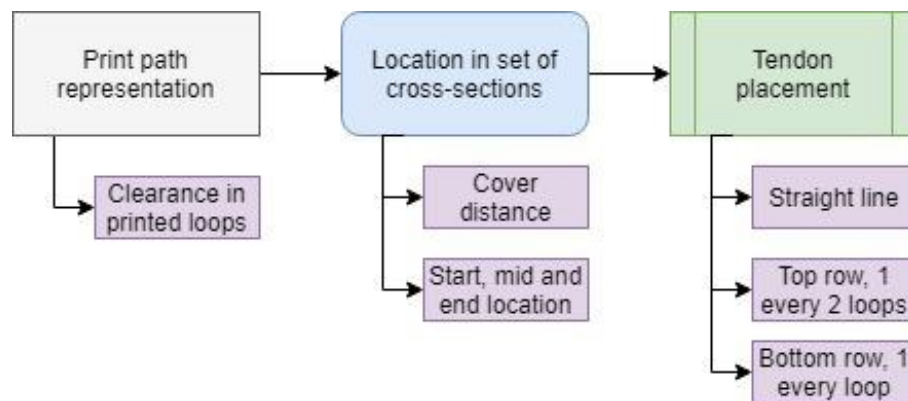


Figure 14; Flowchart visualisation of the calculation of area moments

### 5. Tendon placement

The created set of 3DPC cross-sections created in step 3 are used to identify the area in which post-tensioned tendons should be placed. This “clearance” area is used to identify the possible location of the tendons in the set of cross-sections. In each of the cross-sections a point is placed in the top/bottom row of the inner/outer most print loop. This creates a set of 4 points per cross-section which is the top/bottom & inner/outer location of the tendon in that specific cross-section. Because the shape of the cross-sections can vary along the span, the location of the tendons in the set of cross-sections is compared. The inner most location of the set of tendon location is chosen

on both sides of the structure. This ensures that the tendon will remain straight throughout the span of the structure. At the start- and end- section, the chosen location for the tendons are used to align a number of points. In the top row, 1 tendon will be placed in every 2 print loops. In the bottom row, 1 tendon will be placed in every print loop. These points will be linked to a line element that creates the tendon. This finalises the tendon placement.



**Figure 15; Flowchart visualisation of the placement of tendons in 3DPC cross-sections**

According to the model simulation intent, the main function of the geometry component is to determine the cross-sectional properties (centroidal axis, area and moment of inertia) and locate the tendons. Therefore, the fifth step completes the geometry component.

### 3.3. Application of the methodology

Based on the methodology the following steps have been taken to develop the parametric geometry model. The same structure of the section will be used in this section as in Section 3.2. Each of the steps will be explained and visualised. The visualisations are exported from Rhinoceros 5.0. The Grasshopper script is presented in Annex A.

#### 1. Main geometry

As described, the main geometry is determined by a set of 12 coordinates that represent the top/bottom & left/right point of the start-, mid- and end-section. Because the lines will be modified in the next step, only the results of the coordinates and adjusting the coordinates is presented in this step. The left figure in Figure 16 presents the coordinates according to the Gemert design input. The left figure in Figure 16 shows the effect of adjusting some of the parameters. In this step a total of 12 parameters is used that determine the main geometry; X/Y/Z location of the top/bottom & left/right point of the start-, mid- or end-section.

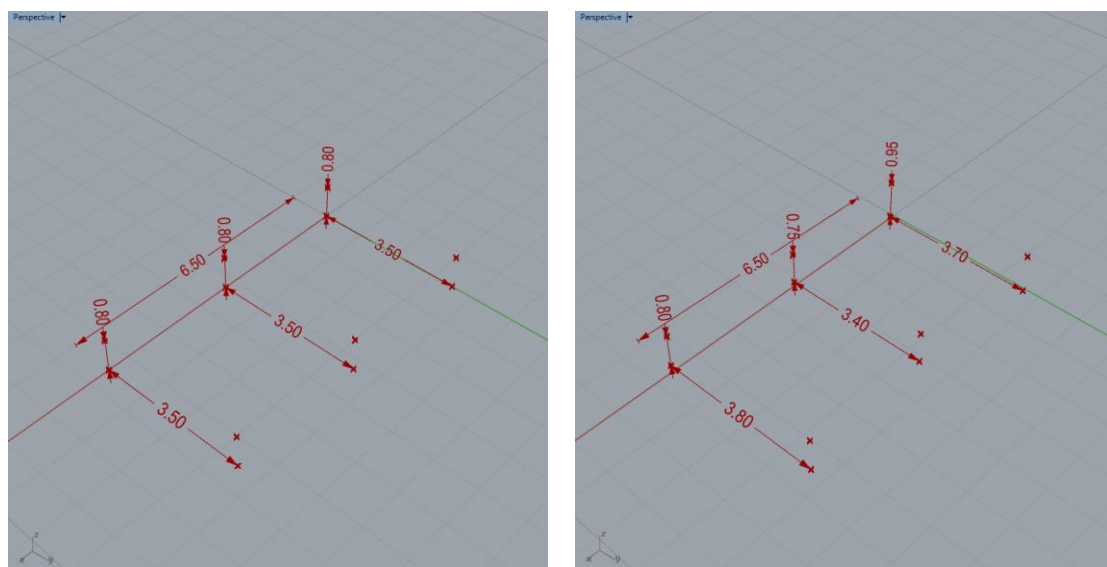
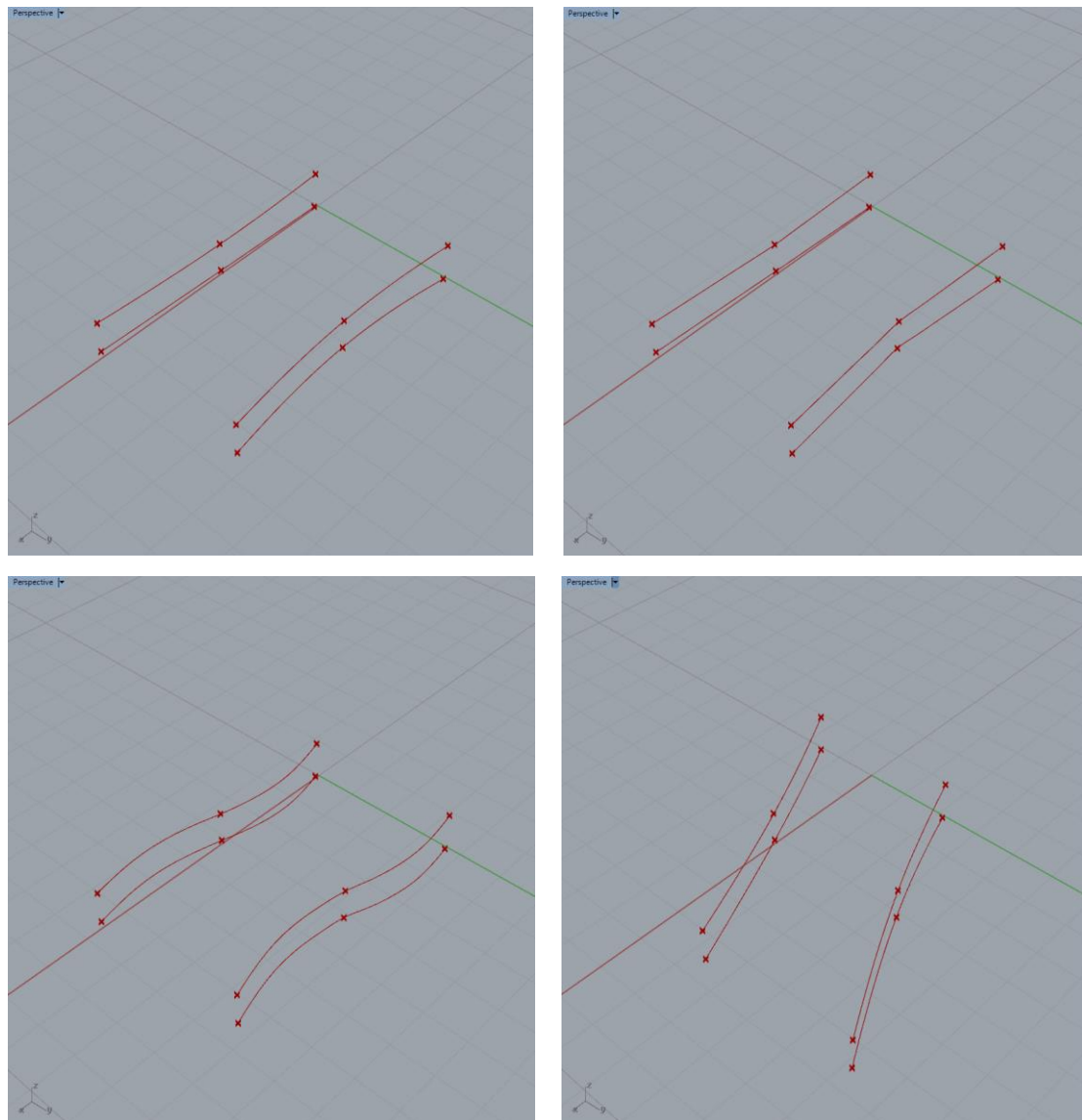


Figure 16; Left; without distortion factors – Right; with distortion factors

#### 2. Modified geometry

A total number of 4 different line types is developed in the parametric geometry component. The first two line types are a straight line- and a smooth line-interpolation between a chosen number of points. The third line type is a sinusoidal line that moves points in a sinusoidal pattern in the Y-direction. The fourth line type is a skewed line configuration. In a skewed configuration, the start and end section of the structure are moved in the opposite Y-direction. The results of the line types are presented in Figure 17. In this step a total of 5 parameters is used. The sections created in this step are presented in the next step.

- |                      |                       |     |
|----------------------|-----------------------|-----|
| • Line type 1&2      | Smooth or Linear      | [-] |
| • Sinusoidal line    |                       |     |
| ○ Amplitude          | between 0.00 and 0.25 | [m] |
| ○ Amount of loops    | between 1 and 3       | [-] |
| • Skewed line        | between -1,5 and 1,5  | [m] |
| • Number of sections | between 2 and 15      | [m] |



**Figure 17; Top left; smooth interpolated line – Top right; linear interpolated line – Bottom left; sinusoidal line – Bottom right; skewed line**

### 3. 3D printed concrete cross-section geometry

Because the exact print path geometry of the Gemert design is not published, a straight line representation of the print path will be generated in this step. However, in figure 5a and 7 of the article of T.A.M. Salet et al [22] a geometry visualisation is presented that can be used in the design model. Based on this print path geometry an approximate shape is created in AutoCAD. This is done for two reasons. The first reason is that generating the shape in a parametric setup in Grasshopper is time consuming. The second is that the accurate representation of the print path is not part of the model simulation intent. The function of the parametric geometry component is to generate geometric properties. Therefore, the print path created in Grasshopper is based on an approximation created in AutoCAD.

The first step of generating the print path in Grasshopper is to divide the cross-section surface by half the filament width. Based on the Gemert design, the grid created by the surface divide component uses a spacing of 30 mm (see Section 2.2). To save time in using the model, only the mid-section is divided into grid points. This section will be used to create the print path geometry in Grasshopper. The other sections are a scaled version of the mid-section.



The second step is to import the AutoCAD file into Grasshopper. After importing the shape it is placed behind the mid-section to identify the key points of the print path. This is done by picking the grid points of the mid-section that are closest to the corners of the AutoCAD approximation of the Gemert design. Two point sets are chosen per corner in the print path, one on the outside of the print path and one on the inside.

The third step is to connect the identified key grid points to create a set of lines that represent the print path geometry in Grasshopper. Because the accurate curvature of the corners of the print path are not published, the lines are connected in a straight manner. Therefore, the print path generated in Grasshopper is a straight line representation of the 3DPC print path used in the Gemert design.

This completes the development of the third step of the parametric geometry component. In this step only one parameter is used which is half of the filament width. The results of the steps used to generate the print path in Grasshopper are presented in Figure 18.

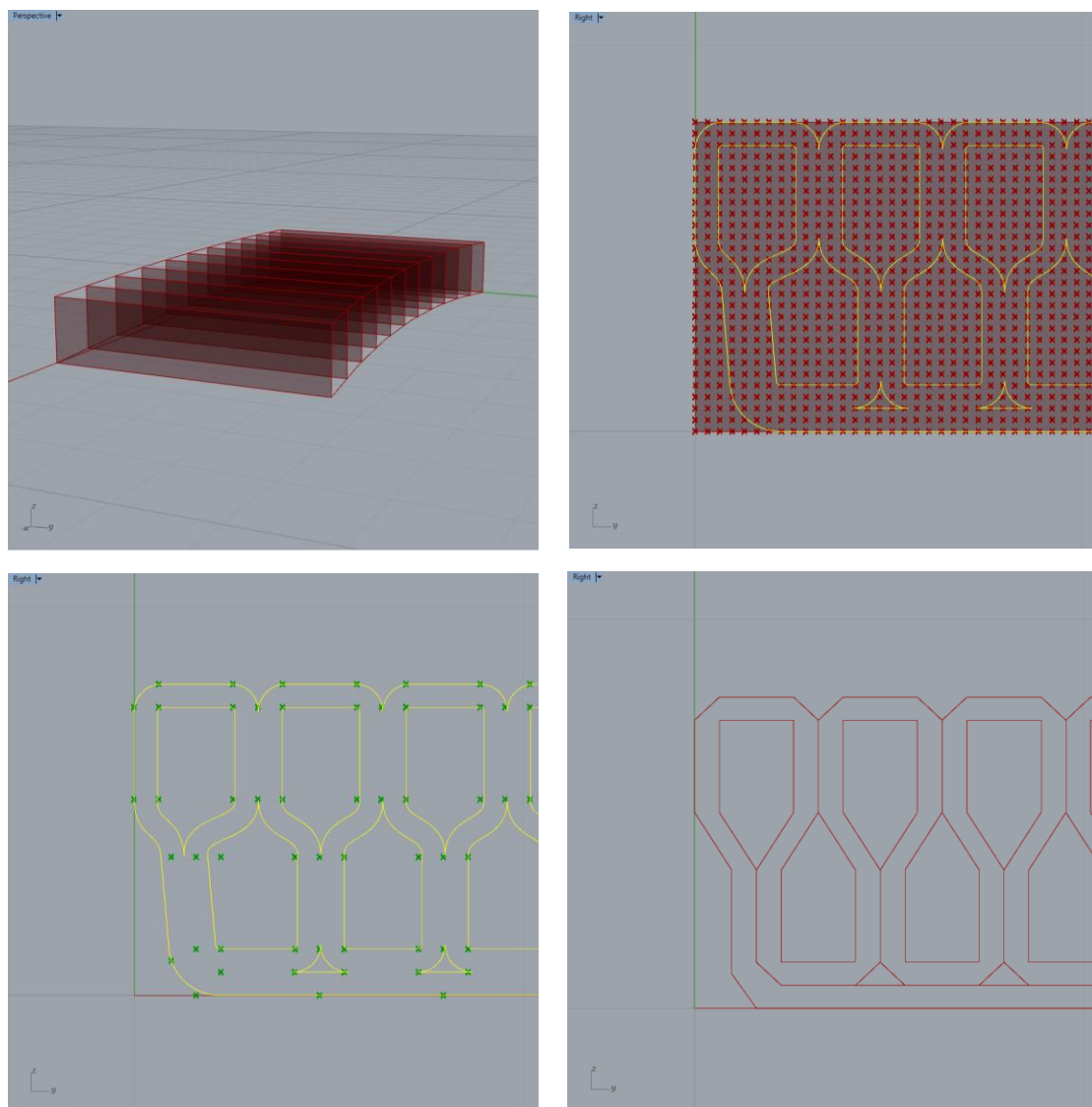


**Figure 18; Top left; generated cross-section – Top right; grid based on half the filament width & AutoCAD approximation – Bottom left; identified key grid points – Bottom right; straight line approximation of the print path**

#### 4. Geometrical properties

Calculation of cross-sectional properties is modelled in a slightly different way than described in Section 3.2. This is chosen based on two reasons. The first reason is related to the straight line representation created in the previous step. Using this cross-section to calculate cross-sectional properties will result in inaccurate values. Therefore, the print path approximation created in AutoCAD will be used to generate geometric properties. The second reason is related to using the model. Calculating cross-sectional properties using the proposed method proved to be time consuming. A reduction in time, when using the model, can be achieved by using the slightly different method proposed in this section.

The alternative method uses conversion factors to determine cross-sectional properties. The proposed conversion factors are calculated based on the difference between the total cross-section and the print path approximation. The total cross-section is the result of step 2 in Section 3.2. The print path approximation value is calculated using the method proposed in step 4 in Section 3.2 using the imported AutoCAD drawing. The calculated conversion factors are used in the Grasshopper model to calculate cross-sectional properties. The equations used to calculate the conversion factors and for using the conversion factors are presented in Equations 1.1-1.3. The results of the conversion factors are presented in Figure 19.

$$\text{Conversion Rate}_{ec} = \frac{h_{total,i}}{e_{c,i}}; \quad ec_i = h_i \times CR_{ec} \quad (1.1)$$

$$\text{Conversion Rate}_A = \frac{A_{print Path}}{b \times h}; \quad A_i = b_i \times h_i \times CR_A \quad (1.2)$$

$$\text{Conversion Rate}_I = \frac{I_{print Path}}{\frac{1}{12} \times b \times h^3}; \quad I_i = \frac{1}{12} \times b_i \times h_i^3 \times CR_I \quad (1.3)$$

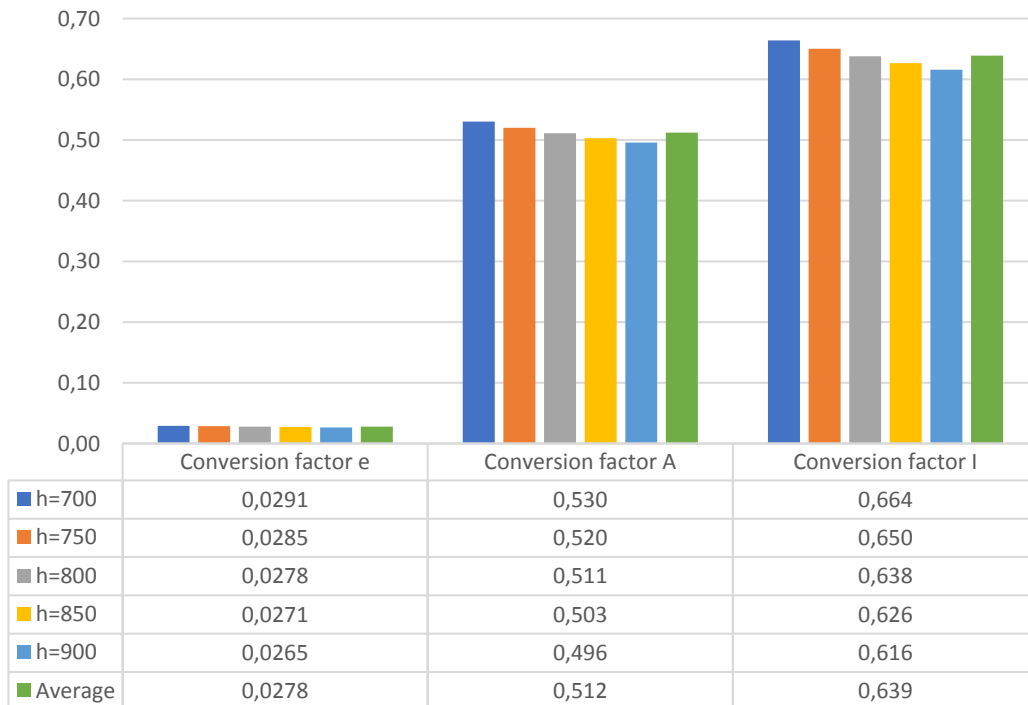
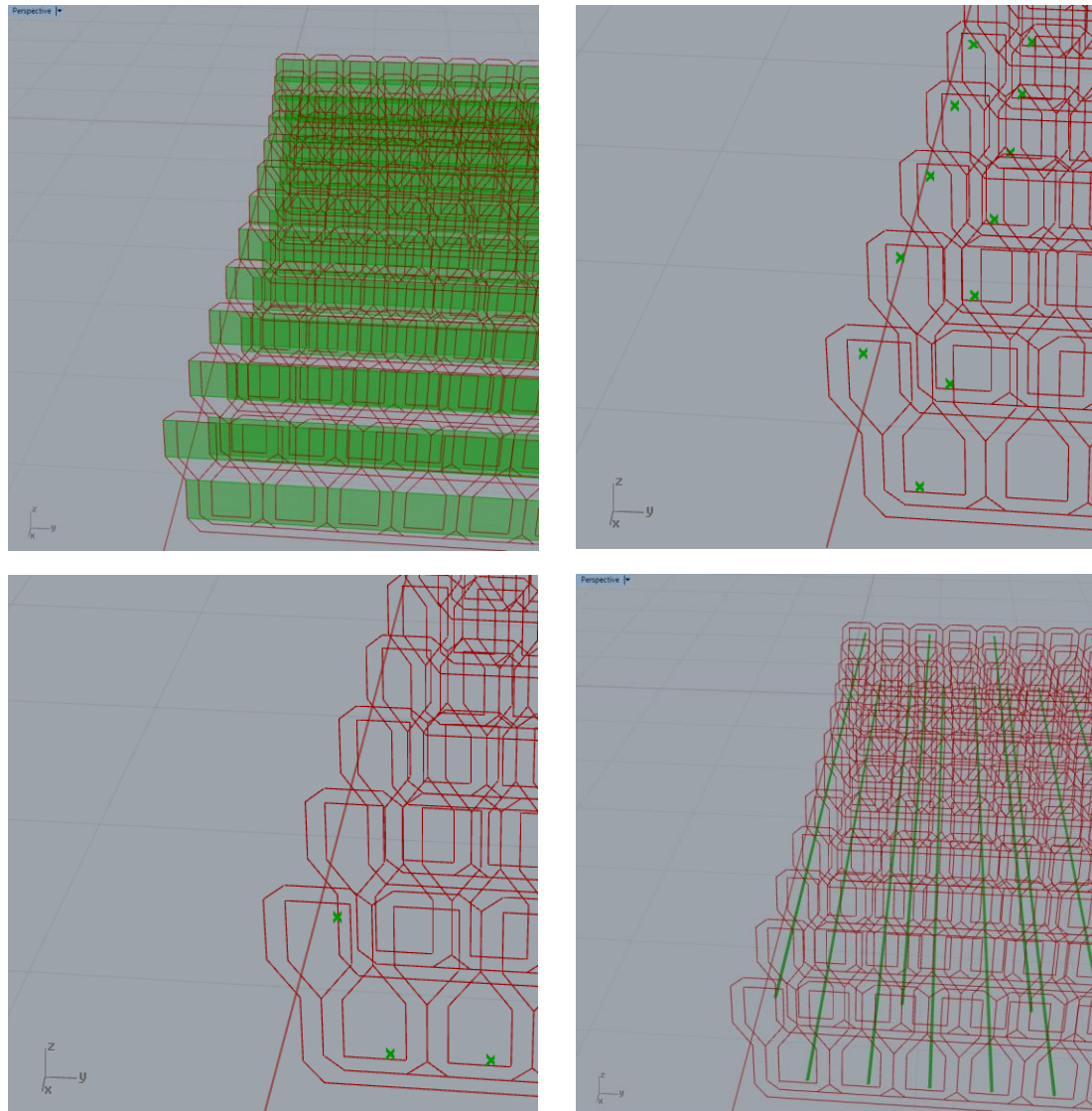


Figure 19; Calculated conversion factors and the average value used in the model

#### 5. Tendon placement

The straight line representation created in step 3 is used to place the tendons. As explained in Section 3.2, the placement of the tendons is performed by comparing the

possible locations along the span. The possible location in each cross-section is the outer most left/right point at the top/bottom row. The Z and Y location of these points in the start-, mid- and end- sections are compared. The Y and Z coordinate closest to the centroidal axis is chosen for tendon placement. This ensures that the tendons remain straight along the span. The described process is visualised in Figure 20. In the top left, the green area indicates the available area for tendon placement. In the top right, the possible location of the outer most left point in the top and bottom row is shown in green. In the bottom left, the resulting point for the comparison is shown in green. The amount of tendons is according to the described pattern in Section 3.2. The start- and end-location of the tendons are then connected to create the tendon configuration presented in green in the bottom right of Figure 20.



**Figure 20; Top left; area for tendon placement – Top right; tendon location per cross-section – Bottom left; resulting location for straight placement per print loop – Bottom right; straight tendon configuration**

The presence of the tendons in the print loops affects the possible range of variation of the cross-sectional shape along the span. Especially the variation in the width of the model is restricted. Placing the tendons requires a continuous clearance in the cross-section throughout the full length of the span. Therefore, the amount of printed loops in which tendons are placed has to stay constant. This requires the width of the printed



loops to decrease/increase in order to decrease/increase the size of the cross-section (see Figure 21). This limits the variation of the width to the maximum clearance inside the printed loops minus the minimum coverage and the diameter of the tendons (see Equations 2.1-2.2).

$$\Delta b_{max} = clearance - (2 \times cover_{min,tendon} + \phi_{tendon}) \quad (2.1)$$

$$\Delta b_{max} \cong 200 - (2 \times 10 + 15,70) = 164,30 \text{ mm} \quad (2.2)$$

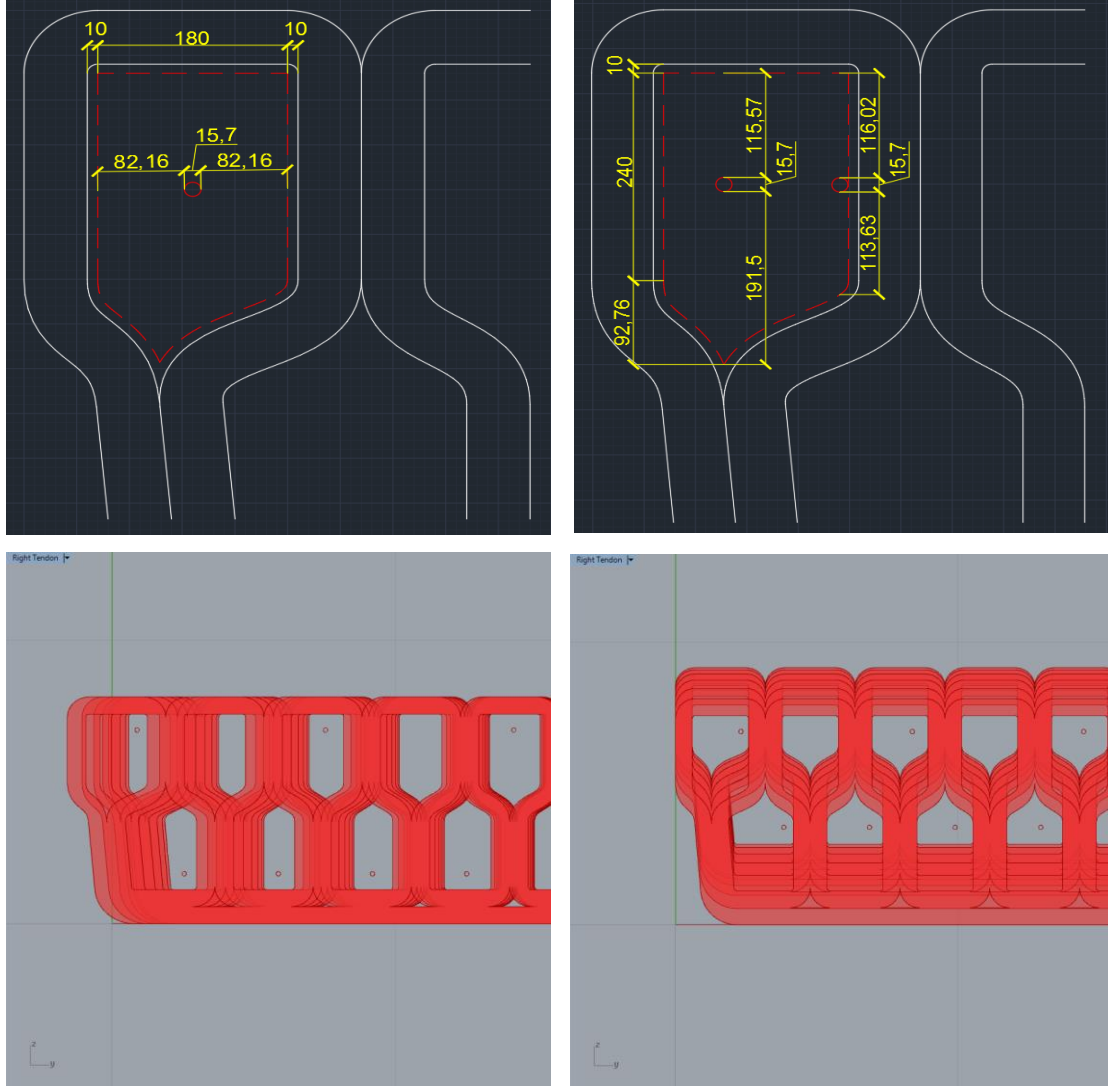


**Figure 21; Top left; possible horizontal tendon movement – Top right; possible vertical tendon movement – Bottom left; effect of horizontal movement on tendon placement – Bottom right; effect of vertical movement on tendon placement**

When compared to the horizontal placement of the tendons, the vertical tendon placement tends to have a higher amount of clearance. Also, the amount of printed loops in the vertical direction is not influenced by changing the height of the section. The maximum variation in the height is calculated in a similar manner as the maximum horizontal variation (see Equations 3.1-3.4).

$$\Delta h_{max} = max \text{ clearance} - (2 \times cover_{min,tendon} + \phi_{tendon}) \quad (3.1)$$

$$\Delta h_{max} \cong 340 - (2 \times 10 + 15,70) = 304,30 \text{ mm} \quad (3.2)$$

$$\Delta h_{min} = \min \text{ clearance} - (2 \times \text{cover}_{min,tendon} + \phi_{tendon}) \quad (3.3)$$

$$\Delta h_{min} \cong 250 - (2 \times 10 + 15,70) = 214,30 \text{ mm} \quad (3.4)$$

This completes the tendon placement. In this step a total of three parameters is used. The first parameter is the tendon placement pattern, the second is the tendon diameter and the third is the cover distance.

To conclude, the model incorporates a total of four parameter categories; main geometric input, modified geometry input, cross-sectional property input, tendon configuration input. The 3D model can be adjusted to the desired configuration by changing the values related to these categories. Most of these input parameters are connected to a number slider. A number slider is a graphic visualisation of the possible input within the boundary conditions. In most cases the input is controlled by a number, that controls the input of a parameter. By using number sliders to control the input for a certain parameter, the functions connected to that parameter will be automatically regenerated after adjusting the slider. The list below presents the four parameters types and value indication.

1. Main geometry
  - a. Length: based on X locations [m]
  - b. Width: based on Y locations [m]
  - c. Height: based on Z locations [m]
2. Modified geometry
  - a. Line type 1&2 Smooth or Linear [-]
  - b. Sinusoidal line
    - i. Amplitude between 0.00 and 0.25 [m]
    - ii. Amount of loops between 1 and 3 [-]
  - c. Skewed line between -1,5 and 1,5 [m]
  - d. Number of sections between 2 and 15 [m]
3. Cross-sectional properties
  - a. Conversion factor ec 0,0278 [-]
  - b. Conversion factor A 0,512 [-]
  - c. Conversion factor I 0,639 [-]
4. Tendon design
  - a. Tendon placement
    - i. Top alternating, 1 in every 2 print loops
    - ii. Bottom all, 1 in each print loop
  - b. Tendon diameter 15,7 [mm]
  - c. Cover distance 10 [mm]

The maximum movement of the model is affected by two factors. The first factor is the result of limits related to geometric restrictions (discussed in this section) and by design standards. The second factor is the result of limits related to the resistance of the sections (discussed in Section 3.4). The geometric restrictions can be described as the result of three groups:

1. Tendon movement limitations due to the print path layout;
  - a. Hmin,bot = 138 [mm]
  - b. Hmax,bot = 352 [mm]
  - c. Hmin,top = 508 [mm]
  - d. Hmax,top = 722 [mm]

2. Tendon movement limitations due to the movability inside the print path
  - a. Max upwards/downwards motion = 214,3 [mm]
  - b. Max inwards/outwards movement = 164,3 [mm]
3. Maximum angle of the deck based on regulations
  - a. Max angle of the slope [43] = 0,075 [°]

The first two limits describe the restrictions related to fitting the tendons in the cross-section. These restrictions are the result of the relative maximum change in position of the start/end section and the mid-section without interference between tendon and cross-section (see Annex B). The origin of these limits is also addressed in this chapter. The third limit is a guideline description regarding the comfort of the angular increase of a bridge deck for cyclists. The final limits for the input of the geometry values and the distortion values will be tested for consistency with the required minimum resistance of the sections, as mentioned before, this topic will be addressed in Section 6.2.



## 4. Structural Analysis

This chapter describes the development of a structural analysis component. As described in the model simulation intent in Section 2.2, the function of the structural analysis component is to determine the structural efficiency. The structural efficiency depends on two aspects. The first aspect is the structural safety and the second is the material application efficiency. To determine these aspects, following information should be generated; the bending induced stress distribution, the shear force distribution and the loss of post-tensioning force due to time dependent behaviour.

Before developing the structural analysis component, this section presents a literature background for describing the function of structural design and the material properties of 3DPC. This information will be used to determine the methodology for developing the component in general. The methodology is used to develop the structural analysis component for the design model. The calculations performed to generate the required output are executed in FEA software.

## 4.1. Structural design

Structural engineering is a branch in engineering in which the goal of the engineer is to formulate and test physics models of structures, materials and load combinations. Structural engineers aim to determine and evaluate the strength, the stability and the rigidity of load-bearing structures or parts of the structure [44]. The structural design process is an iterative process involving four concepts; design principles/conditions, material & structural system, geometric design and SA [45]. Specifically, the last domain is of interest in structural engineering practices because it results in the verification of the structural system. Therefore, the last step evaluates the design. When combined with parametric design, SA can be used to determine limit values for the parametric input. This, however, requires input for determining the material behaviour, the support conditions and the practical limits that influence the geometric limits [29].

When combining parametric and structural design in one model it is crucial to consider the model intent. 3D visualizations, in general, contain a lot of information, especially when creating complex geometry models, that combined with the amount of structural information creates very complex models. This abundance of information can cause the required calculation time to increase rapidly, therefore it can be useful to simplify the geometric model based on the model simulation intent. The most used methods to decrease calculation time are; Fit-for-Purpose modelling and detail reduction of existing models [25]. The first is rather self-explanatory and focusses on modelling only the elements essential for SA. The second method is more complicated since it depends on Mixed-Dimensional Analysis (MDA).

The principle of MDA depends on combining elements with different properties regarding dimensions. MDA processes each of the elements individually and therefore all elements can be adjusted individually. By separating the model, the sections are transformed according to the best representation of that section and using the advantages of the type of element [46]. There are however several downsides to the MDA approach. These downsides mainly depend on the interface behaviour of the different elements and their Degrees of Freedom (DOF) [47]. In MDA the model information is reduced as much as possible by transforming the elements into representative elements. This requires two steps; modification of element and modification of properties [46]. The first step converts the existing elements into 3 base geometries; 1D beam-, 2D shell- and 3D volume-elements. The second step then determines the representative value of each specific element, the interface conditions and the mechanical properties of the elements [47]. Using MDA greatly reduces the model information resulting in a simplified approximation of the model based on the intent of the simplification. This, however, is a downside to the principle. when using approximations, results obtained are also an approximation of which the accuracy depends mainly on the accuracy of the approximation.

A different downside is related to automating the model simplification. The reduction of the DOF of elements can change the mechanical behaviour of the interface areas and the deformation of the entire model, which results in deteriorating structural behaviour. This procedure therefore should be managed carefully. By automating this procedure errors can occur due to incorrectly over-simplification of interfaces and/or elements [48]. Another downside of automated simplification is the lack of traceability of what type of simplifications have occurred for which elements/interfaces [25]. An upside to automated simplification is a significant reduction in the time it takes to use the model. However, it is important for the transparency of the process to carefully document and describe the function of the simplification methods in the model.

Because of the relatively short application of 3DPC in the infrastructure and civil engineering industry, there are quite a few downsides to the technology that have

yet to be improved. When compared to traditionally casted concrete the 3D printed concrete tends to have three characteristics that differ most.

1. Orthotropic material behaviour. Because of the production process, the material characteristics vary over the height of the printed sections. The process and the print material also affect the strength of the cross section. The pressure resistance in X-direction<sup>1</sup> and the Z-direction<sup>1</sup> are approximately 5% lower. The pressure resistance in the Y-direction<sup>1</sup> is slightly higher (2%). [49, 50].
2. Deteriorating structural behaviour, caused by differences in cross-sectional and inter-layer shear behaviour. In general 3D printed concrete tends to have a lower flexural and a comparable compressional/tensional resistance. Especially the interlayer shear resistance and the lower resistance in X-direction<sup>1</sup> and Z-direction<sup>1</sup> reduce the flexural resistance. [49, 51].
3. Reduced ductility, this is mainly due to the problematic implementation of steel reinforcement in the production process. However, the ductility of non-reinforced casted samples is slightly higher than the ductility of printed samples. [52].

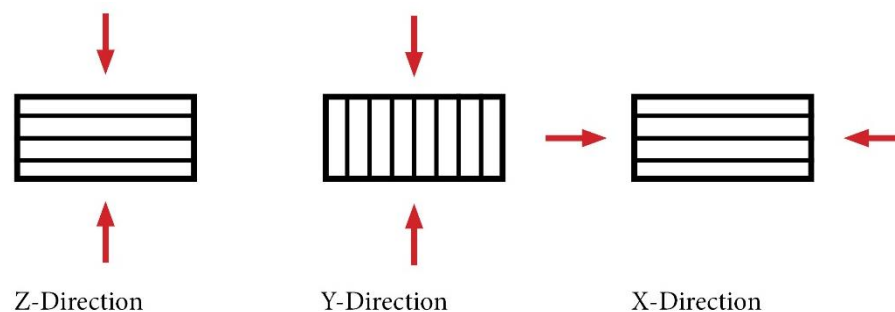


**Figure 22; Schematic visualisation of the stress directions in 3DPC**

Another effect of the relatively new material production method is in the current rate of development of the method. With each new study a different material property is added or changed. Based on the article of T.A.M. Salet et al, the three above described influences turn out to be less influencing than initially determined. To conclude, the inter-layer shear/slip resistance, the tensile resistance and the ductility in 3D printed concrete structures can still be improved. This will benefit large-scale applications structural in the infrastructure and civil engineering industry. The currently used methods to improve these values are being studied. Their main characteristics are based on two methods.

1. Enhancement of printer material
  - a. Fibre reinforced concrete, by adding polymer/steel fibres to the mixture the internal resistance of the filaments increases. Especially the tensional and flexural resistance increase with fibres. It is also studied if the fibres can be used to increase the inter-layer shear/slip resistance. [49, 51].
  - b. Concrete mixture and supply settings. By using more/less coarse granulate in the concrete mixture. More coarse granulate will increase the material interlocking in the layers. By adjusting the pressure in the printer nozzle or the shape of the nozzle the mixture can be compressed or stretched a bit. This can increase/reduce the density and bonding between layers. [53, 54].

<sup>1</sup> The described direction is relative to the orientation of the local axis system of the filament layering (see Figure 22).

- c. Filament surface treatment. The filaments typically have a smooth surface after printing. Disrupting the surface or applying surface additives can mechanically or chemically improve the bond between the layers. [52].
- d. Concrete rheology, influence of concrete mixture properties during the printing process. Two aspects are currently studied to improve the printability of early age concrete.
  - i. Increased hardening, in 3DPC the material is deposited layer by layer while the concrete hardens. As a result, the weight on a layer increases as more layers are applied. Therefore, the yield strength of the concrete should increase in the same speed as the layer built-up to prevent material flow out of the lower layers [55].
  - ii. Stability during printing, a side effect of 3DPC is print path stability during the print process. A low yield strength of early age concrete combined with a low combination of stiffness and Young's modulus reduce the buckling resistance of the print path during printing. [5, 56]
- 2. Optimizing the printing method
  - a. Mechanical interlocking. Notches can be introduced in the freshly printed filament to increase the interaction area between areas. Research shows that the implementation of 1,3 cm deep notches can increase the resistance by 10% and up to 25%. However the failure modes of an interlocked sample have to be explored. [57].
  - b. Printer settings can be optimized. TU Eindhoven is studying the effects of different categories of printer settings to identify their impact on material behaviour and material production repeatability for accurate testing. Research has identified 4 steps of printing process optimization levels:
    - i. Predefined system parameters (printer set-up)
    - ii. Informed system parameters (basic printer settings)
    - iii. Analysed system parameters (linking process and material properties)
    - iv. Optimized system parameters (linking process and structural behaviour)
    - v. These levels describe the area affected by changes in the process and can vary from adjusting the height of the nozzle above the print surface to using algorithms to optimize print path/geometry. [52]

Since the focus of this research project is on the development of a design model based on 3DPC structures, improvement of the 3D printing material or process will not be addressed in this chapter. The properties of 3DPC are rapidly developing as more research is performed and published. However, this research project uses the 3DPC properties described for the Gemert design (as presented in Section 2.2).



## 4.2. Structural analysis context

The simulation intent defined in Section 2.2 determines the function of the structural analysis component but does account for rules and standards for a structural analysis. Rules and standards can require the use of specific material properties, methods or procedures. It is important to consider these requirements because they can influence the content or methodology of the component. Therefore, this section describes the requirements for the structural analysis component. In Europe, design standards and procedures are defined in the Eurocode. The Eurocode defines calculation procedures and input used for calculation procedures. Following Eurocode documents and Dutch regulations are used in this research project to determine the structural analysis procedure and input:

Procedure-related standards	Title
NEN-EN 1990+A1+A1/C2;2011	Basis of structural design
NEN-EN 1990+A1+A1/C2/NB	Dutch national annex to NEN-EN 1990

Load-related standards	Title
NEN-EN 1991-1-1+C1:2011	Actions on structures - Part 1-1: General actions - Densities, Self-weight, imposed loads for buildings
NEN-EN 1991-1-1+C1/NB	Dutch National annex to NEN-EN 1991-1-1
NEN-EN 1991-1-3+C1;2011	Actions on structures - Part 1-3: General actions - Snow loads
NEN-EN 1991-1-3+C1/NB	Dutch National annex to NEN-EN 1991-1-3
NEN-EN 1991-1-4+A1+C2:2011	Actions on structures - Part 1-4: General actions - Wind actions
NEN-EN 1991-1-4+A1+C2/NB	Dutch National annex to NEN-EN 1991-1-4
NEN-EN 1991-2+C1:2011	Actions on structures - Part 2: Traffic loads on bridges
NEN-EN 1991-2+C1/NB	Dutch National annex to NEN-EN 1991-1-2

Design-related standards	Title
NEN-EN 1992-1-1+C2:2011	Design of concrete structures - Part 1-1: General rules and rules for Buildings
NEN-EN 1992-1-1+C2/NB	Dutch national annex to NEN-EN 1992-1-1
NEN-EN 1992-2+C1:2011	Design of concrete structures - Part 2: Concrete bridges - Design and detailing rules
NEN-EN 1992-2+C1/NB	Dutch National annex to NEN-EN 1992-2
RTD 1001:2017 version 1.4	Guidelines for design of artworks (ROK 1.4)
RTD 1009:2012 version 1.0	Directive for the design of asphalt pavements on concrete and steel bridge decks

### 1. Structural analysis procedure

Eurocode NEN-EN 1990 defines a procedure for verifying structural safety by using partial safety factors. In this method, partial safety factors are used to determine the design value of a load or resistance. The safety factors take the effect of uncertainties and undesirable or desirable effects into account. The design values therefore can be used to determine the safety of the structural in ultimate limit state. A structure is assumed to be safe in ultimate limit state if the design value of the resistance is higher than the design value of a load on the structure. This procedure is presented below, used from equation 6.8 of Eurocode document NEN-EN 1990.

$$E_d \leq R_d \quad (6.8)$$

where :

$E_d$  is the design value of the effect of actions such as internal force, moment or a vector representing several internal forces or moments ;

$R_d$  is the design value of the corresponding resistance.

NOTE.1 Details for the methods STR and GEO are given in Annex A.

NOTE 2 Expression (6.8) does not cover all verification formats concerning buckling, i.e. failure that happens where second order effects cannot be limited by the structural response, or by an acceptable structural response. See EN 1992 to EN 1999.

Figure 23; Eurocode NEN-EN 1990 equation 6.8

The design value of the effect of actions can be determined by calculating critical load combinations. The formula used to calculate the critical load combination is determined by the national annex of Eurocode NEN-EN 1990 section A2.

Blijvend en tijdelijke ontwerpsituaties	Blijvende belastingen		Voor-spanning	Overheersende veranderlijke belasting <sup>a)</sup>	Tegelijkertijd optredende veranderlijke belastingen <sup>a</sup>	
	Ongunstig	Gunstig			Belangrijkste (indien aanwezig)	Andere
(Vgl. 6.10a)	$\gamma_{G,j,sup} G_{k,j,sup}$	$\gamma_{G,j,inf} G_{k,j,inf}$	$\gamma_P$		$\gamma_{Q,1} \psi_{0,1} Q_{k,1}$	$\gamma_{Q,i} \psi_{0,i} Q_{k,i}$
(Vgl. 6.10b)	$\xi \gamma_{G,j,sup} G_{k,j,sup}$ waarbij $\xi = 0,80$	$\gamma_{G,j,inf} G_{k,j,inf}$	$\gamma_P$	$\gamma_{Q,1} Q_{k,1}$		$\gamma_{Q,i} \psi_{0,i} Q_{k,i}$

<sup>a</sup> Veranderlijke belastingen zijn die, die zijn beschouwd in tabellen NB.9 – A2.1, NB.10 – A2.2 en A2.3.

Figure 24; Eurocode NEN-EN 1990 critical load combinations

The load factors used in these formulae are presented in table NB.13 of the national annex of Eurocode 1990.

Tabel NB.13 – A2.4(B) — Belastingsfactoren voor wegverkeersbruggen en bruggen voor langzaam verkeer en voetgangers- en fietsbruggen STR/GEO (groep B)

Gevolgklasse	$\beta$	G			Verkeer (met $\psi = 1$ )	Overig veranderlijk (met $\psi = 1$ )
		$\gamma_{G,j,sup}$		$\gamma_{G,j,inf}$		
		6.10a	6.10b (incl. $\xi$ )	6.10a en 6.10b		
CC1	3,3	1,20	1,10	0,9	1,20	1,35
CC2	3,8	1,30	1,20	0,9	1,35	1,5
CC3	4,3	1,40	1,25	0,9	1,5	1,65

$\gamma = 0$  voor gunstig werkende veranderlijke belastingen

Voor  $\gamma_P$  zie de aanbevelingen in de desbetreffende materiaalgebonden Eurocodes 1992 t.m. 1999.

Voor de berekening van het effect van ongelijkmatige zettingen geldt dat  $\gamma_{G,set} = 1,20$  in het geval van een lineaire berekening en  $\gamma_{G,set} = 1,35$  in het geval van een niet lineaire berekening. Gunstig werkende zettingsverschillen worden niet in rekening gebracht. De grootte van de zettingen is bepaald op basis van de karakteristieke belastingscombinatie en de karakteristieke waarden voor de grondeigenschappen.

OPMERKING De factor  $K_F$  volgens B 3.3 is in de waarden van  $\gamma$  verwerkt; voor de zettingsberekening blijft de betrouwbaarheidsdifferentiatie achterwege.

Figure 25; Eurocode NEN-EN 1990 load factors

The load combination factors used in these formulae are presented in table NB.10 of the national annex of Eurocode 1990.

**Tabel NB.10 – A2.2 —  $\psi$ -factoren voor voetgangers- en fietsbruggen**

Belasting	Symbool		$\psi_0$	$\psi_1$	$\psi_2$
Verkeersbelastingen	gr1	Gelijkmatig verdeelde belasting $q_{fk}$	0,4	0,8 <sup>c</sup>	0,4
		Horizontale belasting $Q_{fk}$			
	gr 2	Gelijkmatig verdeelde belasting $q_{fk}$	0,4	0,8 <sup>b</sup>	0
		Dienstvoertuig $Q_{serv}$			
		Horizontale belasting $Q_{fk}$			
	Geconcentreerde belasting $Q_{fwk}$		0	0,8 <sup>b</sup>	0
	Onbedoeld voertuig (zie 5.6.3)		0	0,8 <sup>b</sup>	0
Windkrachten	$F_{wk}$ blijvende ontwerpituatie Uitvoering	0,3 0,8	0,6 <sup>b</sup> 0	0	
Thermische belastingen	$T_k$	0,3	0,8	0,3 <sup>a</sup>	
Sneeuwbelastingen	$Q_{Sn,k}$ blijvende ontwerpituatie Uitvoering		0 0,8	0 0	0
	Belastingen tijdens de bouw		$Q_c$	1,0	0
<sup>a</sup> In de uiterste grenstoestand kan voor $\psi_2$ voor thermische belasting 0 worden aangehouden.					
<sup>b</sup> Voor aanrijding op of onder de brug en aanvaring is $\psi_1 = 0$ .					
<sup>c</sup> Voor aanrijding op of onder de brug en aanvaring is $\psi_1 = 0,4$ .					
OPMERKING Groepen verkeersbelastingen hoeven niet met elkaar te zijn gecombineerd.					

**Figure 26; Eurocode NEN-EN 1990 load combination factors**

The next step in determining the critical load combination is to determine the input for calculating the effect of actions on the structure.

## 2. Load input

The permanent loads used in the structural analysis are the result of following self-weight of materials in the structure;

Material	Self-weight	Unit	Source
3D printed concrete	2000	kN/m <sup>3</sup>	T.A. Salet et al [22]
Pressure layer	33	kN/m <sup>3</sup>	RTD 1009:2012 version 1.0
Finishing layer	25	kN/m <sup>3</sup>	RTD 1009:2012 version 1.0
Y1860 tendon	0,7263	kN/m	Dywidag tendons

Traffic loads determined for a bridge used by pedestrians and cyclists are based on NEN-EN 1991-2 NB section 5 and NEN-EN 1990 A2.

Load name	Load value	Load unit	Source
Distributed traffic	5,0	kN/m <sup>2</sup>	NEN-EN 1990 A2
Concentrated traffic	7,0	kN	NEN-EN 1990 A2

Snow loads are based on NEN-EN 1991-1-3.

Load name	Load value	Load unit	Source
Vertical snow load	0,58	kN/m <sup>2</sup>	NEN-EN 1991-1-3

Wind loads are based on NEN-EN 1991-1-4. In the described design project, only the vertical wind load is taken into account because of a low amount of horizontal surface.

Load name	Load value	Load unit	Source
Vertical wind load	0,59	kN/m <sup>2</sup>	NEN-EN 1991-1-4

The next step is to determine the procedure for calculating the resistance of a structure to effects of actions on the structure.

### 3. Structural resistance

Based on the model simulation intent, defined in Section 2.2, the first resistance that should be checked is the bending resistance of the structure. Bending in the structure causes stress in the cross-section. The value of the stress due to loads on the structure can be calculated using following formulae presented by Walraven & Braam in the TU Delft course CIE4160 (pre-stressed concrete) [58];

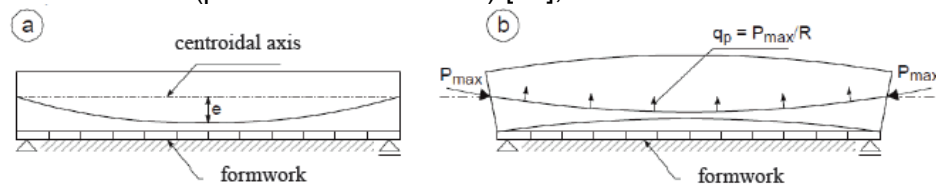


Fig. 4.12 Prestressing with post-tensioned steel  
a. Situation before applying the prestressing force  
b. Situation after applying the prestressing force

When at the manometer of the prestressing jack a force  $P_{\max}$  is indicated, the stresses in the concrete at midspan, at the bottom and at the top are:

$$\text{Bottom:} \quad \sigma_{cb} = -\frac{P_{\max}}{A_c} + \frac{M_g}{W_{cb}} - \frac{P_{\max}e_p}{W_{cb}} \quad (4.12a)$$

$$\text{Top:} \quad \sigma_{ct} = -\frac{P_{\max}}{A_c} - \frac{M_g}{W_{ct}} + \frac{P_{\max}e_p}{W_{ct}} \quad (4.12b)$$

Figure 27; Bending induced stresses in post-tensioned structures

The second resistance that should be verified, based on the simulation intent, is the resistance to shear force. Because the structure has two supports, the value of the shear force can be calculated by deviding the total load on the structure by two. The resistance to shear force is based on the shear capacity of the structure using Eurocode NEN-EN 1992-1-1 section 6.2.2.

#### 6.2.2 Members not requiring design shear reinforcement

(1) The design value for the shear resistance  $V_{Rd,c}$  is given by:

$$V_{Rd,c} = [C_{Rd,c} k (100 \rho_l f_{ck})^{1/3} + k_1 \sigma_{cp}] b_w d \quad (6.2.a)$$

with a minimum of

$$V_{Rd,c} = (V_{\min} + k_1 \sigma_{cp}) b_w d \quad (6.2.b)$$

Figure 28; Eurocode NEN-EN 1992-1-1 equation 6.2a and 6.2b

The third resistance that should be verified, based on the simulation intent, is the loss of post-tensioning force due to time dependent behaviour of concrete. The elongation of the tendons is reduced due to shrinkage of concrete. This can result in a reduction

of stress in the structure. Time dependent shrinkage of concrete should be taken into account in determining the initial post-tensioning force using following equations used from Walraven & Braam [58].

$$\Delta \varepsilon_p = \varepsilon_{c,\infty} - \varepsilon_{c,0}$$

$$\varepsilon_{p,total} = \varepsilon_{p,0} + \Delta \varepsilon_p = \frac{P_m}{A_p \times E_p} + \Delta \varepsilon_p$$

$$P_{m0} = \varepsilon_{p,total} \times E_p \times A_p$$

**Figure 29; Effect of creep on the strain in post-tensioning tendons**

The total amount of shrinkage in the concrete is derived from Eurocode NEN-EN 1990 section 3.1.4.

- (3) The creep deformation of concrete  $\varepsilon_{cc}(\infty, t_0)$  at time  $t = \infty$  for a constant compressive stress  $\sigma_c$  applied at the concrete age  $t_0$ , is given by:

$$\varepsilon_{cc}(\infty, t_0) = \varphi(\infty, t_0) \cdot (\sigma_c / E_c) \quad (3.6)$$

**Figure 30; Eurocode NEN-EN 1990 equation 3.6**

The last step is to determine the resistance of the structure which is determined by the materials used in the structure.

#### 4. Material resistance

The properties of 3D printed concrete used in the structural analysis are derived from the article published by T.A. Salet et al [22]. Based on their study, the 3DPC used in the Gemert design can be compared to concrete described in Eurocode of class C12/15. For this concrete type following strength principles are described in Eurocode NEN-EN 1992-1-1 figure 3.1, section 2.4.2.4 and section 3.1.6.

- (2) Other simplified stress-strain relationships may be used if equivalent to or more conservative than the one defined in (1), for instance bi-linear according to Figure 3.4 (compressive stress and shortening strain shown as absolute values) with values of  $\varepsilon_{c3}$  and  $\varepsilon_{cu3}$  according to Table 3.1.

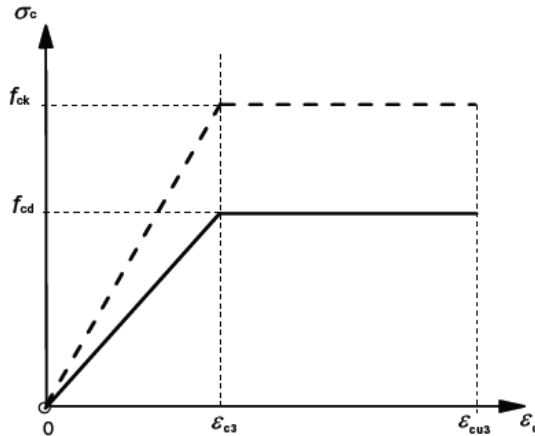


**Figure 3.4: Bi-linear stress-strain relation.**

**Figure 31; Eurocode NEN-EN 1992-1-1 Figure 3.4**

Table 3.1 of the Eurocode document NEN-EN 1992-1-1, specifies the maximum strain values as;

$$\begin{aligned} \varepsilon_{c3} &= 0,175 \% \\ \varepsilon_{cu3} &= 0,350 \% \end{aligned}$$

- (1) Partial factors for materials for ultimate limit states,  $\gamma_c$  and  $\gamma_s$  should be used.

**Note:** The values of  $\gamma_c$  and  $\gamma_s$  for use in a Country may be found in its National Annex. The recommended values for 'persistent & transient' and 'accidental' design situations are given in Table 2.1N. These are not valid for fire design for which reference should be made to EN 1992-1-2.

For fatigue verification the partial factors for persistent design situations given in Table 2.1N are recommended for the values of  $\gamma_{c,fat}$  and  $\gamma_{s,fat}$ .

**Table 2.1N: Partial factors for materials for ultimate limit states**

Design situations	$\gamma_c$ for concrete	$\gamma_s$ for reinforcing steel	$\gamma_s$ for prestressing steel
Persistent & Transient	1,5	1,15	1,15
Accidental	1,2	1,0	1,0

**Figure 32; NEN-EN 1992-1-1 table 2.1**

- (1)P The value of the design compressive strength is defined as

$$f_{cd} = \alpha_{cc} f_{ck} / \gamma_c \quad (3.15)$$

where:

$\gamma_c$  is the partial safety factor for concrete, see 2.4.2.4, and

$\alpha_{cc}$  is the coefficient taking account of long term effects on the compressive strength and of unfavourable effects resulting from the way the load is applied.

**Note:** The value of  $\alpha_{cc}$  for use in a Country should lie between 0,8 and 1,0 and may be found in its National Annex. The recommended value is 1.

- (2)P The value of the design tensile strength,  $f_{ctd}$ , is defined as

$$f_{ctd} = \alpha_{ct} f_{ctk,0.05} / \gamma_c \quad (3.16)$$

where:

$\gamma_c$  is the partial safety factor for concrete, see 2.4.2.4, and

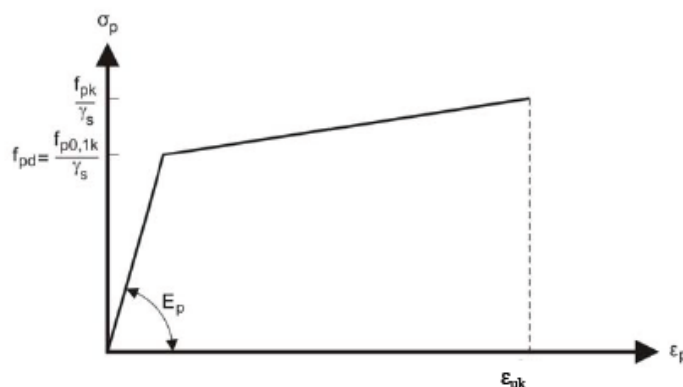
$\alpha_{ct}$  is a coefficient taking account of long term effects on the tensile strength and of unfavourable effects, resulting from the way the load is applied.

**Note:** The value of  $\alpha_{ct}$  for use in a Country may be found in its National Annex. The recommended value is 1,0.

**Figure 33; Eurocode NEN-EN 1992-1-1 equation 3.15 and 3.16**

The properties of post-tensioning steel are based on the TU Delft course CIE 4160, pre-stressed concrete, by Walraven & Braam [58];

*Stress-strain diagram of prestressing steel*



Y1860S7:  $f_{pk} / \gamma_s = 1860 / 1,1 = 1691 \text{ N/mm}^2$   
 $f_{pd} = f_{p0,1k} / \gamma_s = 1674 / 1,1 = 1522 \text{ N/mm}^2$   
 $\epsilon_{uk} = 35 \text{ ‰}$   
max. initial stress  $\sigma_{pi} = \sigma_{pm0} = 1395 \text{ N/mm}^2$ ;  $\sigma_{p,max} = 1488 \text{ N/mm}^2$  (at jacking)  
 $E_p = 195 \cdot 10^3 \text{ N/mm}^2$

**Figure 34; Material properties of post-tensioning tendons of class Y1860S7**



### 4.3. Component methodology

The methodology presented in this section describes the development of a structural analysis component that calculates structural behaviour using FEA software. Five steps are used in the structural analysis component to analyse a structure using FEA software. The first step is to gather all information required for analysis in FEA software. The second step is to determine the correct model representation in the FEA software. The third step is to export all information created in parametric software to the FEA software. The fourth step is to perform the FEA and generate output that can be imported back into the parametric software. The fifth step is to calculate the structural safety by result interpretation. Based on this information the structural efficiency can be determined. The five steps used for the structural analysis component are visualised in Figure 35 as a flowchart.

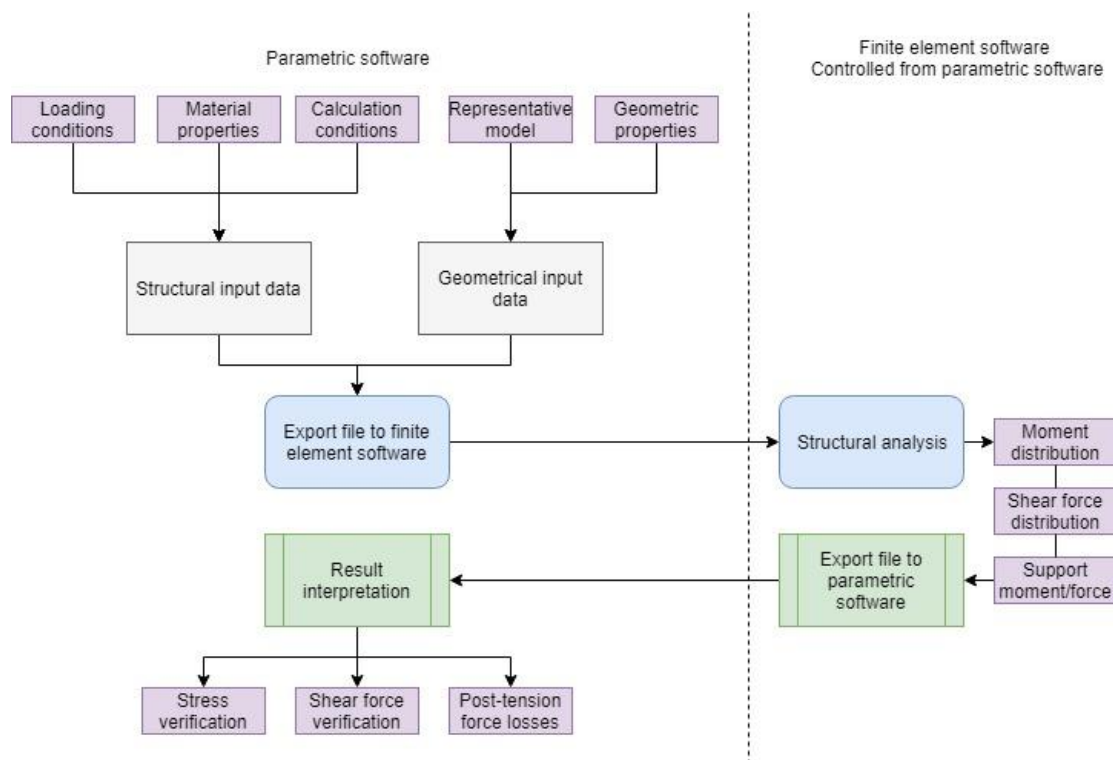


**Figure 35; Flowchart visualisation of the structural analysis component**

#### 1. Required input for finite element analysis

The requirements for SA, by means of FEA, can be defined by a number of key components that should be specified. The first component group contains the calculation conditions, the second contains the material properties, the third contains the geometric properties and the fourth component contains the loading conditions. This division into components is also used for export of the model and its contents to FEA software.

The calculations conditions can be determined based on the model simulation intent, described in Section 2.2, and the context of the structural analysis, described in Section 4.2. The goal of the structural analysis using FEA is to calculate the structural safety. This can be calculated by using ultimate limit state (ULS) design verifications. Only the ULS is considered in the analysis because the serviceability limit state is to be fulfilled by the range of possible input of the parameters. The calculation described in this thesis project is based on the following set of analysis conditions and assumptions.

1. The loading case for the bridge is based on loads imposed on the structure by pedestrians and cyclists. The load values are based on Eurocode NEN-EN1991.
2. The designed lifespan of the structure is 100 years, standard for bridge design. This results in construction class cc1 according to NEN-EN 1991.
3. The bridge is exposed to environmental influences of exposure class XF2 and XF4. These classes indicate environmental influences regarding frost conditions and de-icing salt.
4. The support conditions are similar, but not limited, to a simply supported beam model. A simply supported beam has two different supports, 1 hinge and 1 rolling-hinge support.
5. Other than the post-tensioned tendons no contributions of reinforcements are considered in the analysis.
6. Other conditions not described in the model methodology are chosen similar to the Gemert design.
7. Due to unknown crack behaviour of printed concrete and limited ductility, resulting in limited redistribution of stresses, it is favourable if there is no tensional-stress in the concrete sections as a result of the loading conditions.
8. The material properties in this project are chosen to be similar, but not limited, to the Gemert design. As described in the simulation intent, this is chosen for model evaluation and to determine the accuracy of the design model. The material properties of 3DPC are presented in Table 1.

Property	Dir.	Age	Symbol	Value
Density		28 days	P	2,000 kg/m <sup>3</sup>
Modulus of elasticity		28 days	E	19,000 MPa
Average compressive strength	u	28 days	$f_{ck,u}$	23.2 MPa
	v	28 days	$f_{ck,v}$	21.5 MPa
	w	28 days	$f_{ck,w}$	21.0 MPa
Average tensile strength (also used for flexural tension)	u	28 days	$f_{ct,u}$	1.9 MPa
	v	28 days	$f_{ct,v}$	1.6 MPa
	w	28 days	$f_{ct,w}$	1.3 MPa
Creep factor <sup>a</sup>		7 days	$\psi_7$	1.0
		14 days	$\psi_{14}$	2.5
		56 days	$\psi_{56}$	3.0
Shrinkage		7 days	$\epsilon_7$	0.6
		14 days	$\epsilon_{14}$	1.2
		56 days	$\epsilon_{56}$	1.5

<sup>a</sup>After 28 days.

Notes: For the directional dependency, a relative orientation of axis  $u, v, w$  is used (Bos *et al.*, 2016), indicating the direction parallel to the print in the horizontal plane, perpendicular to the print direction in the horizontal plane, and vertically perpendicular to the print direction (or parallel to the robot arm), respectively.

**Table 1; Material properties determined for the 3DPC bridge in Gemert by T.A.M. Salet et al - [22]**

## 2. Representative model

The objective of model representation is a reduction in the amount of unnecessary information in the model. This can be achieved by using a representative model for the analysis in FEA software. Generating a representative model involves three steps. The first step calculates representative values for the geometry. The second step reduces the amount of degrees of freedom as much as possible. The third step uses the simplification values and the simplified model to create a simplified structure. This is the representative model.

In order to calculate the representative values the information of each of the sections has to be extracted from the geometry model. The most important cross-sectional properties for structural analysis are the centroidal/global location, the area, the moment of inertia. These values are calculated at multiple positions along the span. Geometric properties are automatically calculated in the geometry component, as described in Section 3.2 and 3.3. The geometric properties are used to calculate representative values of the geometry model. The formulae presented in Equations 4.1-4.2 are used to calculate the representative values using the actual values.



$$h_{Rep,A,i} = A_{print\ path,i} \div b_i \quad (4.1)$$

$$h_{Rep,I,i} = \sqrt[3]{\frac{12 * I_{print\ path,i}}{b_i}} \quad (4.2)$$

A benefit of using representative sections is the possibility of simulating both plate and beam behaviour. The two options are 1D analysis and 2D analysis. In 1D analysis, the model is represented as a beam existing of multiple sections. In 2D analysis, the model is represented as a plate existing of multiple sections. Both methods have favourable and non-favourable influences on the results of the analysis and the possible input geometry. This step will focus on determining the most suitable method for reducing the DOF with respect to the model simulation intent. The biggest difference between the 1D and 2D analysis is the capability to take the effect of nonlinear stress distributions into account. The expected stress distribution pattern of a section can be estimated by the ratio between geometric values of the model in two directions (length/width). The first indicator, in plate theory, is the height over span ratio which is divided into three limit cases [59].

1. The first case is the high and thin plate ( $h/l > 1$ ) which result is strong non-linear stress distribution.
2. The second case is the “normal” plate in, the length and height are approximately equal ( $h/l = 1$ ), this shape ratio still result in a nonlinear stress distribution.
3. The third case is the slender beam ( $h/l < 1$ ) in this case the stress distribution is in compliance with the Euler/Bernoulli theory which results in a linear stress distribution.

The second indicator is the height over width ratio. This ratio can be applied similar to the thickness over span ratio and is classified, for identifying nonlinear distribution, in the same manner [59]. Based on these two ratios, the model can be represented by two sets of five different height values; the total height, the representative height for the area (average/max value) and the representative height for the moment of inertia (average/max value). These five values are used to determine if the representative model is best simulated as a 1D beam or 2D plate element (see Figure 36).

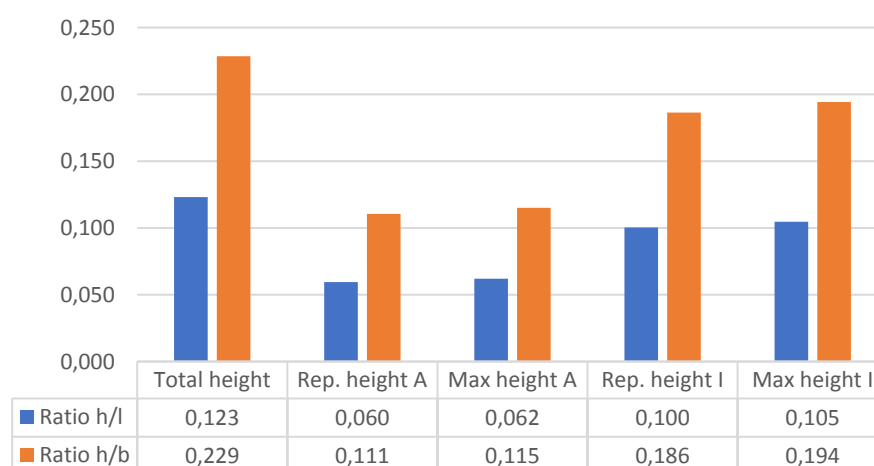


**Figure 36; Height over span length and height over width ratios**

Another factor that can be used to indicate plate behaviour is the typical thickness (height) over width ratio of a plate structure which, according to plate theory, is less than 0.1 [60]. This ratio deviates 0,01 and 0,08 from the boundary condition, thereby indicating that both analysis methods (1D and 2D) can be used. However, it can be

argued that the 1D analysis is preferred since the height over width ratio is slightly higher than the typical value of 0,1 (indicated by plate theory) and because of the simplicity of the approach.

When considering the representative model the second important factor is the loading condition. The dominant loading case according to the article of T.A.M. Salet et al [22] is a uniformly distributed load. Therefore, the model is best represented as a continuous model [61]. Since both the 1D and 2D analysis result in continuous model, this factor should only be considered if the dominant loading case is non-symmetric. The influence of the geometry on the dominant loading case in relation to the model representation will be further addressed in Section 4.4.

Based on the low height over span length/width ratios linear stress distribution in the cross-sections can be expected. The only indicator that is inconclusive is the typical thickness to width ratio which, in case of the Gemert geometry input, is slightly higher. This suggests that, in case of the Gemert geometry input, the model can be represented by the beam. However, in the model simulation intention it is specified that the model should be able to represent but not be limited to the Gemert case. The downside of the 1D beam representation is that the nonlinear stress influences cannot be taken into account while the 2D plate representation can take both linear and non-linear stress influences into account. Therefore, the most suited representation model should be determined based on a comparison. However, this requires input values that will be presented in Section 4.4. For this reason, the model representation will be determined in Section 4.4.

After establishing the degrees of freedom of the representative model the next step is to use the calculated representative values to reduce the model complexity. The representative height value are used to create a simplified representation of the complex shaped of the cross-section. This greatly reduces the model complexity and, while changing the local behaviour, still results in a relatively accurate approximation of the overall structural behaviour. The following steps are used to generate the cross-section representation model;

1. Determine the x-value of the centroidal coordinate at the section interfaces, these coordinates represent the x-location centroidal axis of the interfaces.
2. The width and the y-coordinate of the section interfaces at the centroidal coordinate are used to determine the y-coordinates of the representative model ( $y_{1,i} = y_{ca} - b/2$  and  $y_{2,i} = y_{ca} + b/2$ ).
3. The representative height for the moment of inertia and the z-coordinate of the centroidal coordinate of the section interface are used to determine the z-coordinates of the representative model ( $z_{1,i} = z_{ca} - h_{rep}/2$  and  $z_{2,i} = z_{ca} + h_{rep}/2$ ).
4. The y- and z-coordinate are used to determine the representative sections that is lofted into a 3D model existing of multiple simplified sections (see Figure 37).

### 3. Export to finite element software

The third step is to export the generated information in the required format for the FEA software. However, Grasshopper cannot be linked directly to FEA software due to a different data structure. Software communication between different data structures requires the software to incorporate plugins for data transformation and interpretation. The preferred method for automating communication between two types of software, with different data structurea, is by using an application programming interface (API). Developers use an API to create a data communication tool that can be used to transform data to the required format. Using an API type of data communication tool can significantly speed up back and forth communication of software packages.

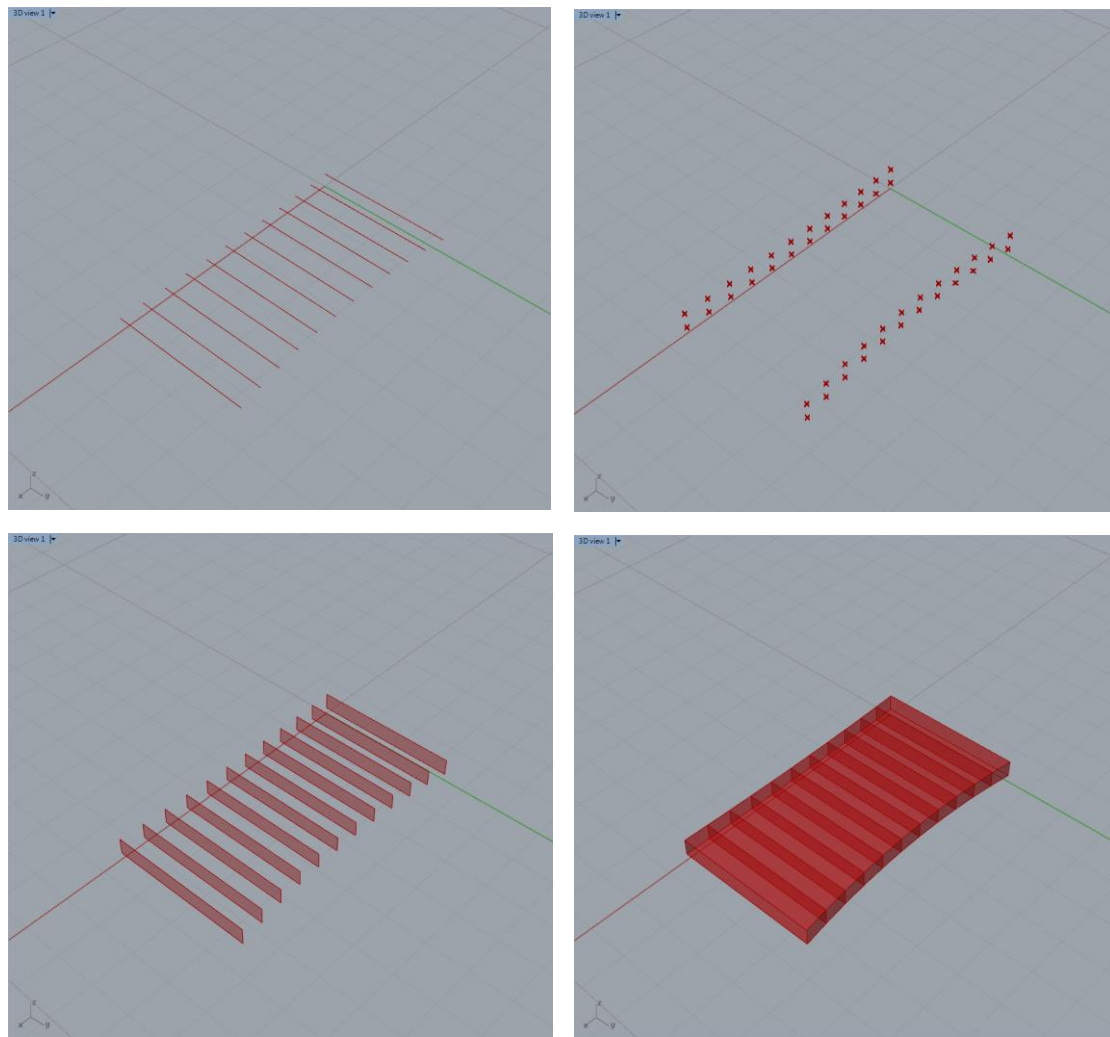


**Figure 37; Top left; centroidal axis of the section interfaces – Top right; coordinates of the representative solid model – Bottom left; representative sections – Bottom right; representative solid model**

However, a downside of using this method is that few FEA software offer open source API platforms. Therefore, a different method for data structure communication and interpretation is used. Before API connections were available, data was transferred by exchanging files in xml format. An xml file contains the data required as input for the FEA software and a coding element to indicate the function of each of the specified lines in the document. A benefit of xml files is that most software packages allow import of this type of format, thereby reducing the time requirements for manual input of values in the FEA software.

When compared to using an API, the reduction of time is smaller. The options for back and forth communication, using xml import/export, are limited. However, a component can be created in Grasshopper that can be used in combination with the Python plugin component to create xml files. The export of xml files can be automated in Grasshopper and executed on command using a switch component. FEA software can read the file directly from a folder specified in the Grasshopper model. For these reasons, the structural analysis component will use import and export of xml files to communicate with FEA software.

A quick method to determine the format required for importing an xml data file in a software package is to manually create a model, that fulfils the model simulation intent, and export that model as an xml file. After exporting the desired model configuration and specifications as xml the file can be modified and customised. Using this method,

the xml data format for SCIA Engineer is determined and verified by editing and importing the script in order to determine the critical information. The complete results of this method are documented in Annex D. A brief preview, of specifying the location of the nodes, is presented below in Figure 38.

```

<container id="{39A7F468-A0D4-4DFF-8E5C-5843E1807D13}"
t="EP_DSG_Elements.EP_StructNode.1">
  <table id="F3A9E1CA-F6A1-4579-8307-BDF4F5CC3A7F"
t="EP_DSG_Elements.EP_StructNode.1" name="Knop">
    <h>
      <h0 t="Naam"/>
      <h1 t="Coördinaat X"/>
      <h2 t="Coördinaat Y"/>
      <h3 t="Coördinaat Z"/>
    </h>
    <obj id="1">
      <p0 v="K1"/>
      <p1 v="0"/>
      <p2 v="0"/>
      <p3 v="0"/>
    </obj>
    <obj id="2">
      <p0 v="K2"/>
      <p1 v="3.25"/>
      <p2 v="0.156187"/>
      <p3 v="0"/>
    </obj>
  </table>
</container>

```

**Figure 38; Example of specifying a node of a structure for import into SCIA**

In the xml example presented in Figure 38, a colour coding system is used to indicate the function of the lines and the text input. This system uses a set of rules to simplify the identification of the script and visualise the location where text should be inserted. The following set of rules have been applied:

- Text written in red;
  - Indicates the beginning/end of sections of similar function of input
  - Specifies the container id, thereby assigning the input to its function
  - Specifies the table id, thereby ensuring that the data lines are assigned to the correct position in the table in SCIA Engineer
- Text marked in grey;
  - Specifies the beginning/end of sections within a container
  - For example the start/end of the specifications of the first node
- Text marked in blue;
  - Indicates the function of the lines in the table assigned to the section by the text written in red
  - For example, line 1 in the nodes specification section assigns that the first line of every green text specifies the name of the node
- Text marked in green:
  - Indicates that these lines are used for specifying information that is to be specified in the Grasshopper model
  - For example the first green line in the node specification section should contain the information related to the first line
- Text written in white;
  - Indicates the location of information that is to be generated by the Grasshopper model and specified in SCIA Engineer

Using these rules, the information is assigned to a location in the xml file based on the function of the information. As mentioned before, the complete overview of all specified information in the xml file is presented in Annex D. Once the required information is

gathered, the sections can be combined to create the final version of the xml file. it is crucial for importing the xml script into SCIA Engineer that the definition file is specified correctly and is present in the same enclosing folder as the xml file. A benefit of using Grasshopper to combine the information required for the xml file is that if parameters are changed the script is updated automatically.

#### 4. Structural analysis using finite element software

The previous step results in an xml file containing all information required for the SA using FEA software. This file is used to calculate the required information in SCIA. If the xml file is generated correctly, importing the xml file will not result in warnings and therefore can directly be used to calculate internal forces. The process of calculating the internal forces is automated using Python components in Grasshopper. In the Python component an external command file is specified that will be opened in the background if the python component is activated. To execute the calculation in FEA software, the following commands have to be executed in the following order;

1. Specify the task that the cmd file executes
2. Sepcify the directory that files should be located and saved in
3. Execute the task using the following settings;
  - a. Type of analysis, in this project linear [LIN]
  - b. Use a specific template file for the analysis [\_Template\_XX.esa]
  - c. Use a specific xml input file for the analysis [SCIA Export.xml]
  - d. Generate output as text file [-tTXT]
  - e. Name the output file [-o"Name\_file.txt"]

After the analysis is completed the generated results are exported as text file in the specified directory. As discussed the analysis should generate four output files; the bending moment & shear force distribution and the bending moment & shear force at the supports. Four template files are used to generate this information. The four output files are required to perform the following critical design checks;

- The start/end section are loaded by shear force and therefore should be verified for shear capacity.
- In the mid-span the shear force is zero but the momentum is at its maximum value. Therefore the mid-span should be tested for bending induced stresses.
- The start- and mid-section are used to determine the required value of the post-tensioned force. The mid-section determines the minimum force, to prevent cracking of the mid-span, and the start-section determines the maximum allowed force, to prevent crushing of the concrete. These values determine the designed range of values suitable for the post-tensioned compression force.
- Inbetween the start- and mid-section, the combination of shear and moment should be verified to stay within the limits of the resistance.

#### 5. Result interpretation

The data imported in parametric software is used to perform design checks. However, the values calculated in FEA software are not directly applicable. The values generated by the analysis in SCIA Engineer are 2D plate results and therefore are internally distributed values. The internal plate values are calculated as an intensity value for a specific element of a plate section and not a reaction value to the applied load [61]. Therefore, the unit is in kNm/m for bending and kN/m for shear force. The reaction force on the structure is required to verify the design checks. Because interal forces for bending and shear distribution can vary over the width of the sections, the reaction value at a section interface should calculated on element level (see Equation 5.1 and

5.2). At the supports the values should be averaged to determine the overall reaction value. Therefore the results of the elements are combined and averaged (see Equation 5.3 and 5.4)

$$M_{i,j} = m_{x,i,j} \times b_{i,j} \quad (5.1)$$

$$V_{i,j} = v_{x,i,j} \times b_{i,j} \quad (5.2)$$

$$R_{z,i} = \frac{\sum_{j=1}^{n-1} [(R_{z,i,j} + R_{z,i,j+1}) \times b_{i,j} / 2]}{\sum_{j=1}^n b_{i,j}} \quad (5.3)$$

$$M_i = \frac{\sum_{j=1}^{n-1} [(M_{i,j} + M_{i,j+1}) \times b_{i,j} / 2]}{\sum_{j=1}^n b_{i,j}} \quad (5.4)$$

Another factor influencing the internal forces along the span is the amount of elements in the mesh used by SCIA to calculate the internal forces. The amount of elements depends on the mesh settings used in SCIA, an example of a result is presented in Figure 39. Because the mesh settings are not specified in the xml, the mesh settings are automatically generated based on the overall geometry of the imported section. Therefore, the amount of elements can vary based on the geometry of the model. This is taken into account by the internal forces conversion process in Grasshopper. Besides the amount of sections, the type of distribution should also be considered. As seen in Figure 39, the value of the internal forces can vary in both x and y direction. Therefore, it is important to create a value interpretation component based on the data structure of the output and the interpretation process in Grasshopper.

Results generated in SCIA Engineer are presented in three different tables; extreme values, element average values and net values. The extreme values results in a simple table only showing the maximum values. This option does not generate the results required for analysis at the interfaces and therefore is not used. The element average values generates the average values of all the elements of the mesh (see Figure 39). This option generates the most important values but does not present extreme values calculated in the model. The net values option generates all the values in all of the nodes of all the mesh elements generated by SCIA Engineer to analyse the geometry. However this option results in a text output files in which the results are scattered; not structured based on the x and y location of the mesh node. Therefore the second option, element average values, will be used to calculate the stresses at the element interfaces.

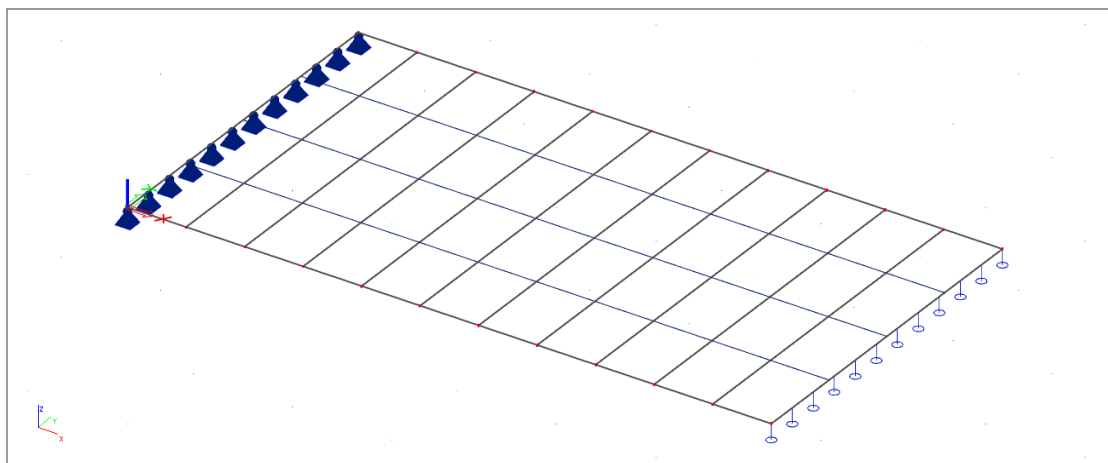


**Figure 39; Exported from SCIA – Mesh generated by SCIA for the Gemert design case**  
After interpreting the data generated in the FEA, the reaction forces in the structure can be calculated. However, it is important to first consider the effect of using the representative model. The representative model does not take the eccentric properties



of 3DPC cross-section into account. Therefore, the stress values calculated in the FEA cannot be used for stress verifications. The formulae presented in Equations 6.1-6.2 include the effect of the eccentricity on the stress distribution in the cross-section [62]. In the equation the stress is calculated as a result in the y- and z-direction. However, since the load case is dominant in the z-direction the influences of the momentum in the y-direction can be neglected in Equation 6.1. The resulting formula is Equation 6.2.

$$\sigma(y, z) = \frac{N}{A} + \frac{M_y \times e_y}{I_{yy}} + \frac{M_z \times e_z}{I_{zz}} \quad (6.1)$$

$$\sigma(z) = \frac{M_z \times e_z}{I_{zz}} \quad (6.2)$$

Besides the effect of the eccentricity, the post-tensioning should also be included in the stress calculation. The tendon eccentricity influences the resistance of sections related to the post-tensioning moment on the sections. To calculate the stresses the combination of the post-tensioning has to be included in Equation 6.2 [58]. This value should be checked at the top and bottom of each of the sections specified in step 2 in Section 3.3. The calculated stress values can be used for the stress verification. The formulae presented in Equations 7.1-7.5 are used to verify the cross-sectional resistance related to the eccentricity of the cross-section and the post-tensioning force.

$$z_{c,top,i} = \frac{h_i}{2} + z_{c,i} \quad (7.1)$$

$$z_{c,bot,i} = \frac{h_i}{2} - z_{c,i} \quad (7.2)$$

$$e_{p,i} = \frac{n_{bot} \times z_{p,bot} + n_{top} \times z_{p,top}}{n_{p,bot} + n_{p,top}} - z_{c,i} \quad (7.3)$$

$$\sigma_{c,top,i} = -\frac{P_m}{A_{c,i}} + \frac{P_m \times e_{p,i} \times z_{top,i}}{I_{c,top,i}} - \frac{M_{Ed,i} \times z_{top,i}}{I_{c,top,i}} \geq f_{cd} \quad (7.4)$$

$$\sigma_{c,bot,i} = -\frac{P_m}{A_{c,i}} - \frac{P_m \times e_{p,i} \times z_{bot,i}}{I_{c,bot,i}} + \frac{M_{Ed,i} \times z_{bot,i}}{I_{c,bot,i}} \leq f_{ctd} \quad (7.5)$$

In Equation 7.1 and 7.2,  $z_{c,i}$  is the centroidal axis of the cross-section in the Z-direction at location (i) along the span. In Equation 7.3,  $e_{p,i}$  is the value of the tendon eccentricity at location (i) along the span. The goal of the post-tensioning is to apply as much force required to ensure that there is no tension in the structure. This condition results in a minimum required amount of prestressing that should be applied to both ends of the structure. The required minimum value can be obtained by rewriting Equations 7 according to the stress limit specified by the calculation condition (in this design, lower than 0 but higher than the compression limit). The result of rewriting Equations 7 is presented in Equations 8. Equations 7 and 8 are based on NEN-EN-1992-1-1 (section 5.10 & 6.1) and NEN-EN-1992-2 (section 5.10 & 6.1).

$$\sigma_{c,top,i}; \quad P_m \geq \frac{f_{cd} + \frac{M_{Ed,i} \times z_{top,i}}{I_{c,top,i}}}{-\frac{1}{A_{c,i}} + \frac{e_{p,i}}{I_{c,top,i}}} \quad (8.1)$$

$$\sigma_{c,bot,i}; \quad P_m \leq \frac{\frac{M_{Ed,i}}{W_{c,bot,i}} - f_{ctd}}{\frac{1}{A_{c,i}} + \frac{e_{p,i}}{I_{c,bot,i}}} \quad (8.2)$$

The above presented equations provide a minimum and a maximum value for the applied post-tensioning force. Values within these ranges can be used to calculate the



final result of the stress distribution. This value can be used to determine the size and the material class of the post-tensioned tendons. Next to the minimum required amount of post-tensioning force, the effect of creep and shrinkage should also be considered. Eurocode NEN-EN 1992-1-1:2004 describes the process of calculating the effect of creep and shrinkage in concrete structures. According to Eurocode section 3.1.4, these effects can be determined by calculating the strain of the concrete at time  $t=\infty$ . The exact value of the strain at time  $t_0=\infty$  can be calculated using Equation 9.1, in which the value of the creep coefficient  $[\varphi(t,t_0)]$  is 3,50 (as determined in the material properties presented in Table 1 and figure 3.1 of NEN-EN 1992-1-1:2004). However, this value is determined for concrete and not 3DPC in particular. Therefore, a different formula is used based on research performed by the TU Eindhoven [55]. According to the article the value of strain at time  $t=\infty$  should be adjusted because of a decrease in stiffness over time. The adjustment of the formula is presented in Equation 9.2.

$$\varepsilon_{cc}(\infty, t_0) = \frac{\sigma_c \times \varphi(\infty, t_0)}{1,05 \times E_{cm}} \quad (9.1)$$

$$\varepsilon_{cc}(\infty, t_0) = \frac{\sigma_c \times [1 + \varphi(\infty, t_0)]}{E_{cm}} \quad (9.2)$$

Because the tendons are post-tensioned, the effect of friction on losses by contact with the concrete section can be neglected. The same logic applies to the curvature induced tension losses in the tendons, related to the straight configuration. Therefore the only factor influencing the tension losses in the tendons is the time dependent creep of the concrete. The loss of stress in the tendons can be determined by subtracting the initial strain from the strain at time  $t=\infty$ , from Equation 9.2. The difference of the two strain values is considered to be the time dependent strain loss related to shrinkage and creep in the concrete. The increases in strain over time results in a decrease in post-tensioning in the tendons over time. To take this effect into account the total expected strain in the tendon should include the creep related strain. The total expected strain can then be used to calculate the initial required amount of post-tensioning force (see Equations 10.1-10.4).

$$\Delta\varepsilon_p = \varepsilon_{c,\infty} - \varepsilon_{c,0} \quad (10.1)$$

$$\varepsilon_{p,total} = \varepsilon_{p,0} + \Delta\varepsilon_p = \frac{P_m}{A_p \times E_p} + \Delta\varepsilon_p \quad (10.2)$$

$$P_{m0} = \varepsilon_{p,total} \times E_p \times A_p \quad (10.3)$$

A benefit of modelling the post-tensioned configuration of tendons in Grasshopper is the possibility of parametrically determining the type and diameter of the tendons. In order to determine the effect of the geometry of the 3DPC sections the initial models should have the same amount and type of tendons. However, as determined in the model simulation intent, the model input should represent but should not be limited to the Gemert design input. The type and the diameter of the tendons can be calculated using the formulas presented in Equations 10.1-10.3. The main parameters influencing the choice for a tendon type are the modulus of elasticity, the tendon area and the strength of the tendon (see Equations 11.1-11.2).

$$E_p \times A_p \geq \frac{P_{m0}}{\varepsilon_{p,total}} \quad (11.1)$$

$$\frac{P_{m0}}{A_p} \leq f_{pd} = f_{p0,1k} / \gamma_p \quad (11.2)$$

Looking at the formulae presented in Equations 10.1-10.3 and 11.1-11.2 it can be noted that the process of determining the tendon properties is an iterative process. Determining the total strain in the tendons and the initial required amount of post-tensioning force, using Equations 10.1-10.3, requires information validated later on by Equations 11.1-11.2. Therefore, a decision for a type of tendon is first estimated to calculate the total strain and then verified to justify the initial decision.

The stress distribution is calculated using the element average force, Equations 5.1-5.4 and Equations 7.1-7.5. The calculated stresses are used to validate the resistance of the sections at cross-section interfaces using Equation 7.1-7.5. In Grasshopper, the design check for compliance to the required minimum and/or maximum stress level in the structure is automated. The shear safety is verified by calculating the shear resistance and comparing the shear force in the sections with the resistance of the section. The shear resistance is calculated using the effective area method based on the minimum shear resistance described in Eurocode NEN-EN1992-1-1 section 6.2.2 formula 6.2b (see Equations 12.1-12.2).

$$V_{Rd,c} = (v_{min} + k_1 \times \sigma_{cp}) \times A_{eff} \quad (12.1)$$

$$v_{min} = 0,0035 \times k^{3/2} \times f_{ck}^{1/2} \quad (12.2)$$

The value of k in the formula for the minimum shear resistance in this design is 1. The value of k1 is determined by the national annex of the Eurocode and is in this design 0,15. For the value of k the most conservative value is used, k=1, to account for the material uncertainties. For determining the effective width of the section the amount of filament widths should be considered. For the effective height of the section the combined height of the verticals in the section should be used. Based on these values the resistance of the model can be tested for shear. However, the effect of the combination of shear and transverse bending should also be determined in the design verification. According to Eurocode NEN-EN1992-2 section 6.2.106 the combination of shear and transverse bending can only be neglected if;

- $V_{Ed}/V_{Rd,max} < 0,2$
- $M_{Ed}/M_{Rd,max} < 0,1$

If not, the effect of combining shear and transversal bending can be taken into account using a simplified version of the Von Mises failure criterion (see Equations 13.1-13.2). The Von Mises failure criterion can be used to determine the simultaneous effect of shear and transversal bending on the stress in a section. In order to apply the Von Mises failure criterion the value of the shear stress has to be calculated. The value of the shear stress can be calculated according to the formula presented in Equations 13.1-13.2. In the equation, S is the first moment of area of the section and I the moment of inertia. The value for S is estimated in the model as half of the area of the print path interface multiplied by half the representative height of the area minus the eccentricity. The width b in the equation is the amount of print path curves in the model.

$$\tau_i = \frac{S_i \times V_i}{b_i \times I_i} ; S_i = A_{print\ path,i} \times \frac{(h_{rep,A,i} - e_{c,i})}{2} \quad (13.1)$$

$$\sigma_{combined,i} = \sqrt{\sigma_i^2 + 3 \times \tau_i^2} \quad (13.2)$$

Equations 7-13 are used from Eurocode ULS and SA theory. To conclude the following checks are checked for determining the structural safety of the model;

- The bending induced stresses should be lower than zero, no tension in the structure
- The shear force should not exceed the effective shear resistance of the print path
- The combined effect of shear and transversal bending should not exceed the limits of the strength of the 3DPC material
- The value of the post-tensioning force losses should be taken into account when applying the initial post-tension force.

If all of these conditions are fulfilled the structure is assumed to be safe to fulfil its designed function within the designed life. This completes the process of developing the structural analysis component. The next step is to verify the generated results. If the accuracy is within an acceptable range the model can be used to create different combinations of parameters. Within the range of applicability, the structural analysis component can be used to test influence of the geometry on the structural efficiency.

## 4.4. Application of the methodology

The five steps described in the methodology can be used to develop a structural analysis component using FEA software. In this section, the same structure will be used to elaborate the application of the development of the component.

### 1. Required input for finite element analysis

The requirements for structural analysis using FEA are partly defined in section 4.3. The calculations and the calculation conditions are the same as described in section 4.3. This information does not need to be repeated in this section. The calculated results of the loads and the cross-sectional properties are presented in this step.

Because the structure can be modelled as a 2D plate or 1D beam, the load is represented in this section as a 2D load. Beam loads can be obtained by multiplying the plate load by the width of the beam. The value of the 2D load is generated by considering the critical combination of loading conditions, resulting in the 2D design load in kN/m<sup>2</sup>. Critical load combinations, load values and load factors are calculated using Section 4.2 step 1 and 2. A complete description of the sections of the codes applied to this thesis work are presented in Annex C. Results of the load generation calculations are presented below. Changing the cross-sectional height affects the self-weight therefore is calculated in kN/m<sup>3</sup>. Variable loads are not affected by changing the height of a cross-section and therefore can directly be applied as 2D load.

1.	Calculation of self-weight	(permanent)
a.	Self-weight of the cross-section	22,563 kN/m <sup>3</sup>
b.	Correction of print process (5%)	1,128 kN/m <sup>3</sup> *
c.	Concrete pressure layer 10 mm	33,000 kN/m <sup>3</sup> *
d.	Extra finishing layer 50 mm	25,000 kN/m <sup>3</sup> *
2.	Traffic	(variable)
a.	Variable traffic; Q <sub>q,z</sub>	5,000 kN/m <sup>2</sup>
3.	Wind load	(variable)
a.	Parallel to deck; Q <sub>w,x</sub>	1,180 kN/m <sup>2</sup>
b.	Along the span; Q <sub>w,y</sub>	0,590 kN/m <sup>2</sup>
c.	Perpendicular to deck; Q <sub>w,z</sub>	0,450 kN/m <sup>2</sup>
4.	Snow load	(variable)
a.	Perpendicular to deck; Q <sub>s,a</sub>	0,560 kN/m <sup>2</sup>
5.	Thermal load	(variable)
a.	Along the span; Q <sub>t,y</sub>	0,120 kN/m <sup>2</sup>
6.	Construction load	(variable)
a.	Perpendicular to deck; Q <sub>t,z</sub>	-
b.	Safety factor for construction <sup>2</sup>	q <sub>G</sub> * × 1,2

These loads can be specified in the FEA software using two methods. The first method models the loads separately as self-weight, permanent and variable loads. The second method combines the load values with combination factors to generate characteristic load values of the 2D plate load. The first method requires load combination after generating the values. The second method can directly be used for the calculation. The design load conditions can be determined by using the fundamental load combination cases and the design load combination factors. The load combination factors, the partial safety factors and the calculation of the combinations are presented in Annex C. When using the first method, the generated loads should be combined with design factors. When using the second method these values should be combined with design

<sup>2</sup> The construction load factor is applied only to the loads indicated with a (\*)

and combination factors. Based on the Gemert design (constant dimensions;  $h=0,80$  m &  $b=3,50$  m) the following loads are calculated as design load (method 1) and design load combinations (method 2):

1. Design loads		
a. Distributed load		
i. Permanent 6.10 a	12,72	kN/m <sup>2</sup>
ii. Permanent 6.10 b	11,66	kN/m <sup>2</sup>
iii. Q1 traffic	6,00	kN/m <sup>2</sup>
iv. Q2 wind	0,61	kN/m <sup>2</sup>
v. Q3 snow	0,76	kN/m <sup>2</sup>
b. Concentrated load		
i. Traffic (vertical)	8,40	kN
ii. Wind (horizontal)	3,30	kN
2. Design load combinations		
a. Distributed load		
i. 6.10 a	17,89	kN/m <sup>2</sup>
ii. 6.10 b	18,03	kN/m <sup>2</sup>
iii. Snow	13,48	kN/m <sup>2</sup>
b. Concentrated load		
i. Permanent	11,66	kN/m <sup>2</sup>
ii. Traffic	8,40	kN

When comparing design load combinations, the loading case resulting in the highest load value is the 2D plate load generated by combination 6.10b. Because the critical load is a distributed load, method 2 will be used in the model to determine the critical load value. The values of the UDL at the section interfaces are automatically generated in Grasshopper and compared to use the highest load. However, since SCIA is not able to model loads varying in the direction of the span the average value of the load in an element is used. Because the highest load is uniformly distributed, the critical cross-sectional resistance is expected to be located in the mid-span of the bridge, due to bending induced stresses. The momentum resulting from loading case 6.10b can be used to determine the minimum required tendon force and eccentricity by substitution in the formulae of equations 7. Geometrical properties used for calculation of the Gemert design using the developed design model are presented below.

1. Main geometry		
a. Length	6,50	[m]
b. Width	3,50	[m]
c. Height	0,80	[m]
2. Line type		
a. Line type 1&2	Straight	[-]
b. Sinusoidal line		
i. Amplitude	0,00	[m]
ii. Amount of loops	1	[-]
c. Skewed line	0,00	[m]
d. Number of sections	11	[-]
3. Cross-sectional properties		
a. Concrete centroidal axis <sup>3</sup>	0,378	[m]
b. Area	1,434	[m <sup>2</sup> ]
c. Moment of inertia	0,096	[m <sup>4</sup> ]

<sup>3</sup> Concrete centroidal axis is measured from the bottom of the section.

#### 4. Post-tension configuration

##### a. Tendon placement

###### i. Top

6 tendons

###### ii. Bottom

10 tendons

##### b. Tendon diameter

12,5 [mm]

##### c. Cover distance

10 [mm]

This completes the first step of the model development.

### 2. Representative model

Although the 2D model representation is preferable, both methods described in step 2 of Section 4.3 are suitable. Therefore, it is important to compare the results obtained by the different analysis types. The structural and geometric data generated in the previous section are used to make a comparison between three different models. As mentioned before, a calculation control document is created in Excel. This documents contains data presented in the previously described methodology and step 1 of this section. The full calculation control document is presented in Annex E. The second model is made in MatrixFrame. This model is setup as a 1D beam model using the data presented in step 1. The third model is made in SCIA Engineer. In SCIA two options are compared; 2D plate analysis and 2D scale analysis. The difference between a scale element and a plate element in SCIA is in the method of creating a surface. A plate element is specified as an infinite number of points that are connected to define a surface. A scale element in SCIA defines a surface based on any geometry made out of 2, 3 or 4 lines. The data presented in step 1 is used in both models in SCIA Engineer. Because the data used in the compared representations is the same, the difference in results only reflects on the difference in analysis type. The difference in the analysis type is related to the degrees of freedom of the representation and the calculation procedure. The results of the comparison are presented in Figure 40 as a percentage of results determined in the calculations control document in Excel. The results of this document are assumed to be the correct design values because the document is based on calculations and procedures specified in Eurocode.

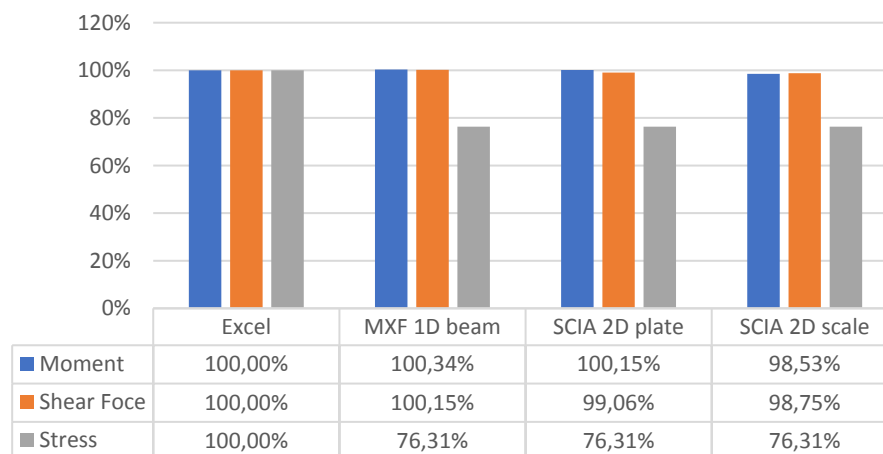


**Figure 40; Percentage based difference between results obtained by the compared model representations.**

Looking at the results presented in Figure 28, the following observations regarding the accuracy of the results are made;

- The 1D beam representation and the 2D plate representation result in the best approximation of results of the calculation control document. The 1D analysis results in the most accurate combination of the results, except for the stress.

- The difference between the results of SCIA and Matrixframe both deviate from the desired result. However, the difference are smaller than 1% in the calculation of the internal force distribution.
- The difference between the stress calculated in the FEA software and the result of the document control document is  $\pm 24\%$ . The reason for the inaccurate approximation of the stress is related to the simplification as determined in step 2 of Section 4.2. Therefore, the stress is calculated in Grasshopper.
- The geometry is considered to be simple. Therefore, analysis using scale elements is not necessary because of the simplicity of the model. The model can be represented by sets of rectangles. Scale models are mostly used for complex shaped elements.

To conclude, the SCIA 2D plate model will be used to represent the print path geometry in the development of the model described in this thesis project. This decision is made based on the model simulation intent and the results of the comparison presented in Figure 40. After choosing the model representation, the next step is to determine the geometric setup of the representative model.

Because of the printing process, in sections, the configuration of a plate as multiple sections is used in this research project. Using multiple 2D plate elements to create the global geometry ensures a smooth transition between plate elements. This configuration allows for accurate control of input values at section interfaces and therefore can approximate the behaviour of a 3DPC bridge. Another benefit of this configuration is the ability to accurately control the curvature along the span in the horizontal and vertical direction. Therefore, the 3DPC bridge is represented as a plate structure existing of multiple 2D plate sections with varying cross-sectional properties in the span direction. The result of the representative model in SCIA is presented in Figure 41.

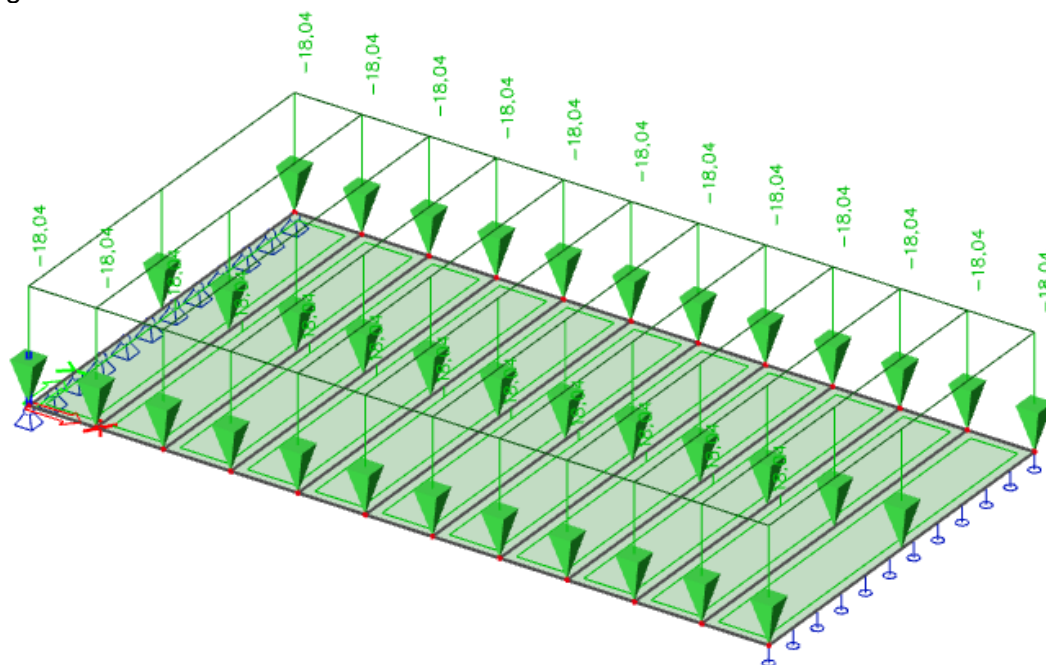


**Figure 41; 2D plate model existing of multiple elements exported from SCIA Engineer**

After selecting the representative model, the equation and solver method used in SCIA Engineer 2D plate sections can be documented. In SCIA Engineer, and other FEA software, a matrix based calculation procedure is used to numerically calculate the structural response to loads on the structure. The relation between the structural response and the load on the structure is determined by the stiffness matrix. The

content and calculation procedure of this matrix can vary between FEA packages and representative models. The finite element analysis performed in a SCIA Engineer 2D plate model uses Matrix notation  $K \times u = F$ . In this equation; K is the stiffness matrix, u is the displacement matrix and F is the force matrix. The displacements are measured in the nodes of the generated finite element matrix. The displacement matrix contains lateral and rotational displacements. The equation in matrix notation is presented below in Figure 42.

$$\begin{bmatrix} M_x \\ M_y \\ M_{xy} \\ T_x \\ T_y \end{bmatrix} = - \begin{bmatrix} D_{11} & D_{12} & 0 & & \\ D_{21} & D_{22} & 0 & & 0 \\ 0 & 0 & D_{33} & & \\ & & & D_{11} & D_3 & 0 & 0 \\ 0 & & & 0 & 0 & D_{22} & D_3 \end{bmatrix} \cdot \begin{bmatrix} w_{xx} \\ w_{yy} \\ 2w_{xy} \\ w_{xxx} \\ w_{yyx} \\ w_{yyy} \\ w_{xxy} \end{bmatrix} \quad \begin{matrix} (1- \\ 6) \end{matrix}$$

**Figure 42; Relation between force and displacement in a SCIA Engineer 2D plate model**

The values of the stiffness matrix entries in Figure 42 are calculated using equations presented in Figure 43. These equations are retrieved from the SCIA helpdesk using following link; [https://help.scia.net/download/16.0/en/OtrhotropTB\\_enu.pdf](https://help.scia.net/download/16.0/en/OtrhotropTB_enu.pdf)

$$D_{11} = \frac{E_1 h^3}{12 (1 - \mu_{12} \mu_{21})}, \quad D_{22} = \frac{E_2 h^3}{12 (1 - \mu_{12} \mu_{21})}$$

$$D_{12} = \mu_{21} D_{11} \equiv D_{21} = \mu_{12} D_{22}$$

$$D_{33} = G_{12} \frac{h^3}{12}$$

$$D_3 = 2D_{33} + D_{12} = 2D_{33} + D_{21}$$

$$\mu_{21} = \mu_{12} \frac{E_2}{E_1} = \mu_{12} \frac{D_{22}}{D_{11}}$$

$$G_{12} = \frac{\sqrt{E_1 E_2}}{2 (1 + \sqrt{\mu_{12} \mu_{21}})}$$

**Figure 43; Stiffness matrix equations used in a SCIA Engineer 2D plate model**

The system of equations is solved based on the Cholesky decomposition method. The solution method is based on decomposition of a matrix into the product of a lower triangular matrix and its conjugate transpose.

### 3. Export to finite element software

In collaboration with SCIA Engineer representatives, it was determined that import and export procedures can be developed by trial and error. The first step used to determine



the requirements for import/export using xml is to create a model in SCIA Engineer. After specifying the desired content of the model, the model is exported as xml file. When exporting the xml file a certain amount of options can be specified for export. The required options for import are determined using different export settings and importing the resulting xml files. If the imported xml file results in the correct model than that xml file can be used in the design model. This process resulted in the following list of requirements for importing a model as xml file in SCIA Engineer:

1. Model properties
  - a. Code definition file that specifies tables and table contents as specified in the xml file. Critical for import in SCIA Engineer.
  - b. Data structure of the xml file is required in UTF-16
2. Project information
  - a. Function of the model, in this project structural analysis model
  - b. Codes and standards, in this project Eurocode & Dutch national database
3. Material properties
  - a. The name of the material
  - b. The modulus of elasticity to determine the deflection
  - c. The density of the material
  - d. The Poisson's ratio
4. Load cases
  - a. Name of load combination
  - b. Dominant load case
5. Load groups
  - a. Name of load group
  - b. Loads associated with a certain loading case
6. Nodes
  - a. Name and number of the node
  - b. Location based on the x, y and z coordinate
7. 2D element
  - a. The name and number of the element
  - b. The nodes that define the edges of the element
  - c. The material of the element
  - d. The start/end height of the element
  - e. The direction of the change in height
8. Boundary conditions
  - a. Name and location of boundary condition
  - b. At the beginning of the first section and at the end of the last section
  - c. The movement restrictions imposed by the boundary condition
9. Load definition
  - a. The name of the load
  - b. The element the load is applied on
  - c. The direction of the load
  - d. Since SCIA is not able to model load varying along the span it is important to model the load as the average value between two section interfaces.

Another aspect encountered by trial and error is the numbering of the nodes. It is important for a tapered geometry that the nodes are numbered per side. This means that, when using 11 elements, the nodes in the X-direction that are closest to the coordinate  $Y=0$  are numbered 1 to 12 in the X-direction (see Figure 44). SCIA Engineer does not automatically use the correct numbers of the node for the variation of the height along the span. Even if the correct numbers are specified in the xml script, for

the nodes that should be used for the tapered direction, SCIA Engineer will pick the numbers closest to each other, based on the X-value of numbers. The result of the incorrect numbering of the nodes results in an incorrect direction of the variation of the height. The standard numbering and corresponding stepwise shape of the cross-section is presented in the bottom of Figure 44. The proposed numbering method results in a smooth transition of the height of sections along the span. The result of this method is presented in the top of Figure 44.

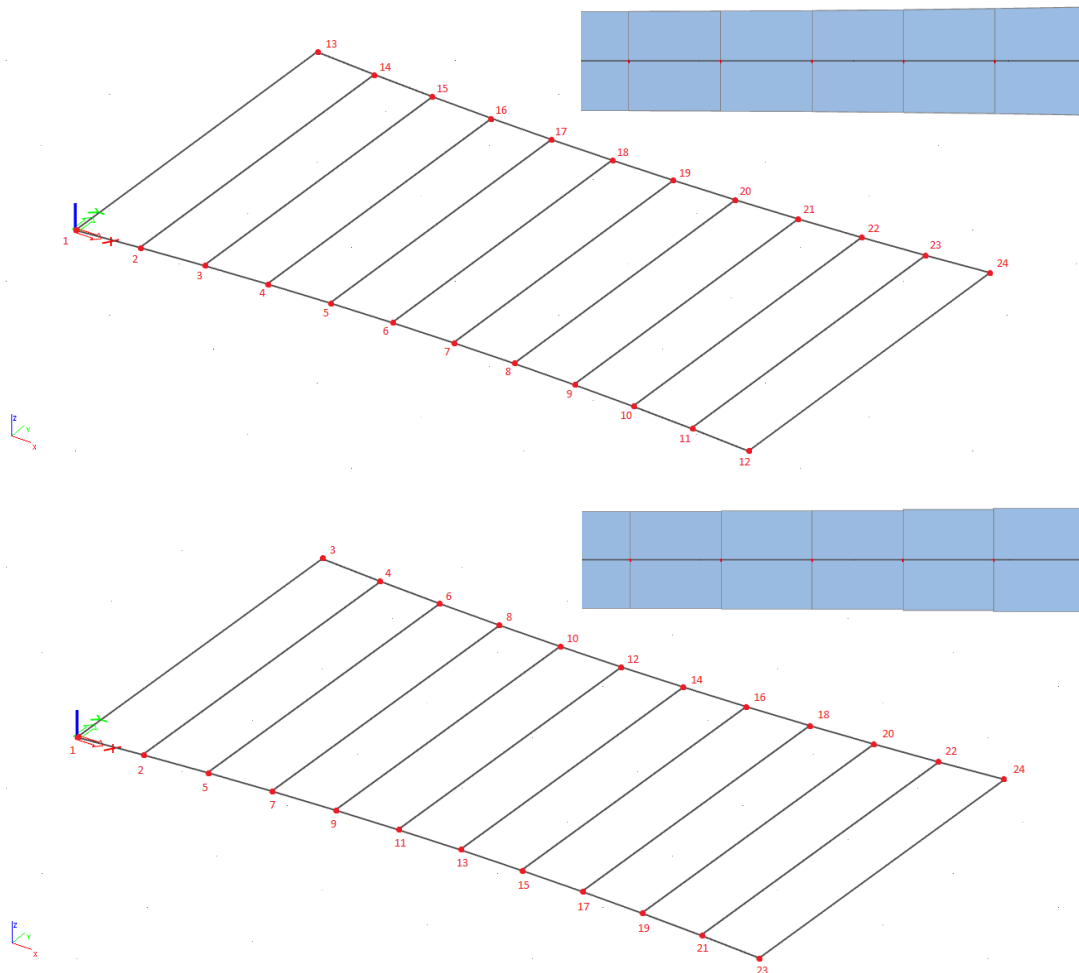


**Figure 44; Above; correct numbering of the nodes and its result – Below; incorrect numbering of the nodes and its result**

A full description of the xml file is presented in Annex D. Data generated and described in this section is used for the validation of the Gemert design case. Conform to the model simulation intent, the information that can be generated in the Grasshopper model is not limited to generating the specific data described in this section.

#### 4. Structural analysis using finite element software

As mentioned in step 4 of Section 4.3, this step describes executing structural analysis in FEA software controlled in parametric software (in this project Grasshopper). Python components are used in the Grasshopper script to execute the structural analysis in SCIA Engineer. In total three Python components are used in Grasshopper to execute the structural analysis in SCIA Engineer. The function of the components are listed below. Because these components have a high amount of similarities in content, only

one component is visualised in this section. The developed Grasshopper script and its components are presented in Annex A. Following Python components are used;

1. Export xml component
  - a. Connects the geometric and structural information to the correct location in the xml file
  - b. When pressing the execute button the component performs its function and writes the xml export file in a specified directory
2. Pre-calculation check
  - a. Removes txt files generated in previous calculations
  - b. This component is used to avoid using the wrong results
  - c. When pressing the execute button the component performs its function. The component deletes the txt files in a specified directory with the same name as the files generated in the SA in SCIA Engineer
3. Execute calculation
  - a. This component specifies the command file created in step 4 in Section 4.2 to execute the calculation in SCIA Engineer without interface
  - b. When pressing the execute button the component performs its function and generates four txt files for importing the results to Grasshopper.
  - c. This component is presented in Figure 45

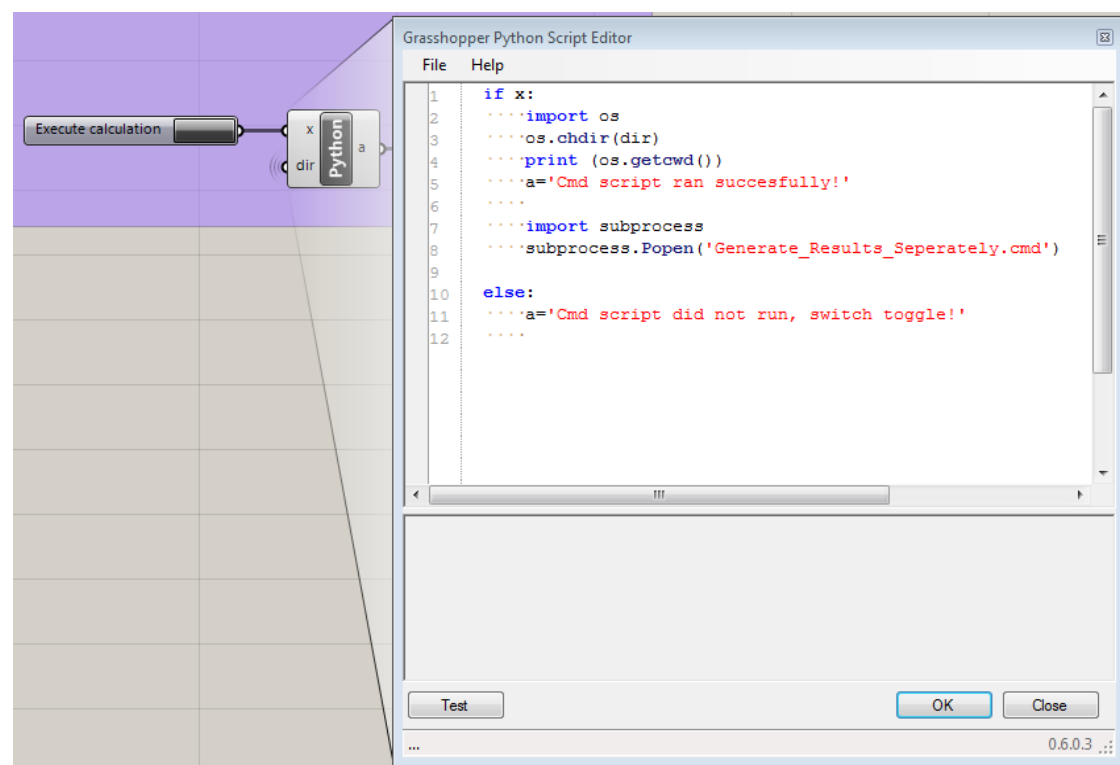


**Figure 45; Python component, Python script and execute button used in Grasshopper**

The command file that the Python component runs is presented in Figure 46. The same commands are used as described in step 4 in Section 4.3. However, the chain of commands is specified 4 times because of output separation using SCIA Engineer. If the output is specified in one template file, the resulting txt output document exists all four internal force distributions required for the structural analysis. These txt files are difficult to correctly interpret in Grasshopper. Therefore, the output is generated separately. This is performed by generating four template files that generate the four required output data for the structural analysis.

```

set esaprog="C:\Program Files (x86)\Scia\Engineer17.01\esa_xml.exe"
C:
cd "C:\Users\karel.van.dongen\Google Drive\Thesis\Calculations\Final results\XML"

%esaprog% LIN "_Template_mx.esa" "SCIA Export.xml" -tTXT -o"GH_Model_Results_mx.txt"
%esaprog% LIN "_Template_vx.esa" "SCIA Export.xml" -tTXT -o"GH_Model_Results_vx.txt"

%esaprog% LIN "_Template_Msup.esa" "SCIA Export.xml" -tTXT -o"GH_Model_Results_Msup.txt"
%esaprog% LIN "_Template_Rz.esa" "SCIA Export.xml" -tTXT -o"GH_Model_Results_Rz.txt"

```

**Figure 46; Command file created for calculating the structural behaviour in SCIA Engineer without an interface**

### 5. Result interpretation

Data generated in the previous step is exported as txt files. These files are linked to a Python component that translates the data to a usable format. The component and the execute button have a similar setup as the calculation component in Figure 30. The import component reads the output txt files in a specified directory. After reading the plate values in the txt files, the values are specified in four lists. Each of the lists contains the information for a specific internal plate force. These values are used to calculate the reaction force on the structure. This is performed using the equations presented in step 5 of Section 4.3. After calculating the reaction forces on the structure, the verification of structural resistance is performed. As described in step 5 of Section 4.3, three resistance verifications are performed. The first verification is the stress resistance, the second is the shear strength verification and the third is the loss of post-tensioning force due to time dependent behaviour of concrete. These verifications are modelled in Grasshopper and therefore are automatically updated if the imported txt files are changed in the specified directory. The design verification check is performed by a unity check for the stress and the shear in the structure. The equations used for performing the unity checks are presented in Equations 14.1-14.3. The presented formulae are based on NEN-EN-1992-1-1 and NEN-EN-1992-2 (section 6.1 and 6.2).

$$UC_{tension} = \frac{Max\ tension}{f_{ctd}} \leq 1,0 \quad (14.1)$$

$$UC_{compression} = \frac{Max\ compression}{f_{cd}} \leq 1,0 \quad (14.2)$$

$$UC_{shear} = \frac{Max\ shear\ force}{V_{rd}} \leq 1,0 \quad (14.3)$$

In the Grasshopper model the UC is performed as a mathematical inequality condition. If the value of the reaction force is lower than the resistance the panel connected to the inequality will read "true". This means that if the control panels all read the word "true" that all structural safety verification indicate the design value of the load is lower than the design value of the resistance. Results of the model are displayed in Table 2.

Description	Specification	Load	Resistance	Unit	UC	Safety
Stress	σ <sub>ed,top</sub>	-2,86	-11,20	N/mm <sup>2</sup>	0,26	<1,0
Stress	σ <sub>ed,bot</sub>	-0,61	0,69	N/mm <sup>2</sup>	-0,80	<1,0
Shear	V <sub>ed</sub>	205,18	302,33	kN	0,68	<1,0
Tension loss	P <sub>m,0</sub>	158,94	-	kN	-	-

**Table 2; Results calculated using the design model and verification of structural safety**

This completes the development of the structural analysis component for the design model. The accuracy of the results are calculated in Section 6.2.



# 5 Environmental analysis

As mentioned in Section 1 and 2.3, the function of the environmental analysis component is to determine the impact of a design. The environmental impact can be calculated using geometric quantities calculated in Section 3. These geometric quantities are combined with environmental impact indicators to determine the impact of quantities used.

Before the environmental impact can be estimated, it is important to determine why the environmental impact should be estimated. This will provide information required for determining which indicators should be used. The next step is to link the indicators to design output of the design model developed in this research project.

After determining the current level of impact, this research project addresses possibilities to mitigate the estimated level of impact. These possibilities will mainly focus on reducing materials and reusing the structure or parts of the structure. The reason for using these methods are described in the Section 1.2.

The obtained results and the developed mitigation measures will be used to conclude on the application possibilities of the design model and its impact on the environmental impact of the design.

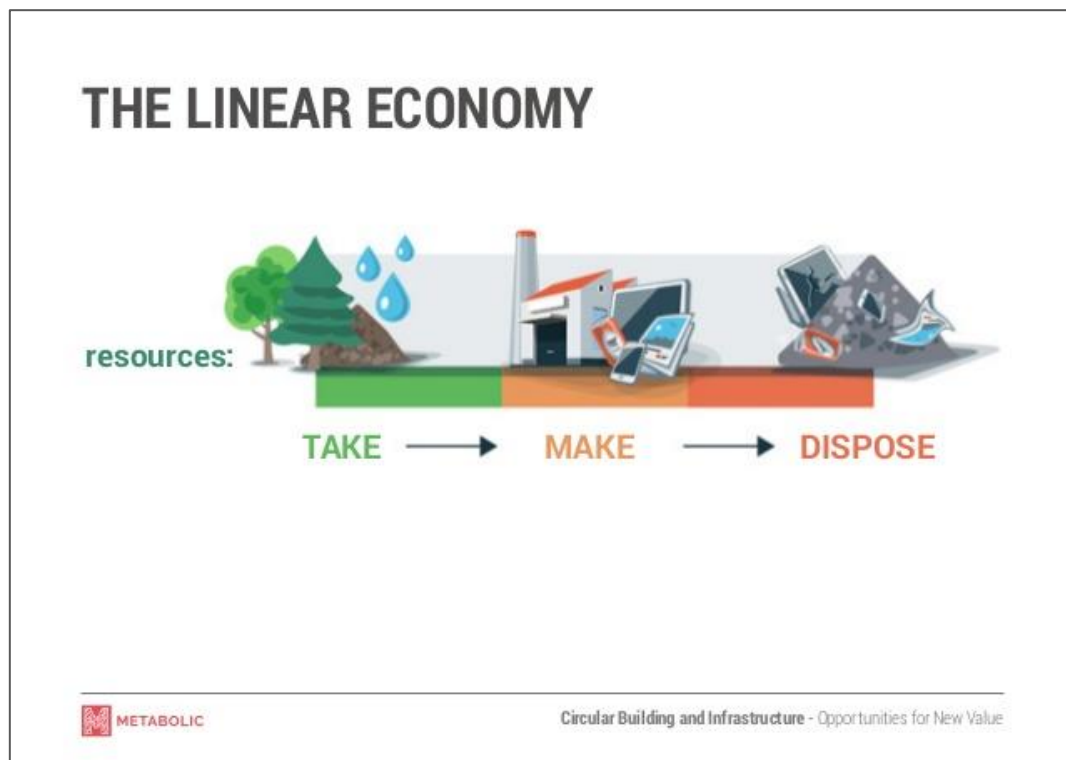


Figure 47; Graphic representation of the current construction economy - [63]

## 5.1. Towards sustainable construction

A definition of sustainable construction can be derived from the definition of sustainable development as determined by the Brundtland commission in 1987. According to the commission sustainable development is *“the kind of development that meets the needs of the present without compromising the ability of future generations to meet their own needs”* [64]. Therefore, sustainable construction can be described, by substituting the word development in the definition of sustainable development for construction, as *“the kind of construction that meets the needs of the present without compromising the ability of future generations to meet their own needs”*.

The book of John Elkington “Cannibals with Forks” describes three main aspects which sustainable construction can affect/benefit. These three categories are people, planet and profit (PPP principle) [65]. The people aspect addresses the importance of social fair and beneficial practices of sustainable development. The planet aspect refers to sustainable environmental practices. The profit aspect deals with the economic value for all entities created by sustainable developments. In the application of sustainable construction in this thesis project, the emphasis is on the planet category of the PPP principle. This category is also referred to as the environmental impact. The environmental impact can be sub-divided into 11 impact categories [66]. Each of these impact categories addresses a specific pollution aspect related to an equivalent measured element. One of the impact categories, used by the European government, is the global warming potential (GWP) which is measured in the amount of CO<sub>2</sub> emission [19]. As described in the introduction one of the European objectives, related sustainable construction, is to limit the emission of green house gases (GHG) such as CO<sub>2</sub>. The GWP environmental impact category can be an indicator for the level of the environmental impact of a structure. The identified eleven impact categories are;

1. Abiotic depletion (non-fuel)	per kg Antimone
2. Abiotic depletion (fuel)	per kg Antimone
3. Global warming potential	per kg CO <sub>2</sub>
4. Ozone layer depletion	per kg CFC-11
5. Photochemical oxidation	per kg Ethene
6. Acidification	per kg SO <sub>2</sub>
7. Eutrophication	per kg PO <sub>4</sub> (3-)
8. Human toxicity	per kg 1,4-dichloro benzene
9. Fresh water aquatic ecotoxicity	per kg 1,4-dichloro benzene
10. Marine aquatic ecotoxicity	per kg 1,4-dichloro benzene
11. Terrestrial ecotoxicity	per kg 1,4-dichloro benzene

Based on research it is possible to quantify the equivalent measured element of a product or process per impact category. These quantities can then be used to determine the shadow price of the product/process. According to the “Shadow prices handbook” published by CE Delft, *“a shadow price can be defined as the infinitesimal change along an objective function e.g. arising from an infinitesimal change in a constraint”* [67]. In other words the shadow price represents the costs required to bring the environmental impacts of a product or process to an acceptable ‘sustainable’ level [66]. The value of the shadow price is calculated using a conversion rate related to the impact categories. These conversion rates are based on studies that are focused on quantifying the environmental damage inflicted by the impact categories. The conversion rates therefor depend on the latest studies and thus are time-dependent. Because the conversion rates are time-dependent they should be updated when new values for the conversion rate are determined.

Shadow costs can be used in combination with Life Cycle Analysis (LCA) to generate information regarding the environmental impact of a structure. The LCA

process consists of three steps [68]. The first step, goal and scope, defines purpose, objectives, functional units and system boundaries. The second step, inventory, consists of collecting, describing and verifying all data regarding input, processes, emissions, etc of the whole life cycle. The third step, quantification, combines the first two steps to list the environmental impacts and used resources. Therefore, the LCA process can be used to couple functional units, such as shadow costs, to develop an inventory of environmental impact of structures throughout the multiple cycles of the life cycle. It can also be used to identify which phases, of the structure's total life cycle, a material and/or process affects. Applying LCA methods to the civil engineering (CE) industry can be useful for determining the environmental bottleneck of the construction process. A study performed by Cabeza et al [17] gives insight into a few environmental bottlenecks of the CE industry;

- Ecotoxicity in CE structures is mainly related to road salting run off, potentially resulting in the pollution of groundwater.
- Production and transportation of materials used in road construction projects result in significant environmental burdens. Especially materials that are used in a single life-cycle of a structure.
- Example of an asphalt pavement project that used 15% recycled asphalt and warm mix asphalt. Resulted in the decrease of climate change potential, fossil-depletion and cumulative energy demand of 13-14 %.

Another design driven objective in sustainable construction material is the application of self-healing agents to structural concrete. According to the study of H.M. Jonkers, application self healing agents to concrete can increase the concrete durability [69]. The self healing agents become activated by water ingress in cracks, in concrete, after which they start to multiply and precipitate minerals such as calcite ( $\text{CaCO}_3$ ). further research can determined if these agents can be used to increase strength of the parent material [70]. Besides improving the materials, the application of the material can also be altered to increase the durability of the material. Designing materials for multiple life cycles makes it possible to use the same structure (or parts of the structure) in multiple life cycles, thus increases the durability. A similar approach is seen in modular construction (MC) practices. MC is a construction principle that uses separation of functional elements to increase the on-site erection time and reduce construction waste [71]. As a result the structure can be divided into parts that can be used for multiple life cycles in similar structures assembled using similar components. According to the literature study performed by Kamali and Hewage [72], this specific application of MC can contribute to an increased level of environmental performance. In their study the following contributions result in the increased performance:

- Reduction of waste generation
- Potential for waste management
- Less disturbance on-site (noise and dust)
- Efficient land resources used
- Reduction in GHG emission

Application of modular construction can also result in a reduction of erection costs/time, increased productivity and product quality [72]. Modular construction can be used to incorporate flexibility and adaptation in a product/process which, according to the presentation of Eva Gladek at Infratech 2017, is one of the transition steps towards a circular building & infrastructure industry [63]. The word circular is related to the definition of circular economy by the Ellen MacArthur Foundation who defined circular economy as *“an industrial economy that is restorative or regenerative by design”* [73].



In other words, a circular setup of the construction industry can be seen as a method to reduce construction waste by using process output, such as construction waste, as a secondary resource. Currently the circularity of the construction sector and built environment is estimated as 6% [74]. This estimate suggests that about 94% of the output of the construction sector and built environment is currently disposed. Below listed principles of circularity are applicable to this research project [63];

1. Dematerialisation; reduce the amount of materials of similar functionality
2. Impact reduction; decrease the environmental impact of materials/processes
3. Design for flexibility and adaptation; increase product/process value by preparing for multi-purpose applicability
4. Design for disassembly; reduce the required amount of resources and effort required at the end of a life cycle
5. Multiple values from single assets; create added value to a process/product by integrating multiple functionalities

These principles will be used to determine, reduce and compare the environmental impact of multiple bridge-deck desing configurations. Application of these principles to the construction industry can result in an increased involvement of governmental organisations, industrial actors and clients. The increased involvement can result in increase in knowledge of sutainable construction practices. Ultimately this contributes to transitioning to a more circular and more sustainable construction industry [74].

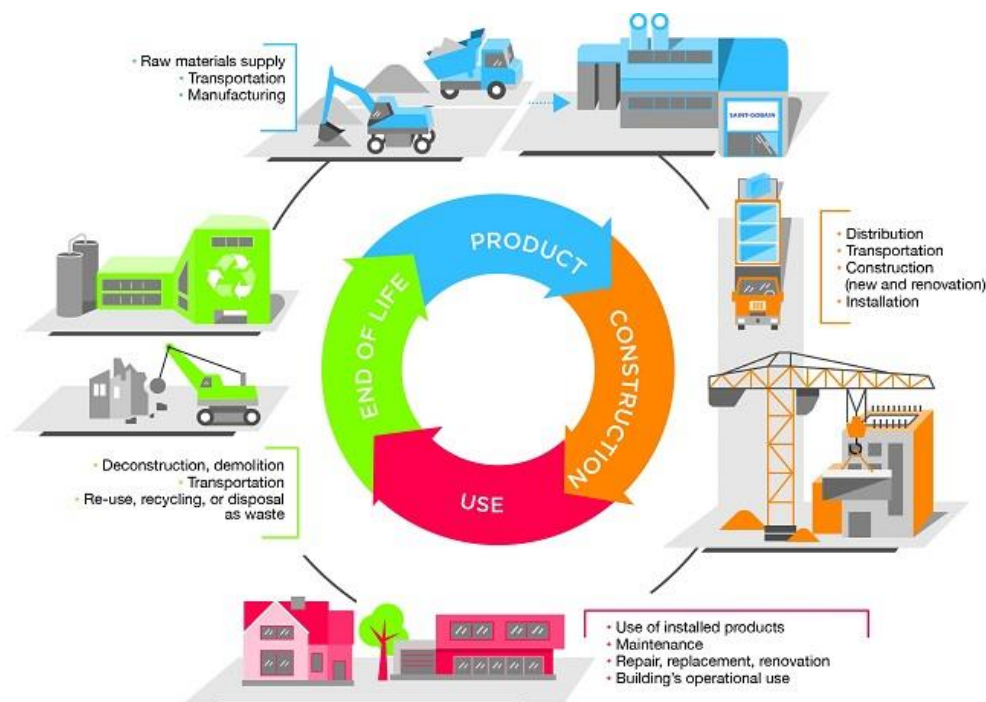


Figure 48; Graphic representation of a circular built environment - [75]

## 5.2. Component methodology

As determined in the previous section, the model should determine, reduce and compare the environmental impact of multiple design configurations. Therefore, the process of generating information regarding the environmental impact of the model contains three steps;

1. Determine the current impact level of the design; link the design output (volumes, dimensions) to environmental impact indicators (shadow costs)
2. Reduce the impact of the design; determine the effect of changes in geometric/material values on the environmental impact
3. Reuse the design; design for changes in the use of the structure and thereby increase end of life applicability

### 1. Indication of environmental impact

The environmental impact of the designed configuration of the model can be calculated as the sum of three steps; the raw materials used, the production process and the transport of elements. The first step is visualised in Figure 49.

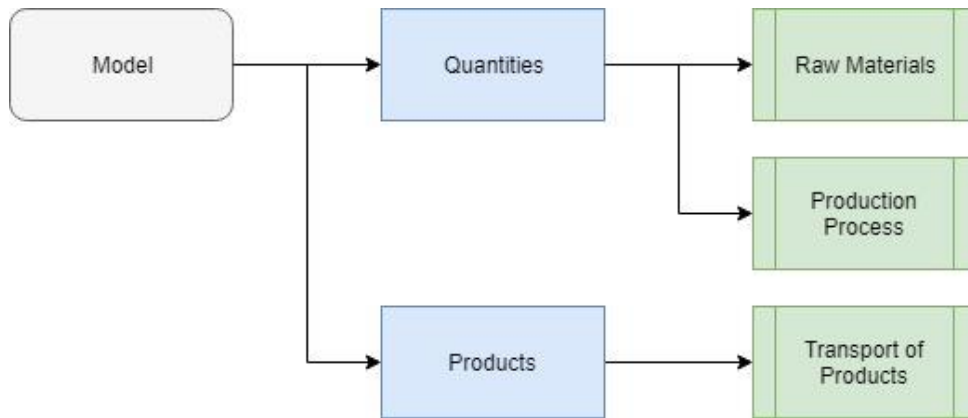


**Figure 49; Flow chart for determining the environmental impact**

The impact of the raw materials depends on the values of the quantities of materials which are calculated in the model by using volumetric calculation components in Grasshopper. These components calculate the concrete volume, the tendon volume and determine the length of the print path. The calculated quantities are linked to a multiplication element, thereby connecting a specific quantity to the shadow cost conversion rate of that specific item. This process is automated in grasshopper and the value is changed as the shape of the geometry is changed. The shadow cost conversion rate is calculated as the sum of the product of the impact equivalent unit and the related cost estimate of all eleven categories, indicated in Section 5.1 (see Equation 15).

$$CR_{shadow\ cost,i} = \sum_{i=1}^n (Equivalent\ Unit_i \times Shadow\ Price_i) \quad (15)$$

The calculated shadow cost conversion rates can be multiplied with the quantities in the model to determine the cost. The resulting formula is presented in Equation 16.

$$Shadow\ Cost_{Raw\ materials} = \sum_{i=1}^n (Q_i \times CR_i) \quad (16)$$

The impact of the 3D printing process is calculated based on the 3DPC volume. The value of the volume is the same as used to calculate the impact of the raw material.

This value can be connected to process energy use values determined by BAM Infraconsult. The energy use per m<sup>3</sup> is then coupled to the shadow cost related to energy use. The obtained shadow cost is used to determine the environmental impact of the production process related to the required energy for the specified volumetric quantity of 3DPC. Because of the relatively new application of 3D printing in concrete, an accurate value for indication of the effect of the print time on the energy use is not available. Therefore, the process impact will be limited to the indication based on the printed quantity. The resulting formula is presented in Equation 17.

$$\text{Shadow Cost}_{\text{process}} = \text{Energy use} \times CR_{\text{Energy use}} \quad (17)$$

The transport costs are calculated using the dimensions of the printed sections obtained from the model. Two transport scenarios are considered for calculating a transport scenario based on the restrictions of transport vehicles. The first scenario transports the section modules in the height direction of the section. The second scenario transports the section modules in the width direction of the section. The required amount of vehicles is calculated using the dimensions of the section modules, the weight of the section modules and the capacity of the transport vehicles. The calculated amount of vehicles is linked to the fuel index of the transport type. The calculated fuel usage is used to determine the fuel required for the transport scenarios. The calculated required fuel is used to estimate the shadow cost of the transport of the sections using the conversion rate for fuel presented by the NDEI. The calculated shadow cost therefore is related to a specific combination of section module, vehicle and transport scenario. The workflow of calculating the transport cost is presented in Figure 50.

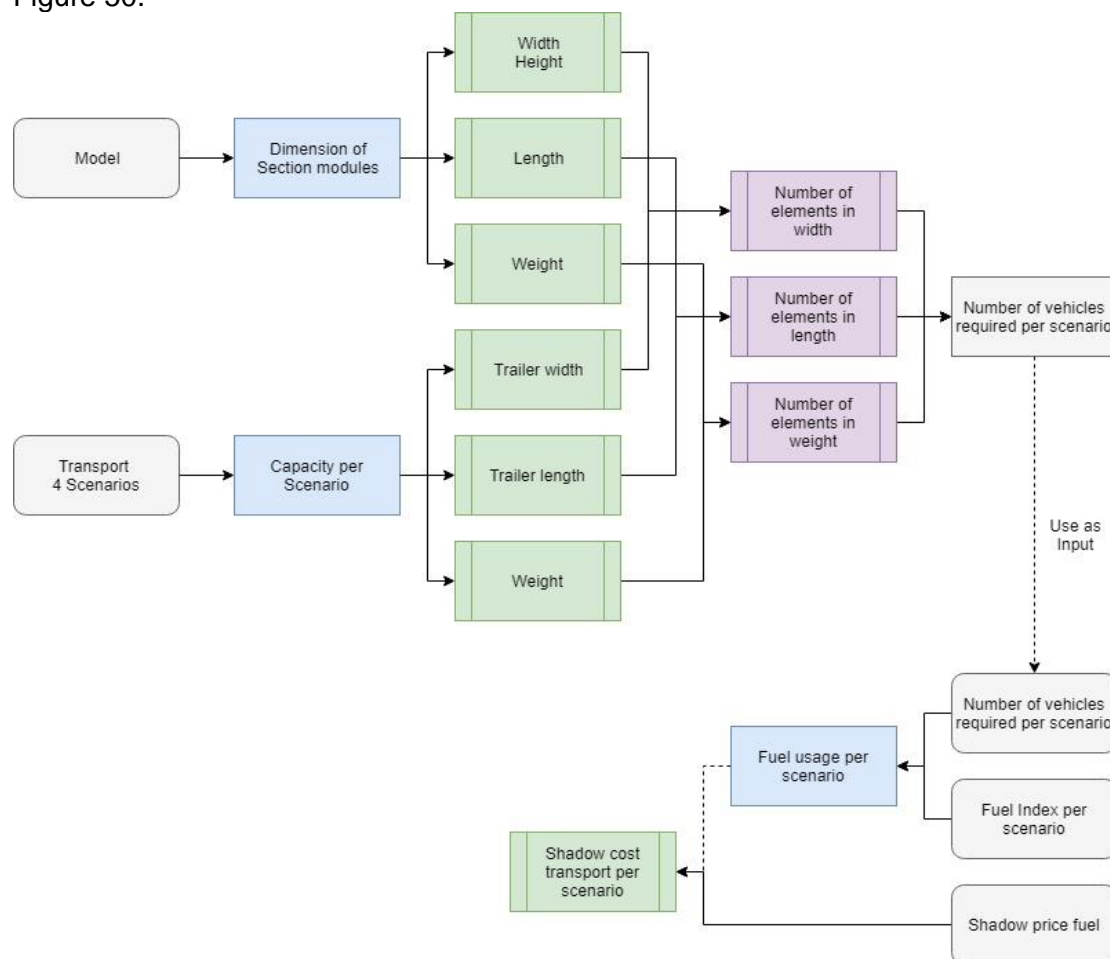


**Figure 50;** Flow chart for determining the shadow cost related to transport of final product

The sum of the calculated values is used to indicate the estimated environmental impact of specific combination of parameters used in the model. This values is automatically updated with changes in the parameters. Therefore, the process of indicating the current level of impact of the design is completed. The influence of changing parameters will be discussed in Section 6.3 and compared for multiple combinations of parameters.

## **2. Reduction of impact**

The impact indication procedure described in the first step is used to determine the impact of changes in the combination of parameters. Changing the material, for example, can result in a reduction of required material if a higher strength grade is used. Another option is to change the shape of the cross-section along the span. As discussed in Section 4.2. the structural efficiency can be increased by applying only the required amount of materials at the required location. This method can result in a reduction of material use and therefore in a reduction of the environmental impact of the design. Based on the method described in this section, an automated tool is created that calculates the effect of changes in parameters on the environmental impact. Therefore, a reduction in environmental impact is automatically calculated by adjusting parameters. The effect of adjusting parameters is described in Section 6.3. This completes the reduction of impact methodology used in the model.

## **3. Design for reusability**

Another method used to reduce the impact of a structure is design for multiple future applications. This can be achieved by separation of function of elements in the structure. Separating elements based on function is an established method in architecture. The first person who described and applied this principle is Le Corbusier, a famous French architect. In his vision of “the Five Points of New Architecture” he describes a separation between the exterior and the structural function, in the third point [76]. The same principle can be applied to the design of concrete bridges. In designing for adaptability of bridges, two main functions can be identified; primary systems (structural resistance) and secondary systems (aesthetics). The primary system fulfils the requirements for the use of the bridge in a certain application. The secondary system fulfils the aesthetical requirements for a specific application. Separating these systems can result in reuse of the primary system for multiple applications by combination with multiple secondary systems. Reusing parts of the structure results in an elongation of the life cycle of the structure. Therefore, reusability can result in a lower environmental impact over time. In the environmental analysis component, the following steps are used to create a secondary structure.

1. In the model, the appearance of the design can be adjusted by using a component that creates a secondary structure. The first step of generating the secondary structure is to identify the edges of the primary structure. Based on these edges, the starting points of the secondary structure are identified by a specified distance from the primary structure and a required number of points.
2. By connecting the above identified points, a set of lines is created. These lines are used to create the inner layer of the secondary structure. The shape of the secondary structure is based on the distance between the inner and the outer layer which is generated by an offset component. In this thesis project two offset components are developed; a linear interpolation- and a sinusoidal-component. The offset component moves points in a direction and pattern based on the specified input. The outer layer is connected to the inner layer, creating a surface between the inner and outer layer of the secondary structure. These surfaces are connected to create the volume of the secondary structure.

In the described separation of primary- and secondary-structure, the secondary structure is developed to fulfil specific requirements regarding the exterior shape of the model. The configuration of the secondary structure is project-specific. Therefore, the exact value of input parameters of the secondary structure is not presented in this research project. To create a specific shape of the secondary structure, the following input should be specified in the design model:

1. Distance between the primary structure and inner layer of secondary structure
  - a. In width direction
  - b. In height direction
2. Shape configuration
  - a. Sinusoidal
  - b. Linear interpolated
3. Symmetrical setup
  - a. Yes
  - b. No
4. Distance between inner and outer layer of secondary structure
  - a. Start
  - b. Mid-span
  - c. End
  - d. Both sides of the model separately
5. Number of secondary offset elements along the span
  - a. Number of sinusoidal periods
  - b. Number of linear-interpolated sections

The resulting volume of the secondary shape is used to calculate the material required for the secondary structure. Because the secondary structure has no structural function it is not required to use reinforcements or post-tensioning. Therefore, the quantity of secondary material can be directly linked to a shadow price to calculate the shadow cost of including a secondary structure. The benefit of designing for adaptability is hard to quantify because the benefit relies on the amount of life cycles the primary structure can fulfil. This topic will be further elaborated Section 6.3.

This completes the description of the environmental analysis component. To conclude, this section described;

- The method of generating the shadow cost related to the material input/process requirements of a combination of parameters.
- The method of determining the effect of changes in the geometry on the calculated environmental impact.
- The method of developing a component that uses a separation in function to design the structure for adaptability to multiple applications.

## 5.3. Application of the methodology

### 1. Indication of environmental impact

The shadow prices and equivalent units indicated using Equation 15 are based on values used from the national database of environmental impact (NDEI). The values, presented in the database, are provided by the organisations “Nationale MilieuDatabase” and “Stichting Bouwkwiteit”, in the Netherlands. These organisations specialise in governing the use of the database and keeping the values up to date. The specific version used in this thesis project is the database of September 2016 (see Annex F). The exact environmental impact of the 3DPC mixture is not known/shared with BAM, therefore an estimated impact value is used. The estimated impact value provided by Prof.dr.ir. H.E.J.G. Schlangen. Based on this value, the estimated difference in the environmental impact of a 3DPC mixture is 1,50 times higher than the mixture of a traditionally cast concrete mixture of the same strength class. This estimate will be used in section 5.3 to compare the results between the impact of 3DPC and traditionally casted concrete.

The values for the process impact are provided by BAM Infraconsult. The energy used for preparing the mixture for printing is 32 kWh per m<sup>3</sup> and the energy used for the actual printing is 93 kWh per m<sup>3</sup>.

The information used to determine the capacity of transport vehicles is presented in Annex F. The combinations of truck types and trailers for transport are based on a Eurocode document regarding transport on public roads (see Annex F). The fuel index used to calculate the shadow cost is based on a document published by Volvo that indicates the fuel use of 4 categories of trucks (see Figure 51).

Typical fuel consumption in litres per 100 km				
	Payload in tons	Total weight in tons	litres / 100 km empty*	litre / 100 km full load*
Truck, distribution traffic	8.5	14	20-25	25-30
Truck, regional traffic	14	24	25-30	30-40
Tractor and semi-trailer, long-haul traffic	26	40	21-26	29-35
Truck with trailer, long-haul traffic	40	60	27-32	43-53

**Figure 51; Fuel index based on a publication of the Volvo company - [77]**

### 2. Reduction of impact

The impact indication procedure described in step 2 of Section 5.2 is modelled in Grasshopper. This step does not require additional input other than described in step 2 of Section 5.2. As mentioned, the impact of adjusting parameters on the environmental impact is presented in Section 6.3. Therefore, no further elaboration is required in this step.

### 3. Design for reusability

Based on the description of the model functions and parameters the following input is used in the visualisations presented in this section.

1. Distance between the primary structure and inner layer of secondary structure
  - a. In width direction 0,10 [m]
  - b. In height direction 0,20 [m]
2. Shape configuration
  - a. Sinusoidal yes [-]
  - b. Linear interpolated yes [-]
3. Symmetrical setup
  - a. No



4. Distance between inner and outer layer of secondary structure
  - a. Start 0,20 [m]
  - b. Mid-span 0,05 [m]
  - c. End 0,10 [m]
  - d. Both sides of the model reversed setup
5. Number of secondary offset elements along the span
  - a. Number of sinusoidal periods 20 [-]
  - b. Number of linear-interpolated sections 20 [-]

Based on the methodology presented in step 3 of Section 5.2, the result of the first phase of the secondary structure is a set of points. This set of points is generated using the described data. The generated set of points are presented in Figure 52.

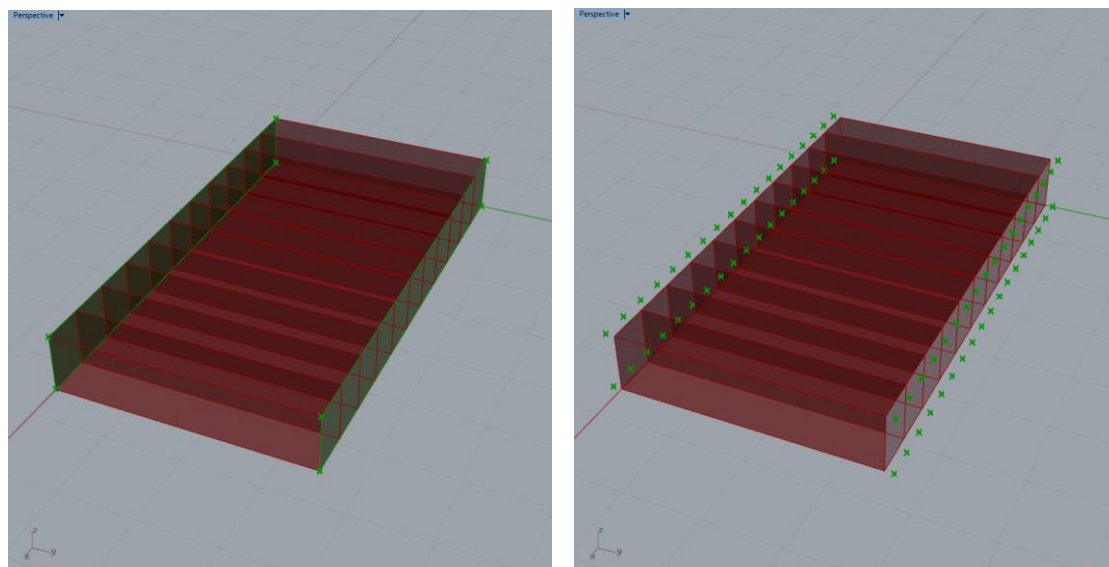


**Figure 52; Left; identified edges of the primary structure in green – Right; generated start points in green**

The shape of the secondary structure is generated based on the set of start points created in the previous phase. In the description of the development, the linear interpolated and the sinusoidal secondary structure are visualised (see Figure 53). To show the possible options, the model is setup as non-symmetric in two directions. The displacement pattern used to create the shape is reversed in two directions. The top and bottom displacement are reversed, top starts at  $x=0$  and bottom starts at  $x=L$ . The left and right side are reversed. The  $y=0$  side starts with the max displacement and  $y=b$  side ends with the max displacement specified in the beginning of this step (see Figure 53).

The component developed in this section is used to generate information regarding the environmental impact of the design. The generated information will be used in Section 6.3 to compare the influence between combinations of parameters and to conventional production methods. This completes the description of the developing the environmental analysis component for the design model.



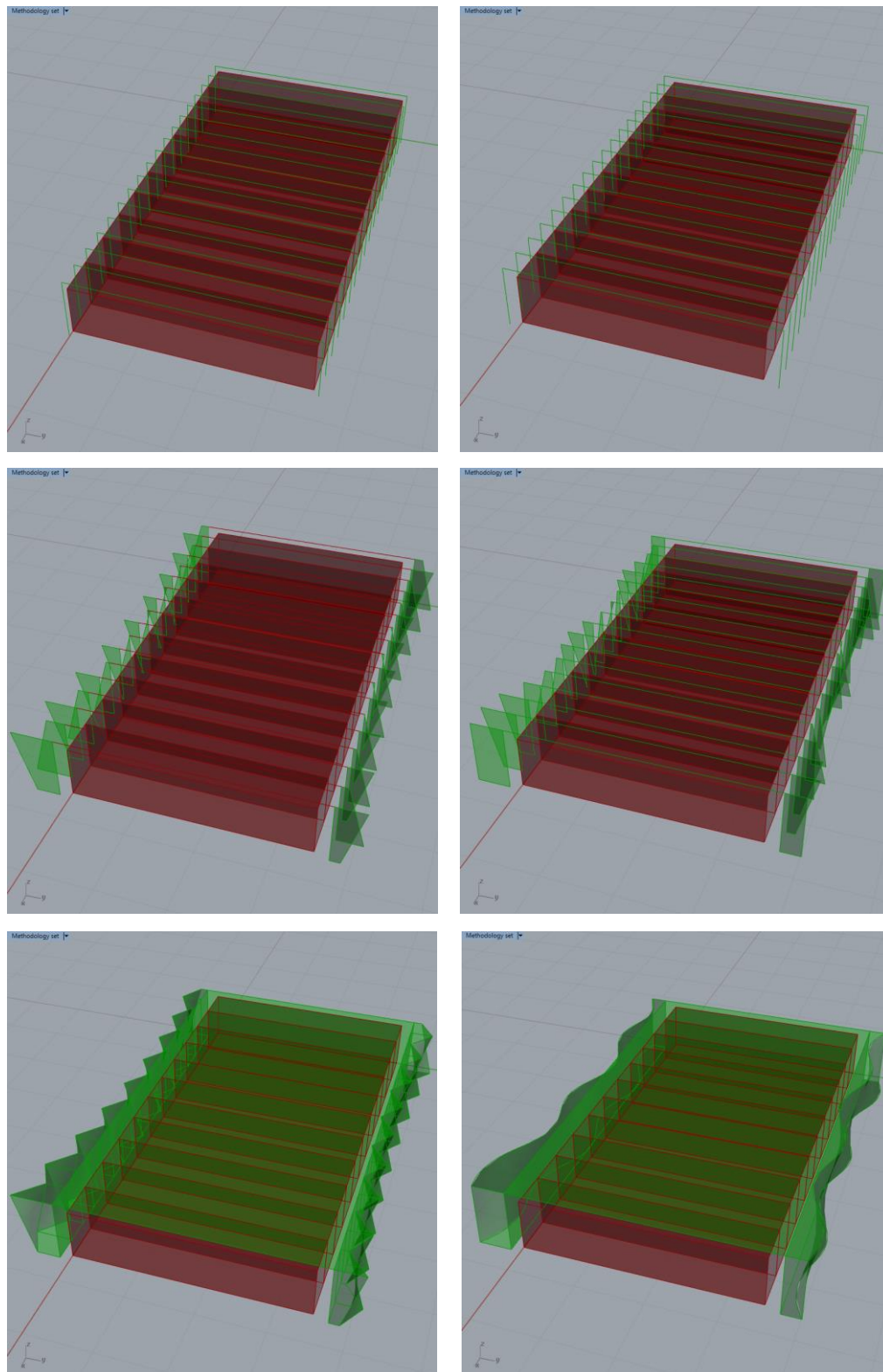


**Figure 53; Left side, top to bottom; inner layer, secondary shape and volume in the linear interpolated configuration – Right side, top to bottom; inner layer, secondary shape and volume in the sinusoidal configuration**



## 6. Model analysis

The components described in Chapter 3, 4 and 5 are used to generate data. This data is used to determine the structural efficiency and environmental impact of a 3DPC bridge. A parametrical setup of a design process allows the process to develop multiple design configurations that can be verified using the same model. However, it is important to determine the accuracy of the results generated by the design model before using results of the design model. A possible method to validate obtained results is by comparison to a benchmark problem. If the simulation of the test case fulfils the accuracy check, the results generated for other designs are assumed to be accurate as well, in the range of applicability of the model.

Because the application of 3DPC in infrastructure and civil engineering is rather new, few test cases exist to validate the accuracy of the model. The most comparable test case is the Gemert design. However, the results of this test case are not public and therefore cannot be used to validate the results of the design model. For this reason, a calculation control document, in excel, is created in this research project. This document, described in Section 4.3 and 4.4, will be used to verify the results of the design model in Grasshopper. Because the excel model is based on calculation procedures described in Eurocode NEN-EN-1992-1-1 and NEN-EN-1992-2, the results of the Excel document are assumed to be accurate.

Once the model accuracy has been validated, the difference between the results can be discussed. The results of the comparison can be used to reflect on the possibilities of using the design model and the options for further development. If the design model produces accurate results it can be used to determine the relation between the structural efficiency and the environmental impact. The structural efficiency is calculated as the material utilisation rate of the load and the resistance of the sections in the structure. Determining the result between structural efficiency and environmental can be used to reflect on the potential benefit of applying 3DPC in the construction industry (see Section 1.1 and 1.2).

If the model does not produce accurate results, this chapter will reflect on the changes that should be applied to correct the approach. After the correction have been applied and the model produces accurate results, the same approach will be used as mentioned before. Possible inaccuracies of the design model are used to indicate the restrictions of using the design model.

## 6.1. Model accuracy

As described in the introduction of Chapter 6, the verification method used in this research project is a comparison to a manually performed calculation. The manual calculation is performed in Excel. The methodology used to develop the document is the same as the methodology used to develop the structural analysis component of the design model (presented in Section 4.3 and 4.4). The methodology is based on Eurocode document NEN-EN-1992-1-1 and NEN-EN-1992-2 sections 5.10, 6.1 & 6.2 as presented in Section 4.2. The manually performed calculation control document does not use simplifications in the calculation procedure. Therefore, this is assumed to be an accurate method for performing the design verification based on the simulation intent presented in Section 2.2.

There can be multiple reasons for differences in results between the design model and the calculation control document. This section aims to address these reasons and thereby reflect on the accuracy of the design model and the used components. The first identified deviation in results is related to the calculation process of the cross-sectional properties. This deviation is a result of the simplifications and therefore conversion factors used to calculate cross-sectional properties. The difference between cross-sectional values generated using the method described in step 5 of Section 3.2 and the values generated by the design model are presented in Figure 54. The deviation of the cross-sectional values presented in Figure 54 are expressed in a percentage. This is chosen for determining the expected deviation of the model because percentage based deviations can be summed into an expected total deviation.

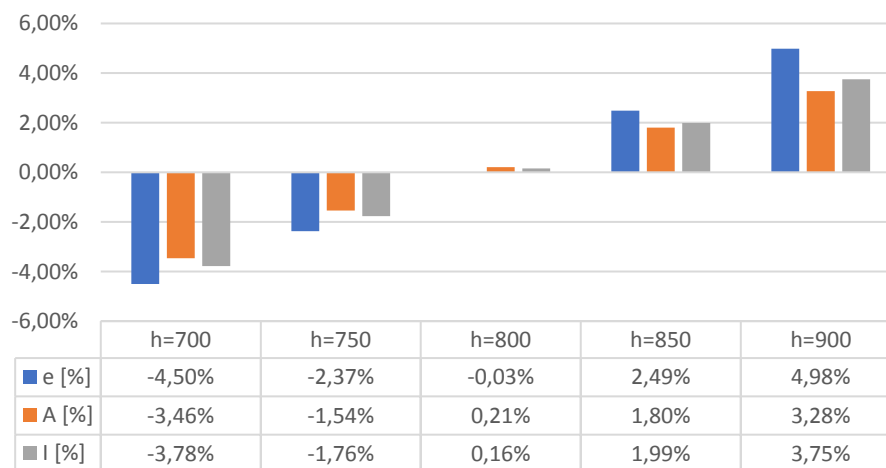


**Figure 54; Calculated accuracy of the conversion rate method**

As presented in Figure 54, the cross-sectional properties calculated for the Gemert design case (h=800 mm) will deviate 0,11% in average and up to 0,34% in total. In other words, the impact of the results is affected before any calculations are performed. Therefore, the total result deviation is expected to increase related to deviations of other input used in the SA. Based on the values presented in Figure 40, the deviates of the analysis at least -0,40% and -0,80% at most. Therefore, the total expected variation is at least -0,29% and -0,46% at most. This value is based on accuracy estimations of model simplifications. The indicated expected deviation is not based on a comparison between generated data and the calculation control document.

The Gemert design case (height=800 mm, width=3,50 m and length is 6,50 m) is used to determine the accuracy of the design model. The developed design model generates the design verification performed in the Gemert design, as described by

T.A.M. Salet et al in their publication in the “Virtual and Physical prototyping” journal. A comparison between the extreme values of the model and the control document is presented in Table 3.

Description	Unit	Control document	Design model	Difference [-]	Difference [%]
q	kN/m	18,03	18,04	0,01	0,06%
M	kNm	333,27	332,06	-1,21	-0,36%
V	kN	205,09	205,18	0,09	0,04%
max S	N/mm2	-2,84	-2,86	-0,02	0,70%
min S	N/mm2	-0,62	-0,61	0,01	-1,61%

**Table 3; Comparison of the obtained results**

Based on the results of the comparison the following observations are made;

- The difference in the values does not relate to the expected deviation determined in the beginning of this section.
- The reaction forces calculated by the model are considered as less favorable than the values presented in the test case.
- The percentage based difference of the minimum stress is higher than expected. However, this is related to the low value of the minimum stress.
- Therefore the model results in a safe and accurate approximation of the structural behaviour in the deck section.

Besides comparing the results it is also important to validate the results of the FEA. A simple method to validate the results is done by confirming boundary conditions/sanity checks and value/unit control. The following checks can be performed on the obtained results;

- The bending moment at the supports should be zero because the supports are not able to resist rotations.
- The total support force should approximately be  $\frac{1}{2} \cdot b \cdot l \cdot q = 0,5 \cdot 6,5 \cdot 18,03 = 205,09$  kN.
- The internal bending moment at mid-span should approximately be equal to  $1/8 \cdot q \cdot l^2 = 0,125 \cdot 19,21 \cdot 6,5^2 = 95,22$  kNm/m.
- The Gemert design is symmetrical in the width (at  $y=b/2$ ) and in the length (at  $x=l/2$ ) of the model. Therefore, the calculated internal forces should be symmetrical in these axes as well.

Msup [kNm]			Vsup [kN]		
Mesh Element	1	11	Mesh Element	1	11
1	0	0	1	32,81	32,81
2	0	0	2	48,54	48,54
3	0	0	3	42,48	42,48
4	0	0	4	48,54	48,54
5	0	0	5	32,81	32,81
			Total	205,18	205,18

**Table 4; Support reactions calculated in SCIA Engineer**

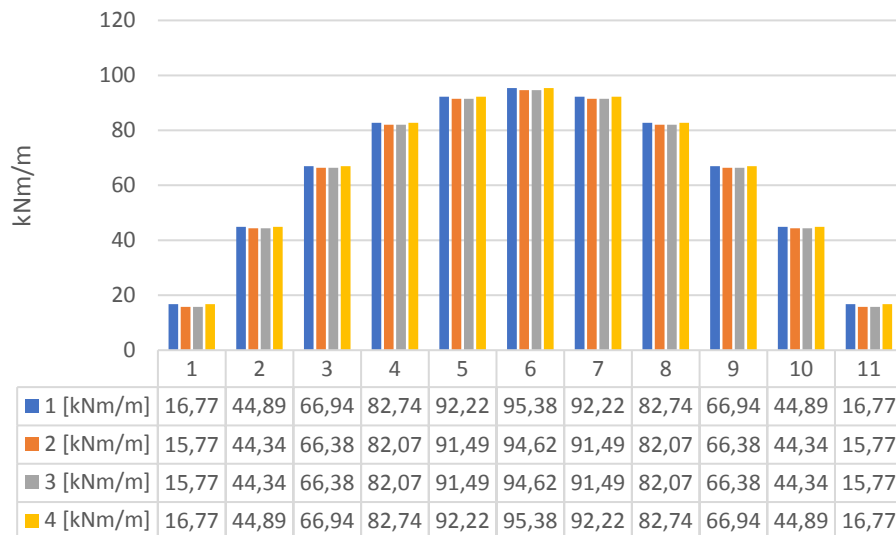


**Figure 55; Internal moment distribution calculated in SCIA Engineer**

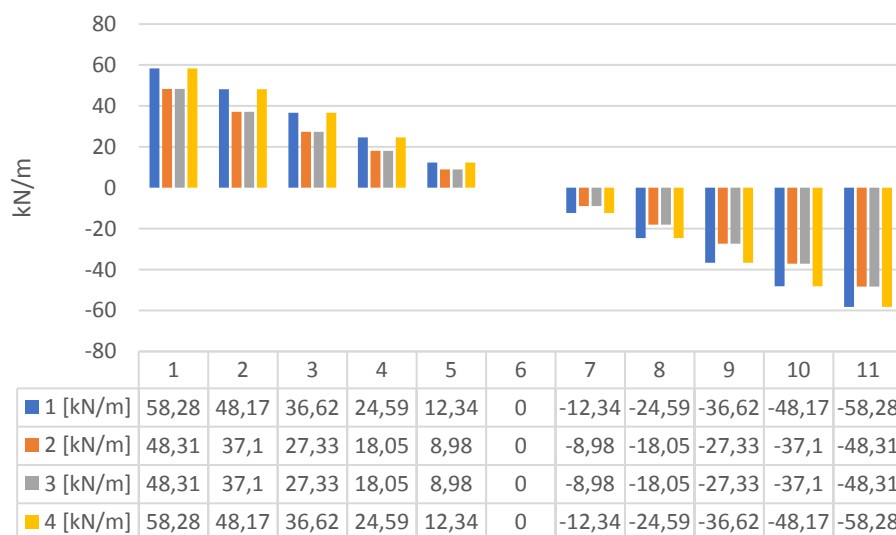


**Figure 56; Internal shear force distribution calculated in SCIA Engineer**

Based on the results presented in Table 4 and Figures 55 and 56, the following observations are made regarding the accuracy of the FEA;

- The bending moment at the supports is as expected; there is no bending moment.
- The support force at the supports is approximately equal to the expected value.
- The bending moment at mid-span is approximately equal to the expected value.
- The internal forces show a symmetrical pattern in width & length of the model.

Other results generated by the model result in similar behaviour compared to the results generated using the controll document.

- The required total amount of post-tensioning force calculated by the model is 158,94 kN (in tension) per tendon (total of 2543,00 kN). The required amount of post-tensioning force calculated in the control document is 155.52 kN, the accuracy of the approximation therefore is 0,022%. This value is a bit higher and therefore is on the safe side.

- The stresses calculated in the control document are  $-2,84 \text{ N/mm}^2$  in the top fibre and  $-0,62 \text{ N/mm}^2$  in the bottom fibre. The values calculated in the design model are  $-2,86 \text{ N/mm}^2$  in the top fibre and  $-0,61 \text{ N/mm}^2$  in the bottom fibre. The model values slightly differ from the control document values. The value in the top fibre is a bit higher while the value in the bottom fibre is a bit lower.
- The shear force calculated in the control document is  $205,09 \text{ kN}$ , which is exactly the same as the value calculated in the sanity check. The value calculated in the design model is  $205,18 \text{ kN}$ . This value is slightly higher than the control document value and therefore is on the safe side.

The accuracy of the developed model is determined by comparison to a manually performed calculation document based on Eurocode. The comparison of the results generated by the design model and the control document indicate that using the design model results in a good approximation of design values, the difference is smaller than 10%. The FEA model results in reliable values for internal forces. As mentioned before, the loads and reaction force/stress values generated by the model are approximately equal to the values in the calculation control document. Therefore, it is concluded that the model results in an accurate and safe approximation of the structural behaviour. As a result, it is possible to determine the structural efficiency based on the utilisation ratios calculated in the design model.



## 6.2. Structural efficiency comparison

After determining the accuracy of the design model, the next step is to test the effect of the geometry on the structural efficiency. This is done by comparing possible scenarios and their effect on the structural efficiency. The first goal of the result verification process is to test whether the calculated forces are within the acceptable range of the resistance. The second goal of the result verification process is to determine the effect of changes in the geometry on the material utilisation ratio. It is possible to comment on the efficiency of the application of the material by comparing multiple utilisation ratios. A high utilisation ratio indicates that the value of the structural resistance is close to the load applied on the structure. A low utilisation ratio indicates that the value of the structural resistance is higher to the load applied on the structure. Therefore, a low utilisation ratio can indicate that the material efficiency is low and the structure can be considered as overdimensioned for the designed application.

Both objectives can be tested simultaneously by running the model for multiple combinations of parameters. However, testing all possible options of a model is a time consuming process due to the number of possible combinations. The total amount of options for adjusting the geometry is equal to  $6 \times 8 \times 2 \times 6 = 567$  combinations (6 main, 8 section distortion, 2 smooth/kinked, 6 sinusoidal). A limit case study can be used to reduce the amount of combinations. A limit case study only considers the combinations of parameters that result in the most unfavourable value of the resistance. Engineering assumptions can be used to reduce the number of limit cases that should be verified. Below listed assumptions are used to make a selection of limit case combinations.

- The mid-section determines the tensional stress compliance which in this design is a critical design check. Reducing the height and width of the mid-section reduces the section modulus and therefore increases the stress.
- The start & end section are critical for the shear force resistance. Decreasing the height of these sections reduces the shear modulus and therefore the shear resistance.
- The span-length increases the load, therefore the longest possible length results in the highest possible load.
- The option for kinked/smooth and sinusoidal lines influence local geometry. However, the model simplification only considers the section interfaces and therefore does not account for local differences in the geometry. These options therefore are not considered to affect the structural resistance. This influence is further elaborated in the model restriction section.

As described in Section 2.2, a goal of the project is to determine the influence of the printed geometry on the structural behaviour. Therefore the calculation and model conditions used in the limit cases are chosen similar to the original design. This includes variables such as the material properties, the post-tensioning and the loads acting on the sections. Based on these criteria four limit cases are considered for the result verification (see Figure 57).

1. Modified Gemert
  - a. Length is increased to 7,00 m
  - b. Width is reduced to 3,00 m
  - c. Height is reduced to 0,75 m
2. Maximum inwards distortion of the mid-section
  - a. Height of the mid-section is reduced to 0,375 m
  - b. Width of the mid-section is reduces to 2,740 m
  - c. Other variables are equal to the modified Gemert setup

3. Upwards and flat distortion
  - a. The top coordinate at mid-span stays at 0,750 m high
  - b. The bottom coordinate at mid-span is moved to 0,187 m high
  - c. Other variables are equal to the max inwards setup
4. Minimum shear resistance at start/end
  - a. Height of the start/end section is reduced to 0,372 m
  - b. Other variables are equal to the modified Gemert setup

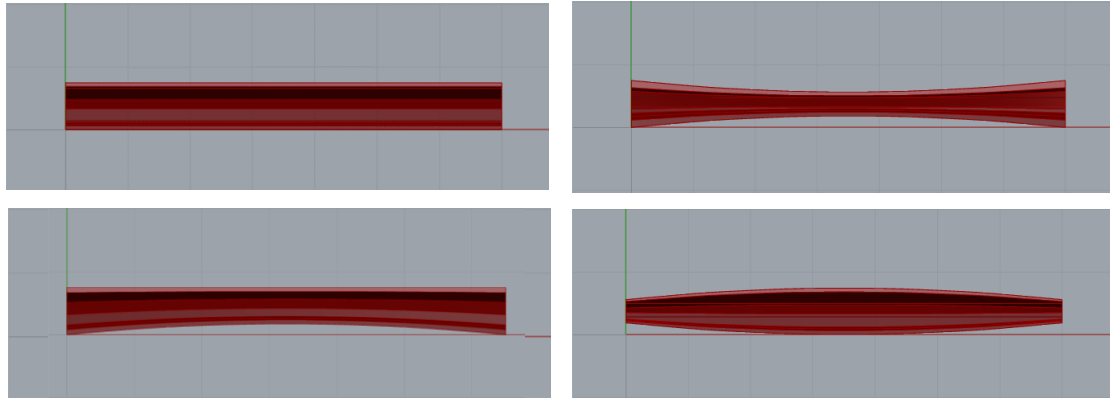


**Figure 57; Top left; Limit case 1 – Top right; Limit case 2 – Bottom left; Limit case 3 – Bottom right; Limit case 4**

The limit case variables are entered in the model after which the limit case entry is processed according to the procedures determined in the methodology section. The main goal of the limit case study is to obtain extreme stress and shear values from the model. As mentioned in the engineering assumptions, the limit case studies should provide feedback for the influence of the geometry on the desired values. Changing the geometry along the span also influences the tendon design, in particular the tendon eccentricity, and the eccentricity of the 3DPC section. The value of the tendon and 3DPC section eccentricity should therefore be part of the limit case study. The load, resistance and eccentricity values of the of the limit case study are presented in Table 5. In Table 5 the location is indicated by a number, 0 represents the value of the first and last section interface and 1 represents the mid-span section.

Model	Location	Unit	Control doc	LMC1	LMC2	LMC3	LMC4
<b>M</b>	1	kNm	332,060	320,190	236,098	266,531	345,873
<b>V</b>	0	kN	205,180	183,220	143,900	158,140	185,880
<b>Comp</b>	1	N/mm2	-2,860	-3,360	-10,391	-5,174	-2,938
<b>Tens</b>	1	N/mm2	-0,610	-0,200	2,695	0,456	-0,124
<b>Vrd</b>	0	kN	301,220	223,120	170,305	176,946	123,862
<b>h</b>	0	m	0,800	0,750	0,750	0,750	0,327
<b>h</b>	1	m	0,800	0,750	0,374	0,681	0,750
<b>ec</b>	0	m	0,022	0,021	0,021	0,022	0,021
<b>ec</b>	1	m	0,022	0,021	0,021	0,266	0,021
<b>ep</b>	0	m	0,028	0,019	-0,236	-0,070	-0,002
<b>ep</b>	1	m	0,028	0,019	-0,236	0,003	-0,002

**Table 5; Result comparison of the limit case study**

After calculating the results, the limit cases should be tested for compliance with the calculation conditions discussed in the SA section of the methodology chapter. This procedure should include three critical design checks, as previously discussed.

Because 3DPC has different resistance values for two directions, perpendicular and parallel to the print direction, the lowest value will be chosen for the verification checks. The lowest resistance value of 3DPC is the resistance perpendicular to the print path. The first design check is the maximum allowable compression which is related to the compression strength of the material. The second design check is the maximum allowable tension which is related to the tensional strength of the material and the 7<sup>th</sup> calculation condition (preferably no tension in the geometry). The third design check is the maximum allowable shear force which is related to the cross-section geometry, the stress in the section and the compression strength of the material.

Based on the identified checks four critical verifications can be performed (see Equations 18.1-18.4). The process of performing verifications is automated in the model. In this thesis project these verifications. The utilisation ratios can be determined based on the four verifications by using the calculated load and resistance values. Since it is difficult to determine the utilisation ratio of a zero-stress criterion only three utilisation ratios are calculated (max compression, max tension and max shear). The results of the utilisation ratios of the limit case study is presented in Figure 58.

$$UR_{Compression} = \frac{\sigma_{max,compression}}{f_{cd}} ; f_{cd} = \frac{f_{ck} \times \alpha_{cc,pl}}{\gamma_M} = \frac{21,00 \times 0,80}{1,50} = 11,20 \text{ N/mm}^2 \quad (18.1)$$

$$UR_{Tension} = \frac{\sigma_{max,tension}}{f_{ctd}} ; f_{ctd} = \frac{f_{ctk} \times \alpha_{cc,pl}}{\gamma_M} = \frac{1,30 \times 0,80}{1,50} = 0,69 \text{ N/mm}^2 \quad (18.2)$$

$$UR_{Shear} = \frac{V_{max}}{V_{Rd}} \quad (18.3)$$

$$\text{Preferably no tension; } \sigma_{max,tension} \leq 0 \text{ N/mm}^2 \quad (18.4)$$

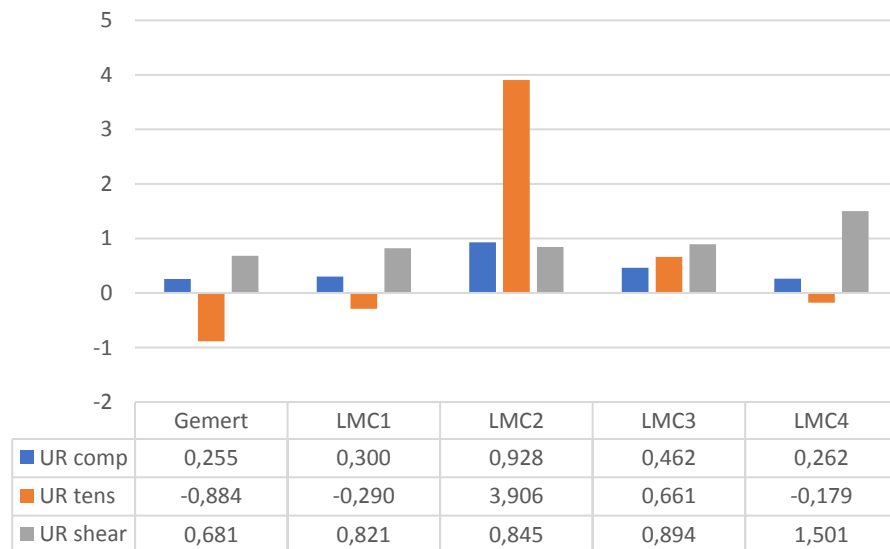


**Figure 58; Utilisation ratio comparison between the limit cases**

Using results presented in table 5 and figure 58, following observations are made based on the limit case study;

- When compared to the Gemert design configuration, limit case 1 results in a similar compression efficiency. However, the tension and shear utilisation ratios are much higher. The decrease in height results in an decreased shear resistance and thus results in a higher shear strength efficiency. The higher tension utilisation ratio is explained by comparing the eccentricity of the tendons in the

two configurations. The eccentricity of the concrete remains relatively unchanged while the position of the tendon eccentricity decreases by 32%. This causes the increase in tensional efficiency while still meeting the requirements for no tension in the model.

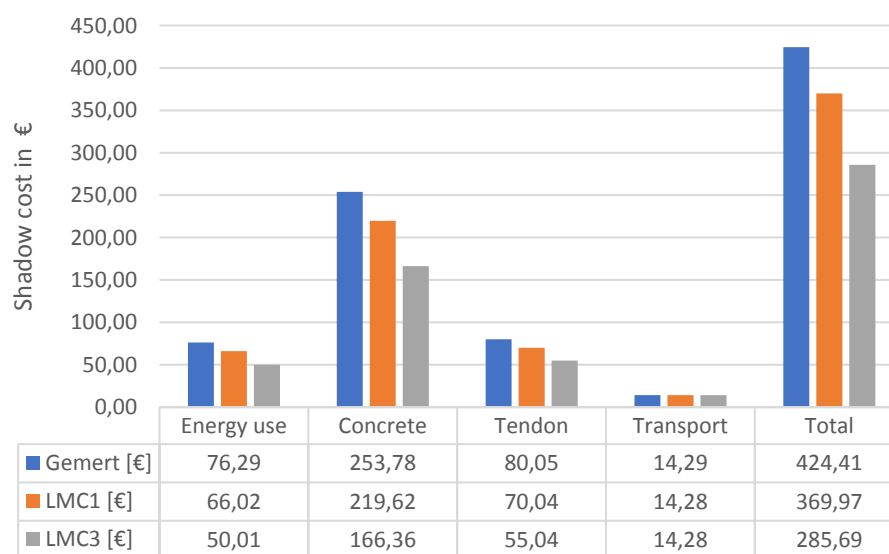
- When compared to the Gemert design configuration, limit case 2 results in a higher compression and shear efficiency. The higher shear efficiency can be explained by considering the lower shear resistance. As presented in formula 12.1, the post-tensioning stress in the sections influences the shear resistance. In this design configuration the tendon eccentricity is negative along the entire span. In this case, the eccentricity negatively influences the shear resistance and therefore increases the shear utilisation efficiency. The same effect is noticed in the tension and compression utilisation. Because of the negative eccentricity, the post-tensioning moment works in the same direction as the loading momentum. This increases the compression and tension in the mid-span section. Since the compression resistance is much higher than the tension resistance, this results in a safe compression utilisation ratio but an unsafe tension utilisation ratio.
- When compared to the Gemert design configuration, limit case 3 results in a higher compression, shear and tension efficiency. The tendon placement results in a low negative eccentricity at the start/end-section and a very low positive eccentricity at mid-span. Therefore, the post-tensioning results in an increased moment resistance in mid-span while not endangering the shear resistance at the supports. This limit case therefore results in the most efficient use of material, when compared to the other limit cases and the Gemert design. However, this limit case fails to meet the requirement for no tension in the model.
- When compared to the Gemert design configuration, limit case 4 results in similar compression and in a higher tension efficiency. The tendon eccentricity at the start is similar while the eccentricity at mid-span is slightly negative. This results in a similar effect of post-tensioning at the supports and an increased tension stress in the bottom of the section at mid-span. Because of the shape of the structure, the amount of material at the supports is much lower than the Gemert design. This results in an unsafe shear utilisation ratio of 1,501. The increased tension in the bottom section at mid-span and the reduced height results in a tension utilisation ratio closer to zero than the Gemert design. Because the compression strength is much higher the utilisation ratio of compression remains relatively unchanged compared to the Gemert design.

These observations are used for discussing the effect of the geometry on the structural efficiency and to determine restrictions of using the model in Section 7.1. The results of the limit case study are used to determine the effect of changes in the geometry on the structural efficiency of the structure.

## 6.3. Environmental impact comparison

The methods described in the Sections 5.2 and 5.3 are used to determine the environmental impact of combinations of parameters. Three design configurations are used to determine the impact of changes in the geometry on the environmental impact. The combination of parameters representing the Gemert design ( $l=6,5$   $b=3,5$   $h=0,80$  [m]) is used as a benchmark result. Two of the limit cases presented in Section 6.2 are compared to the Gemert result (see Figure 59). The two chosen limit cases are limit case 1 and limit case 3. However, the length of the limit cases in the impact comparison is similar. The combination of parameters used for the two limit cases are listed below.

- Limit case 1
  - Length 6,50 [m]
  - Height 0,75 [m]
  - Width 3,00 [m]
- Limit case 3
  - Similar global setup as limit case 1
  - Height at mid-span 0,563 [m]
  - Width at mid-span 2,740 [m]



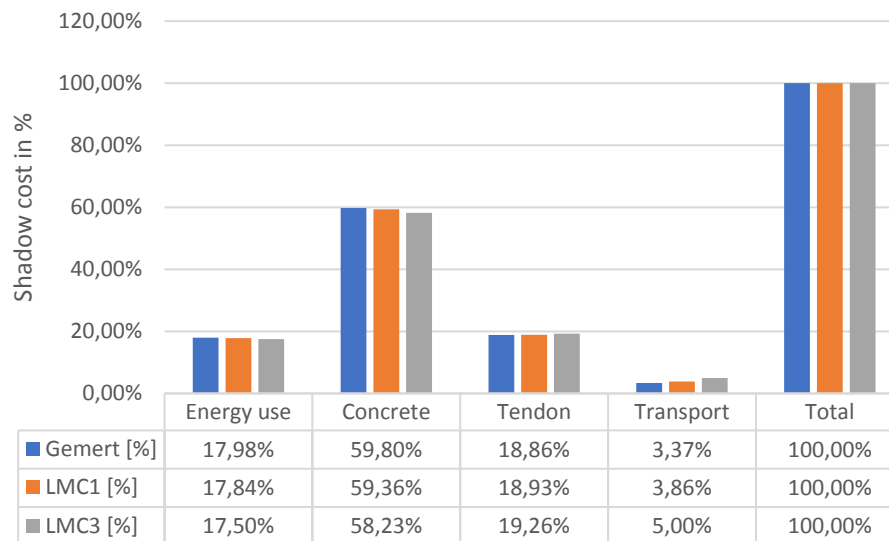
**Figure 59; Comparison of environmental impact expressed in shadow costs**

Figure 59 compares the initial impact of the specified combinations of parameters expressed in shadow cost. These values do not consider the negative impact of customised sections on the reusability of the section modules. However, the results show that a decrease in the dimensions along the span result in a reduction of the initial shadow cost. This is an expected result because a reduction in volumes used in the model should result in a reduction of the initial impact. The conversion rates presented in Table 6 are used to calculate the shadow cost presented in Figure 59.

Shadow cost item	Functional unit	Conversion rate	Largest impact category
Concrete C12	€ per kg	0,007894134	GWP 67,58 %
Pre-stressing steel (average)	€ per kg	0,656817339	Human toxicity 52,26 %
Energy use	€ per MJ	0,018193755	GWP 56,63 %
Transport	€ per l	0,446394021	GWP 60,37 %

**Table 6; Shadow cost conversion rates used in the model, based on the NDEI of 2009**

Another interesting comparison is the variation of the weighted percentage of the impact categories in the different combination of parameters. The weighted percentage compares the specific impact of a measurement to the total calculated impact. Therefore, the weighted percentage can be used to indicate the largest contributor to the total impact (see Figure 60).



**Figure 60; Weighted factor of the calculated impacts**

The largest contributor to the total impact is concrete. The average contribution of concrete to the total calculated impact is 59,13%. The relative contribution of concrete decreases for the three compared combinations of parameters with a standard deviation of 0,60%. However, changing the volume of concrete used in the model results in a low decrease of shadow cost percentage. A similar effect is seen in the contribution of the energy use related to printing the final result. This can be explained by considering the calculation method of the shadow cost related to the use of concrete and the printing process. Both shadow costs are related to the concrete volume calculated in the model (in m<sup>3</sup>). Therefore, their contribution to the total calculated relative impact should vary similarly with changes in the geometry.

A different effect occurs in the weighted percentages of the impact of the transport. Looking at Figure 60, the impact of the transport is similar for all three combinations of parameters while the total impact reduces. The constant transport impact is related to the constant amount of sections and total length of the model. Therefore, the required amount of transport vehicles remains the same, thus resulting in the same impact in all three combinations of parameters. As a result, the weighted percentage will increase because of the decrease in total shadow cost.

The opposite effect occurs in the contribution of the impact of the amount of tendons. The weighted percentage of the tendons increases with a decrease in concrete volume. A small increase in relative impact of 0,07% is measured in the transition from 3,50 m to 3,00 m in width. However, the total shadow cost is reduced by €20,01. A reduction in width at mid-span from 3,00 m to 2,740 m increases the relative impact with 0,33%. However, the total shadow cost of the tendons is reduced by €15,00. The measured shadow cost reduction is related to the amount of tendons in the cross-section. In the Gemert design a total of 16 tendons is used, while in limit case 1 a total of 12 tendons is used and in limit case 3 a total of 11 tendons is used. The increased relative shadow cost is related to a decrease in concrete used in the structure. Because the total cost related to concrete reduces much more than the cost related to the tendons, the relative impact of the tendon on the total impact increases.

As mentioned before, it is difficult to estimate the reduction of the environmental impact related to reusing parts of a structure. This is related to a high amount of factors

influencing the possible reduction. Each of these factors has a related uncertainty factor and by increasing the amount of factors the uncertainty is increased. However, Marit van Lieshout presented an estimated value in her study *“Update prioritering handelingsperspectieven verduurzaming betonketen”*, published by CE Delft in 2015. According to the calculation presented in this study, the reduction in CO<sub>2</sub> emissions related to reusing demountable standardized plate elements is estimated between 0,07 and 0,095 metric ton CO<sub>2</sub> per square meter [78]. This estimate is calculated for reusing hollow-core slab (HCS) elements in residential construction (see Figure 61). From a structural engineering point of view, a HCS is comparable to a 3DPC slab. The application to residential construction is also comparable to the application as a small and single-span pedestrian/cyclists bridge. Both loading cases are symmetric and can be verified for structural safety using linear elastic calculations/safety factors. Therefore, the presented estimate can be used to calculate the estimated reduction in CO<sub>2</sub> emission related to reusing the primary structure.

Omschrijving	Woonhuis	Appartement	
Vrijmaken van vloer uit gebouw	31,6	31,6	€/m <sup>2</sup>
Opslag voor een jaar	2,6	2,6	€/m <sup>2</sup>
Leggen van de hergebruikte vloer	7,65	15,6	€/m <sup>2</sup>
Uitgespaarde nieuwe vloer	-35,00	-45,00	€/m <sup>2</sup>
Onzekerheidsmarge op inschatting meerkosten	20%	20%	%
Ondergrens meerkosten	6,11	12,46	€/m <sup>2</sup>
Bovengrens meerkosten	9,17	18,68	€/m <sup>2</sup>
CO <sub>2</sub> -besparing laag	0,04	0,07	ton CO <sub>2</sub> /m <sup>2</sup>
CO <sub>2</sub> -besparing hoog	0,04	0,095	ton CO <sub>2</sub> /m <sup>2</sup>
Reductiekosten (laag)	152,8	131	€/ton CO <sub>2</sub>
Reductiekosten (hoog)	229	267	€/ton CO <sub>2</sub>

**Figure 61; Calculated CO<sub>2</sub> reduction related to reusing demountable standardized elements - [78]**

Based on the values presented in Figure 61, the reduction of the GWP related to reusing demountable standardised elements is calculated as 0,0825 ton CO<sub>2</sub>/m<sup>2</sup>. The shadow cost related to the GWP is €0,05 per kg CO<sub>2</sub>, as presented in the NDEI. Therefore the shadow cost reduction is estimated at  $0,0825 \times 0,05 \times 1000 = 4,125$  €/m<sup>2</sup>. This value is used to calculate the impact reduction potential of using a modular construction setup (see Figure 62). The calculated reduction only indicates the potential for reuse of the primary structure because the secondary structure is assumed not to be reusable.

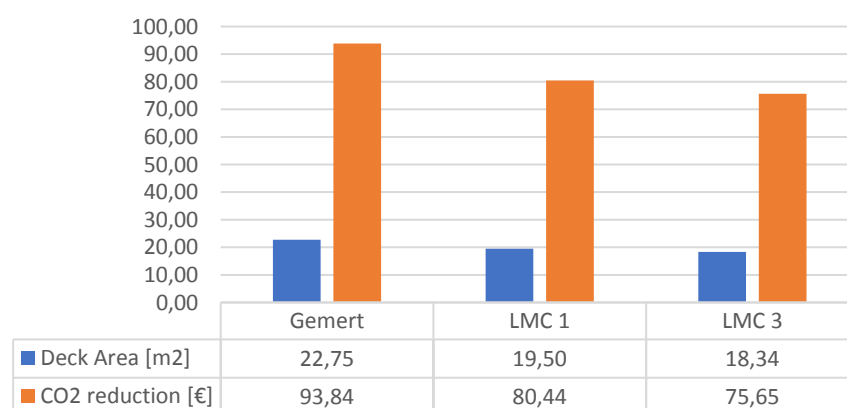


**Figure 62; Comparison between shadow cost reduction of applying modular construction to the project**



A HCS can also be used for the comparison between the environmental impact of 3DPC and traditional construction methods. In the application to this thesis project the HCS represents the traditional construction method. The design curves presented in Figure 63 can be used to indicate the required height of HCS for the designed span.

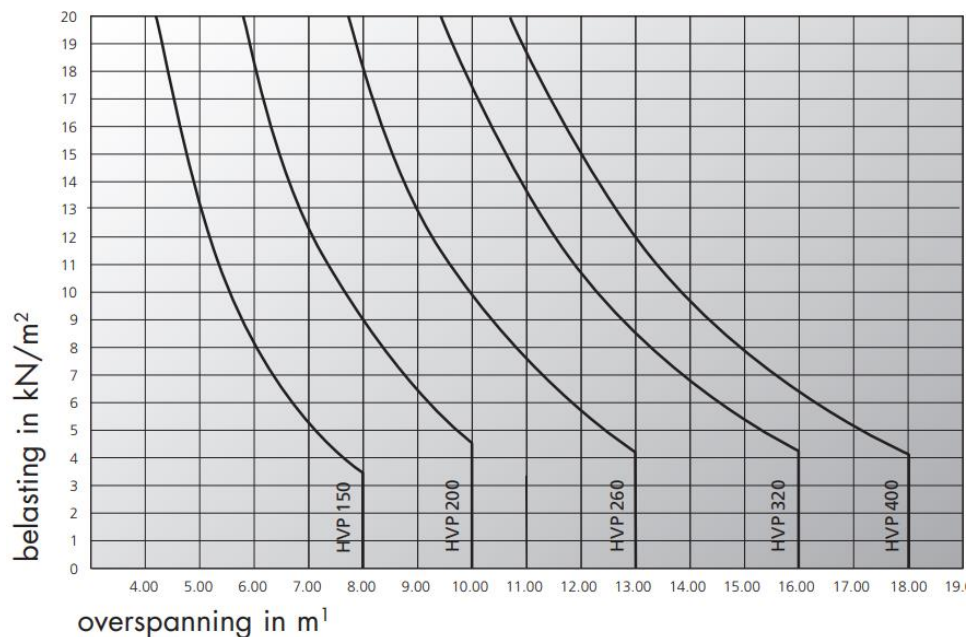


**Figure 63; Load in relation to span curve to determine the required type of slab - [79]**

In the Gemert design configuration the span-length is 6,5 m and the load is 18,30 kN/m<sup>2</sup>. Using Figure 63, the required height of a HCS for the specified input is HVP 260. Based on this slab type, the shadow cost related to using the slab type presented in Figure 64 can be used to determine the initial impact and the recycled impact.

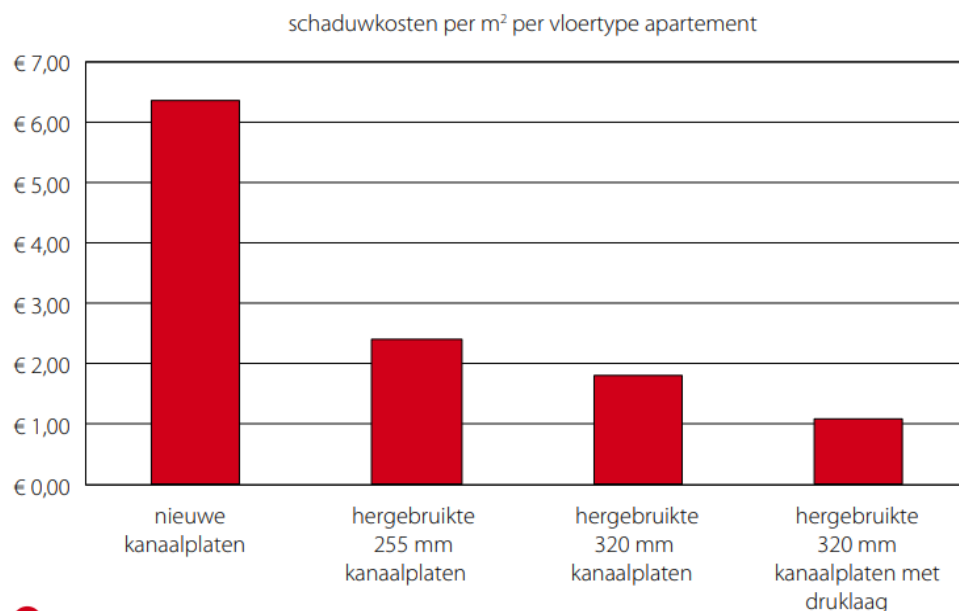


**Figure 64; Indication of shadow cost related to new and reused hollow-core slabs - [80]**

The bridge deck area, in the Gemert design configuration, is equal to 3,5x6,5=22,75 m<sup>2</sup>. Therefore, the initial environmental impact of a HCS, using the values presented in Figure 64, is estimated at 22,75x6,20=141,05 €. This value is lower than the

calculated shadow cost related to the volume of concrete present in the 3DPC Gemert configuration, which is €253,78. The calculated shadow cost of the 3DPC model is an indicative value that does not account for the actual environmental impact. Because approximated values are used to calculate the impact and not all contributors are included in the model, the calculated value is an approximation of the actual value. The actual environmental impact of 3DPC material can be even higher than the calculated impact in the design model. As a result, the shadow cost related to 3DPC is likely to be higher when compared to traditional methods such as prefabricated HCS. The difference between initial impact of 3DPC compared to HCS is a factor 1,80 higher (253,78/141,05).

Based on the data presented in Figure 64, reusing HCS elements once results in an impact of 8,4 €/m<sup>2</sup>. This value is calculated for the initial application and one reuse application. The relative shadow cost per application is 4,2 €/m<sup>2</sup>. Compared to the initial impact of 6.2 €/m<sup>2</sup>, reusing HCS elements results in a reduction of 32,26 %. Using these values, the shadow cost related reusing HCS 255 mm is  $22,75 \times 4,2 = 95,55$  €. When including the reduction of shadow cost related to the modular setup the total shadow cost related to concrete use only is  $\text{€}253,78 - \text{€}93,80 = \text{€}159,98$ . Therefore, the difference between reusing 3DPC and reusing HCS is a factor 1,67 in the favour of reusing HCS ( $159,98/95,55$ ). However, the reduction potential of the impact related to reusing the 3DPC is calculated based on the GWP only. Therefore, the total reduction of impact of reusing 3DPC structures can be higher.

Due to the limited amount of information publicly available, a more accurate comparison is not possible based on the data generated in this research study. It is estimated that the difference of initial environmental impact of 3DPC structures is 1,80 times higher than conventional methods. The impact of reusing 3DPC structures is estimated as 1,67 times higher than reusing a conventional product.

## 7. Discussion

This section describes if the results obtained using the design model (Section 6.2 and 6.3) satisfy the research questions, hence the research objective. Next, the limitations of the developed design model are discussed and its applicability for future projects.

## 7.1. Reflection on research project

The main research question in this project was:

*“Does increasing the structural efficiency in a 3D printed concrete bridge result in a decreased environmental impact that is lower compared to a conventional method?”*

This research question was split into a set of three sub-questions. The findings to these sub-questions are discussed to determine if the research project fulfils its intended purpose.

### 1) What is the effect of changing the geometry on the structural efficiency?

Based on results and the novel design model, it was found that the main influence of changes in the geometry on the structural behaviour is related to the vertical position of the tendons. The relative vertical position of the tendons influences the tendon eccentricity in the model. Therefore, the tendon eccentricity can be changed by varying the distance between the top and/or bottom fibre and the tendons along the span. If the tendon eccentricity is positive the post-tensioning moment works in the opposite direction of the bending moment caused by the load on the structure. This is considered to be a positive post-tensioning moment.

The stress capacity in a cross-section is increased by a positive post-tensioning moment (see Equations 7.1-7.5). Changes in the tendon eccentricity therefore influence the stress utilisation efficiency (see Table 5 & Figure 58). Another aspect that is influenced by changes in the tendon eccentricity is the shear capacity (see Equations 12.1-12.2). The width and height at the supports determine the shear capacity and tendon eccentricity at the start/end of the structure. These values therefore affect the shear force utilisation efficiency at the support.

*The findings used to comment on the first sub-question are generated using the parametric geometry component and the structural analysis component (Chapter 3 & 4). The proposed relation between geometry and structural efficiency is defined as described above. The relation describes the main parameters and limits of the proposed relation. The accuracy of the model is determined in Section 6.1. Restrictions to using the model and the validity of its results are described in Section 7.2.*

### 2) What is the effect of changing the geometry on the environmental impact?

Based on results and the novel design model, it was found that the main influence of changes in the geometry on the initial environmental impact is related to quantities of 3D printed of concrete material. The average contribution of concrete to the total calculated impact is 59% (see Figures 44 & 45). Reducing the amount of concrete in the structure results in a reduction in shadow cost of €54 and €139 (for limit cases 1 & 3 compared to the Gemert design). The use of concrete results in CO<sub>2</sub> emission which is the functional unit for the global warming potential. The global warming potential therefore is an important environmental impact category for a 3DPC bridge. A separation between primary and secondary functions can be used to reuse parts of the structure. An average reduction of environmental impact of reusing structural elements is calculated as 30%. When comparing the impact of the Gemert design to the limit cases, limit case 1 reduces the impact by 13% and limit case 3 reduces the impact by 33%. In combination with reduction of material, the total reduction measured in limit case 1 is 42% and the total reduction in limit case 3 is 51%.

*The findings used to comment on the first sub-question are generated using the parametric geometry component and the environmental analysis component (Chapter 3 & 5). The proposed relation between geometry and environmental impact is determined for the influence of material reduction and for the impact of reuse of the structure. The above described influence of geometry on environmental impact is based on results described in Section 6.3. Limitations related to reuse of the structure and the validity of obtained results are described in Section 7.2.*

3) Does the application of 3D printed concrete to bridge design result in a lower environmental impact when compared to a conventional method?

Based results and information generated to answer the first two sub-questions, the initial environmental impact of a 3D printed concrete bridge is compared to a hollow-core-slab element with a similar functionality. The result of the comparison show that the initial environmental of 3D printed concrete is a factor 1,8 higher than a hollow-core-slab element. When including the effect of reusing parts of the structure, the environmental impact of 3D printed concrete is 1,7 times as high as hollow-core-slab. These difference factors are calculated based on initial impact and single reuse.

*The findings of the first and second sub-question are used to comment on the third sub-question (Section 6.3). The conventional method used in the comparison is a hollow-core-slab element. The impact of material reduction and reuse of the structure on the comparison are presented above and in Section 6.3. The validity of the comparison is described in Section 7.2.*

## 7.2. Project limitations

Data obtained to comment on the sub-questions in the previous section are only valid for the application described in this research project. This imposes limitations on the validity of the design model and method for future applications. Following limitations are identified in this research project:

### 1) Determining the structural efficiency;

- The main restriction of the design model to changing the geometry is the cross-section, especially in combination with the tendon placement in the print path. The current design of the print path restricts varying the width of the sections along the span to a maximum value of 164 mm. The maximum vertical variation of the section height along the span is not restricted by the print path. This value is restricted in the mid-section by the tensional/compressional resistance and at the supports by shear capacity.
- Another restriction related to the print path is the accuracy of the cross-sectional properties. The most accurate approximation method uses reduction values to calculate the representative value of the cross-sectional properties (see Figure 19). However, the accuracy of the approximation depends on the height of the section (see Figure 31). If the height deviates from the Gemert design value (0,80 m) the accuracy of the cross-sectional properties reduces. Less accurate cross-sectional properties result in a less accurate simulation of the structural behaviour. Therefore, the design model is restricted to the range in which the determined reduction factors can be verified (0,70-0,90 [m]).
- The process of 3D printing concrete currently cannot add reinforcement in the sections. Because of the low-tension resistance of 3DPC this material should not be designed to sustain tension. This limits possible geometric configurations of the shape of a structure. The low-tension resistance also influences the tendon configuration. The 3D printing processes currently do not allow the placement of tendon deviators along the span. The tendons therefore must remain straight throughout the span of the sections. This limits the options varying the shape of the structure along the span.
- The calculation setup as a plate structure allows the model to calculate a large range of values of the width of the sections. However, the structural analysis is based on a load configuration for a symmetrical loaded pedestrian bridge. If the value of the width increases the loading case is likely to include asymmetrical load configurations, related to asymmetrical placement of vehicles on the bridge deck. Asymmetrical load cases are currently not included in the model and thus restrict the value of the width.
- The structural behaviour calculated in the design model developed in this research project only determines global behaviour (bending & shear). Local effects of the load on the structure are not calculated in the design model. The stability of the cross-section should be determined manually.
- Adjusting geometrical properties results in a different load value for the structural analysis. The structural analysis is performed in a different software than the geometry generation. Therefore, the model cannot be verified without the structural analysis output of the adjusted model, in SCIA, as input for the verification, in Grasshopper. Unfortunately, the automated connection with SCIA does not allow forwards and backwards communication (from GH to SCIA and from SCIA to GH). Therefore, the model is restricted to linear design processes starting from geometry and finishing with the structural analysis results.

## 2) Determining the environmental impact;

- Modular construction is only effective when a structure can be deconstructed without significant effort and waste production. This complicates the connection between the primary and secondary structure. This should be considered in the design and production of the 3DPC bridge.
- Optimizing the design of the shape along the span can result in a reduced amount of possibilities for end of life applications. By designing a bridge to optimally perform in one specific case, the primary structure will not be optimally designed to fit other specifications. Therefore, optimizing the shape for maximum structural efficiency in a specific configuration will reduce the applicability of the primary structure to other applications. As a result, the reduction of 51% can only be achieved if the exact same parameters as initially used can directly be applied to another project.
- The calculated environmental impact using the design model does not consider all impacts during the total life cycle of the structure. Because of the relatively new application of the material to civil and infrastructure projects, there is few information available regarding the environmental impact of the material. The calculated impact therefore represents the initial impact of the materials used in the structure only. Including the effects of other aspects in the total life cycle will influence the environmental impacts. Including these factors requires further studies and publications.

## 3) Comparison of environmental impact;

- The environmental impact calculation procedure of hollow-core-slab elements, related to Figure 49, is not fully documented in the article of Naber et al [80]. The environmental impact factors therefore could be based on different impact categories and processes. This can influence the validity of obtained results. Complete transparency of the input data for the comparison can result in a more accurate result of the comparison.





## 8. Conclusions

As the objectives of this research project were to study the relation between the structural efficiency and environmental impact of a 3D printed concrete (3DPC) bridge, following research question has been studied. The research question focuses on a) *“Does increased structural efficiency in 3DPC bridges result in a decreased environmental impact”* and b) *“Is the environmental impact of 3DPC bridges lower compared to a conventional method”*. Using a novel design model and based on the results described in Section 6.2 and 6.3, following two conclusions can be drawn;

1. Increasing structural efficiency can decrease the environmental impact of a 3DPC bridge.
2. Considering the state of 3D printing concrete technology at present, applications of this technology for bridges can result in a higher environmental impact than the compared conventional method.

Looking at these conclusions, the claimed potential of applications of 3DPC in the construction industry needs further evidence. E.g. the environmental impact can be reduced by increasing the structural efficiency, using other compositions of concrete mixtures and including reinforcement in the printing process. Here, the reuse of 3DPC materials and its' initial environmental impact are other important topics for further research.

The novel design model developed in this research project is not limited to the application of design of 3DPC bridges. This model can be used for other applications & materials by adjusting the input and critical design checks. The component-based design setup of the model and the connection to automated manufacturing can contribute to the transition to digital construction.

## 9. Recommendations

The design model developed in this research project successfully performs its intended function within the described limitations (Section 7.2). Increasing applicability of the model and the validity of its result requires further development. Therefore, following recommendations are suggested for further development of the model;

### 1) Parametric geometry component;

- Include a cross-section optimisation tool in the design model. This allows the model to accurately calculate cross-sectional properties for the structural analysis component. Another benefit of implementing such a tool is the possibility to determine the effect of the shape of the cross-section on the structural efficiency and environmental impact.

### 2) Structural analysis component;

- Develop a representative model in a FEA environment that can accurately visualise the complex shape of the cross-section. This can result in the possibility of calculating local behaviour as well as overall behaviour of the structure. Including this option will also allow the model to reflect on the stability of the cross-section.
- Include an asymmetric loading case in the load combinations. This will increase the range of applicability of the design model to larger span bridges and loading cases other than pedestrian/cyclists.

### 3) Environmental analysis component;

- Include information of multiple phases of the life cycle of the structure. The model currently is focussed on design aspects only. Including information regarding the on-site erection, maintenance and deconstruction phase increases the amount of information the design model can generate. This extra information can be used for a more accurate comparison and to generate a more complete environmental impact assessment.

Besides recommendations for the design model, following recommendations for future scientific research are suggested;

### 4) Research required for further development of structural parametric & environmental design of 3DPC bridges;

- Include reinforcement and tendon deviators in the 3D printing process. This will result in an increased manufacturing freedom of cross-sections for design of 3DPC bridges. This can influence the structural efficiency of a 3DPC bridge.
- Material and failure behaviour of 3DPC. Currently the validation process is based on standard concrete calculations. Accurate studies to determine the material and failure behaviour of 3DPC can increase the accuracy of validation models of the structural safety of 3DPC bridges.
- Composition of concrete mixtures for 3D printing. Reducing the environmental impact of a concrete mixture can significantly reduce the initial impact. Increasing the tension strength of mixture can result in a higher structural efficiency.
- Studying these topics, or a combination of, can increase structural efficiency and/or reduce environmental impact. This can decrease the difference in impact compared to hollow-core-slab elements.

# Bibliography

1. Lenard, D. *Promoting the development of an innovative culture through the strategic adoption of advanced manufacturing technology in construction*. in *Proceedings of CIB World Building Congress: Performance in Product and Practice*. 2001.
2. Holness, G., *Building information modeling*. ASHRAE journal, 2006. **48**(8): p. 38-46.
3. theaecassociates1. *Building information modeling services*. 2015 23-10-2018]; Available from: <https://visual.ly/community/infographic/business/building-information-modeling-services>.
4. Bernal, M., J.R. Haymaker, and C. Eastman, *On the role of computational support for designers in action*. Design Studies, 2015. **41**: p. 163-182.
5. De Schutter, G., et al., *Vision of 3D printing with concrete—Technical, economic and environmental potentials*. Cement and Concrete Research, 2018.
6. Dubois, A. and L.-E. Gadde, *The construction industry as a loosely coupled system: implications for productivity and innovation*. Construction Management & Economics, 2002. **20**(7): p. 621-631.
7. Al Hattab, M. and F. Hamzeh, *Analyzing Design Workflow: An Agent-based Modeling Approach*. Procedia engineering, 2016. **164**: p. 510-517.
8. herigemblong. *Flow chart template Xls fresh critical path method Cpm spreadsheet Pert algorithm*. 2018 23-10-2018]; Available from: <http://dailyrevshare.com/flow-chart-template-xls/flow-chart-template-xls-fresh-critical-path-method-cpm-spreadsheet-pert-algorithm/>.
9. Rezgui, Y. and A. Zarli, *Paving the way to the vision of digital construction: a strategic roadmap*. Journal of construction engineering and management, 2006. **132**(7): p. 767-776.
10. Mihindu, S. and Y. Arayici. *Digital construction through BIM systems will drive the re-engineering of construction business practices*. in *International Conference Visualisation*. 2008. IEEE.
11. Merschbrock, C. and B.E. Munkvold, *Effective digital collaboration in the construction industry—A case study of BIM deployment in a hospital construction project*. Computers in Industry, 2015. **73**: p. 1-7.
12. Halfawy, M.M. and T.M. Froese, *Component-based framework for implementing integrated architectural/engineering/construction project systems*. Journal of Computing in Civil Engineering, 2007. **21**(6): p. 441-452.
13. Conner, B.P., et al., *Making sense of 3-D printing: Creating a map of additive manufacturing products and services*. Additive Manufacturing, 2014. **1**: p. 64-76.
14. Myung, S. and S. Han, *Knowledge-based parametric design of mechanical products based on configuration design method*. Expert Systems with applications, 2001. **21**(2): p. 99-107.
15. Lepech, M.D., V.C. Li, and G.A. Keoleian, *Sustainable infrastructure material design*. 2005.
16. Yılmaz, M. and A. Bakış, *Sustainability in construction sector*. Procedia-Social and Behavioral Sciences, 2015. **195**: p. 2253-2262.
17. Cabeza, L.F., et al., *Life cycle assessment (LCA) and life cycle energy analysis (LCEA) of buildings and the building sector: A review*. Renewable and sustainable energy reviews, 2014. **29**: p. 394-416.
18. Karaś, S. and J. Bohatkiewicz, *Sustainable Bridge Design*. 2015.

19. *A Roadmap for moving to a competitive low carbon economy in 2050*. 2011, European Commission: Brussels.
20. Yepes, V., J.V. Martí, and T. García-Segura, *Cost and CO2 emission optimization of precast–prestressed concrete U-beam road bridges by a hybrid glowworm swarm algorithm*. Automation in Construction, 2015. **49**: p. 123-134.
21. Petzet, M. and F. Heilmeyer, *Reduce Reuse Recycle*. Architecture as Resource, Hatje Cantz Verlag, Berlin, 2012.
22. Salet, T.A., et al., *Design of a 3D printed concrete bridge by testing*. Virtual and Physical Prototyping, 2018: p. 1-15.
23. Grondin, F. and M. Matallah, *How to consider the Interfacial Transition Zones in the finite element modelling of concrete?* Cement and Concrete Research, 2014. **58**: p. 67-75.
24. Huang, Z. and J.R. Liew, *Nonlinear finite element modelling and parametric study of curved steel–concrete–steel double skin composite panels infilled with ultra-lightweight cement composite*. Construction and Building Materials, 2015. **95**: p. 922-938.
25. Nolan, D.C., et al., *Defining simulation intent*. Computer-aided design, 2015. **59**: p. 50-63.
26. García-Segura, T. and V. Yepes, *Multiobjective optimization of post-tensioned concrete box-girder road bridges considering cost, CO2 emissions, and safety*. Engineering Structures, 2016. **125**: p. 325-336.
27. Rumpf, M., et al. *Structural Surface–multi parameter structural optimization of a thin high performance concrete object*. in *Proceedings of the IASS Conference 2015, Amsterdam*. 2015.
28. Bletzinger, K.-U., et al., *Computational methods for form finding and optimization of shells and membranes*. Computer Methods in Applied Mechanics and Engineering, 2005. **194**(30-33): p. 3438-3452.
29. Coenders, J.L. *Parametric and associative strategies for engineering*. in *IABSE Symposium Report*. 2008. International Association for Bridge and Structural Engineering.
30. Aish, R., *Introduction to GenerativeComponents, a parametric and associative design system for architecture, building engineering and digital fabrication*. 2005, White Paper.
31. Lai, Y., et al., *Integrating CAD with Abaqus: a practical isogeometric analysis software platform for industrial applications*. Computers & Mathematics with Applications, 2017. **74**(7): p. 1648-1660.
32. Yousefzadeh, S., et al., *Building Information Modelling (BIM) Software Interoperability: A Review of the Construction Sector*. 2015.
33. Shahbazi, S. and I. Rasoolan, *Meso-scale finite element modeling of non-homogeneous three-phase concrete*. Case studies in construction materials, 2017. **6**: p. 29-42.
34. Rolvink, A., R. van de Straat, and J. Coenders, *Parametric structural design and beyond*. International Journal of Architectural Computing, 2010. **8**(3): p. 319-336.
35. Nembrini, J., S. Samberger, and G. Labelle, *Parametric scripting for early design performance simulation*. Energy and Buildings, 2014. **68**: p. 786-798.
36. Mitchel, M., J. Codling, and J. Gell. *Parametric concept bridge*. 2015 23-10-2018]; Available from: <https://miketmitch.wordpress.com/2015/05/18/parametric-concept-bridge/>.
37. Shea, K., R. Aish, and M. Gourtovaia, *Towards integrated performance-driven generative design tools*. Automation in Construction, 2005. **14**(2): p. 253-264.
38. Coenders, J.L. *Interfacing between parametric associative and structural software*. in *Proceedings of the 4th International Conference on Structural and Construction Engineering, Melbourne, Australia*. 2007. Citeseer.

39. Georgiou, O. *Interactive structural analysis and form finding*. in *IABSE IASS Conference*. 2011.
40. Singh, M.M., A. Sawhney, and A. Borrmann, *Modular coordination and BIM: development of rule based smart building components*. *Procedia Engineering*, 2015. **123**: p. 519-527.
41. Danhaive, R.A. and C.T. Mueller, *Combining parametric modeling and interactive optimization for highperformance and creative structural design*. *Proceedings of the International Association for Shell and Spatial Structures (IASS)*, 2015.
42. Abrishami, S., et al., *Virtual generative BIM workspace for maximising AEC conceptual design innovation: A paradigm of future opportunities*. *Construction Innovation*, 2015. **15**(1): p. 24-41.
43. ter Braack, C., R. Andriesse, and O. van Boggelen, *Hellingen in fietsroutes Onderzoeksrapport*. 2009: p. 52.
44. *Track: Structural Engineering*. n.d. [27-05-2018]; Describes structural engineering practices]. Available from: <https://www.tudelft.nl/onderwijs/opleidingen/masters/ce/msc-civil-engineering/msc-programme/track-structural-engineering/>.
45. Pavlovic, M., *Lecture 2; Structural Design*, in *Steel Bridges*, M. Pavlovic, Editor. 2018, TU Delft: Delft.
46. Cuillière, J.-C., S. Bournival, and V. François, *A mesh-geometry-based solution to mixed-dimensional coupling*. *Computer-aided design*, 2010. **42**(6): p. 509-522.
47. Bournival, S., J.-C. Cuillière, and V. François, *A mesh-geometry based method for coupling 1D and 3D elements*. *Advances in Engineering Software*, 2010. **41**(6): p. 838-858.
48. Robinson, T., C. Armstrong, and R. Fairey, *Automated mixed dimensional modelling from 2D and 3D CAD models*. *Finite elements in analysis and design*, 2011. **47**(2): p. 151-165.
49. Panda, B., S.C. Paul, and M.J. Tan, *Anisotropic mechanical performance of 3D printed fiber reinforced sustainable construction material*. *Materials Letters*, 2017. **209**: p. 146-149.
50. Kim, K., et al., *Evaluation of Shear Strength of RC Beams with Multiple Interfaces Formed before Initial Setting Using 3D Printing Technology*. *Materials*, 2017. **10**(12): p. 1349.
51. Farina, I., et al., *On the reinforcement of cement mortars through 3D printed polymeric and metallic fibers*. *Composites Part B: Engineering*, 2016. **90**: p. 76-85.
52. Salet, T.A., et al., *3D concrete printing—a structural engineering perspective*, in *High Tech Concrete: where Technology and Engineering Meet*. 2018, Springer Cham.
53. Panda, B., et al., *Additive manufacturing of geopolymers for sustainable built environment*. *Journal of Cleaner Production*, 2017. **167**: p. 281-288.
54. Le, T.T., et al., *Hardened properties of high-performance printing concrete*. *Cement and Concrete Research*, 2012. **42**(3): p. 558-566.
55. Reiter, L., et al., *The role of early age structural build-up in digital fabrication with concrete*. *Cement and Concrete Research*, 2018.
56. Buswell, R.A., et al., *3D printing using concrete extrusion: a roadmap for research*. *Cement and Concrete Research*, 2018.
57. Zareian, B. and B. Khoshnevis, *Effects of interlocking on interlayer adhesion and strength of structures in 3D printing of concrete*. *Automation in Construction*, 2017. **83**: p. 212-221.
58. Walraven, J.C. and C.R. Braam, *Prestressed Concrete*, in *CIE4160*. 2015, Delft Technical University of Technology: Delft. p. 4.8-4.13.



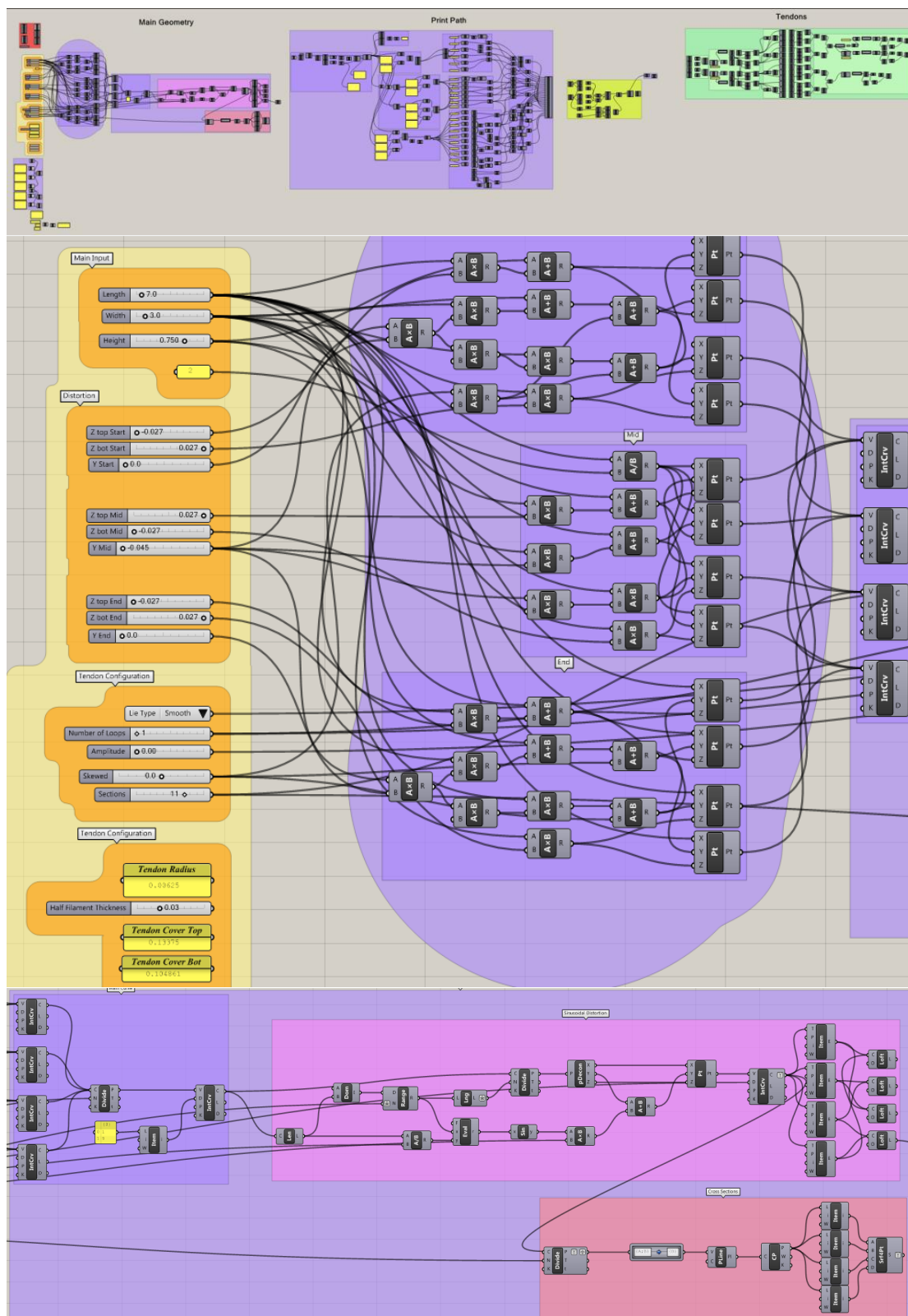
59. Blaauwendraad, J., *Theory. Plate analysis, theory and application*. Vol. 1. 2006, Delft: Technical University Delft. 96.
60. Hendriks, M.A.N., *Lecture 1: Introduction to Plate analysis, theory and applications*. 2017, Technical University Delft: Delft. p. 6.
61. Blaauwendraad, J., *Numerical methods. Plate analysis, theory and application*. Vol. 2. 2006, Delft: Technical University Delft. 136.
62. Welleman, J.W. and C. Hartsuijker, *Structural Mechanics 4, in Non-Symmetrical and Inhomogeneous cross sections*. 2017, TU Delft: Delft. p. 20.
63. Gladek, E., *Circular building & infrastructure - Metabolic at Infratech 2017 [powerpoint slides]*, in *Opportunities for new value*. 2017.
64. Brundtland, G.H., *Our common future (Report for the World commission on Environment and Development, United Nations)*. Our common future: report for the World Commission on Environment and Development, United Nations, 1987.
65. Elkington, J., *Cannibals with forks: The triple bottom line of twentieth century business*. Capstone: Oxford, 1997.
66. Jonkers, H.M., *Lifecycle Assessment (LCA)*, in *Reader for TU Delft course "Materials and Ecological Design"*. 2016, TU Delft.
67. De Bruyn, S., et al., *Shadow prices handbook: valuation and weighting of emissions and environmental impacts*. CE Delft, Delft, the Netherlands.[online] Ecology and Society, 2010. **21**(2): p. 10.
68. Buyle, M., J. Braet, and A. Audenaert, *Life cycle assessment in the construction sector: A review*. Renewable and Sustainable Energy Reviews, 2013. **26**: p. 379-388.
69. Jonkers, H.M., *Self healing concrete: a biological approach*, in *Self healing materials*. 2007, Springer. p. 195-204.
70. Li, V.C. and E. Herbert, *Robust self-healing concrete for sustainable infrastructure*. Journal of Advanced Concrete Technology, 2012. **10**(6): p. 207-218.
71. Generalova, E.M., V.P. Generalov, and A.A. Kuznetsova, *Modular buildings in modern construction*. Procedia engineering, 2016. **153**: p. 167-172.
72. Kamali, M. and K. Hewage, *Life cycle performance of modular buildings: A critical review*. Renewable and Sustainable Energy Reviews, 2016. **62**: p. 1171-1183.
73. MacArthur, E., *Towards the circular economy*. J. Ind. Ecol, 2013: p. 23-44.
74. Stephan, A. and A. Athanassiadis, *Towards a more circular construction sector: Estimating and spatialising current and future non-structural material replacement flows to maintain urban building stocks*. Resources, Conservation and Recycling, 2018. **129**: p. 248-262.
75. Saint-Gobain. *Preserving natural resources*. 2015 23-10-2018]; Available from: <https://www.saint-gobain.com/en/preserving-natural-resources>.
76. Corbusier, L. and J.-L. Cohen, *Le Corbusier: an atlas of modern landscapes*. 2013: Museum of Modern Art.
77. Martensson, L. *Emissions from Volvo's trucks*. 2018 23-10-2018]; Available from: [https://www.volvotrucks.com/content/dam/volvo/volvo-trucks/markets/global/pdf/our-trucks/Emis\\_eng\\_10110\\_14001.pdf](https://www.volvotrucks.com/content/dam/volvo/volvo-trucks/markets/global/pdf/our-trucks/Emis_eng_10110_14001.pdf).
78. Van Lieshout, M. and S. Nusselder, *Update prioritering handelingsperspectieven verduurzaming betonketen* 2016. 2016, CE Delft, Delft.
79. Vree, J.d. *Kanaalplaatvloeren*. 2011 23-10-2018]; Available from: [http://www.joostdevree.nl/bouwkunde2/jpgk/kanaalplaatvloer\\_9\\_brochure\\_betonson\\_web-juni-2011\\_www\\_betonson\\_com.pdf](http://www.joostdevree.nl/bouwkunde2/jpgk/kanaalplaatvloer_9_brochure_betonson_web-juni-2011_www_betonson_com.pdf).
80. Naber, N., D.v. Keulen, and M. Haas, *Milieuwinst bij hergebruik kanaalplaten*. Cement, 2013.

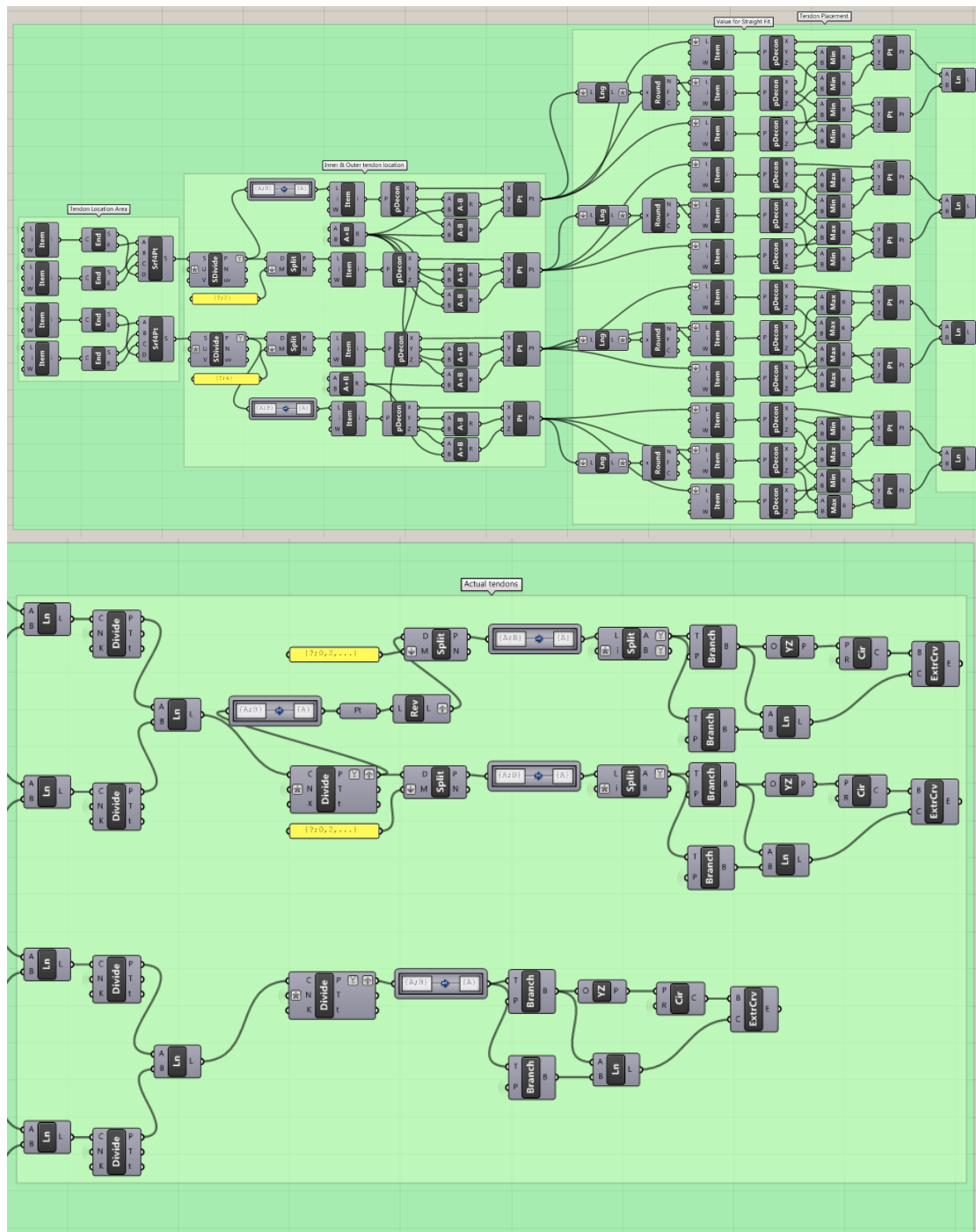


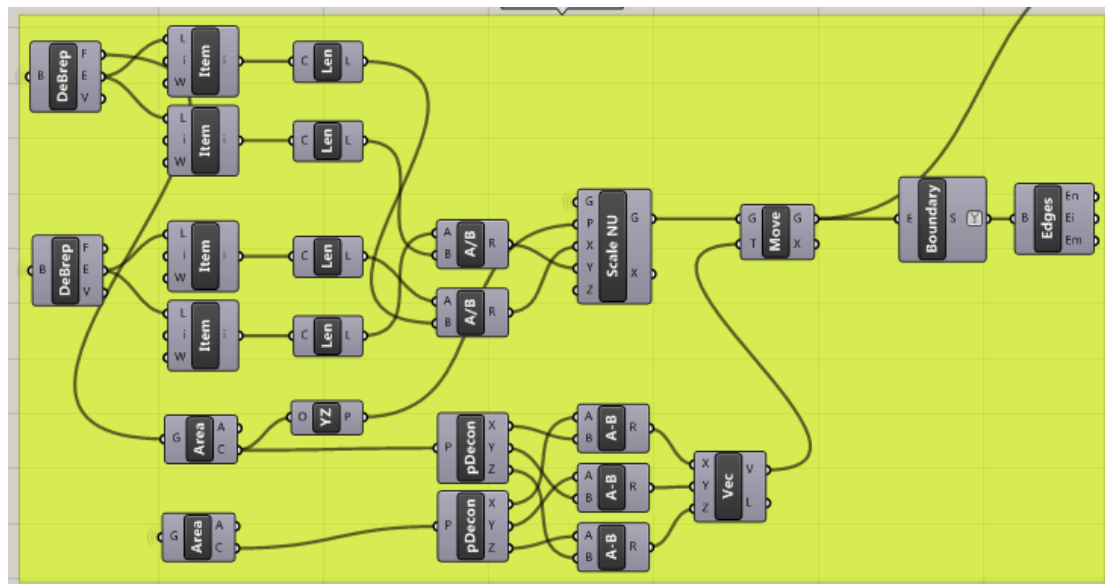
## Annex A Grasshopper components

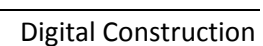
- A1 Geometry component
- A2 Pre-processing component
- A3 XML export and execute analysis component
- A4 Result interpretation component
- A5 Sustainable analysis component

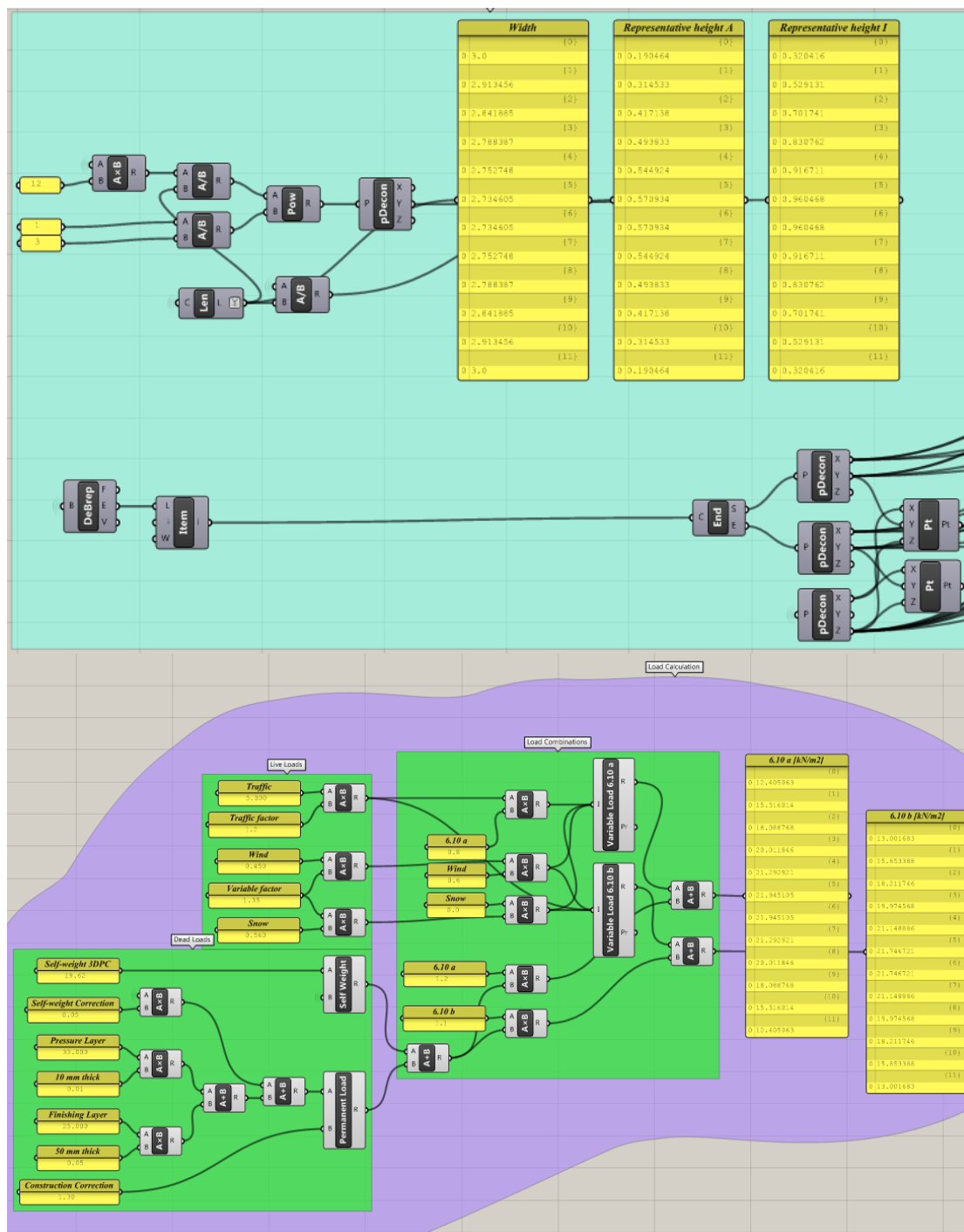
# A1 Geometry Component



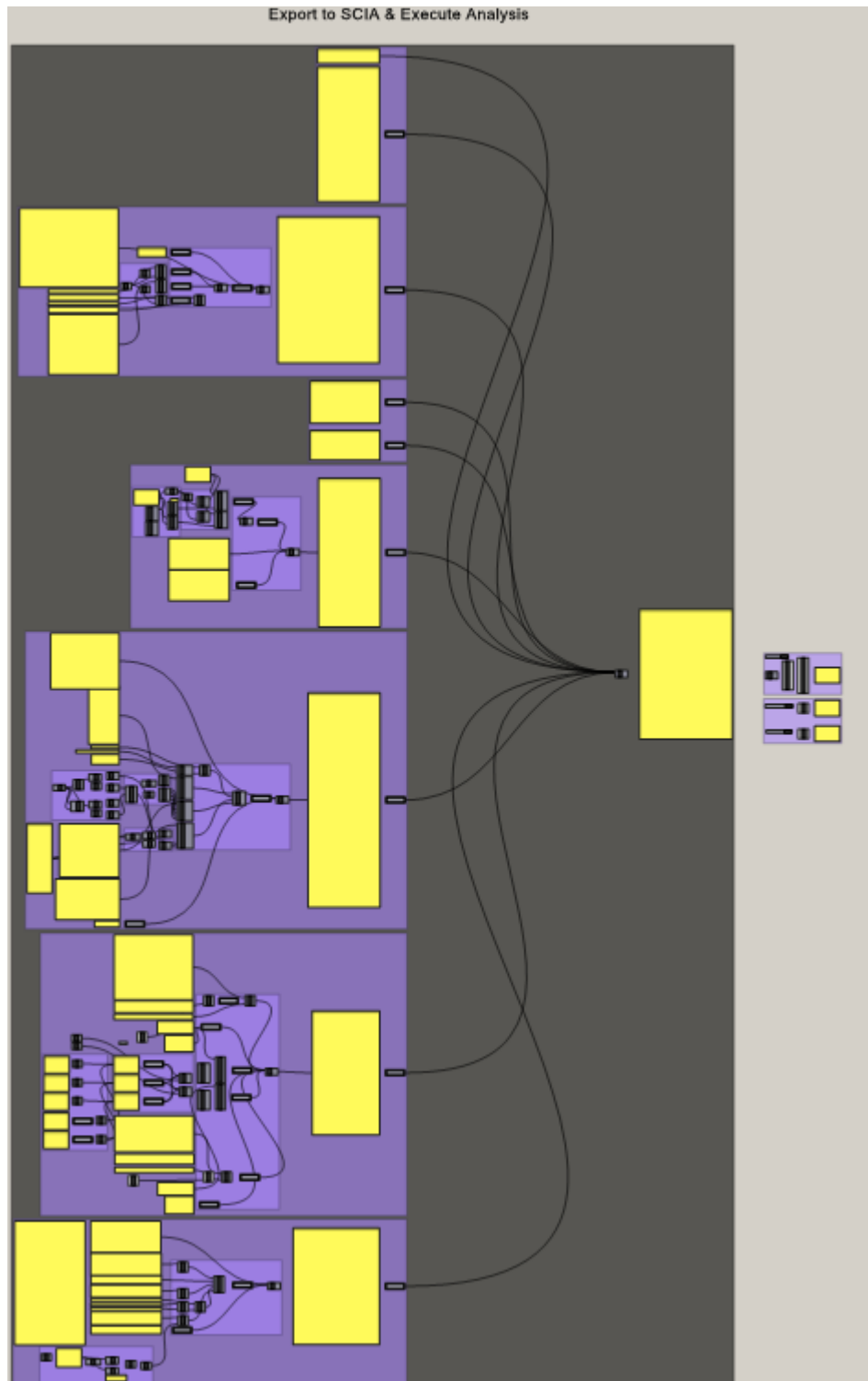




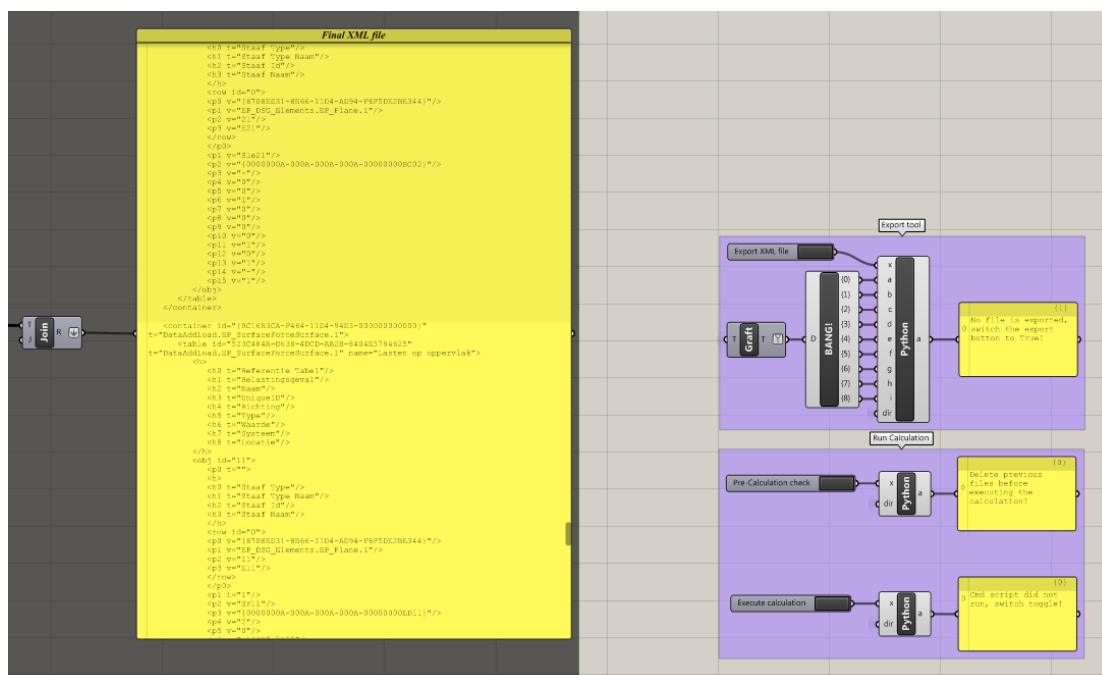




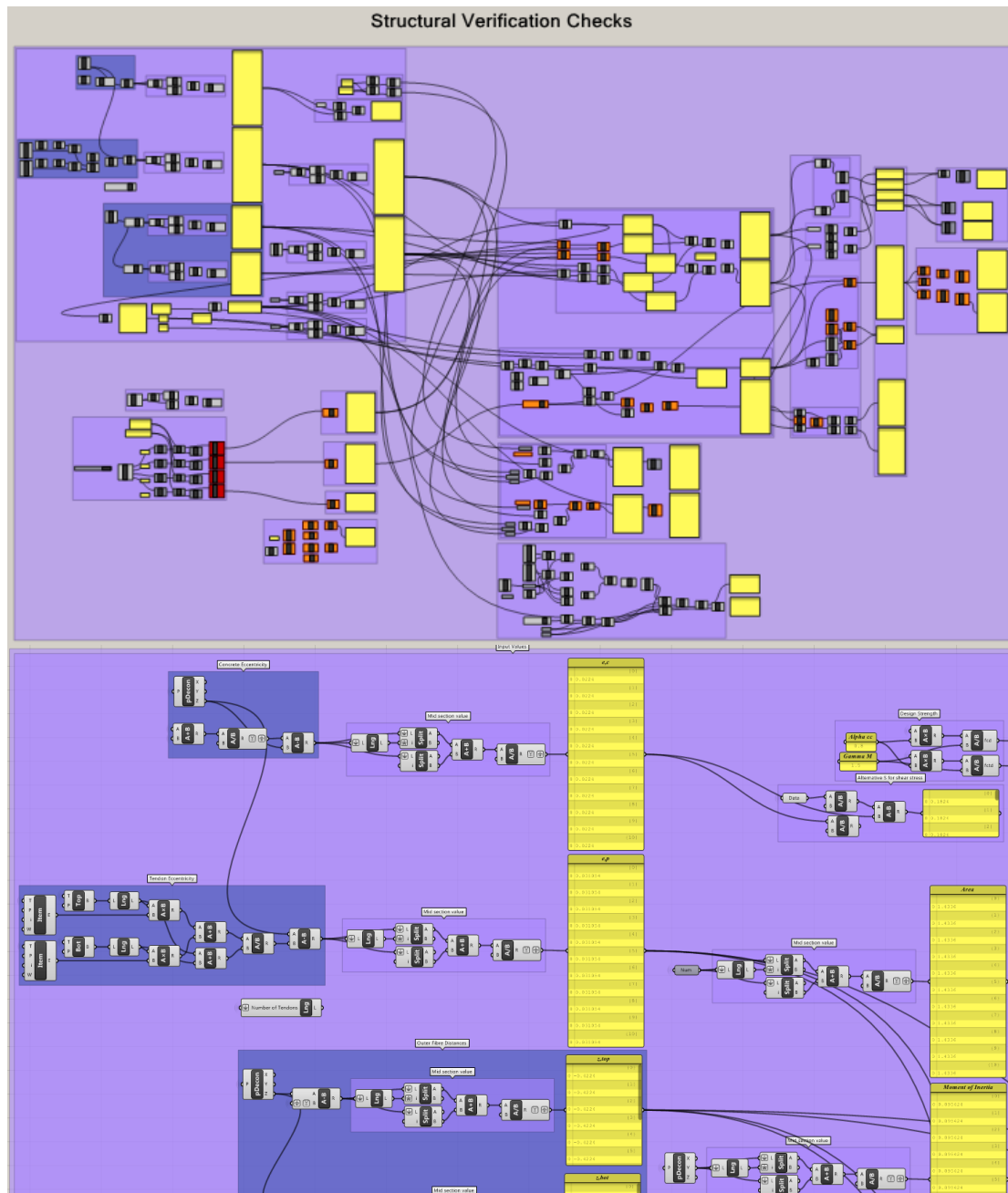
## A3 XML export and execute analysis component



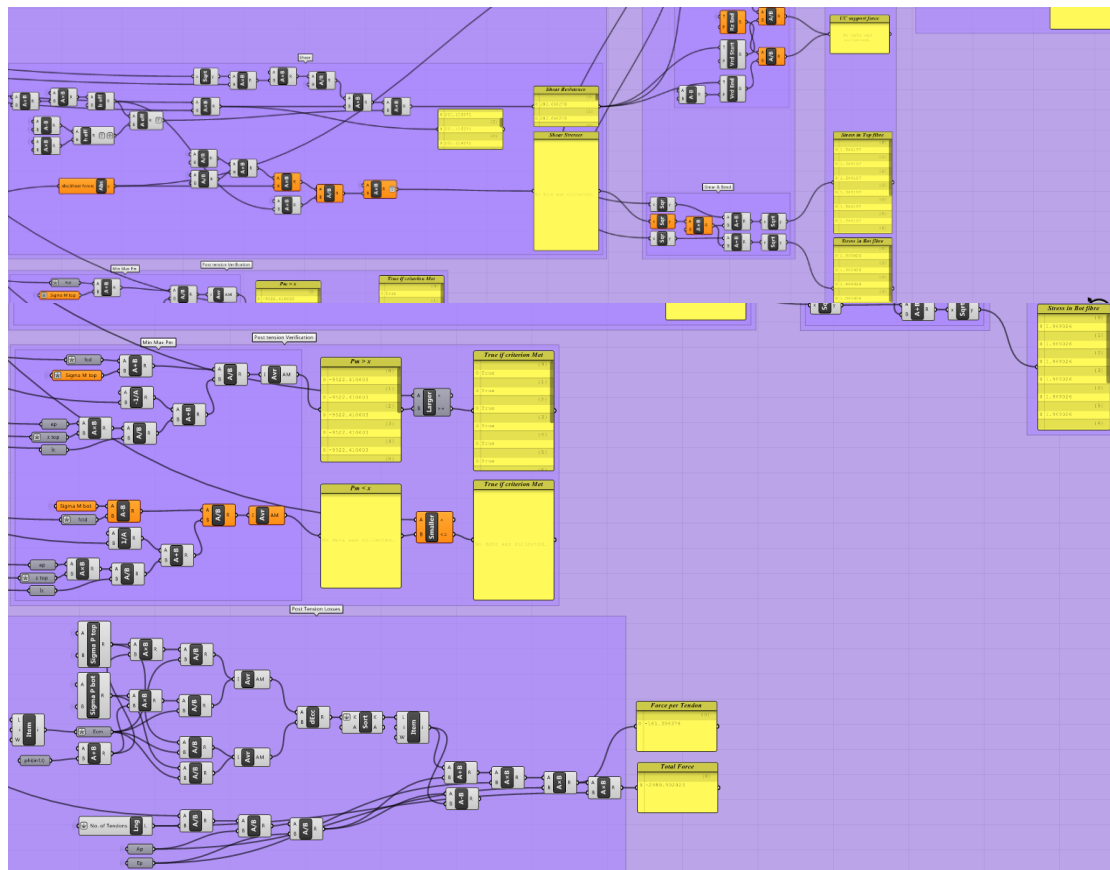




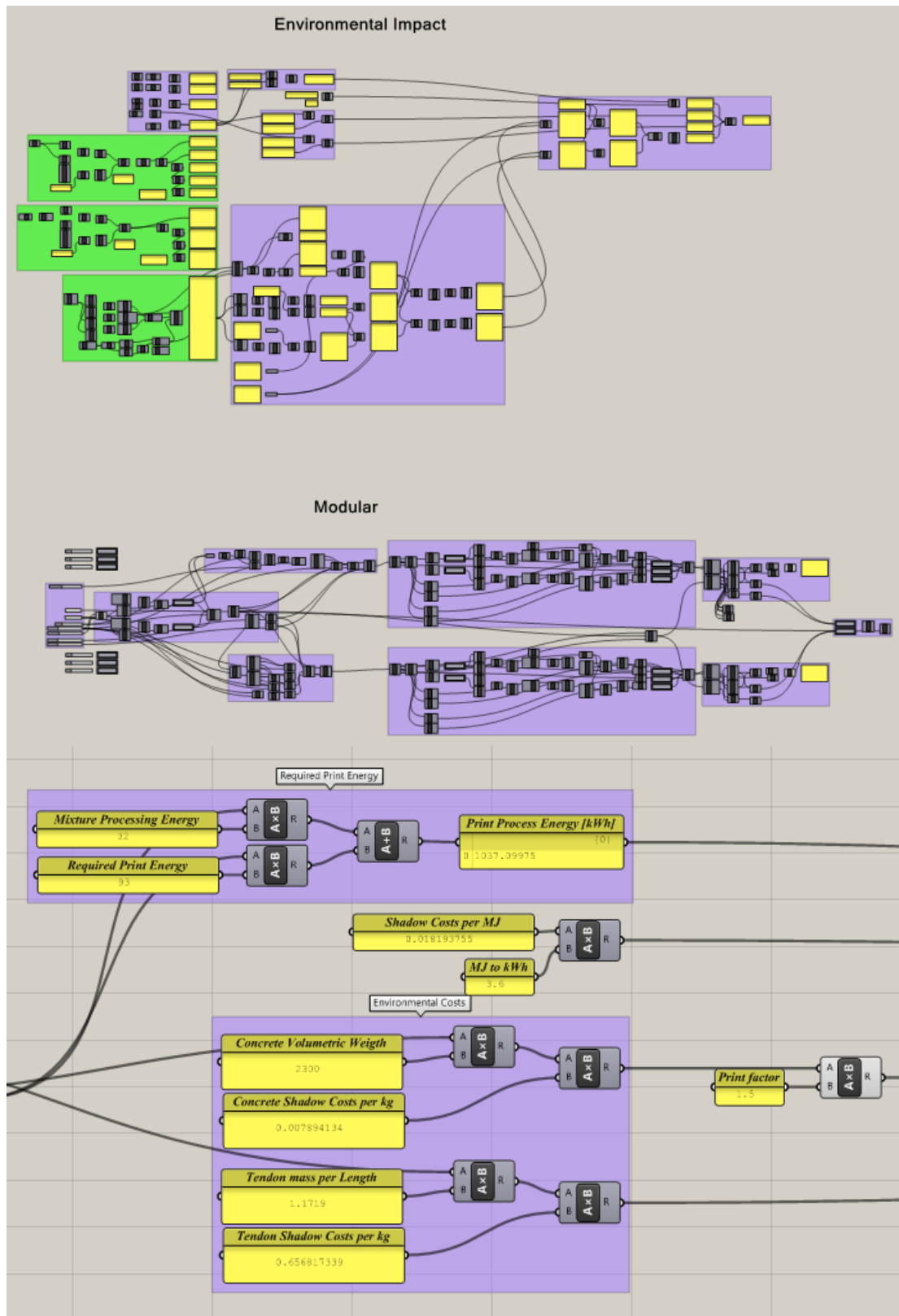
## A4 Result interpretation component

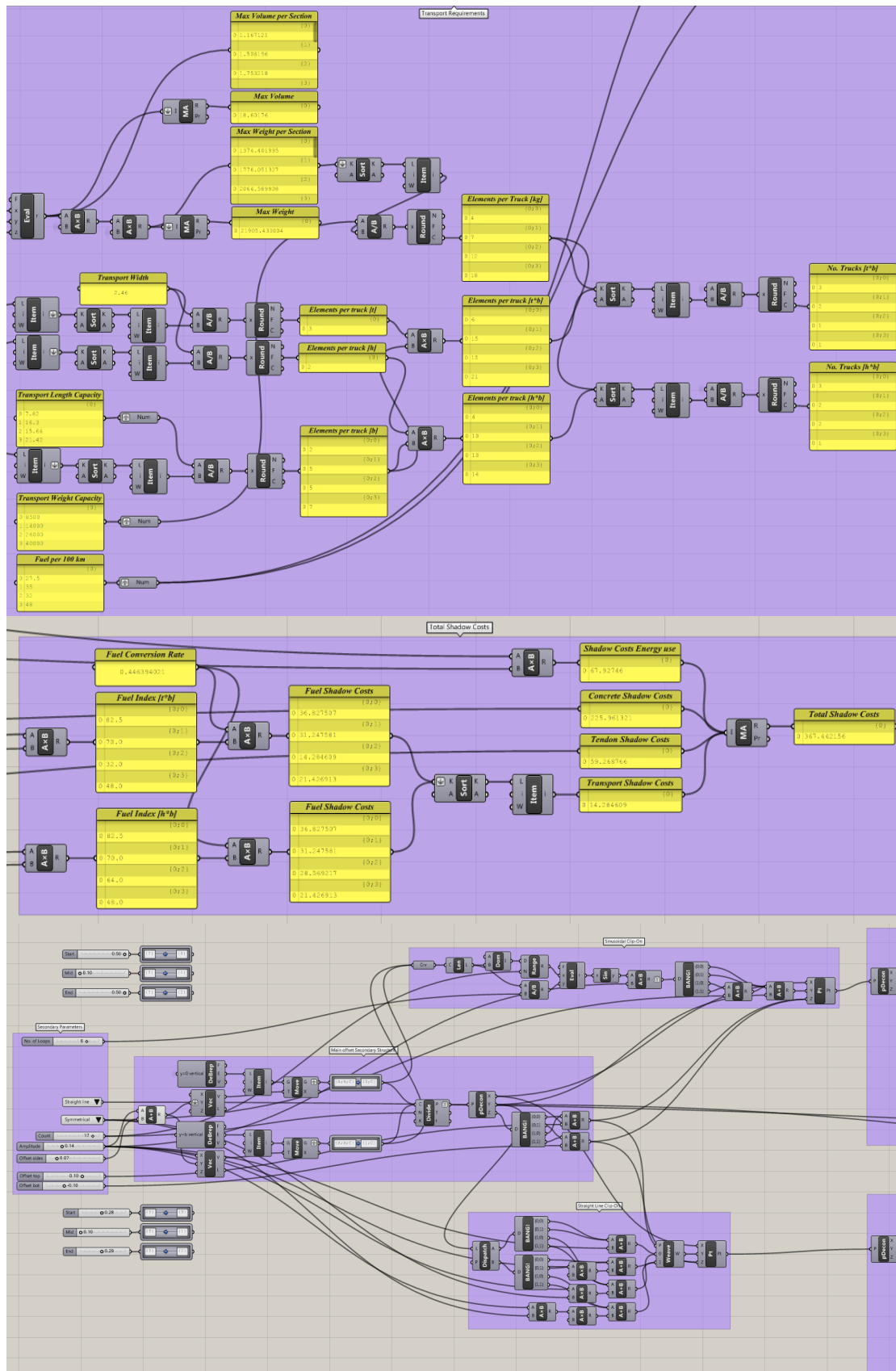


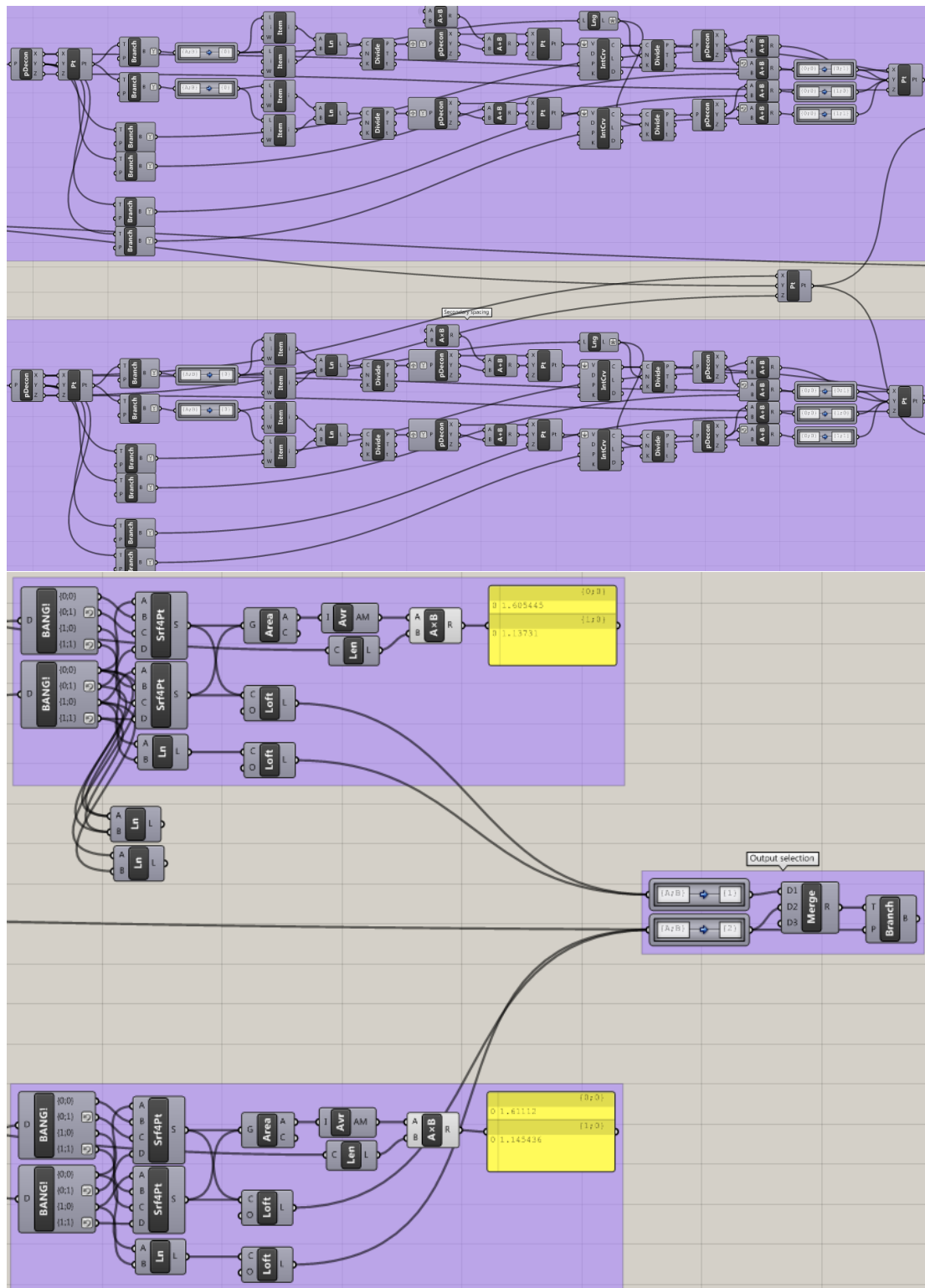




## A5 Environmental analysis component





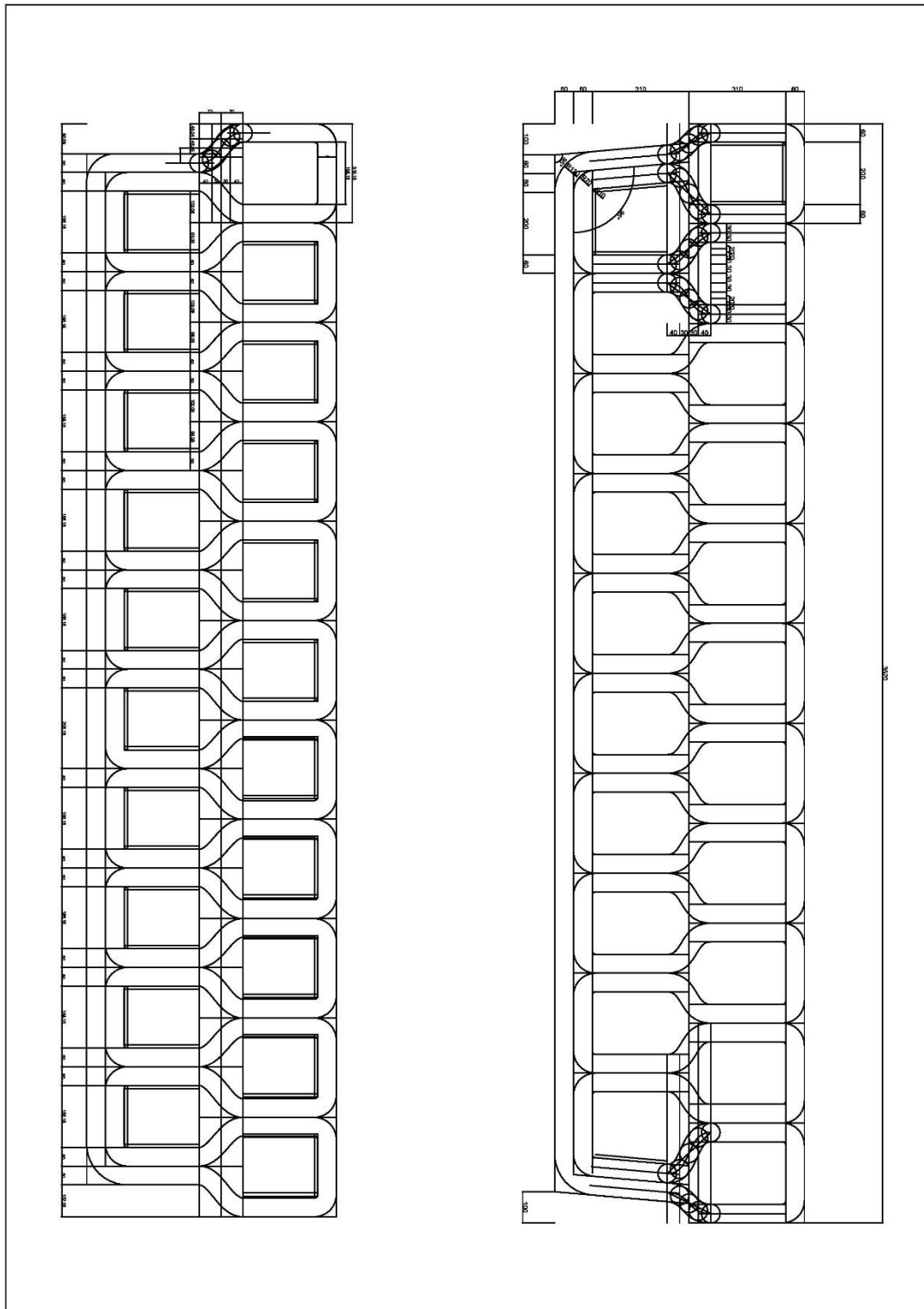


## Annex B Design drawings

- B1 Print path design
- B2 Varying tendon location in print path
- B3 Inner/outer tendon location



## B1 Print path design







# Annex C Eurocode documentation

- C1 Eurocode load combinations
- C2 Eurocode standards
- C3 Method statement

# C1 Eurocode load combinations

Tabel NB.10 – A2.2 —  $\psi$ -factoren voor voetgangers- en fietsbruggen

Belasting	Symbool		$\psi_0$	$\psi_1$	$\psi_2$
Verkeersbelastingen	gr1	Gelijkmatig verdeelde belasting $q_{fk}$	0,4	0,8 <sup>c</sup>	0,4
		Horizontale belasting $Q_{fk}$			
	gr 2	Gelijkmatig verdeelde belasting $q_{fk}$	0,4	0,8 <sup>b</sup>	0
		Dienstvoertuig $Q_{serv}$			
		Horizontale belasting $Q_{fk}$			
	Geconcentreerde belasting $Q_{fkk}$		0	0,8 <sup>b</sup>	0
Onbedoeld voertuig (zie 5.6.3)		0	0,8 <sup>b</sup>	0	
Windkrachten	$F_{wk}$ blijvende ontwerpsituatie Uitvoering		0,3 0,8	0,6 <sup>b</sup> 0	0
Thermische belastingen	$T_k$		0,3	0,8	0,3 <sup>a</sup>
Sneeuwbelastingen	$Q_{sn,k}$ blijvende ontwerpsituatie Uitvoering		0 0,8	0 0	0
	Belastingen tijdens de bouw		$Q_c$	1,0	0

<sup>a</sup> In de uiterste grenstoestand kan voor  $\psi_2$  voor thermische belasting 0 worden aangehouden.

<sup>b</sup> Voor aanrijding op of onder de brug en aanvaring is  $\psi_1 = 0$ .

<sup>c</sup> Voor aanrijding op of onder de brug en aanvaring is  $\psi_1 = 0,4$ .

OPMERKING Groepen verkeersbelastingen hoeven niet met elkaar te zijn gecombineerd.

Tabel NB.12 – A2.4(B) — Rekenwaarden voor de belastingen in CC2 (STR/GEO) (groep B)

Blijvend en tijdelijke ontwerpsituaties	Blijvende belastingen		Voor-spanning	Overheersende veranderlijke belasting <sup>a)</sup>	Tegelijkertijd optredende veranderlijke belastingen <sup>a</sup>	
	Ongunstig	Gunstig			Belangrijkste (indien aanwezig)	Andere
(Vgl. 6.10a)	$\gamma_{G,j,sup} G_{k,j,sup}$	$\gamma_{G,j,inf} G_{k,j,inf}$	$\gamma_P$		$\gamma_{Q,1} \psi_{0,1} Q_{k,1}$	$\gamma_{Q,i} \psi_{0,i} Q_{k,i}$
(Vgl. 6.10b)	$\xi \gamma_{G,j,sup} G_{k,j,sup}$ waarbij $\xi = 0,80$	$\gamma_{G,j,inf} G_{k,j,inf}$	$\gamma_P$	$\gamma_{Q,1} Q_{k,1}$		$\gamma_{Q,i} \psi_{0,i} Q_{k,i}$

<sup>a</sup> Veranderlijke belastingen zijn die, die zijn beschouwd in tabellen NB.9 – A2.1, NB.10 – A2.2 en A2.3.

Tabel NB.13 – A2.4(B) — Belastingsfactoren voor wegverkeersbruggen en bruggen voor langzaam verkeer en voetgangers- en fietsbruggen STR/GEO) (groep B)

Gevolgklasse	$\beta$	G			Verkeer (met $\psi = 1$ )	Overig veranderlijk (met $\psi = 1$ )
		$\gamma_{G,j,sup}$		$\gamma_{G,j,inf}$		
		6.10a	6.10b (incl. $\xi$ )	6.10a en 6.10b		
CC1	3,3	1,20	1,10	0,9	1,20	1,35
CC2	3,8	1,30	1,20	0,9	1,35	1,5
CC3	4,3	1,40	1,25	0,9	1,5	1,65

$\gamma = 0$  voor gunstig werkende veranderlijke belastingen

Voor  $\gamma_P$  zie de aanbevelingen in de desbetreffende materiaalgebonden Eurocodes 1992 t.m. 1999.

Voor de berekening van het effect van ongelijkmatige zettingen geldt dat  $\gamma_{G,set} = 1,20$  in het geval van een lineaire berekening en  $\gamma_{G,set} = 1,35$  in het geval van een niet lineaire berekening. Gunstig werkende zettingsverschillen worden niet in rekening gebracht. De grootte van de zettingen is bepaald op basis van de karakteristieke belastingscombinatie en de karakteristieke waarden voor de grondeigenschappen.

OPMERKING De factor  $K_{F1}$  volgens B 3.3 is in de waarden van  $\gamma$  verwerkt; voor de zettingsberekening blijft de betrouwbaarheidsdifferentiatie achterwege.

Tabel NB.17 – A2.2 —  $\psi$ -waarden voor voetgangers- en fietsbruggen

Belasting	Belastingscombinaties									
	gr1	gr2	$Q_{fwk}$	Onbedoeld voertuig <sup>b</sup>	$W^c$		$T^d$		S	A1 <sup>a,c</sup>
Gelijkmatig verdeelde belasting	1	0,8	0	0	0,4	0,32	0,4	0,32	0	0,4
Horizontale belasting	1	1,0	0	0	0,4	0,4	0,4	0,4	0	0,4
Dienstvoertuig $Q_{serv}$	0	1,0	0	0	0	0,4	0	0,4	0,8	0
Geconcentreerde belasting $Q_{fwk}$	0	0	1	0	0	0	0	0		0
Onbedoeld voertuig	0	0	0	1	0		0		0	0
Wind $F_{wk}$	0,3	0,3	0	0	1,0	1,0	0,3	0,3	0,3	0
Temperatuur	0,3	0,3	0	0	0,3	0,3	1,0	1,0	0,3	0
Sneeuw	0	0	0	0	0	0	0	0	1,0	0
Impact op of onder de brug	0	0	0	0	0	0	0	0	0	1
Aardbevingsbelasting	0	0	0	0	0	0	0	0	0	0
<sup>a</sup> A1 = aanrijding op of onder de brug en aanvaring.										
<sup>b</sup> Te beschouwen als gewoon belastingsgeval (geen calamiteit); zie 5.6.3.										
<sup>c</sup> Bij deze combinatie is in eerste kolom de verticale belasting vermenigvuldigd met $\psi_0$ en de horizontale met $\psi_0^2$ ; in de tweede kolom is dat omgekeerd; dit is gedaan om consistent te zijn met het gebruik van de groepen verkeersbelastingen.										

Bovenstaande tabel is de uitwerking van uitdrukking (6.10b). In de tabel zijn de blijvende belastingen en de voorspanning niet aangegeven. Voor ongunstig werkende blijvende belastingen is  $\gamma$  afhankelijk van de gevolgklasse en voor gunstig werkende blijvende belastingen geldt  $\gamma = 0,90$ . Voor de voorspanning moet de voorgeschreven waarde voor  $\gamma$  overeenkomstig het relevante Eurocodedeel worden aangehouden.

## C2 Eurocode standards

Eurocode chapters of interest:

1. NEN-EN 1990 Basis of structural design;
  - a. A2 annex for application of general rules and guidelines on concrete bridge design
  - b. The other chapters in the code mainly describe the meaning of the rules and in which cases the rules are of application
  - c. Table A2.1 and A2.2 show the values of the combination coefficients in Case of pedestrian/bicycle bridges
  - d. Table A2.4 shows contains the design values of the different types of loads for ULS combination cases
  - e. Table A2.6 is used for the SLS combinations of the load combinations
  - f. 6.4.3.2 describes the formulae for combining different loading cases to determine the most unfavourable loading situations. See picture snaps.
  - g. 6.5.3 can be used to determine the characteristic values of the loads that have to be checked for SLS purposes.
  - h. National Annex;
    - i. Table NB.10 A2.2 should be used for combination factors (see snap)
    - ii. Table NB.12 A2.4 Calculation value
    - iii. Table NB.13 A2.4 Partial safety factors
    - iv. Table NB.17 A2.2 Combination factors
  - i.  $\Psi_0$  is used for a basic variable load
  - j.  $\Psi_1$  is used for a frequent variable load
  - k.  $\Psi_2$  is used for a quasi-permanent variable load
2. NEN-EN 1991-2 Traffic Loads on Bridges
  - a. Chapter 4; Traffic Bridges in General
    - i. Only applicable for vehicles
  - b. Chapter 5; Pedestrian and Bicycle Bridges
    - i.  $Q_{fk} = 2.0 + 120 / (L + 30)$  [kN/m<sup>2</sup>]
    - ii.  $Q_{fk} \leq 5.0$  and  $Q_{fk} \geq 2.5$
    - iii. Concentrated load by Eurocode standards should be equal to 10 kN concentrated on an area of 0.1x0.1 m<sup>2</sup>.
    - iv. The load can vary based on the value of the national annex. The value of service vehicles should be used if the structure is to be able to carry such service vehicles.
    - v. Horizontal load along the deck upper surface layer
      1. 10% of the UDL value
      2. 60% of the service vehicle (if specified)
    - vi. Load groups:
      1.  $q_{fk}$  and  $Q_{fk}$
      2.  $Q_{ser}$  and  $Q_{flk}$
    - vii. Relevant eigenfrequencies of the structure (for vertical, horizontal and torsional vibrations) have to be tested to deviate from loading frequencies.
    - viii. Railing system is loaded with a vertical or horizontal UDL load of 1.0 kN
  - c. National Annex
    - i. In case of a publicly accessible bridge the railing structure needs to be designed to withstand a UDL of 3.0 kN/m<sup>2</sup> in horizontal and vertical direction separately.'

- ii. 5.3.2.1 describes the formula for determining the value of  $Q_{fk}$ , which in this case is equal to 5 kN/m<sup>2</sup>
    - iii. 5.3.2.2 describes the configuration of the concentrated load  $Q_{fvd}$ , which in this case is equal to 7 kN on a surface of 0.1x0.1 m<sup>2</sup>.
  - d. National Annex NB.A; Models for dynamic loading of pedestrian/bicycle bridges;
    - i. Not required in this case?
- 3. NEN-EN 1991-1-1; Actions on structures;
  - a. Section 5; Self-weight of construction works ;
    - i. The self-weight of the construction works includes structural elements, non-structural elements and earth/ballast.
  - b. 5.2.3; Additional provisions for bridges;
    - i. This section mainly addresses large bridge structures such as railway bridges.
  - c. Section 6; Imposed loads on buildings
    - i. This section identifies commonly used values of loading cases
    - ii. The section is organized based on the type of use and equipment related to the purpose of the section. For example, load configuration and impact areas due to traffic.
  - d. Annex A addresses different types of construction materials and their average density.
  - e. National Annex;
    - i. Table 6.1 addresses loads for multiple types of uses of a structure.
    - ii. This entire document is not really relevant for bridges.
- 4. NEN-EN 1991-1-3; Snow loading
  - a. Section 5 Snow load on roofs:
    - i. 5.2 (3) c; Accidental snow action  $s = \mu_i \cdot S_k$
    - ii. 5.3.2 according to table 5.2 the load shape coefficient for a flat roof (<30) is 0.8
    - iii. Can't find the characteristic snow load in the NEN code, however in the Dutch code, EN, the snow load is defined as 0.7 kN/m<sup>2</sup>.
    - iv. Because of the accidental load combination the combination factors are all zero.
  - b. Annex C
    - i. Shows the maps with the ground snow load per area in Europe.
    - ii. The Netherlands are shown in the Western European map.
    - iii. According to the colour coding the zone of Gemert is zone 2 which leads to a snow load of 0.2 kN/m<sup>2</sup>
    - iv. In the design however the load is used as 0.7 kN/m<sup>2</sup>
- 5. NEN-EN 1991-1-4; Wind loading
  - a. Section 4; Wind velocity and velocity pressure
    - i. Basic wind velocity;  $v_b = C_{dir} \cdot C_{season} \cdot v_{b,0}$
    - ii. These values can depend on the height of testing of the structure
    - iii. Table 4.1 terrain category; Terrain category 3 [ $z_0 = 0.3$  m and  $z_{min} = 5$  m]
    - iv. Correction value for the probability;  $C_{prob} = ((1 - K \cdot \ln(-\ln(1-p)))) / (1 - K \cdot \ln(-\ln(0.98)))^n$
    - v. Mean wind value;  $V_m(z) = C_r(z) \cdot C_o(z) \cdot v_b$
    - vi. Use  $z_{min}$  as value for height, this makes the roughness factor;  $C_r(z) = K_r \cdot \ln(z/z_0)$
    - vii. The terrain factor depends on;  $K_r = 0.19 \cdot (z_0/0.05)^{0.07}$



- viii. The terrain orography is less than 3% therefore;  $C_o=1.0$
- ix. Wind turbulence intensity;  $I_v(z)=\sigma_{vav}/V_m(z)$
- x. The standard deviation of turbulence is;  $\sigma_{vav}=K_r \cdot V_b \cdot K_I$
- xi. The recommended value for the turbulence factor  $K_I$  is 1.0
- xii. The peak velocity pressure is;  $q_p(z) = (1+7 \cdot I_v(z)) \cdot 1/2 \cdot \rho \cdot V_m(z)^2$  in which  $\rho$  is the air density ( $\rho=1.25 \text{ kg/m}^3$ )
- xiii. The basic velocity pressure is;  $q_b=1/2 \cdot \rho \cdot V_b^2$
- xiv. The exposure factor is;  $C_e(z)=q_p(z)/q_b$
- b. Section 5; Wind actions
  - i. Table 5.1; calculation procedure; section 4 is for velocity, section 5 and 7 for pressure and section 6 for the structural factor.
  - ii. Wind pressure;  $w_e=q_p(z_e) \cdot C_{pe}$  [e is for external]
- c. Section 6; Structural factor  $C_s C_d$ 
  - i. Not applicable to bridge design
  - ii. Therefore  $C_s=C_d=1.0$
- d. Section 7; Pressure and force coefficients
  - i. Mainly used for special structures (such as canopies and rooftops with multiple sections)
- e. Section 8; Wind action on bridges
  - i. Only applicable to bridge design with a constant depth
  - ii. Directions:
    - 1. X; parallel to the deck
    - 2. Y; along the span
    - 3. Z; perpendicular to the deck
  - iii. Recommended value for  $v_{b,0}=23 \text{ m/s}$
  - iv. Figure 8.3; Force coefficient for bridges  $C_{fx,0}$ 
    - 1.  $b/d_{tot}=3500/(850+2 \cdot 1200)=1.09$
    - 2. Type a; open parapets (more than 50%)
    - 3.  $C_{fx,0}=2.4-[(2.4-1.3)/(4-0.5)] \cdot [(1.09-0.5)/(4-0.5)]=2.3$
  - v. In the absence of wind tunnel testing the recommended value for the force coefficient is  $\pm 0.9$
  - vi. Wind forces in the Y-direction depend on the national annex and on the shape of the bridge design. Recommended values are 25% of the x-direction for plated and 50% of the x-direction for truss bridges.
- f. National Annex NL
  - i. Zone 3 according to figure NB.1;
    - 1.  $v_{b,0}=24,5 \text{ m/s}$
  - ii.  $C_{dir}=C_{season}=1.0$
  - iii.  $K=0.281$  [shape parameter]
  - iv.  $n=0.5$  [exponent]
  - v. Terrain class 3 (urban environment) [NB.3-4.1]
    - 1.  $Z_0=0.5 \text{ m}$
    - 2.  $Z_{min}=7 \text{ m}$
    - 3.  $P=0.01$  [wind exceedance probability]
  - vi.  $Q_{w,x}=0,5 \cdot \rho \cdot C_{fx} \cdot C_e(z) \cdot (C_{prob} \cdot V_b)^2$
  - vii.  $Q_{w,x}=0,5 \cdot \rho \cdot C_{f,z} \cdot C_e(z) \cdot (C_{prob} \cdot V_b)^2$
  - viii.  $Q_{w,y} = ?$
- g. Annex A.3 ; Numerical Calculation of orography coefficients;
  - i. Contains the formulas to calculate the effect of the wind slopes on the wind loading. If the value is smaller than 0.3 than the coefficient for orography is equal to 1.0.

- ii. Slope factor is;  $\Phi = H/L_u$ 
      - 1. H is the effective height of the slope;  $H=0$
      - 2.  $L_u$  is the actual length of the upwind slope in the wind direction;  $L_u=10$  m
    - iii. Therefore  $\Phi=0/10=0$  so  $C_o=1.0$
  - 6. NEN-EN 1991-1-5; Thermal actions
    - a. Stresses and strains in the structure due to seasonal variation in temp., solar radiation, shading and such. Stresses and strains depend on the variation of the temperature throughout the cross-section
    - b. Uniform temperature component;  $dT_u = T - T_0$
    - c. Section 6 ; Bridge design
      - i. Concrete is considered to be of type 3
      - ii. T is used for the shade air temperature
      - iii.  $T_e$  is used for the uniform bridge temp
      - iv. Table 6.1 addresses the recommended values of linear temperature differences. Concrete box girders have a recommended value of 10 degrees C for a warm top and 5 degrees C for a warm bot. Other designs have a value of 15 and 8 respectively
      - v. Table 6.2 addresses the effect of the surface thickness.
    - d. The code does not specify any loads due to the thermal actions imposed on the bridge.
    - e. However, since the bridge is not clamped on either side the structure is free to deform and therefore will not be influenced by temperature induced stress.
  - 7. NEN-EN 1991-1-6; Loading during the construction phase;
    - a. Table 4.1 shows the characteristic loads for construction activities.
      - i. Personnel and hand tools;  $Q_{ca}=1.0$  kN/m<sup>2</sup>
      - ii. Storage of movable items;  $Q_{cb}=0.2$  kN/m<sup>2</sup> and  $F_{cb}=100$  kN
      - iii. Non-permanent equipment;  $Q_{cc}=0.5$  kN/m<sup>2</sup>
    - b. NB. A1.1(1) representative values of the variable actions due to construction loads :
      - i. Combination factor  $\Psi_0=1.0$
      - ii. Combination factor  $\Psi_1=0.2$
    - c. A1.3(2) characteristic value of the horizontal load shall be taken as 3% of the vertical load in the most unfavourable combination of actions.
    - d. Annex A2 supplementary rules for bridges;
      - i. Design value of horizontal friction forces shall be taken as 10%
      - ii. The friction coefficient  $\mu_{min}=0$  and  $\mu_{max}=0.04$
  - 8. NEN-EN 1992-1-1; Design of concrete structures;
    - a. 4 Environmental influence
      - i. XF means freeze or thaw attack
      - ii. Class 2 represents moderate saturation of fluids with de-icing agents
      - iii. Class 4 represents high saturation of fluids with de-icing agents
      - iv. Concrete cover;  $C_{nom} = C_{min} + dC_{dev}$
      - v. 4.4.1.2 can be used to determine the value of  $C_{nom}$ . However the application in this case maybe rather insignificant because of the application of the tendons in the centre of the print path geometry.
    - b. 5 Structural analysis
      - i. Accurate description of the calculation procedure and the scope of the application of certain formulas.
      - ii. Not necessary for my research, maybe for model verification

- c. 5.10 Prestressed members and structures
  - i. Description of the different types of prestressing configuration and their respective formulas.
  - ii.
- d. 6 ULS (page 22-34)
  - i. 6.1 Bending;
    - 1. For prestressed members with permanently unbonded tendons see 5.10.8
  - ii. 6.2.2 Shear in members not requiring design shear reinforcement:
    - 1. Formula 6.4 (see snapshots) explains the procedure of calculating the regions un-cracked in bending where the flexural tensile stress is smaller than  $f_{ctk0,05}/\gamma_{mac}$ .
    - 2. Formula 6.2a is to be used in prestressed single span members without shear reinforcement see snapshot.
  - iii. 6.2.3 Shear in members requiring design shear reinforcements
- e. 7 SLS
  - i. 7.2 Stress limitations:
    - 1. In the absence of measures such as an increase in the cover to reinforcement in the compressive zone or confinement by transverse reinforcement, it may be appropriate to limit the compressive stress to a value of  $k_1 \cdot f_{ck}$  in areas exposed to environment classes (XD, XF a XS) see table 4.1.
  - ii. 7.3 Crack Control
    - 1. For members with only unbonded tendons, the requirements for reinforced concrete elements apply.
  - iii. 7.4 Deflection control
    - 1. In general the deflection of a slab or member should not exceed a maximum value of the span length divided by 250. Calculated under quasi-permanent loading.
- f. 8 Detailing of reinforcement and prestressing
- g. National Annex;
  - i. 2.4.2.2 Partial factors for prestressing stress
    - 1. 1.0 for favourable behaviour
    - 2. 1.2 for unfavourable behaviour
  - ii. Table 2.1 N Partial factors for materials in ULS
    - 1. Temp and perm concrete  $\gamma_c=1.5$
    - 2. Temp and perm rebar  $\gamma_s=1.15$
    - 3. Temp and perm prestress  $\gamma_p=1.1$
  - iii. 3.1.6; Calculation value of  $\alpha_{acc}=\alpha_{act}=1.0$
  - iv. Table 4.3 Construction class
    - 1. Designed life 100 year; XC1 and XC4 additional two classes
    - 2. Irrelevant because of the design,
  - v. Table 4.4 & 4.5 Minimum coverage values
    - 1. Dependent on the construction class and the environment class
    - 2. Should include the additional two classes for the designed life
  - vi. 5.2 Geometrical imperfection  $\Theta_0=1/300$
  - vii. 5.5 Elastically redistribution of forces
  - viii. 5.8.3.1; Slenderness criterion for isolated members;

1. Limit value for the slenderness ratio, if the slenderness is below this ratio the second order effects may be ignored.
  - ix. 6.2.2 formula 6.2 b for non-reinforced cracked concrete zones
    1.  $K1=0.15$
    2.  $V_{min}=0.035 \cdot k^{3.2} \cdot f_{ck}^{1/2}$
  - x. 6.2.2 formula 6.4 for cracked regions of non-reinforced concrete zone
    1. Depends on the values of  $f_{ctd}$  and  $f_{ctd,0.05}$
    2. Alpha I for non pretensioned tendons is 1.0
  - xi. The national annex does not provide extra formulas and does not require extra formulas on top of the NEN code.
9. NEN-EN-1992-2; Design and detailing of concrete bridges:
- a. Same setup as NEN-EN-1992-1-1, provides additional rules specifically for the design of concrete bridges.
  - b. The code and the national annex do not provide extra checks or values compared to NEN-EN-1992-1-1 in the cases of ULS bending and Shear design verification.
  - c.

## C3 Method statement

# Method Statement; Structural Analysis

Following topics are addressed in this document:

1. Project information
  - 1.1. General information
  - 1.2. Design description and objective
  - 1.3. Design standards and regulations
    - 1.3.1. Load-related standards
    - 1.3.2. Materials-related standards
    - 1.3.3. Other standards
2. Structural information
  - 2.1. Safety and construction class
  - 2.2. Materials properties
  - 2.3. Durability class
  - 2.4. Software
3. Loading condition
  - 3.1. Loads on structure
    - 3.1.1. Permanent loads
    - 3.1.2. Variable loads
    - 3.1.3. Load groups
  - 3.2. Load combinations
  - 3.3. Load factors
  - 3.4. Combination factors
4. Model and design verifications
  - 4.1. Design model
    - 4.1.1. Schematic representation
    - 4.1.2. Finite Element Analysis
  - 4.2. Design verifications
    - 4.2.1. Bending verification
    - 4.2.2. Shear force verification
    - 4.2.3. Creep and shrinkage
    - 4.2.4. Resistance verification ULS

## 1. Project information

### 1.1 General information

This document presents fundamental information used to develop a structural analysis model of a 3D printed concrete (3DPC) bridge. The structural analysis model is used in a research project as part of a novel design model. In the research project, the design model is used to study the relation between the structural efficiency and environmental impact of a 3DPC bridge. This document aims to increase the transparency and reproducibility of the structural analysis. The structural analysis performed by the design model is based on published information regarding the design of the 3DPC bridge in Gemert.

### 1.2 Design description and objective

The structural analysis described in this document aims to verify the structural safety of a 3DPC pedestrian/cyclist bridge. The structural analysis is based on the design of the 3DPC bridge in Gemert (Brabant, The Netherlands). The content of the structural analysis is based on an article published by T.A. Salet et al [1]. The article describes design verifications performed to verify the structural safety of the Gemert bridge.

The objective of the structural analysis is to express the structural safety in a material utilisation ratio, also referred to as a unity check. The performed checks are described in Section 4.2 and based on the mentioned article published by T.A. Salet et al. The objective of this document is to document the method used for the structural analysis. Following input is used in the design of the 3DPC bridge in Gemert;

- The span-length is 6,5 meter.
- The width of the bridge is 3,5 meters and the height of the bridge is 0,80 meters. Both width and height remain constant along the span.
- The structure built up of several 3D printed elements between two clamping blocks.
- The bridge is post-tensioned using 16 tendons, 6 in the top row and 10 in the bottom row.
- The structure is simply supported; one hinge connection and one slider connection.



Figure 1; Visualisation of the Gemert design in the article of T.A.M. Salet et al - [1]

### 1.3 Design standards and regulations

#### 1.3.1 Load-related Standards

Standard	Title
NEN-EN 1990+A1+A1/C2;2011	Basis of structural design
NEN-EN 1990+A1+A1/C2/NB	Dutch national annex to NEN-EN 1990
NEN-EN 1991-1-1+C1:2011	Actions on structures - Part 1-1: General actions - Densities, Self-weight, imposed loads for buildings
NEN-EN 1991-1-1+C1/NB	Dutch National annex to NEN-EN 1991-1-1
NEN-EN 1991-1-3+C1;2011	Actions on structures - Part 1-3: General actions - Snow loads
NEN-EN 1991-1-3+C1/NB	Dutch National annex to NEN-EN 1991-1-3
NEN-EN 1991-1-4+A1+C2:2011	Actions on structures - Part 1-4: General actions - Wind actions
NEN-EN 1991-1-4+A1+C2/NB	Dutch National annex to NEN-EN 1991-1-4
NEN-EN 1991-2+C1:2011	Actions on structures - Part 2: Traffic loads on bridges
NEN-EN 1991-2+C1/NB	Dutch National annex to NEN-EN 1991-1-2



### 1.3.2 Material-related standards

Standard	Title
NEN-EN 1992-1-1+C2:2011	Design of concrete structures - Part 1-1: General rules and rules for Buildings
NEN-EN 1992-1-1+C2/NB	Dutch national annex to NEN-EN 1992-1-1
NEN-EN 1992-2+C1:2011	Design of concrete structures - Part 2: Concrete bridges - Design and detailing rules
NEN-EN 1992-2+C1/NB	Dutch National annex to NEN-EN 1992-2

### 1.3.3 Other standards

Standard	Title
RTD 1001:2017 version 1.4	Guidelines for design of artworks (ROK 1.4)
RTD 1009:2012 version 1.0	Directive for the design of asphalt pavements on concrete and steel bridge decks

## 2. Structural information

### 2.1 Safety and construction class

The structural design is based on following two conditions regarding the safety and use of the structure:

1. The safety class is CC1, conform Eurocode NEN-EN 1991; standard in design of bridges.
2. The calculation life span is 100 years, conform Eurocode NEN-EN 1991; standard in design of bridges.

### 2.2 Material properties

The properties of 3D printed concrete used in the structural analysis are derived from the article published by T.A. Salet et al [1].

Property	Dir.	Age	Symbol	Value
Density		28 days	$\rho$	2,000 kg/m <sup>3</sup>
Modulus of elasticity		28 days	$E$	19,000 MPa
Average compressive strength	$u$	28 days	$f_{ck,u}$	23.2 MPa
	$v$	28 days	$f_{ck,v}$	21.5 MPa
	$w$	28 days	$f_{ck,w}$	21.0 MPa
	$u$	28 days	$f_{ct,u}$	1.9 MPa
Average tensile strength (also used for flexural tension)	$v$	28 days	$f_{ct,v}$	1.6 MPa
	$w$	28 days	$f_{ct,w}$	1.3 MPa
Creep factor <sup>a</sup>		7 days	$\Psi_7$	1.0
		14 days	$\Psi_{14}$	2.5
		56 days	$\Psi_{56}$	3.0
		56 days	$\epsilon_{56}$	1.5
Shrinkage		7 days	$\epsilon_7$	0.6
		14 days	$\epsilon_{14}$	1.2
		56 days	$\epsilon_{56}$	1.5

<sup>a</sup>After 28 days.

Notes: For the directional dependency, a relative orientation of axis  $u$ ,  $v$ ,  $w$  is used (Bos *et al.*, 2016), indicating the direction parallel to the print in the horizontal plane, perpendicular to the print direction in the horizontal plane, and vertically perpendicular to the print direction (or parallel to the robot arm), respectively.

Table 1; Material properties determined for the 3DPC bridge in Gemert by T.A.M. Salet et al - [1]

Because a limited amount of research has been published regarding structural behaviour of 3DPC, other properties of concrete are chosen similar to concrete class C12/15. These properties are based Eurocode standards document number NEN-EN 1992-1-1.

The values of the strain indicated in figure 3.4 of Eurocode NEN-EN 1992-1-1 are listed, in table 3.1 of the Eurocode document, as;

$$\epsilon_{c3} = 0,175 \%$$

$$\epsilon_{cu3} = 0,350 \%$$

(2) Other simplified stress-strain relationships may be used if equivalent to or more conservative than the one defined in (1), for instance bi-linear according to Figure 3.4 (compressive stress and shortening strain shown as absolute values) with values of  $\varepsilon_{c3}$  and  $\varepsilon_{cu3}$  according to Table 3.1.

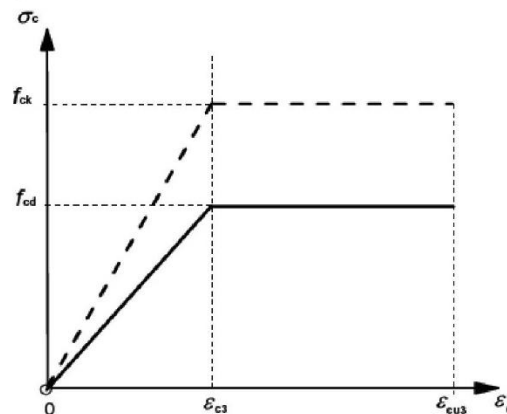


Figure 3.4: Bi-linear stress-strain relation.

#### 2.4.2.4 Partial factors for materials

(1) Partial factors for materials for ultimate limit states,  $\gamma_c$  and  $\gamma_s$  should be used.

**Note:** The values of  $\gamma_c$  and  $\gamma_s$  for use in a Country may be found in its National Annex. The recommended values for 'persistent & transient' and 'accidental, design situations are given in Table 2.1N. These are not valid for fire design for which reference should be made to EN 1992-1-2.

For fatigue verification the partial factors for persistent design situations given in Table 2.1N are recommended for the values of  $\gamma_{c,fat}$  and  $\gamma_{s,fat}$ .

Table 2.1N: Partial factors for materials for ultimate limit states

Design situations	$\gamma_c$ for concrete	$\gamma_s$ for reinforcing steel	$\gamma_s$ for prestressing steel
Persistent & Transient	1,5	1,15	1,15
Accidental	1,2	1,0	1,0

#### 3.1.6 Design compressive and tensile strengths

(1)P The value of the design compressive strength is defined as

$$f_{cd} = \alpha_{cc} f_{ck} / \gamma_c \quad (3.15)$$

where:

$\gamma_c$  is the partial safety factor for concrete, see 2.4.2.4, and

$\alpha_{cc}$  is the coefficient taking account of long term effects on the compressive strength and of unfavourable effects resulting from the way the load is applied.

**Note:** The value of  $\alpha_{cc}$  for use in a Country should lie between 0,8 and 1,0 and may be found in its National Annex. The recommended value is 1.

(2)P The value of the design tensile strength,  $f_{ctd}$ , is defined as

$$f_{ctd} = \alpha_{ct} f_{ctk,0,05} / \gamma_c \quad (3.16)$$

where:

$\gamma_c$  is the partial safety factor for concrete, see 2.4.2.4, and

$\alpha_{ct}$  is a coefficient taking account of long term effects on the tensile strength and of unfavourable effects, resulting from the way the load is applied.

**Note:** The value of  $\alpha_{ct}$  for use in a Country may be found in its National Annex. The recommended value is 1,0.

The properties of the post-tensioning tendons represent Y1860 high grade tendons. These properties are derived from the TU Delft course CIE 4160 – Prestressed concrete;



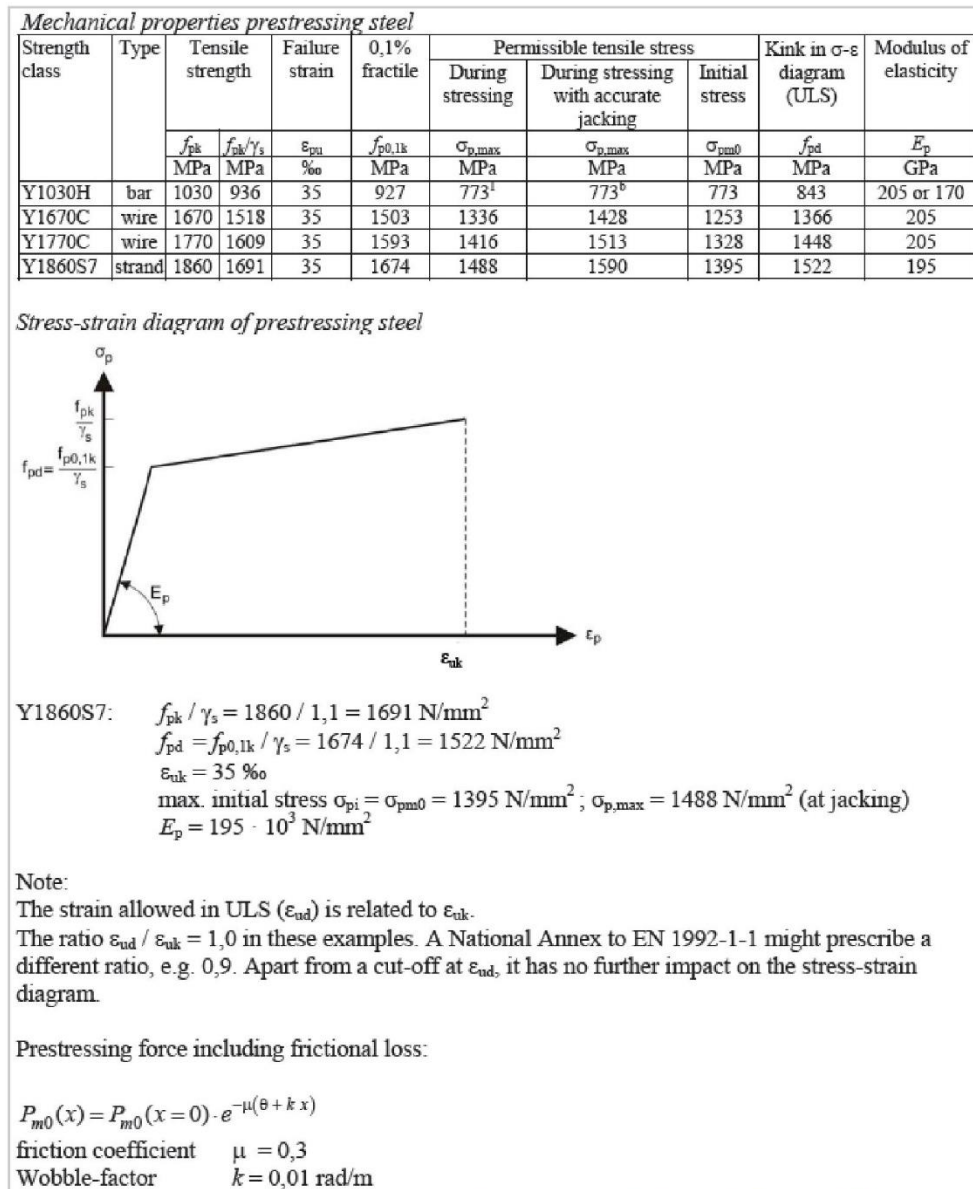


Figure 2; Pre/Post-tensioning steel properties by Walraven & Braam - [2]

### 2.3 Environmental influence class

The durability class is based on the use of the bridge, pedestrian & cyclists, and the location of the bridge, Gemert - Brabant - The Netherlands. Based on these properties the environmental influence class of the bridge is determined by the presence of de-icing salt. During winter season, the chance of de-icing salt very high. The environmental influence class of the structure is therefore identified as XF4. This environmental influence class indicates a high saturation of fluids with de-icing agents.

### 2.4 Software used for analysis

The software used for calculating and simulating structural behaviour is as follows;

- Microsoft Excel; calculation control document and geometric properties
- Rhinoceros 5.0; 3D visualisation of the structure
- Grasshopper 0.9.0076; visual script environment for parametrically control of Rhino
- SCIA Engineer 17.01; finite element analysis software for structural analysis

### 3. Loading condition

#### 3.1 Loads on structure

##### 3.1.1 Permanent loads

The permanent loads used in the structural analysis are the result of following self-weight of materials in the structure;

Material	Self-weight	Unit	Source
3D printed concrete	2000	kN/m <sup>3</sup>	T.A. Salet et al [1]
Pressure layer	33	kN/m <sup>3</sup>	RTD 1009:2012 version 1.0
Finishing layer	25	kN/m <sup>3</sup>	RTD 1009:2012 version 1.0
Y1860 tendon	0,7263	kN/m	Dywidag tendons

##### 3.1.2 Variable loads

Traffic loads determined for a bridge used by pedestrians and cyclists are based on NEN-EN 1991-2 NB section 5 and NEN-EN 1990-1 A2. Using these documents, the following vehicle loads are used;

Load name	Load value	Load unit	Source
Distributed traffic	5,0	kN/m <sup>2</sup>	NEN-EN 1990 A2
Concentrated traffic	7,0	kN	NEN-EN 1990 A2

Snow loads are based on NEN-EN 1991-1-3. Using the Eurocode document and the deck area of the structure, the following snow load is calculated;

Load name	Load value	Load unit	Source
Vertical snow load	0,58	kN/m <sup>2</sup>	NEN-EN 1991-1-3

Wind loads are based on NEN-EN 1991-1-4. In the described design project, only the vertical wind load is taken into account because of a low amount of horizontal surface/exposure to wind. Using the Eurocode document, the following vertical wind load is calculated;

Load name	Load value	Load unit	Source
Vertical wind load	0,59	kN/m <sup>2</sup>	NEN-EN 1991-1-4

##### 3.1.3 Load groups

Because of the limited amount of loads, a singular load group is used in the described project. This load groups contains all loads described in Section 1.3.

#### 3.2 Load combinations

The load combination used to generate the critical load on the structure is based on Eurocode document NEN-EN 1990 section A2 and the Dutch national annex. The load combination standards for determining the critical load combination for design of bridge structures are;

Blijvend en tijdelijke ontwerpsituaties	Blijvende belastingen		Voor-spanning	Overheersende veranderlijke belasting <sup>3)</sup>	Tegelijkertijd optredende veranderlijke belastingen <sup>a</sup>	
	Ongunstig	Gunstig			Belangrijkste (indien aanwezig)	Andere
(Vgl. 6.10a)	$\gamma_{G,j,sup} G_{k,j,sup}$	$\gamma_{G,j,inf} G_{k,j,inf}$	$\gamma_P P$		$\gamma_{Q,1} \psi_{0,1} Q_{k,1}$	$\gamma_{Q,i} \psi_{0,i} Q_{k,i}$
(Vgl. 6.10b)	$\xi \gamma_{G,j,sup} G_{k,j,sup}$ waarbij $\xi = 0,80$	$\gamma_{G,j,inf} G_{k,j,inf}$	$\gamma_P P$	$\gamma_{Q,1} Q_{k,1}$		$\gamma_{Q,i} \psi_{0,i} Q_{k,i}$

<sup>a</sup> Veranderlijke belastingen zijn die, die zijn beschouwd in tabellen NB.9 – A2.1, NB.10 – A2.2 en A2.3.

### 3.3 Load factors

The load factors used to determine the critical load combination are based on Eurocode document NEN-EN 1990 and the Dutch national annex. The following load factors are used;

**Tabel NB.13 – A2.4(B) — Belastingsfactoren voor wegverkeersbruggen en bruggen voor langzaam verkeer en voetgangers- en fietsbruggen STR/GEO) (groep B)**

Gevolgklasse	$\beta$	G			Verkeer (met $\psi = 1$ )	Overig veranderlijk (met $\psi = 1$ )
		$\gamma_{G,i,sup}$		$\gamma_{G,i,inf}$		
		6.10a	6.10b (incl. $\xi$ )	6.10a en 6.10b		
CC1	3,3	1,20	1,10	0,9	1,20	1,35
CC2	3,8	1,30	1,20	0,9	1,35	1,5
CC3	4,3	1,40	1,25	0,9	1,5	1,65

$\gamma = 0$  voor gunstig werkende veranderlijke belastingen

Voor  $\gamma_F$  zie de aanbevelingen in de desbetreffende materiaalgebonden Eurocodes 1992 t.m. 1999.

Voor de berekening van het effect van ongelijkmatige zettingen geldt dat  $\gamma_{G,set} = 1,20$  in het geval van een lineaire berekening en  $\gamma_{G,set} = 1,35$  in het geval van een niet lineaire berekening. Gunstig werkende zettingsverschillen worden niet in rekening gebracht. De grootte van de zettingen is bepaald op basis van de karakteristieke belastingcombinatie en de karakteristieke waarden voor de grondeigenschappen.

OPMERKING De factor  $K_{FI}$  volgens B 3.3 is in de waarden van  $\gamma$  verwerkt; voor de zettingsberekening blijft de betrouwbaarheidsdifferentiatie achterwege.

### 3.4 Load combination factors

The load combination factors used to determine the critical load combination are based on Eurocode document NEN-EN 1990 and the Dutch national annex. The following load combination factors are used;

**Tabel NB.10 – A2.2 —  $\psi$ -factoren voor voetgangers- en fietsbruggen**

Belasting	Symbool		$\psi_0$	$\psi_1$	$\psi_2$
Verkeersbelastingen	gr1	Gelijkmatig verdeelde belasting $q_{fk}$	0,4	0,8 <sup>c</sup>	0,4
		Horizontale belasting $Q_{fk}$			
	gr 2	Gelijkmatig verdeelde belasting $q_{fk}$	0,4	0,8 <sup>b</sup>	0
		Dienstvoertuig $Q_{serv}$			
		Horizontale belasting $Q_{fk}$			
	Geconcentreerde belasting $Q_{fkk}$		0	0,8 <sup>b</sup>	0
	Onbedoeld voertuig (zie 5.6.3)		0	0,8 <sup>b</sup>	0
Windkrachten	$F_{wk}$ blijvende ontwerpituatie		0,3	0,6 <sup>b</sup>	0
	Uitvoering		0,8	0	
Thermische belastingen	$T_k$		0,3	0,8	0,3 <sup>a</sup>
Sneeuwbelastingen	$Q_{Sn,k}$ blijvende ontwerpituatie		0	0	0
	Uitvoering		0,8	0	
Belastingen tijdens de bouw	$Q_c$		1,0	0	1,0

<sup>a</sup> In de uiterste grenstoestand kan voor  $\psi_2$  voor thermische belasting 0 worden aangehouden.

<sup>b</sup> Voor aanrijding op of onder de brug en aanvaring is  $\psi_1 = 0$ .

<sup>c</sup> Voor aanrijding op of onder de brug en aanvaring is  $\psi_1 = 0,4$ .

OPMERKING Groepen verkeersbelastingen hoeven niet met elkaar te zijn gecombineerd.



## 4. Model and design verifications

### 4.1 Design model

#### 4.1.1 Schematic representation

Internal force distribution in the structure is calculated in SCIA Engineer. A total of four output distributions is generated; internal bending moment  $m_x$  [kNm/m], internal shear force  $v_x$  [kN/m], support moment  $M_x$  [kNm] and support force  $R_z$  [kN].

In SCIA Engineer, the structure is modelled as a number of 2D plates on two supports. The result of the modelling and the finite element mesh of the structure is presented in Figure 3. In Figure 3, the hinge support is located on the left side of the structure and the slider connection is located on the right side of the structure.

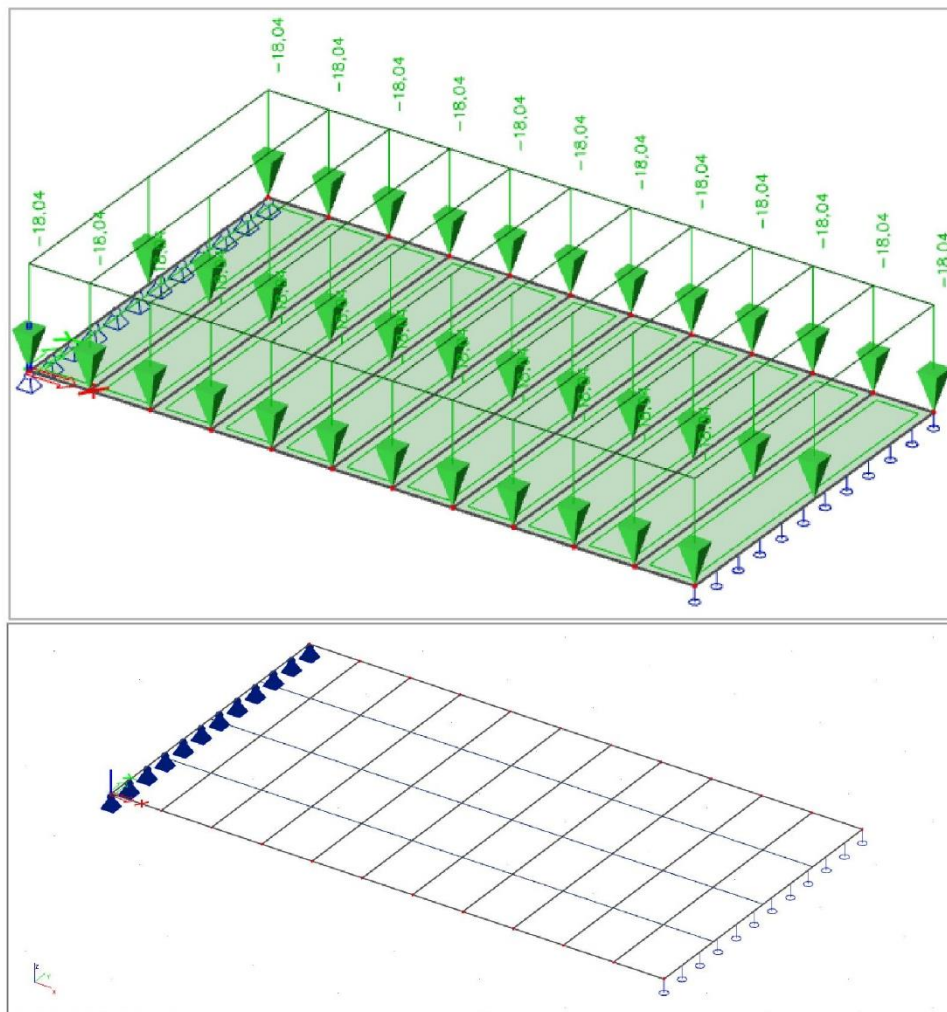


Figure 3; Model of the Gemert design case exported from SCIA Engineer – Top; representation as a number of plate elements including the load – Bottom; generated mesh for analysis

#### 4.1.2 Finite Element Analysis

The finite element analysis performed in SCIA Engineer uses a numerical approach based on matrix equations using the relation between displacement, stiffness and force. This formula can be presented in Matrix notation as  $K \times u = F$ . In this equation;  $K$  is the stiffness matrix,  $u$  is the displacement matrix and  $F$  is the force matrix. The displacements are measured in the nodes of the generated finite element matrix. The

displacement matrix contains lateral and rotational displacements. In matrix rotation, the equation can be presented as;

$$\begin{bmatrix} M_x \\ M_y \\ M_{xy} \\ T_x \\ T_y \end{bmatrix} = - \begin{bmatrix} D_{11} & D_{12} & 0 & & \\ D_{21} & D_{22} & 0 & & \\ 0 & 0 & D_{33} & & \\ & & & D_{11} & D_3 & 0 & 0 \\ & 0 & & 0 & 0 & D_{22} & D_3 \end{bmatrix} \cdot \begin{bmatrix} w_{xx} \\ w_{yy} \\ 2w_{xy} \\ w_{xxx} \\ w_{yyx} \\ w_{yyy} \\ w_{xxy} \end{bmatrix} \quad (1-6)$$

In the figure presented above the formula is written as  $F = K \times u$ . The values of the stiffness matrix can be calculated using the following equations;

$$D_{11} = \frac{E_1 h^3}{12(1 - \mu_{12} \mu_{21})}, \quad D_{22} = \frac{E_2 h^3}{12(1 - \mu_{12} \mu_{21})}$$

$$D_{12} = \mu_{21} D_{11} \equiv D_{21} = \mu_{12} D_{22}$$

$$D_{33} = G_{12} \frac{h^3}{12}$$

$$D_3 = 2D_{33} + D_{12} = 2D_{33} + D_{21}$$

$$\mu_{21} = \mu_{12} \frac{E_2}{E_1} = \mu_{12} \frac{D_{22}}{D_{11}}$$

$$G_{12} = \frac{\sqrt{E_1 E_2}}{2(1 + \sqrt{\mu_{12} \mu_{21}})}$$

The above presented equations are retrieved from the SCIA helpdesk using following link; [https://help.scia.net/download/16.0/en/OtrhotropTB\\_enu.pdf](https://help.scia.net/download/16.0/en/OtrhotropTB_enu.pdf)

The system of equations is solved based on the Cholesky decomposition method. The solution method is based on decomposition of a matrix into the product of a lower triangular matrix and its conjugate transpose. More information regarding this solution method can be found using following link;

[https://en.wikipedia.org/wiki/Cholesky\\_decomposition#Generalization](https://en.wikipedia.org/wiki/Cholesky_decomposition#Generalization)

#### 4.2 Design verifications

The internal force distributions calculated in SCIA Engineer are extracted as an element average value of an internal force for each of the mesh elements presented in Figure 3. As a result of the 2D plate analysis, the internal forces are expressed as a force intensity rather than a reaction force. The resulting internal forces therefore should be multiplied by the width

of the corresponding mesh element to obtain the reaction forces. This process is based on following equations;

$$M_{i,j} = m_{x,i,j} \times b_{i,j}$$

$$V_{i,j} = v_{x,i,j} \times b_{i,j}$$

$$R_{z,i} = \frac{\sum_{j=1}^{n-1} [(R_{z,i,j} + R_{z,i,j+1}) \times b_{i,j}/2]}{\sum_{j=1}^n b_{i,j}}$$

$$M_i = \frac{\sum_{j=1}^{n-1} [(M_{i,j} + M_{i,j+1}) \times b_{i,j}/2]}{\sum_{j=1}^n b_{i,j}}$$

These equations are derived from the TU Delft course CIE 4180 – Plate analysis and theory by Prof.dr.ir. J. Blaauwendraad [3, 4]. After obtaining the average reaction force in each of the mesh elements, the structural safety can be determined using Eurocode standards and equations from the TU Delft course pre-stressed concrete.

#### 4.2.1 Bending verification

#### 4.4 Prestressing with post-tensioned steel

In the case of prestressing with post-tensioned steel, the tendons are positioned in empty ducts that are installed before casting. After hardening of the concrete, the tendons are applied (or were already in the ducts before casting) and stressed. The ducts are injected with a special grout. After hardening of the grout, the cross-sections behave like composite cross-sections: steel and concrete work together. In that stage the prestressing steel behaves in the same way as the reinforcing steel in a non-prestressed structure.

##### 4.4.1 The transmission of the prestressing forces

When the prestressing force is exerted on the post-tensioned steel, this force does not act on the composite cross-section, because there is no bond yet between the prestressing steel and the concrete. Due to the prestressing, the beam will deform, which activates the selfweight as a load, see fig. 4.12.

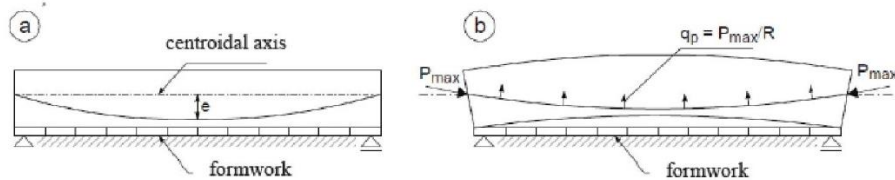


Fig. 4.12 Prestressing with post-tensioned steel  
a. Situation before applying the prestressing force  
b. Situation after applying the prestressing force

When at the manometer of the prestressing jack a force  $P_{\max}$  is indicated, the stresses in the concrete at midspan, at the bottom and at the top are:

Bottom:

$$\sigma_{cb} = -\frac{P_{\max}}{A_c} + \frac{M_g}{W_{cb}} - \frac{P_{\max} e_p}{W_{cb}} \quad (4.12a)$$

Top:

$$\sigma_{ct} = -\frac{P_{\max}}{A_c} - \frac{M_g}{W_{ct}} + \frac{P_{\max} e_p}{W_{ct}} \quad (4.12b)$$

Figure 4; calculation of the bending moment in post-tensioned structures by Walraven & Braam - [2]

#### 4.2.2 Shear force verification

The value of the shear capacity of the structure is calculated using Eurocode NEN-EN 1992-1-1 section 6.2.2.

##### 6.2.2 Members not requiring design shear reinforcement

(1) The design value for the shear resistance  $V_{Rd,c}$  is given by:

$$V_{Rd,c} = [C_{Rd,c} k (100 \rho_l f_{ck})^{1/3} + k_1 \sigma_{cp}] b_w d \quad (6.2.a)$$

with a minimum of

$$V_{Rd,c} = (v_{min} + k_1 \sigma_{cp}) b_w d \quad (6.2.b)$$

where:

$f_{ck}$  is in MPa

$$k = 1 + \sqrt{\frac{200}{d}} \leq 2,0 \text{ with } d \text{ in mm}$$

$$\rho_l = \frac{A_{sl}}{b_w d} \leq 0,02$$

$A_{sl}$  is the area of the tensile reinforcement, which extends  $\geq (l_{bd} + d)$  beyond the section considered (see Figure 6.3).

85

Dit document is door NEN onder licentie verstrekt aan: / This document has been supplied under license by NEN to:  
TU Delft gb\_tude 14-2-2018 17:18:41

##### EN 1992-1-1:2004 (E)

$b_w$  is the smallest width of the cross-section in the tensile area [mm]

$$\sigma_{cp} = N_{Ed}/A_c < 0,2 f_{cd} \text{ [MPa]}$$

$N_{Ed}$  is the axial force in the cross-section due to loading or prestressing [in N] ( $N_{Ed} > 0$  for compression). The influence of imposed deformations on  $N_E$  may be ignored.

$A_c$  is the area of concrete cross section [mm<sup>2</sup>]

$V_{Rd,c}$  is [N]

**Note:** The values of  $C_{Rd,c}$ ,  $v_{min}$  and  $k_1$  for use in a Country may be found in its National Annex. The recommended value for  $C_{Rd,c}$  is  $0,18/\gamma_c$ , that for  $v_{min}$  is given by Expression (6.3N) and that for  $k_1$  is 0,15.

$$v_{min} = 0,035 k^{3/2} \cdot f_{ck}^{1/2}$$

(6.3N)

#### 4.2.3 Creep and shrinkage

The value of the creep and shrinkage due to time dependent behaviour of concrete influences the post-tensioning force in the tendons. The elongation of the tendons is reduced due to shrinkage of concrete and therefore results in a reduction of stress in the structure. As a result, the time dependent shrinkage of concrete should be taken into account in determining the minimum post-tensioning force using following equations derived from Walraven & Braam [2].

$$\Delta \varepsilon_p = \varepsilon_{c,\infty} - \varepsilon_{c,0}$$

$$\varepsilon_{p,total} = \varepsilon_{p,0} + \Delta \varepsilon_p = \frac{P_m}{A_p \times E_p} + \Delta \varepsilon_p$$

$$P_{m0} = \varepsilon_{p,total} \times E_p \times A_p$$

The amount of shrinkage in the concrete is derived from Eurocode NEN-EN 1990 section 3.1.4.



### 3.1.4 Creep and shrinkage

(1)P Creep and shrinkage of the concrete depend on the ambient humidity, the dimensions of the element and the composition of the concrete. Creep is also influenced by the maturity of the concrete when the load is first applied and depends on the duration and magnitude of the loading.

(2) The creep coefficient,  $\varphi(t, t_0)$  is related to  $E_c$ , the tangent modulus, which may be taken as  $1,05 E_{cm}$ . Where great accuracy is not required, the value found from Figure 3.1 may be considered as the creep coefficient, provided that the concrete is not subjected to a compressive stress greater than  $0,45 f_{ck}(t_0)$  at an age  $t_0$ , the age of concrete at the time of loading.

**Note:** For further information, including the development of creep with time, Annex B may be used.

(3) The creep deformation of concrete  $\varepsilon_{cc}(\infty, t_0)$  at time  $t = \infty$  for a constant compressive stress  $\sigma_c$  applied at the concrete age  $t_0$ , is given by:

$$\varepsilon_{cc}(\infty, t_0) = \varphi(\infty, t_0) \cdot (\sigma_c / E_c) \quad (3.6)$$

(4) When the compressive stress of concrete at an age  $t_0$  exceeds the value  $0,45 f_{ck}(t_0)$  then creep non-linearity should be considered. Such a high stress can occur as a result of pretensioning, e.g. in precast concrete members at tendon level. In such cases the non-linear notional creep coefficient should be obtained as follows:

$$\varphi_k(\infty, t_0) = \varphi(\infty, t_0) \exp(1,5 (k_\sigma - 0,45)) \quad (3.7)$$

where:

$\varphi_k(\infty, t_0)$  is the non-linear notional creep coefficient, which replaces  $\varphi(\infty, t_0)$   
 $k_\sigma$  is the stress-strength ratio  $\sigma_c / f_{cm}(t_0)$ , where  $\sigma_c$  is the compressive stress and  $f_{cm}(t_0)$  is the mean concrete compressive strength at the time of loading.

### 4.2.4 Resistance verification ULS

$$E_d \leq R_d \quad (6.8)$$

where :

$E_d$  is the design value of the effect of actions such as internal force, moment or a vector representing several internal forces or moments ;

$R_d$  is the design value of the corresponding resistance.

NOTE.1 Details for the methods STR and GEO are given in Annex A.

NOTE 2 Expression (6.8) does not cover all verification formats concerning buckling, i.e. failure that happens where second order effects cannot be limited by the structural response, or by an acceptable structural response. See EN 1992 to EN 1999.

## Bibliography

1. Salet, T.A., et al., *Design of a 3D printed concrete bridge by testing*. Virtual and Physical Prototyping, 2018: p. 1-15.
2. Walraven, J.C. and C.R. Braam, *Prestressed Concrete*, in *CIE4160*. 2015, Delft Technical University of Technology: Delft. p. 4.8-4.13.
3. Blaauwendraad, J., *Theory*. Plate analysis, theory and application. Vol. 1. 2006, Delft: Technical University Delft. 96.
4. Blaauwendraad, J., *Numerical methods*. Plate analysis, theory and application. Vol. 2. 2006, Delft: Technical University Delft. 136.



# Annex D XML documentation

D1 XML identification document

# D1 XML identification document

```
<?xml version="1.0" encoding="UTF-16" standalone="yes"?>
```

```
<project xmlns="http://www.scia.cz">
```

Section 1 - XML identification code

```
<def uri="Model import test-3.xml.def"/>
```

Section 2 - Code definition file

```
<container id="{AC021036-C943-4B46-88E4-72CFB9D9391C}"
```

```
t="EP_GraphicDsObjects.EP_BaseDataProjectHeader.1">
```

```
<table id="{EF67D65A-95AC-4AD2-86C7-5FACD814BF57}"
```

```
t="ProjectData.EP_ProjectData.1" name="Project">
```

```
<h>
```

```
<h0 t="Licentienaam"/>
```

```
<h1 t="Licentienummer"/>
```

```
<h2 t="Nationale norm"/>
```

```
<h3 t="Versie"/>
```

```
<h4 t="Constructie"/>
```

```
<h5 t="Aantal knopen"/>
```

```
<h6 t="Aantal staven"/>
```

```
<h7 t="Aantal platen"/>
```

```
<h8 t="Aantal vaste lichamen"/>
```

```
<h9 t="Aantal gebruikte doorsneden"/>
```

```
<h10 t="Aantal belastingsgevallen"/>
```

```
<h11 t="Aantal gebruikte materialen"/>
```

```
<h12 t="Projectbestandsnaam"/>
```

```
<h13 t="Project bestandspad"/>
```

```
<h14 t="Project"/>
```

```
<h15 t="Onderdeel"/>
```

```
<h16 t="Omschrijving"/>
```

```
<h17 t="Auteur"/>
```

```
<h18 t="Datum"/>
```

```
<h19 t="Gravitatieversnelling"/>
```

```
<h20 t="Beton"/>
```

```
<h21 t="Staal"/>
```

```
<h22 t="Hout"/>
```

```
<h23 t="Ander materiaal"/>
```

```
<h24 t="Aluminium"/>
```

```
<h25 t="Metselwerk"/>
```

```
<h26 t="Standaard betonmateriaal"/>
```

```
<h27 t="Standaard wapeningsmateriaal"/>
```

```
<h28 t="Functionaliteit"/>
```

```
<h29 t="Nationale Bijlage"/>
```

```
</h>
```

```
<obj id="1">
```

```
<p0 v="Royal BAM Group"/>
```

```
<p1 v="631486"/>
```

```
<p2 v="EC - EN"/>
```

```
<p3 v="SCIA Engineer 17.01.2031"/>
```

```
<p4 v="8" t="Algemeen XYZ"/>
```

```
<p5 v=""/>
```

```
<p6 v=""/>
```

```
<p7 v=""/>
```

```
<p8 v=""/>
```

```
<p9 v=""/>
```

```
<p10 v=""/>
```

```
<p11 v=""/>
```

```
<p12 v="Model import test.ESA"/>
```

```
<p13 v="C:\Users\karel.van.dongen\Google Drive\Thesis\Calculations\XML\Tests"/>
```

**Met opmerkingen [DKv1]:** Definition document specification. The .def document contains all the table and data specification input required for importing the xml document in SCIA.

**Met opmerkingen [DKv2]:** Specification of container contents

**Met opmerkingen [DKv3]:** Specification of the table format

```

<p14 v=""/>
<p15 v=""/>
<p16 v=""/>
<p17 v=""/>
<p18 v=""/>
<p19 v="9.810000000000005"/>
<p20 v=""/>
<p21 v=""/>
<p22 v=""/>
<p23 v=""/>
<p24 v=""/>
<p25 v=""/>
<p26 v=""/>
<p27 v=""/>
<p28 v="Constructiemodel"/>
<p29 v="Standaard EN"/>
</obj>
</table>
</container>

```

Section 3 – Project Information

```

<container id="(77705284-EEB9-11D4-B450-00104BC3B531)"
t="EP_MaterialEP_Material.1">
  <table id="18B21719-5348-44DC-B1C4-171985C1E0C7"
t="EP_MaterialEC_EP_MaterialCrIEC_EN.1" name="Materialen">
    <h>
      <h0 t="Naam"/>
      <h1 t="UniquelD"/>
      <h2 t="Materiaaltype"/>
      <h3 t="Thermische uitzetting"/>
      <h4 t="Massa eenheid"/>
      <h5 t="Dichtheid in natte toestand"/>
      <h6 t="E-modulus"/>
      <h7 t="Poisson coeff."/>
      <h8 t="Onafhankelijke G-modulus"/>
      <h9 t="G-modulus"/>
      <h10 t="Log. decrement (niet-uniforme damping enkel)"/>
      <h11 t="Kleur"/>
      <h12 t="Specifieke hitte"/>
      <h13 t="Thermische geleiding"/>
      <h14 t="Volgorde in norm"/>
      <h15 t="Korrel diameter (dg)"/>
      <h16 t="Cementklasse"/>
      <h17 t="Karakteristieke cilinderdruksterkte fck(28)"/>
      <h18 t="Berekende afhankelijke waarden"/>
      <h19 t="Gemiddelde druksterkte fcm(28)"/>
      <h20 t="fcm(28) - fck(28)"/>
      <h21 t="Gemiddelde treksterkte fctm(28)"/>
      <h22 t="fctk 0,05(28)"/>
      <h23 t="fctk 0,95(28)"/>
      <h24 t="Rekenwaarde van de druksterkte - permanent (fcd = fck / gamma c_p)"/>
      <h25 t="Rekenwaarde van de druksterkte - buitengewoon (fcd = fck / gamma c_a)"/>
      <h26 t="Rek bij het bereiken van maximale sterkte eps c2"/>
      <h27 t="Uiterste rek eps cu2"/>
      <h28 t="Rek bij het bereiken van maximale sterkte eps c3"/>
      <h29 t="Uiterste rek eps cu3"/>
      <h30 t="n"/>
      <h31 t="Toeslagmateriaal"/>
      <h32 t="Gemeten waarden van gemiddelde druksterkte (invloed van ouderdom)"/>
    </h>
  </table>
</container>

```

```

<h3 t="Diagramtype"/>
</h>

<obj id="461" nm="3DPC">
  <p0 v="0P">
  <p1 v="0000000A-000A-000A-000A-00000003DPC"/>
  <p2 v="" />
  <p3 v="" />
  <p4 v="000" />
  <p5 v="" />
  <p6 v="000000000" />
  <p7 v="20" />
  <p8 v="" />
  <p9 v="" />
  <p10 v="" />
  <p11 v="" />
  <p12 v="" />
  <p13 v="" />
  <p14 v="1" />
  <p15 v="" />
  <p16 v="" />
  <p17 v="" />
  <p18 v="" />
  <p19 v="" />
  <p20 v="" />
  <p21 v="" />
  <p22 v="" />
  <p23 v="" />
  <p24 v="" />
  <p25 v="" />
  <p26 v="" />
  <p27 v="" />
  <p28 v="" />
  <p29 v="" />
  <p30 v="" />
  <p32 v="" />
  <p33 v="1" />
</obj>
</table>
</container>

Section 4 - Material properties

<container id="(0908D21F-481F-11D4-AB84-00C06C452330)"
t="DataSetScia.EP_LoadCase.1">
  <table id="A54A5684-B86A-4295-B603-E1EDBF65F382"
t="DataSetScia.EP_LoadCase.1" name="Belastingsgevallen">
    <h>
      <h0 t="Naam"/>
      <h1 t="UniqueID"/>
      <h2 t="Actie type"/>
      <h3 t="Lastgroep"/>
      <h4 t="Belastingtype"/>
    </h>
    <obj id="1" nm="BG1">
      <p0 v="0P">
      <p1 v="0000000A-000A-000A-000A-00000000DC01"/>
      <p2 v="0" t="Permanent"/>
      <p3 v="1" t="Standaard"/>
      <p4 v="1" t="Standaard"/>
    </obj>
  </table>
</container>

```

**Met opmerkingen [DKv4]:** Material name

**Met opmerkingen [DKv5]:** Specification of the type of the material, [0] is for concrete

**Met opmerkingen [DKv6]:** Volumetric weight input

**Met opmerkingen [DKv7]:** Modulus of Elasticity

**Met opmerkingen [DKv8]:** Poisson's ratio

**Met opmerkingen [DKv9]:** Load case name/number, not required to change in the case of different bridges!

**Met opmerkingen [DKv10]:** Load group, also not required to change for different design parameters.

```

</obj>
</table>
</container>

```

Section 5 – Load cases

```

<container id="{F9D4AA72-49D5-11D4-A3CF-000000000000}"
  t="DataSetScia.EP_LoadGroup.1">
  <table id="E2AE0020-D1C2-4BE9-8B5F-57F52CD42E78"
    t="DataSetScia.EP_LoadGroup.1" name="Lastgroepen">
    <h>
      <h0 t="Naam"/>
      <h1 t="Last"/>
    </h>
    <obj id="1" nm="LG1">
      <p0 v="1"/>
      <p1 v="0" t="Permanent"/>
    </obj>
  </table>
</container>

```

**Met opmerkingen [DKv11]:** Load group, also not required to change for different design parameters.

Section 6 – Load groups

```

<container id="{39A7F468-A0D4-4DFF-8E5C-5843E1807D13}"
  t="EP_DSG_Elements.EP_StructNode.1">
  <table id="F3A9E1CA-F6A1-4579-8307-BDF4F5CC3A7F"
    t="EP_DSG_Elements.EP_StructNode.1" name="Knoop">
    <h>
      <h0 t="Naam"/>
      <h1 t="Coördinaat X"/>
      <h2 t="Coördinaat Y"/>
      <h3 t="Coördinaat Z"/>
    </h>
    <obj id="1">
      <p0 v="K1"/>
      <p1 v=""/>
      <p2 v=""/>
      <p3 v="0"/>
    </obj>
    <obj id="2">
      <p0 v="K2"/>
      <p1 v="3.25"/>
      <p2 v="0.156187"/>
      <p3 v="0"/>
    </obj>
    <obj id="3">
      <p0 v="K3"/>
      <p1 v="6.5"/>
      <p2 v="0"/>
      <p3 v="0"/>
    </obj>
    <obj id="4">
      <p0 v="K4"/>
      <p1 v="0"/>
      <p2 v="3.5"/>
      <p3 v="0"/>
    </obj>
  </table>
</container>

```

**Met opmerkingen [DKv12]:** Input parameters for the x & y coordinate of the nodes

```

<obj id="5">
  <p0 v="K6"/>
  <p1 v="3.25"/>
  <p2 v="3.343813"/>
  <p3 v="0"/>
</obj>

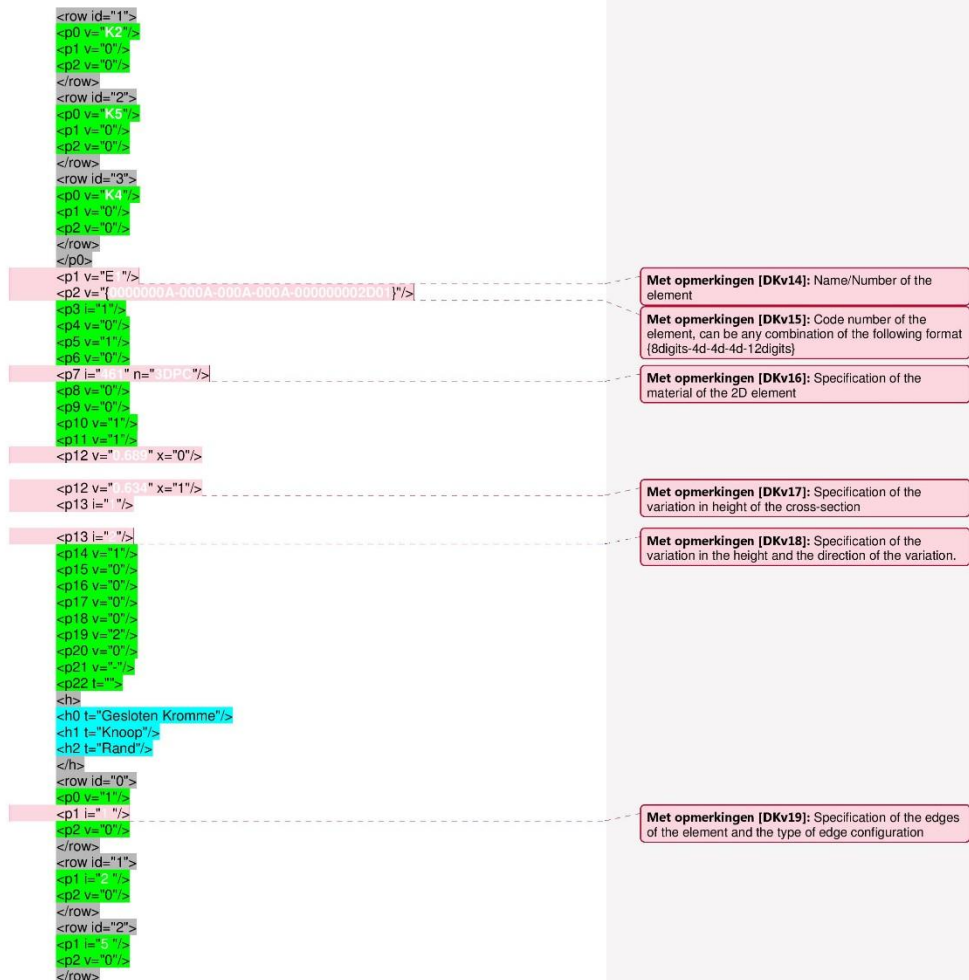
<obj id="6">
  <p0 v="K7"/>
  <p1 v="6.5"/>
  <p2 v="3.5"/>
  <p3 v="0"/>
</obj>
</table>
</container>

Section 7 - Nodal coordinates

<container id="{8708ED31-8E66-11D4-AD94-F6F5DE2BE344}"
t="EP_DSG_Elements.EP_Plane.1">
  <table id="05617FAC-DEAE-446C-9940-DB8496ED48C7"
t="EP_DSG_Elements.EP_Plane.1" name="2D-element">
    <h>
      <h0 t="Elke knoop parameters"/>
      <h1 t="Naam"/>
      <h2 t="UniquelD"/>
      <h3 t="Laag"/>
      <h4 t="Type"/>
      <h5 t="Element type"/>
      <h6 t="Element behaviour"/>
      <h7 t="Materiaal"/>
      <h8 t="EEM model"/>
      <h9 t="EEM niet-lineair model"/>
      <h10 t="Dikte type"/>
      <h11 t="Richting"/>
      <h12 t="Dikte"/>
      <h13 t="Punt 1"/>
      <h14 t="2D-element systeemvlak op"/>
      <h15 t="Excentriciteit z"/>
      <h16 t="LCS type"/>
      <h17 t="Keer oriëntatie om"/>
      <h18 t="LCS hoek"/>
      <h19 t="Modus"/>
      <h20 t="Versleutelde geometrie"/>
      <h21 t="Paneel oppervlak"/>
      <h22 t="Tabel van geometrie"/>
    </h>
    <obj id="1">
      <p0 t=">
      <h>
        <h0 t="Knoop"/>
        <h1 t="Dx"/>
        <h2 t="Dy"/>
      </h>
      <row id="0">
        <p0 v=""/>
        <p1 v="0"/>
        <p2 v="0"/>
      </row>

```

Met opmerkingen [DKv13]: Specification of the nodes that shape the element



```
<row id="3">
  <p1 l="1"/>
  <p2 v="0"/>
</row>
</p22>
</obj>

<obj id=" " >
  <p0 l=" " >
    <h>
      <h0 l="Knoop"/>
      <h1 l="Dx"/>
      <h2 l="Dy"/>
    </h>
    <row id="0">
      <p0 v="K2"/>
      <p1 v="0"/>
      <p2 v="0"/>
    </row>
    <row id="1">
      <p0 v="K3"/>
      <p1 v="0"/>
      <p2 v="0"/>
    </row>
    <row id="2">
      <p0 v="K6"/>
      <p1 v="0"/>
      <p2 v="0"/>
    </row>
    <row id="3">
      <p0 v="K5"/>
      <p1 v="0"/>
      <p2 v="0"/>
    </row>
    <p0>
      <p1 v="E2"/>
      <p2 v="0000000A-000A-000A-000A-000000002D02"/>
      <p3 l="1"/>
      <p4 v="0"/>
      <p5 v="1"/>
      <p6 v="0"/>
      <p7 l="461" n="3DPC"/>
      <p8 v="0"/>
      <p9 v="0"/>
      <p10 v="1"/>
      <p11 v="1"/>
      <p12 v="0.634" x="0"/>
      <p12 v="0.689" x="1"/>
      <p13 l="2"/>
      <p13 l="0"/>
      <p14 v="1"/>
      <p15 v="0"/>
      <p16 v="0"/>
      <p17 v="0"/>
      <p18 v="0"/>
      <p19 v="2"/>
      <p20 v="0"/>
      <p21 v="0"/>
```



```

<p22 t="n">
<h>
<h0 t="Gesloten Kromme"/>
<h1 t="Knoop"/>
<h2 t="Rand"/>
</h>
<row id="0">
<p0 v="1"/>
<p1 v="2"/>
<p2 v="0"/>
</row>
<row id="1">
<p1 v="3"/>
<p2 v="0"/>
</row>
<row id="2">
<p1 v="6"/>
<p2 v="0"/>
</row>
<row id="3">
<p1 v="5"/>
<p2 v="0"/>
</row>
</p22>
</obj>
</table>
</container>

```

Section 8 - Element definition

```

<container id="[24449635-FE8C-46B5-8C97-9E0CA33F0E70]"
t="DataAddSupport_EP_LineSupportSurface.1">
  <table id="AB97FC66-C426-46AE-B9BC-F322C7E8EC0C"
t="DataAddSupport_EP_LineSupportSurface.1" name="Lijnondersteuning op 2D
elementrand">
    <h>
<h0 t="Referentie Tabel"/>
<h1 t="Naam"/>
<h2 t="UniqueID"/>
<h3 t="Restrictie"/>
<h4 t="X"/>
<h5 t="Y"/>
<h6 t="Z"/>
<h7 t="Rx"/>
<h8 t="Ry"/>
<h9 t="Rz"/>
<h10 t="Systeem"/>
<h11 t="Coördinaatdefinitie"/>
<h12 t="Positie x1"/>
<h13 t="Positie x2"/>
<h14 t="Oorsprong"/>
<h15 t="Rand"/>
    </h>
    <obj id="1">
      <p0 t=">
<h>
<h0 t="Staal Type"/>
<h1 t="Staal Type Naam"/>
<h2 t="Staal Id"/>
<h3 t="Staal Naam"/>

```

```

</h>
<row id="0">
  <p0 v="{8708ED31-8E66-11D4-AD94-F6F5DE2BE344}" />
  <p1 v="EP_DSG_Elements.EP_Plane.1" />
  <p2 v=" " />
  <p3 v=" " />
</row>
<p0>
  <p1 v="Sle1" />
  <p2 v="{0000000A-000A-000A-000A-00000000BC01}" />
  <p3 v=" " />
  <p4 v=" " />
  <p5 v=" " />
  <p6 v=" " />
  <p7 v=" " />
  <p8 v=" " />
  <p9 v=" " />
  <p10 v="0" />
  <p11 v="1" />
  <p12 v="0" />
  <p13 v="1" />
  <p14 v=" " />
  <p15 v="1" />
</obj>
<obj id="2">
  <p0 t=" " />
  <h>
    <h0 t="Staat Type" />
    <h1 t="Staat Type Naam" />
    <h2 t="Staat Id" />
    <h3 t="Staat Naam" />
  </h>
  <row id="0">
    <p0 v="{8708ED31-8E66-11D4-AD94-F6F5DE2BE344}" />
    <p1 v="EP_DSG_Elements.EP_Plane.1" />
    <p2 v="1" />
    <p3 v="E1" />
  </row>
  <p0>
    <p1 v="Sle2" />
    <p2 v="{0000000A-000A-000A-000A-00000000BC02}" />
    <p3 v=" " />
    <p4 v="1" />
    <p5 v="1" />
    <p6 v="1" />
    <p7 v="0" />
    <p8 v="0" />
    <p9 v="0" />
    <p10 v="0" />
    <p11 v="1" />
    <p12 v="0" />
    <p13 v="1" />
    <p14 v=" " />
    <p15 v="3" />
  </obj>
</table>
</container>

```

Section 9 - Boundary conditions

**Met opmerkingen [DKv20]:** Specification of the element

**Met opmerkingen [DKv21]:** Unique ID for the boundary condition BC01 and BC02

**Met opmerkingen [DKv22]:** Specification of the restrictions of the per degree of freedom [0] is for free and [1] is for restricted

```

<container id="[BC16B3CA-F464-11D4-94D3-000000000000]"
t="DataAddLoad.EP_SurfaceForceSurface.1">
  <table id="523C484A-D638-4DCD-AB2B-8404E5794625"
t="DataAddLoad.EP_SurfaceForceSurface.1" name="Lasten op oppervlak">
    <h>
      <h0 t="Referentie Tabel"/>
      <h1 t="Belastingsgeval"/>
      <h2 t="Naam"/>
      <h3 t="UniquelD"/>
      <h4 t="Richting"/>
      <h5 t="Type"/>
      <h6 t="Waarde"/>
      <h7 t="Systeem"/>
      <h8 t="Locatie"/>
    </h>
    <obj id="*" ">
      <p0 t=">
        <h>
          <h0 t="Staal Type"/>
          <h1 t="Staal Type Naam"/>
          <h2 t="Staal Id"/>
          <h3 t="Staal Naam"/>
        </h>
        <row id="0">
          <p0 v="{8708ED31-8E66-11D4-AD94-F6F5DE2BE344}"/>
          <p1 v="EP_DSG_Elements.EP_Plane.1"/>
          <p2 v="1"/>
          <p3 v="{0000000A-000A-000A-000A-00000000ED01}"/>
          <p4 v="2"/>
          <p5 v="0"/>
          <p6 v="{00000000}"/>
          <p7 v="1"/>
          <p8 v="0"/>
        </row>
      </obj>
      <obj id="*" ">
        <p0 t=">
          <h>
            <h0 t="Staal Type"/>
            <h1 t="Staal Type Naam"/>
            <h2 t="Staal Id"/>
            <h3 t="Staal Naam"/>
          </h>
          <row id="0">
            <p0 v="{8708ED31-8E66-11D4-AD94-F6F5DE2BE344}"/>
            <p1 v="EP_DSG_Elements.EP_Plane.1"/>
            <p2 v="2"/>
            <p3 v="E2"/>
          </row>
          <p1 t="1"/>
          <p2 v="SF2"/>
          <p3 v="{0000000A-000A-000A-000A-00000000ED02}"/>
          <p4 v="2"/>
          <p5 v="0"/>

```

Met opmerkingen [DKv23]: Load case the load is a part of

Met opmerkingen [DKv24]: Element the load is imposed on

Met opmerkingen [DKv25]: Load name/number and ID

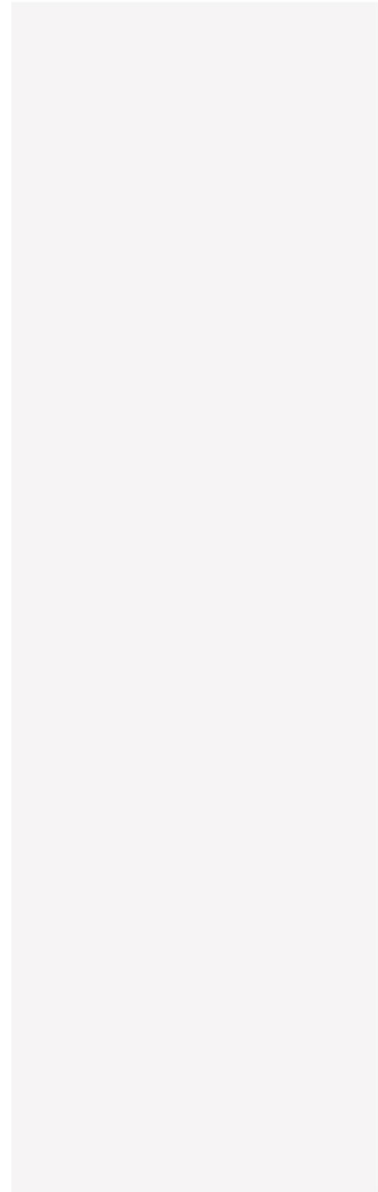
Met opmerkingen [DKv26]: Value of the load

```
<p6 v=-19100"/>  
<p7 v="1"/>  
<p8 v="0"/>  
</obj>  
</table>  
</container>
```

Section 10 - Load definition

```
</project>
```

Section 11 - End of script

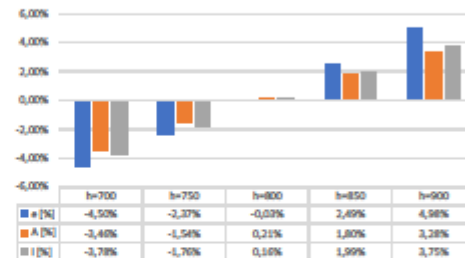
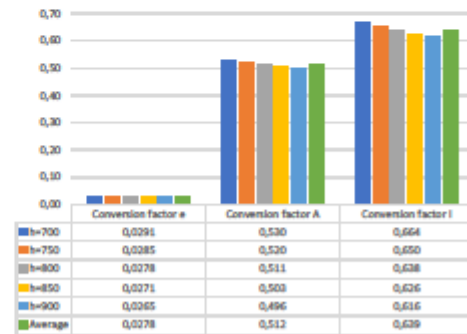


## Annex E Calculation control document

- E1 Geometric properties
- E2 Load generation
- E3 Bending induced stresses
- E4 Shear force
- E5 Post-tensioning force losses

# E1 geometric properties

Group	Description	Value	Unit	Specification
h=700	Height	0,700	m	
	Width	3,520	m	
	Centroidal height	0,330	m	
	Eccentricity	0,020	m	
	Area	1,307	m <sup>2</sup>	
	First moment of area	1,308	m <sup>3</sup>	
	Moment of Inertia	0,067	m <sup>4</sup>	
	CR e	0,0291	-	
	CR A	0,530	-	
	CR S	0,514	-	
	CR I	0,664	-	
h=750	Height	0,750	m	
	Width	3,520	m	
	Centroidal height	0,354	m	
	Eccentricity	0,021	m	
	Area	1,373	m <sup>2</sup>	
	First moment of area	1,376	m <sup>3</sup>	
	Moment of Inertia	0,080	m <sup>4</sup>	
	CR e	0,0285	-	
	CR A	0,520	-	
	CR S	0,505	-	
	CR I	0,650	-	
h=800	Height	0,800	m	
	Width	3,520	m	
	Centroidal height	0,378	m	
	Eccentricity	0,022	m	
	Area	1,439	m <sup>2</sup>	
	First moment of area	1,445	m <sup>3</sup>	
	Moment of Inertia	0,096	m <sup>4</sup>	
	Conversion factor e	0,0278	-	
	Conversion factor A	0,511	-	
	Conversion factor S	0,497	-	
	Conversion factor I	0,638	-	
h=850	Height	0,850	m	
	Width	3,520	m	
	Centroidal height	0,402	m	
	Eccentricity	0,023	m	
	Area	1,505	m <sup>2</sup>	
	First moment of area	1,514	m <sup>3</sup>	
	Moment of Inertia	0,113	m <sup>4</sup>	
	CR e	0,0271	-	
	CR A	0,503	-	
	CR S	0,490	-	
	CR I	0,626	-	
h=900	Height	0,900	m	
	Width	3,520	m	
	Centroidal height	0,426	m	
	Eccentricity	0,024	m	
	Area	1,571	m <sup>2</sup>	
	First moment of area	1,581	m <sup>3</sup>	
	Moment of Inertia	0,132	m <sup>4</sup>	
	CR e	0,0265	-	
	CR A	0,496	-	
	CR S	0,483	-	
	CR I	0,616	-	
Average	CR e	0,0278	-	
	CR A	0,512	-	
	CR S	0,498	-	
	CR I	0,639	-	



## E2 Load generation

Group	Description	Value	Unit	Specification	Eurocode Reference
Geometry	<b>Bridge deck</b>				
	Length	6,5	m	Span Width	
	Width	3,5	m	Outermost	
	Height CS	0,8	m	Outermost	
	Filament width	0,06	m		
	Element width	0,5	m		
Material Class	Coverage	0,05	m		
	<b>Concrete</b>				
	3DPC	C12/15			
	In Situ	C30/37			
	Blinding	C12/15			
	Finishing	C30/37			
Material Class	Impact Layer	C35/45			
	<b>Steel</b>				
	Prestressing	Y1860			
	Reinforcement	B500			
Environment Class	Top side	XF4		Derived from Eurocode	
	Bot side	XF2		Derived from Eurocode	
	Structure class	CC1		Derived from Eurocode	
	Designed life	100	year	Standard for bridge design	
Calculation Conditions	Designed life	100	year		
	Gevolg klasse	CC1		Omdat de referentieperiode afwijkt van de standaard referentieperiode van 50 jaar moeten de belastingen conform NEN-EN 1991 worden verhoogd. Indien NEN-EN geen regels geeft mag zijn uitgegaan	
				Because of the new nature of the material not all conditions can be conform the Eurocode. Some features may deviate from the design standard, if so an explanation will be given.	
Material Properties	<b>3DPC</b>				
	Density	2000	kg/m3		Material is tested after 28 days
	E modulus	19000	N/mm2		Material is tested after 28 days
	Ftk //	1,60	N/mm2		Material is tested after 28 days
	Ftk pp	1,30	N/mm2		Material is tested after 28 days
	Fck //	21,50	N/mm2		Material is tested after 28 days
	Fck pp	21,00	N/mm2		Material is tested after 28 days
				De TU/e hanteert een andere definitie van de kruipfactor. In deze berekening wordt uitgegaan van een	
	Creep coeff	3,50		vermindering van de stijfheid $E_{c,eff} = E_{cm} / (1 + \phi_{t,10})$	Material is tested after 28 days
	Shrinkage coeff	2,00		Yet to be tested	
	acc,pl	?		Plastic reduction factor for compression	Used instead of 1.0 for material strength reduction
	act,pl	?		Plastic reduction factor for compression	Used instead of 1.0 for material strength reduction
Prestressing	<b>Top</b>			7 wire strand	
	Tendon	6			
	P0	150	kN	Initial post-tensioning force	
	Tendon Area	93	mm2		
	Tendon Diameter	12,5	mm		
	<b>Bot</b>				EN 10138
	Tendon	10			
	P0	150	kN	Initial post-tensioning force	
	Tendon Area	93	mm2		
	Tendon Diameter	12,5	mm		
	<b>Both</b>				EN 10138
	Tendon class	1860	N/mm2		
	Bond factor	0		Unbonded tendons	
	Pm,0	150	kN		
Cross sectional values	Pm,inf	160	kN	Estimated as $1,2 * P_{m,0}$ (should later on be verified)	
	E modulus	195000	N/mm2		
	Weight	0,7263	kg/m		
	<b>800 mm high section</b>				
	A	1,4388	m2	Area	
	Iy	0,095807	m4	Moment of inertia around the y axis	
	Wy	0,013363	m3	First moment of area	
	Eccentricity	0,022248	m	Vertical distance of the neutral axis to the midline of the section (pos z is down)	
	Wy,top	-0,2269	m3		
	Wy,bot	0,253624	m3		
Loading conditions	<b>Self weight</b>				
	Concrete	8,07	kN/m2		
	Prestressing	0,03	kN/m2		
	Rebar	0	kN/m2		
	<b>Permanent</b>				
	Finishing Layer	0,33	kN/m2	10 mm high	
	Filament correction	0,5	kN/m2	5% of self weight	
	Pressure layer	1,25	kN/m2	50 mm high (only if required for impact resistance)	
	Calculation value	2,5	kN/m2	Including correction for taking temporary structures into account	
	<b>Variable</b>				
	Traffic UDL (qfk)	5	kN/m2	Standard value by Eurocode Loading cases	NEN-EN 1991-2 ch. 5
	Traffic PL (Qfk)	7	kN	0.1m x 0.1m footprint (standard Eurocode loading value)	NEN-EN 1991-2 ch. 5
	<b>Prestressing</b>				
	Pretensioning force	2400	kN		
	Force per tendon	150	kN		
	Distance ten to edge	0,2	m		
	Distance NA to top	-0,42225	m		
	Eccentricity top	-0,22225	m	Measured from centroidal axis concrete	
	Eccentricity bot	0,177752	m	Measured from centroidal axis concrete	
	Check	1		If 1 than check is ok	
	Mp,top,ch	-200,023	kNm		

	Mp,bot,ch	266,628 kNm	
<b>Wind Load</b>			NEN-EN 1991-1-4
	Vb,0	24,5 m/s	Average wind speed
	Cdir	1	Directional correction factor
	Cseason	1	Seasonal correction factor
	Vb	24,5 m/s	Corrected wind speed
	n	0,5	Terrain exponent
	K	0,281	Terrain shape factor
	p	0,01	Wind exceedence probability
	Cprob	1,05	Probabilistic correction factor
	Calc value Cprob	1,05	
	z	7 m	Height
	z0	0,5 m	Lowest possible height
	zmin	7 m	Minimum calc height
	Kr	0,22	Terrain factor
	Cr(z)	0,58	Terrain roughness factor
	CO(z)	1	Terrain orography is 1,0 due to a slope <3%
	Vm(z)	14,21 m/s	Mean wind velocity
	kl	1	Turbulence factor
	Sigma v	5,39	Wind standard deviation
	Iv(z)	0,38	Turbulence intensity factor
	ro	1,25 kg/m3	Air density
	Qp(z)	0,46 kN/m2	Peak wind pressure
	Qb(z)	0,38 kN/m2	Basic wind pressure
	Ce(z)	1,21	Exposure factor
	b	3500 mm	Width of the structure
	dtot	3200 mm	Total depth of the structure
	b/dtot	1,09	
	Cfx0	2,35	Force coefficient in the x direction
	Cfz	0,9	Force coefficient in the z direction
	Cfy	0,5	Force coefficient in the y direction
	Qw,x	1,18 kN/m2	Wind pressure in the x-direction
	Qw,z	0,45 kN/m2	Wind pressure in the z-direction
	Qw,y	0,59 kN/m2	Wind pressure in the y-direction
<b>Snow load</b>			
	μi	0,8	Shape coefficient for slopes smaller than 30 degrees
	Sk	0,7 kN/m2	Cannot be found in the national Annex nor in the Eurocode
	ψ	0	Due to accidental loading case no combination possibilities
	Qsa	0,56 kN/m2	Snow load to be used for calculations
<b>Construction loads</b>	Qc	0 kN/m2	Because the bridge deck is constructed in prefab situation and then lifted into the location in one sitting there are no relevant loads on the structure during construction
<b>Partial safety factors</b>	<b>Action CC1</b>		
	Beta	3,3	
	Yg,sup 6.10a	1,2	
	Yg,sup 6.10b	1,1	To be used in combination with Xi reduction factor
	Yg,inf	0,9	
	Traffic factor	1,2	(ψ=1)
	Other variable	1,35	(ψ=1)
	<b>Material strength</b>		
	Prestressing favour	1	
	Prestressing unfavour	1,2	
	Concrete ULS	1,5	
	Rebar ULS	1,15	
	Prestressing ULS	1,1	
	ξ	0,89	Reduction factor permanent weight
	<b>Calculation values</b>		
	acc.pl	0,8	Non-reinforced concrete is less ductile, therefore a reduction in strength is required
	acc.pl	0,8	Non-reinforced concrete is less ductile, therefore a reduction in strength is required
<b>Load Combination factors</b>	<b>Combination value ψ0</b>		
	gr 1	0,4	
	gr 2	0,4	
	Qfwk	0	
	Unwanted vehicle	0	
	Wind Fwk permanent	0,3	
	Wind Fwk temp	0,8	
	Thermal	0,3	
	Snow load permanent	0	
	Snow load temp	0,8	
	Construction	1	
	<b>Combination value ψ1</b>		
	gr 1	0,8	
	gr 2	0,8	
	Qfwk	0,8	
	Unwanted vehicle	0,8	
	Wind Fwk permanent	0,6	
	Wind Fwk temp	0	
	Thermal	0,8	
	Snow load permanent	0	
	Snow load temp	0	
	Construction	0	
	<b>Combination value ψ2</b>		
	gr 1	0,4	
	gr 2	0	
	Qfwk	0	
	Unwanted vehicle	0	
	Wind Fwk permanent	0	
	Wind Fwk temp	0	
	Thermal	0,3	
	Snow load permanent	0	
	Snow load temp	0	
	Construction	1	
<b>Vertical loading</b>	<b>Total combinations</b>		
	6.10a no snow loading	413,59 kN	Fundamental load combination for ULS, snow load is very low relative to other loads
	6.10 b no snow loading	387,6 kN	Fundamental load combination for ULS, snow load is very low relative to other loads



	Variable loading only	151,51 kN	Not Including combination factors
	Variable loading only	158,72 kN	Including combination factors
	Prestressing	150 kN	
	<b>Specific loading</b>		
	UDL 6.10a	18,01 kN/m <sup>2</sup>	
	UDL 6.10b	16,74 kN/m <sup>2</sup>	
	CL 6.10 a/b	6,72 kN	
	<b>SLS loading</b>		
	UDL characteristic	16,05 kN/m <sup>2</sup>	
	CL characteristic	7 kN	
<b>Characteristic loads</b>	<b>Distributed</b>		<b>Orientation</b>
	Selfweight	8,1 kN/m <sup>2</sup>	Vertical
	Permanent load	2,5 kN/m <sup>2</sup>	Vertical
	Traffic	5 kN/m <sup>2</sup>	Vertical
	Wind	0,45 kN/m <sup>2</sup>	Vertical
	Snow	0,56 kN/m <sup>2</sup>	Vertical
	<b>Concentrated</b>		
	Traffic	7 kN	Vertical
	Prestressing	2400 kN	Horizontal
	Wind	3,3 kN	Horizontal
<b>Design Loads</b>	<b>Distributed</b>		<b>Orientation</b>
	Permanent 6.10a	12,72 kN/m <sup>2</sup>	Vertical
	Permanent 6.10b	11,66 kN/m <sup>2</sup>	Vertical
	Q1 traffic	6 kN/m <sup>2</sup>	Vertical
	Q2 wind	0,61 kN/m <sup>2</sup>	Vertical
	Q3 snow	0,76 kN/m <sup>2</sup>	Vertical
	<b>Concentrated</b>		
	Traffic	8,4 kN	Vertical
	Prestressing	2400 kN	Horizontal
	Wind	4,46 kN	Horizontal
<b>Design combinations</b>	<b>Distributed</b>		
	6.10 a	17,89 kN/m <sup>2</sup>	Vertical
	6.10 b	18,03 kN/m <sup>2</sup>	Vertical
	Snow	13,48 kN/m <sup>2</sup>	Vertical
	<b>Concentrated</b>		
	Permanent	11,66 kN/m <sup>2</sup>	Vertical
	Traffic	8,4 kN	Vertical

Horizontal loading does not need to be considered in the design of pedestrian bicycle bridges

## E3 Bending induced stresses

Action	Description	Location	Value	Unit	Specification		
Moment	Max UDL	Mid	333,27	kNm	6.10 b		
	Mid UDL	Mid	330,69	kNm	6.10 a		
	Low Udl	Mid	249,17	kNm	Snow		
	Max CL	Mid	229,18	kNm	Traffic load applied in mid span		
	Max CL	Mid	215,53	kNm	Traffic load applied at support		
	Max G,ch	Mid	149,72	kNm	Due to selfweight only		
Shear Force	Max UDL	Mid	205,09	kN	6.10 b		
	Mid UDL	Mid	203,50	kN	6.10 a		
	Low Udl	Mid	153,34	kN	Snow		
	Max CL	Mid	136,83	kN	Traffic load applied in mid span		
	Max CL	Support	132,63	kN	Traffic load applied in mid span		
Prestressing	zp	Constant	0,35	m	Tendon eccentricity measured from bot		
	ep	Constant	0,0278	m	Measured from concrete COG		
	Mp,ch	Constant	-66,60	kNm	Hogging moment		
Stresses	op,ep,top	Top	0,29	N/mm2	Due to eccentricity		
	op,ep,bot	Bot	-0,26	N/mm2	Due to eccentricity		
	opm	Constant	-1,67	N/mm2	Due to force		
	op,top	Top	-1,37	N/mm2	Combined		
	op,bot	Bot	-1,93	N/mm2	Combined		
	oG,top	Top	-0,71	N/mm2	Due to Selfweight & Prestress		
	oG,bot	Bot	-1,34	N/mm2	Due to Selfweight & Prestress		
	oUDL,top	Top	-1,47	N/mm2	Due to UDL		
	oUDL,bot	Bot	1,31	N/mm2	Due to UDL		
	oed,top	Top	-2,84	N/mm2	Total load on structure		
	oed,bot	Bot	-0,62	N/mm2	Total load on structure		
Action	Description	Location	Value Rd	Value Ed	Unit	Specification	UC
Stress	Check 1	Top	0,69	-0,71		No tension due to self load and Prestressing	-1,03
		Bot	0,69	-1,34		No tension due to self load and Prestressing	-1,93
	Check 2	Top	0,69	-2,84		Tension due to total load on structure	-4,10
		Bot	0,69	-0,62		Tension due to total load on structure	-0,89
		Top	-11,20	-2,84		Compression due to total load on structure	0,25
		Bot	-11,20	-0,62		Compression due to total load on structure	0,06
	Check 3	Top	-12,6	-2,84		Limited compression in the section <0.6*fck	0,23
		Bot	-12,6	-0,62		Limited compression in the section <0.6*fck	0,05

## E4 Shear force

Group	Description	Value	Unit	Specification	Eurocode Reference
Shear 1				Effective web area	
	k1	0,15			
	d	560	mm		
	bw,top	1320	mm		
	bw,bot	1320	mm		
	k	1,5976143			
	k*	1		k<2,0	
	Ned	2400	kN		
	Ac	1,4388	m2		
	σcp	1,67	N/mm2	Not taking the eccentricity into account	
	σcpm	1,65	N/mm2	Taking the eccentricity into account	
	fck	21	N/mm2		
	vmin	0,16	N/mm2		
	vrd	0,4075	N/mm2		
	Aw	739200	mm2		0,7392
	Area %	51,38	%	Web area percentage of total concrete area	
	Vrd,c	301,22	kN		
Shear 2				Total web area	
	Ac	1438800	mm2		
	k	1			
	vrd	0,4075	N/mm2		
	Area%	100	%		
Shear 3				Due to the tensional resistance in uncracked regions	
	Iy	9,581E+10	mm4		
	bw	1320	mm		
	S	288987800	mm3		
	fctd	0,69	N/mm2	Flexural tensional strength (design)	
	Alpha I	1		Stress reduction factor for non pretensioned tendons	
	σcp	1,65	N/mm2		
Unity Checks	Vrd,c	556	kN		
	Ved	205,09	kN		
	UC1	0,68			
	UC2	0,35			
	UC3	0,37			

## E5 Post-tensioning force losses

Group	Description	Value	Unit	Specification	Eurocode Reference
Geometry	Length	6500	mm		
	Width	3500	mm		
	Ac	1438800	mm <sup>2</sup>		
	Ecm	19000	N/mm <sup>2</sup>		
	$\phi(=\infty, t_0)$	3,5		For axial loads on concrete loaded after 3 days	NEN-EN-1992-1-1 Fig 3.
	Ec,eff	4222,2222	N/mm <sup>2</sup>		
Stresses	Ep	195000	N/mm <sup>2</sup>		
	Ap	93	mm		
	$\sigma_{c,top}$	-1,37	N/mm <sup>2</sup>		
	$\sigma_{c,bot}$	-1,93	N/mm <sup>2</sup>		
	$\sigma_{c,average}$	-1,65	N/mm <sup>2</sup>		
Strains	$\epsilon_{c,top,0}$	-0,007234	%		
	$\epsilon_{c,bot,0}$	-0,010161	%		
	$\epsilon_{c,average,0}$	-0,008684	%		
	$\epsilon_{c,top,\infty}$	-0,032554	%		
	$\epsilon_{c,bot,\infty}$	-0,045726	%		
	$\epsilon_{c,avg,\infty}$	-0,039079	%		
	$\Delta\epsilon_{c,creep,top}$	-0,02532	%		
	$\Delta\epsilon_{c,creep,bot}$	-0,035565	%		
	$\Delta\epsilon_{c,creep,avg}$	-0,030395	%		
Prestress	Pm, $\infty$	150	kN		
	$\sigma_{pm,\infty}$	1612,9032	N/mm <sup>2</sup>		
	$\epsilon_{pm,\infty}$	0,8271299	%		
	$\epsilon_{pm,0}$	0,8575246	%		
	$\sigma_{pm,0}$	1672,173	N/mm <sup>2</sup>		
	Pm,0	155,52	kN	Minimal amount of prestressing force required	

## Annex F Environmental analysis input

- F1 Volvo Truck emissions
- F2 Road transport truck dimension
- F3 National database environmental impacts incl FA-GWW\_Eng

# F1 Volvo truck emissions

VOLVO TRUCKS



Company name	Type of document		
Volvo Truck Corporation	PM		
Name of document	Issue	Reg. No.	Page
Emissions from Volvo's trucks	3	1320018003	1 (3)
Issuer (name, phone)	Sign	Date of meeting	Info class
Lars Mårtensson, +46 31 3226527		2018-03-09	Open
Approved by (name, phone)	Sign	Date	Valid

## Emissions from Volvo's trucks

To facilitate emission calculation from transport, Volvo Trucks has summarised emission factors per litre fuel consumed. The summary is applicable primarily for trucks using standard diesel fuel. The stated values are based on certification measurements and can be used for outlined calculations. In an actual traffic situation the values vary due to individual conditions such as vehicle status, driving method, traffic situation etc.

Typical values, based on certification measurements, for the more common Volvo engines, with EU certification diesel fuel [g/litre fuel]						
	Law from	Volvo from	NO <sub>x</sub> g/litre	PM g/litre	HC g/litre	CO g/litre
Typical	1980		58±5	4±2	6±2	8±3
Euro 0	1990	1987	41-44	1.5-1.7	1.5-1.8	3-6
Euro 1	1993	1991	28-32	0.2-0.6	0.5-1.2	2-8
Euro 2	1996	1993	25-28	0.2-0.5	0.4-1.0	1-7
Euro 3, D6, 180-220	2001	2000	18	0.35	1.3	2.6
Euro 3, D6, 250	2001	2000	18	0.25	1.3	2.6
Euro 3, D7, 250	2001	2000	18	0.25	0.4	2.3
Euro 3, D7, 290-310	2001	2000	18	0.30	0.4	2.3
Euro 3, D9, 260	2001	2001	18	0.30	0.8	2.3
Euro 3, D9, 300	2001	2001	18	0.35	0.8	2.3
Euro 3, D9, 340-380	2001	2001	19	0.30	0.8	2.4
Euro 3, D12, 340-420	2001	2000	19	0.25	0.8	2.4
Euro 3, D12, 460	2001	2001	20	0.35	0.4	2.5
Euro 3, D12, 500	2001	2001	20	0.30	0.4	2.5
Euro 3, D16, 550	2001	2003	17	0.25	0.8	2.7
Euro 3, D16, 610	2001	2003	17	0.25	0.8	3.9
Euro 4	2006	2005	13	0.10	0.04	1.0
Euro 5	2009	2005	7	0.10	0.00	1.2
Euro 6	2013	2013	0.9	0.01	0.06	0.13

Note: in order to be able to compare the same test cycle (steady state) was used up to Euro 5. For Euro 6 WHTC (transient) was used. Data from different cycles are not directly comparable.



Company name	Type of document		
Volvo Truck Corporation	PM		
Name of document	Issue	Reg. No.	Page
Emissions from Volvo's trucks	3	1320018003	2 (3)

## Legal requirements

The legal requirements for diesel engines have been tightened several times. Diesel engines are used in various types of vehicles, for various types of traffic, and with varying loads. To be able to measure emissions in a comparable way, they are measured in relation to the work performed by an engine and the units used are grams per kilowatt-hour. For certification, a well defined fuel is used, very similar to standard fuel but with closer tolerances. (figures vary based on test cycle)

Legal requirements and limit values					
	Law from	NOx g/kWh	PM g/kWh	HC g/kWh	CO g/kWh
R49.00	1982	18	-	3.50	14
Euro 0	1990	14.4	-	2.40	11.2
Euro 1	1993	8.0	0.36	1.10	4.5
Euro 2	1996	7.0	0.15	1.10	4.0
Euro 3	2001	5.0	0.10	0.66	2.1
Euro 4	2006	3.5	0.02	0.46	1.5
Euro 5	2009	2.0	0.02	0.46	1.5
Euro 6	2013	0.4	0.01	0.13	1.5

Table 2

## Emission factors

Volvo engines comply with the legal requirements and many engines have even been introduced a couple of years before the legal requirements have come into force.

Certification values are converted in various connections into emissions per vehicle kilometre or per ton-kilometre. They are based on assumptions of a certain type of traffic, driving method, and load utilisation, and are therefore uncertain especially as payload is defined differently in different connections. Transporters and transport buyers need better and better data for their environmental reports and calculations. To facilitate this type of work, Volvo has converted the certification values into emissions per litre of fuel, see table 1.

Using fuel consumption as a base, it is possible to calculate the emissions in a better way compared to earlier and to take into consideration load utilisation, road choice, speed, driving method, etc. The data is based on measurements according to the applicable standard for certification that deviates from a real traffic situation. Emissions from vehicles in traffic may differ from these data. The tables should not be used to make direct comparisons between different vehicles.

### Example:

A truck and trailer are fully loaded with a total weight of 40 tons of which the payload is 26 tons. For a certain type of transport on the motorway (freeway), the fuel consumption is 0.275 litres per km. Of course the consumption can be lower for other types of transport and when the truck is not fully loaded. The 2009 truck has an engine that complies with Euro 5. The emissions per ton-km can be calculated as follows:

Nitrogen oxides, NOx     $0.275 \text{ l/km} \cdot 7 \text{ g/l per 26 tons} \approx 0,074 \text{ g/ton-km}$   
 Particulates, PM         $0.275 \text{ l/km} \cdot 0,1 \text{ g/l per 26 tons} \approx 0,0011 \text{ g/ton-km}$

The emissions of carbon dioxide depend on the fuel consumption. It can be calculated using the fuel data described in the section Fuel Quality below.

Carbon dioxide, CO<sub>2</sub>     $0.275 \text{ l/km} \cdot 2.6 \text{ kg/l per 26 tons} \approx 0.0275 \text{ kg/ton-km}$



Company name	Type of document		
Volvo Truck Corporation	PM		
Name of document	Issue	Reg. No.	Page
Emissions from Volvo's trucks	3	1320018003	3 (3)

## Fuel consumption

Fuel consumption varies considerably depending on the type of traffic, roads, driving behaviour, etc. It is therefore advisable to base calculations on the actual fuel consumption for a certain transport. When there is no data available for the fuel consumption, the data in the table can be used as a guiding value for vehicles. Please contact your Volvo dealer for information about a specific type of transport.

Typical fuel consumption in litres per 100 km				
	Payload in tons	Total weight in tons	litres / 100 km empty*	litre / 100 km full load*
Truck, distribution traffic	8.5	14	20-25	25-30
Truck, regional traffic	14	24	25-30	30-40
Tractor and semi-trailer, long-haul traffic	26	40	21-26	29-35
Truck with trailer, long-haul traffic	40	60	27-32	43-53

Table 3

## Fuel quality

Carbon dioxide is formed by combustion. The carbon content of the fuel determines the amount. One litre of standard diesel fuel (EN590) creates about 2.6 kg carbon dioxide.

The fuel contains residues of sulphur. The sulphur content must since January 1<sup>st</sup> 2009 not exceed 0.001% (10 ppm) according to EU Directive and the EN590 standard. There could be variations from one country to another. Fuel suppliers can provide more detailed information about the quality of fuel.

## Transporters and carriers have a key role

It is essential to select the correct type of vehicle with the correct powertrain for the respective transport assignment, the right route, and to have a good load utilisation.

Emissions per ton-kilometre can therefore only be calculated with detailed knowledge about the particular transport, load utilisation, route selection, vehicle, etc.

## More information

More information about Volvo Trucks and how we take care of environmental issues can be found at [www.volvotrucks.com](http://www.volvotrucks.com).

An Environmental Footprint Calculator is also available on internet.

\* Add ~4 % AdBlue consumption (volume) for Euro 4 and ~5 % AdBlue consumption (volume) for Euro 5. For Euro 6: Engines D5K, D8K and D16K ~5 % AdBlue consumption (volume) and D11K and D13K ~8 % AdBlue consumption (volume). The main difference for Euro 6 is between cooled and non-cooled EGR.



## F2 Road transport truck dimensions



13,6 lm STANDARD TRUCK		
LENGTH	WIDTH	HEIGHT
13.60 m	2.46 m	2.65 m – 2.80 m
CAPACITY		
Up to 24.000 kg/90cbm		
UPGRADE		
TARPAULIN		

MEGA TRUCK		
LENGTH	WIDTH	HEIGHT
13.60 m	2.46 m	3.05 m – 3.10 m
CAPACITY		
Up to 24.000 kg/100cbm		
UPGRADE		
TARPAULIN		



TRAILER		
LENGTH	WIDTH	HEIGHT
6.50+7.5 m	2.46 m	2.65 m – 2.80 m
CAPACITY		
Up to 24.000 kg/90cbm		
UPGRADE		
TARPAULIN		

TANDEM		
LENGTH	WIDTH	HEIGHT
6.50-7+7.5-8 m	2.46 m	2.80 m – 3.00 m
CAPACITY		
Up to 24.000 kg/120cbm		
UPGRADE		
TARPAULIN		



SMALL TRUCK		
LENGTH	WIDTH	HEIGHT
6.20 m	2.46 m	2.20 m – 2.70 m
CAPACITY		
2.700 – 3.300 kg/40cbm		
UPGRADE		
TARPAULIN		



13,6 Im STANDARD TRUCK		
LENGTH	WIDTH	HEIGHT
13.60 m	2.45 m	2.65 m – 2.80 m
CAPACITY		
22.000 – 23.000 kg/85cbm		
UPGRADE		
FRIGO/FURGON		



SMALL TRUCK		
LENGTH	WIDTH	HEIGHT
6.20 m	2.45 m	2.20 m – 2.70 m
CAPACITY		
Up to 3.000 kg/35cbm		
UPGRADE		
FRIGO/FURGON		



VAN		
LENGTH	WIDTH	HEIGHT
4.00 m	1.8 – 2.0 m	1.8 m – 1.9 m
CAPACITY		
Do 1.500 kg		
UPGRADE		
/		

# F3 National database environmental impacts

GWW Materials												
Shadow prize (Euro) per kg equivalents		0.16	0.05	30	0.09	0.03	0.0001	0.06	2	4	9	
Impact category	unit	Abiotic depletion (GWP100)	Global warming (CO2 eq)	Ozone layer depletion (CFC-11 eq)	Human toxicity (HWP100)	Fresh water aquatic ecotox	Marine aquatic ecotox	Terrestrial ecotox	Photochemical oxidation	Acidification (SO2 eq)	Eutrophication (PO4-- eq)	
AGRAC (asphalt granulate cement stabilization)	kg	0.000201354	0.050317117	3.8184E-09	0.019408371	0.021918904	19.28079709	9.50197E-05	5.61318E-06	0.000165345	3.32266E-05	
Aluminium	kg	0.048509574	8.257769559	5.09090E-07	37.8599885	3.862235439	4601.232587	0.097582596	0.003307357	0.039533435	0.003481249	
Aluminium, thermal sprayed, 350 um layer	m2	0.123924589	19.72064569	1.12898E-06	76.16103001	7.768798265	9453.291919	0.202519852	0.006820901	0.083591599	0.007567971	
Asphalt (DAB) Partial Recycled 0%	kg	0.00164017	0.09244974	3.19977E-08	0.030602769	0.005389545	19.4783372	0.000182104	2.96558E-05	0.000527984	7.41651E-05	
Asphalt (DAB) Partial Recycled 20%	kg	0.001392008	0.084867206	2.70365E-08	0.033535625	0.005512857	17.1781987	0.000161281	2.55691E-05	0.000482417	7.20438E-05	
Asphalt (EME) averaged	kg	0.001013134	0.060210441	2.53402E-08	0.031098533	0.004977693	15.9004942	0.000152966	2.43719E-05	0.000446335	6.58451E-05	
Asphalt (LTA)	kg	0.001232414	0.072497799	2.42648E-08	0.026722399	0.004788643	15.1804621	0.000142904	2.29199E-05	0.000395503	5.52520E-05	
Asphalt (OAB) Partial Recycled 20%	kg	0.001257479	0.077663512	2.43066E-08	0.030791596	0.004112978	14.80627652	0.000147799	2.30828E-05	0.000441184	6.69028E-05	
Asphalt (STAB) Partial Recycled 20%	kg	0.00110781	0.074877476	2.14252E-08	0.028649847	0.004023293	13.43593074	0.000138332	2.10016E-05	0.000407293	6.32455E-05	
Asphalt (STAB) Partial Recycled 50%	kg	0.000677119	0.05450269	1.28362E-08	0.021137749	0.002519854	8.02538155	8.55421E-05	1.35698E-05	0.000295621	5.08773E-05	
Asphalt application-finish machine (averaged, per type)	h	0.305657055	45.35488997	5.71395E-06	29.11203021	1.190649005	3937.726479	0.049680113	0.000989795	0.353691478	0.075780292	
Asphalt mastic	kg	0.004319517	0.196457148	8.45713E-08	0.006843461	0.011493416	49.47506345	0.000385517	7.1108E-05	0.000713892	0.000117923	
Asphalt truck 16 t: 270 kW, 6x4	tkm	0.000968145	0.132885527	1.24352E-08	0.027608086	0.006020356	10.98214999	0.000286614	2.18457E-05	0.000721348	0.000155184	
Asphalt truck 25 t: 240 kW, 8x4	tkm	0.001396074	0.193452818	1.31263E-08	0.03610029	0.007655307	14.92870231	0.000387887	3.74669E-05	0.001060875	0.000229989	
Asphalt truck 34 t: 240 kW, 10x4	tkm	0.001014705	0.136442423	2.25935E-08	0.026371138	0.006307255	11.31146979	0.000301839	2.61876E-05	0.000718492	0.000153459	
AVI bottom ash	kg	0	0	0	0	0	0	0	0	0	0	
Backhoe excavating equipment	h	1.807743392	271.7903492	3.3794E-05	172.1768644	7.041838402	23288.83946	0.293822381	0.053812875	2.091832455	4.44816298	
Bentonite mats	kg	0.001889448	0.131462787	1.72773E-07	0.015945039	0.005552387	6.867947915	0.000138485	3.15138E-05	0.00045087	4.58213E-05	
Benzine / petrol (led free)	l	0.004472849	5.390152536	7.45906E-07	0.866538103	0.079823422	326.1987897	0.005516149	0.001438562	0.01109223	0.00205482	
Bio-diesel	l	0.006450968	1.716915803	9.45979E-08	0.027950116	0.030599218	64.3934584	0.007973649	0.000648566	0.003316347	0.000368498	
Bitumen emulsion medium layer	kg	0.011494845	0.227370816	2.21722E-07	0.17550204	0.020422609	127.6413024	0.000961772	7.62497E-06	0.002376505	0.000287197	
Black furnace slag mixture (averaged)	kg	0.003152425	0.45024188	3.44795E-08	0.216320641	0.006898934	37.5658454	0.000656093	7.5758E-05	0.002591388	0.000538511	
Breaker machine, hydraulic 600-1500 kg	h	1.091632483	164.124607	2.0407E-05	103.9715365	4.252317875	14063.30885	0.177428974	0.032495698	1.26313385	0.2706439	
Brick clicker, Waal-format (average)	kg	0.001650226	0.183313509	4.88867E-09	0.020329774	0.005734373	8.065758313	0.000266509	2.87045E-05	0.000531287	6.3654E-05	
Brushwood, mats, fences	kg	0.023486236	0.0721418	0.00778972	0.002789728	0.007049639	10.98028603	0.000299158	4.01467E-05	0.000395278	6.76432E-05	
Bulldozer 12-35 t dry/wet	h	0.42684076	64.45173318	8.01382E-08	40.8266237	1.86989523	552.661387	0.069676359	0.01276106	0.496052298	1.06281859	
Cast iron	kg	0.013882539	1.501158032	1.05945E-08	0.983628905	0.9237326	895.059705	0.007752274	0.000844004	0.00777019	0.000553581	
Clay (averaged)	kg	1.93926505	0.00291563	6.62525E-05	0.001847027	7.55413E-05	0.24983096	3.15198E-06	5.72777E-07	2.24401E-05	4.80792E-06	
Clay granules, expanded	kg	0.002014946	0.359744064	6.52462E-08	0.041474367	0.006831369	25.84071194	0.000338305	0.000115591	0.002787555	0.000138175	
Clay, from dredging sludge	kg	0.166153583	21.61568673	1.50028E-06	2.831265161	0.224828156	1364.832816	0.030873512	0.016464614	0.02464614	0.003150539	
Cleaning truck - sweep/vacuum 6-8m3	tkm	0.001396074	0.193452818	1.31263E-08	0.03610029	0.007655307	14.92870231	0.000387887	3.74669E-05	0.001060875	0.000229989	
Coating for steel conservation (averaged)	kg	0.034289963	10.17531257	2.01921E-06	0.01050304	0.032589794	12063.2153	0.025042993	0.001424681	0.026174418	0.00271825	
Concrete (mats and membranes)	kg	0.001711274	0.233493691	1.55342E-08	0.25593844	0.048246477	73.85641893	0.002407954	6.88118E-05	0.00137474	0.00227681	
Cold mixed aggregate material (averaged)	kg	2.18262E-05	0.003282492	4.0814E-06	0.002079431	8.50464E-05	0.281266177	3.54858E-06	6.49914E-07	2.52637E-07	5.41288E-06	
Company car (averaged)	tkm	0.013496567	1.957139481	2.69282E-07	0.631472599	0.12637103	204.8921676	0.00619334	0.000724234	0.007383925	0.002117024	
Compressor diesel 3.5-10.0 m3/min	h	0.29474077	44.3136439	5.50988E-06	28.07231484	1.148125826	3797.09339	0.047805823	0.000773838	0.341059939	0.073073863	
Concrete column	kg	0.000278286	0.005619857	4.57604E-07	0.01050304	0.002118827	6.637096749	0.000184777	6.82497E-06	0.000228545	4.05999E-06	
Concrete companding (vibration needle)	kg	7.4413E-07	9.57674E-05	3.253E-12	1.37700E-05	1.3244E-06	0.007494144	2.19741E-07	6.16041E-09	1.3483E-07	1.80902E-08	
Concrete granulate / concrete rubble	kg	0.004774059	0.715063683	8.93972E-08	0.470261386	0.053534883	89.98280472	0.000806609	0.000141535	0.005484782	0.001175998	
Concrete mortar C12/15 (CEM I)	kg	0.000279732	0.1066953	4.46904E-09	0.009109928	0.001912038	3.190198499	0.000171122	7.45059E-06	0.000230925	4.10374E-05	
Concrete mortar C12/15 (CEM II)	kg	0.000243534	0.079868847	4.01828E-09	0.009235507	0.002038118	3.320184061	0.000155494	6.67407E-06	0.000202989	3.6664E-05	
Concrete mortar C20/25 (100% granulate)	kg	0.000529427	0.596434222	6.53095E-08	0.327489877	0.036667013	64.86543592	0.000762604	0.000139353	0.003638848	0.000833722	
Concrete mortar C20/25 (20% granulate)	kg	0.00093366	0.212702356	1.93529E-08	0.071808174	0.006552929	15.74355795	0.000338958	2.70014E-05	0.000855408	0.000198501	
Concrete mortar C20/25 (CEM I)	kg	0.000312369	0.123241332	4.95195E-09	0.010029126	0.00201553	3.408307694	0.000195946	8.3489E-06	0.000254503	4.46204E-05	
Concrete mortar C20/25 (CEM II)	kg	0.00027105	0.093270597	4.42066E-09	0.01026255	0.002171646	3.572933923	0.00018065	7.4021E-06	0.00022232	3.93859E-05	
Concrete mortar C30/37 (100% granulate)	kg	0.003534144	0.610327457	6.53134E-08	0.325296598	0.038438097	64.33663072	0.00079193	0.00010403	0.00382457	0.000828845	
Concrete mortar C30/37 (20% granulate)	kg	0.000938389	0.216727982	1.66444E-08	0.07156622	0.006527234	15.71446925	0.000347247	2.71297E-05	0.000595957	0.000193117	
Concrete mortar C30/37 (CEM I)	kg	0.000320046	0.12754589	5.1096E-09	0.010319382	0.002057054	3.480190756	0.000202592	8.61122E-06	0.00026003	4.586E-05	
Concrete mortar C30/37 (CEM II)	kg	0.00027569	0.094493546	4.50443E-09	0.010418311	0.002199242	3.627124452	0.000183449	7.53166E-06	0.000228284	0.01583E-05	
Concrete mortar C35/45 (CEM II)	kg	0.000279286	0.095490857	4.57604E-09	0.01050634	0.002188287	3.637086743	0.000184777	7.62497E-06	0.000228545	4.05999E-06	
Concrete mortar C55/67 (CEM I-CEM II)	kg	0.000330558	0.118053376	5.15393E-09	0.011925113	0.0023673	3.936360579	0.000217018	8.86497E-06	0.000260373	4.52897E-05	
Concrete mortar C70/85 (CEM I-CEM II)	kg	0.000454525	0.160572173	6.76381E-09	0.019084163	0.00341663	6.334907297	0.000334068	1.2537E-05	0.000350207	5.64382E-05	
Concrete pump incl. truck	m3	0.044931979	6.76532885	8.4007E-07	4.28007683	0.175050278	578.5280569	0.007304014	0.001337713	0.052000036	0.011142286	
Concrete reinforcement steel (averaged)	kg	0.012737595	1.487306959	5.6546E-08	0.658503497	0.633223299	590.001295	0.027548661	0.000847148	0.00515538	0.001052688	
Concrete, aerated - lightweight	kg	0.00087965	0.401043089	1.31839E-08	0.036748079	0.006406319	10.25238247	0.000695896	2.57933E-05	0.000838398	0.00010036	
Concrete, under-water C20/25	kg	0.000225207	0.075660072	6.88338E-09	0.008264596	0.001783401	2.924167471	0.00043279	6.04634E-06	0.00018068	3.22981E-05	
Concrete, under-water C30/37	kg	0.000249438	0.083974578	4.11919E-09	0.009110949	0.001947707	3.268541972	0.000192578	6.74589E-06	0.00020652	3.70874E-05	
Copper	kg	0.01542076	2.0241918	1.45501E-07	88.3830473	2.59301868	4373.67236	0.36870585	0.005289893	0.139898312	0.004199987	
Copper, hydraulic (averaged)	kg	0.57579812	86.5701056	1.074E-05	54.84129496	7.41718057	241.8051987	0.00358066	0.000744034	0.006625498	0.14275234	
Crusher rock (averaged)	kg	0.00136444	0.020195127	2.19767E-09	0.01137299	0.000648853	2.055085827	4.0891E-05	3.95272E-06	0.00030642	3.3031E-05	
Crusher sand	kg	1.33884E-05	0.001640694	6.68261E-10	0.000355892	0.00157396	4.022079584	6.61436E-06	6.18357E-07	1.00288E-05	2.27422E-06	
Cutter sucker 350-600 mm suction tube	h	3.897172964	595.98248471	7.28529E-09	37.1738351	15.18077482	5026.0126	6.63342147	1.6100694	4.59566343	0.96198742	
Diesel	l	0.02183266	3									



Polyester foil	kg	0,057321197	8,025203611	1,109006E-06	7,093815307	0,42746251	718,5485826	0,029895422	0,002041415	0,021237507	0,004110783
Polyester membrane, reinforced	kg	0,057321197	8,025203611	1,109006E-06	7,093815307	0,42746251	718,5485826	0,029895422	0,002041415	0,021237507	0,004110783
Polyethylene membrane	kg	0,03696254	2,58434842	2,67102E-08	0,299249997	0,11715631	136,20065	0,002678162	0,00053916	0,010009224	0,00076637
Polypropylene membrane	kg	0,036962001	2,47497005	2,66104E-08	0,272962602	0,105399482	127,5213109	0,002650713	0,000595509	0,008261485	0,000793027
Polypropylene membrane, reinforced	kg	0,04131168	3,862534452	2,97226E-07	1,978175816	0,185915247	275,2781298	0,00942814	0,000565986	0,011505491	0,001622941
PP (polypropylene)	kg	0,035126227	2,327429762	2,29468E-08	0,255059761	0,08385057	111,3110418	0,003010384	0,000583372	0,008079357	0,000760948
Pressure sprayer for applying paint layers	m2	0,072938686	10,96617534	1,36352E-06	6,946978396	0,284123534	939,656238	0,011855122	0,002171238	0,084401089	0,018083385
Pressure tubing land (averaged)	tkm	4,36653E-05	0,006564984	8,16279E-10	0,004158861	0,000170093	0,562532354	7,09716E-06	1,29983E-06	0,505274E-05	1,08258E-05
Prestressing steel (average)	kg	0,015351254	1,79136736	7,16698E-08	3,813593993	1,487281841	1315,591287	0,031816387	0,00928571	0,007384261	0,001343378
Propane	kg	0,024413656	0,601122586	4,71348E-07	0,369870987	0,046117595	280,5246229	0,00260507	0,000377692	0,006839789	0,000607988
Pump, diesel-fueled 4-15 kW	h	0,026444737	3,975918605	4,94359E-07	2,518710471	0,103012401	340,636567	0,004298217	0,000787208	0,030600629	0,006556348
PVC (averaged)	kg	0,022624127	1,960688109	2,94826E-09	0,592970223	0,152997418	40,86137661	0,006836077	0,00031303	0,005352097	0,000760211
PVC-foil	kg	0,026213566	2,485102958	2,94E-08	0,777970357	0,213599123	151,9070416	0,009350839	0,000406994	0,007420747	0,000902803
Rammer hammer, hydraulic stroke 50-200	h	1,091632483	164,124607	2,0407E-05	103,9715365	4,252317875	14063,30885	0,177428974	0,032495698	1,26318395	0,2706439
Rammer rig (small setting)	h	0,348543596	52,40283832	6,51568E-06	33,19675904	1,357709427	4430,230401	0,056850748	0,010373451	0,403318966	0,089413054
Rammer rig, mobile 300-500kN	h	0,435677393	65,50354789	8,1446E-06	41,495598	1,697136783	5612,788001	0,070813436	0,012969313	0,504147592	0,108016317
Rammer, diesel-fueled (averaged, per tonnage) hour	h	0,619585055	93,1532867	1,15825E-05	59,01181133	2,413516129	7982,005047	0,100704534	0,018443798	0,716953597	0,153611145
Rammer, hydraulic	h	1,091632483	164,124607	2,0407E-05	103,9715365	4,252317875	14063,30885	0,177428974	0,032495698	1,26318395	0,2706439
Rammer, vibration - electric (averaged)	h	0,151324582	23,69459434	2,92307E-06	3,04767099	0,304243583	1737,583978	0,01861165	0,007931606	0,244039512	0,052121397
RE-HDPE (averaged)	kg	0,031300031	1,431772024	6,5827E-11	0,043378806	0,031302793	6,164844033	7,6667E-05	0,000289074	0,003269912	0,000294074
RE-PE (averaged)	kg	0,031300031	1,431772024	6,5827E-11	0,043378806	0,031302793	6,164844033	7,6667E-05	0,000289074	0,003269912	0,000294074
RE-PVC	kg	0,022624127	1,960688109	2,94826E-09	0,592970223	0,152997418	40,86137661	0,006836077	0,00031303	0,005352097	0,000760211
Road marking / line drawing machine	h	0,104796718	15,75596227	1,95907E-06	9,9812675	0,408222516	1350,07765	0,017033181	0,003119587	0,12126565	0,025981814
Road roller machine (average)	m2	0,000436653	0,065649843	8,16279E-09	0,041588615	0,001700927	5,625323541	7,09716E-05	1,29983E-05	0,000505274	0,000108258
Sand (average)	kg	3,34652E-05	0,004895269	5,39801E-10	0,002731243	0,000115055	0,410185438	6,11267E-06	8,67858E-07	3,23939E-05	6,58115E-06
Sand for drainage	kg	2,00081E-05	0,002694296	3,02429E-10	0,001250503	6,51851E-05	0,240267225	3,81337E-06	4,8849E-07	1,8322E-05	3,86255E-06
Sand, Dutch Jslasmeer (land raising)	kg	7,8019E-06	0,001144299	1,4211E-10	0,000724036	2,96122E-05	0,097833906	1,23558E-06	2,86293E-07	8,79954E-06	1,88471E-06
Sand, polymer-bentonite	kg	8,90002E-05	0,009174527	5,57018E-10	0,003245872	0,000278945	0,560065116	1,0428E-05	1,45748E-06	4,14046E-05	7,53484E-06
Sand, rural (land raising)	kg	2,05143E-05	0,00286283	2,4393E-10	0,001210207	5,50189E-05	0,230222898	4,42948E-06	4,01946E-07	1,43255E-05	2,9461E-06
Sandcement (stabilized)	kg	0,108971834	16,38671498	2,14976E-06	3,258620734	1,214009622	1886,859002	0,03284026	0,002725626	1,033758899	0,022169539
Seasons - landscaping	kg	0,001000534	0,014974154	1,74458E-09	0,009318449	0,000461822	1,623165908	3,13676E-05	0,000281728	2,91526E-05	0,000108258
Shells, clay-mixture	kg	1,93926E-05	0,00291553	3,62525E-10	0,001847027	7,55413E-05	0,24983098	5,77277E-07	2,24401E-05	4,80792E-06	0,000108258
Shovel	h	0,287754322	43,26324641	5,37928E-06	27,40689701	1,120910992	3707,088214	0,046770278	0,008565667	0,332917563	0,071341732
Silpform paver	h	0,746676618	112,2612132	1,39584E-05	71,11653093	2,908585427	9619,303255	0,121361418	0,022225077	0,864017723	0,185102427
SMA stone mass asphalt 0/11 (averaged)	kg	0,593821287	85,64163883	1,11979E-05	41,67621582	8,863272851	12673,67148	0,33129593	0,015268991	0,510569927	0,102782203
Softwood FSC	kg	0,001633563	0,229483334	1,88198E-08	0,112002129	0,023371255	38,44507463	0,001190516	0,000109536	0,001378257	0,000225018
Soil	kg	0	0	0	0	0	0	0	0	0	0
Soil, cleaned	kg	7,44824E-05	0,01037607	1,65378E-09	0,002250631	0,000400991	0,806706955	2,01548E-05	2,01262E-06	5,84577E-05	1,26594E-05
Soil, mildly polluted	kg	0	0	0	0	0	0	0	0	0	0
STAB (steenslagasfaltbeton) 0% PR (asfaltgranulaat)	kg	0,001301134	0,082010441	2,53402E-08	0,031098553	0,004976633	15,90804942	0,000152966	2,43719E-05	0,000446335	6,58451E-05
Steel fibres	kg	0,015351254	1,79136736	7,16698E-08	3,813593993	1,487281841	1315,591287	0,031816387	0,00928571	0,007384261	0,001343378
Steel GWW (averaged)	kg	0,015351254	1,79136736	7,16698E-08	3,813593993	1,487281841	1315,591287	0,031816387	0,00928571	0,007384261	0,001343378
Steel reinforcement net FeB 500 HKN	kg	0,012739756	1,487306595	5,6546E-08	0,658503497	0,633223299	590,0001295	0,027549861	0,000847148	0,00515538	0,001052698
Steel slag	kg	0,012571986	1,796706031	1,73192E-07	0,86269448	0,038939616	149,8242973	0,002616524	0,000281475	0,010334541	0,002151589
Steel, heavy duty - 90% Beam steel (BlastFurnace and Electric Arc F	kg	0,015644102	1,819644381	5,65569E-08	0,602423921	0,456673579	426,5800965	0,010842716	0,001082834	0,006160042	0,001317667
Stone, quarried	kg	0,001810059	0,262682605	3,42598E-08	0,117213776	0,008242238	24,09703059	0,001033894	4,67675E-05	0,00156234	0,000313237
Stone, re-used	kg	6,6222E-05	0,010097563	1,20989E-09	0,00556865	0,000324427	1,029252913	2,04458E-05	4,68136E-06	0,000150321	1,65155E-05
Street tiles (average)	kg	0,004257845	0,575471898	2,25359E-08	0,216164434	0,197083943	185,0566733	0,009690508	0,000269147	0,001821085	0,000360587
Suction hopper dredger 10.000 m3	h	6,103886346	904,7513043	0,000101742	57,7548866	30,2283723	108777,4999	2,373050361	6,828130345	22,26239996	1,901806592
Suction hopper dredger 20.000 m3	h	12,20777699	1809,502609	0,000203484	111,5509774	60,45674461	217554,9998	4,746100723	1,656260991	44,52479993	3,803613185
Suction hopper dredger 5.000 m3	h	3,051944173	452,3756522	5,0871E-05	278,8774434	15,11418615	54388,74995	1,186525181	0,0414065173	11,13119998	0,959030396
System formwork application (average)	m2	0,104375209	59,36954086	2,96023E-07	5,603853727	2,325255626	2241,655578	0,056924305	0,02436374	0,024671841	0,044229916
Thermoplastic road marking	kg	0,022232526	2,599156289	2,15022E-07	2,18023812	1,526955266	336,9522961	0,015068022	0,000643387	0,01638504	0,001971813
Timber crossol impregnated	kg	0,013683015	5,739611446	3,4151E-08	1,626124464	0,180152942	96,77890793	0,003355986	0,000194231	0,002924903	0,000345107
Timber, chrome - copper - arsenic (volmanized) impregnated	kg	0,001770848	0,253315555	2,03818E-08	1,16795338	0,043704879	57,23649312	0,0153394	0,000120715	0,001672013	0,000240686
Timber, cut European hardwood (averaged)	kg	0,008648205	5,448919422	1,11154E-08	0,068056603	0,014801985	24,06827043	0,000790419	6,15438E-05	0,000849399	0,000137362
Timber, cut tropical hardwood (averaged)	kg	1,445024733	6,757603841	6,68336E-08	0,261550536	0,027295513	63,24254269	0,001445312	0,000236251	0,006769516	0,000768244
Timber, FSC label	kg	0,003656013	0,607603941	6,68336E-08	0,261550536	0,027295513	63,24254269	0,001445312	0,000236251	0,006769516	0,000768244
Timber, secondary	kg	9,68145E-05	0,01328953	1,14352E-09	0,002760809	0,000602036	1,098214999	2,88614E-05	2,18457E-06	7,21348E-05	1,55184E-05
Tractor 40-110 kW; 4x4	h	0,208720131	31,38062486	3,90181E-06	19,87935777	0,813043178	2688,904653	0,0392442	0,006213177	0,241520752	0,051747114
Traditional formwork application (average)	m2	0,082883454	56,88262697	1,95685E-07	1,164822137	0,243061049	399,8287761	0,012381363	0,001139174	0,014333875	0,002340188
Transport bulk (over road)	tkm	0,001396074	0,193452818	1,31263E-08	0,03610029	0,007655307	14,92870231	0,000387887	3,74669E-05	0,001060875	0,000229989
Transport bulk (over water)	tkm	0,000262893	0,046380953	4,83522E-09	0,007345362	0,001682516	4,315341706	9,35E-05	6,59858E-06	0,000336376	7,11491E-05
Transport steel	tkm	0,001396074	0,193452818	1,31263E-08	0,03610029	0,007655307	14,92870231	0,000387887	3,74669E-05	0,001060875	0,000229989
Transport synthetic polymers	tkm	0,000968145	0,132885527	2,14352E-08	0,027608086	0,006020356	10,98214999	0,000288614	2,18457E-05	0,000721348	0,000155184
Transport timber	tkm	0,001253574	0,17328301	2,80326E-08	0,033272386	0,007110868	13,61450039	0,000354829	3,22651E-05	0,000947813	0,000205079
Truck 25-28t; 240kW; 8x4/8x6	tkm	0,001396074	0,193452818	1,31263E-08	0,03610029	0,007655307	14,92870231	0,000387887	3,74669E-05	0,001060875	0,000229989
Truck+crane 120-220 kW; 4x2/6x4	tkm	0,000914802	0,116789237	1,8803E-08	0,034036146	0,008483075	12,51190817	0,000390064	1,82914E-05	0,000473223	8,85502E-05
Truckmixer 15 m3	tkm	0,000914802	0,116789237	1,8803E-08	0,034036146	0,008483075	12,51190817	0,000390064	1,8		